# Reaction-diffusion Equations with Nonlinear and Nonlocal Advection Applied to Cell Co-culture

Xiaoming Fu

Institut de Mathématiques de Bordeaux

université de BORDEAUX

# THÈSE

PRÉSENTÉE À

# L'UNIVERSITÉ DE BORDEAUX

ÉCOLE DOCTORALE DE MATHÉMATIQUES ET D'INFORMATIQUE

par **Xiaoming Fu**

POUR OBTENIR LE GRADE DE

# DOCTEUR

SPÉCIALITÉ : MATHÉMATIQUES

---

## Reaction-diffusion Equations with Nonlinear and Nonlocal Advection Applied to Cell Co-culture

---

**Date de soutenance :** 19 Novembre 2019

**Devant la commission d'examen composée de :**

| | | |
|---|---|---|
| Vincent Calvez ..... | Directeur de recherche CNRS, Université Claude Bernard Lyon 1 | Examinateur |
| Jacques Demongeot | Professeur, Université de Grenoble ..... | Président du jury |
| Arnaud Ducrot .... | Professeur, Université Le Havre Normandie ..... | Examinateur |
| Quentin Griette ... | Maître de conférences, Université de Bordeaux ..... | Examinateur |
| Pierre Magal ..... | Professeur, Université de Bordeaux ..... | Directeur |
| Alain Miranville .. | Professeur, Université de Poitiers ..... | Rapporteur |
| Glenn Webb ..... | Professeur, Vanderbilt University ..... | Rapporteur |

– 2019 –

# Reaction-diffusion Equations with Nonlinear and Nonlocal Advection Applied to Cell Co-culture

Xiaoming Fu

Institut de Mathématiques de Bordeaux UMR 5251
Université de Bordeaux
351, cours de la Libération - F 33405 TALENCE

**Résumé**

Cette thèse est consacrée à l'étude d'une classe d'équations de réaction-diffusion avec advection non-locale. La motivation vient du mouvement cellulaire avec le phénomène de ségrégation observé dans des expérimentations de co-culture cellulaire. La première partie de la thèse développe principalement le cadre théorique de notre modèle, à savoir le caractère bien posé du problème et le comportement asymptotique des solutions dans les cas d'une ou plusieurs espèces.

Dans le Chapitre 1, nous montrons qu'une équation scalaire avec un noyau non-local ayant la forme d'une fonction étagée, peut induire des bifurcations de Turing et de Turing-Hopf avec le nombre d'ondes dominant aussi grand que souhaité. Nous montrons que les propriétés de bifurcation de l'état stable homogène sont intimement liées aux coefficients de Fourier du noyau non-local.

Dans le Chapitre 2, nous étudions un modèle d'advection non-local à deux espèces avec inhibition de contact lorsque la viscosité est égale à zéro. En employant la notion de solution intégrée le long des caractéristiques, nous pouvons rigoureusement démontrer le caractère bien posé du problème ainsi que la propriété de ségrégation d'un tel système. Par ailleurs, dans le cadre de la théorie des mesures de Young, nous étudions le comportement asymptotique des solutions. D'un point de vue numérique, nous constatons que sous l'effet de la ségrégation, le modèle d'advection non-locale admet un principe d'exclusion.

Dans la deuxième partie de la thèse (Chapitre 3), nous nous intéressons à l'application de nos modèles aux expérimentations de co-culture cellulaire. Pour cela, nous choisissons un modèle hyperbolique de Keller-Segel sur un domaine borné. En utilisant les données expérimentales, nous simulons un processus de croissance cellulaire durant 6 jours dans une boîte de pétri circulaire et nous discutons de l'impact de la propriété de ségrégation et des distributions initiales sur les proportions de la population finale.

**Mots clés:** Diffusion non-locale et non-linéaire, Equation hyperbolique de Keller-Segel, Ségrégation, Bifurcation de Turing-Hopf, Co-culture cellulaire

**Abstract**

This thesis is devoted to the study for a class of reaction-diffusion equations with nonlocal advection. The motivation comes from the cell movement with segregation phenomenon observed in cell co-culture experiments. The first part of the thesis mainly develops the theoretical framework of our model, namely the well-posedness and asymptotic behavior of solutions in both single-species and multi-species cases.

In Chapter 1, we show that a single scalar equation with a step function kernel may display Turing and Turing-Hopf bifurcations with the dominant wavenumber as large as we want. We find that the bifurcation properties of the homogeneous steady state are closely related to the Fourier coefficients of the nonlocal kernel.

In Chapter 2, we study a two-species nonlocal advection model with contact inhibition when the viscosity equals zero. By employing the notion of solution integrated along the characteristics, we rigorously prove the well-posedness and segregation property of such a hyperbolic nonlocal advection system. Besides, under the framework of Young measure theory, we investigate the asymptotic behavior of solutions. From a numerical perspective, we find that under the effect of segregation, the nonlocal advection model admits a competitive exclusion principle.

In the second part of the thesis (Chapter 3), we are interested in applying our models to a cell co-culturing experiment. To that aim, we choose a hyperbolic Keller-Segel model on a bounded domain. By utilizing the experimental data, we simulate a 6-day cell growth process in a circular petri dish and discuss the impact of both the segregation property and initial distributions on the population proportions.

**Key words:** Nonlocal and nonlinear diffusion, Hyperbolic Keller-Segel equation, Segregation, Turing-Hopf bifurcation, Cell co-culture

# Acknowledgments

First of all, I am grateful to my supervisor Pierre Magal during my doctoral study. It's because of his dedication, availability, and professional advice that I can focus on my doctoral research at the Institut de Mathématiques de Bordeaux. It is him who led me into the field of applied mathematics in biology and taught me how to do research and work with people.

I would also like to express my gratitude to all the other members of the jury. I'd like to thank two referees: Professor Alain Miranville and Professor Glenn Webb for their precious time to read my thesis and give me useful suggestions. I'd like to thank Professor Vincent Calvez and Professor Jacques Demongeot for their acceptance to be part of the jury. I'd like to thank Professor Arnaud Ducrot for all the guidance of my work. I'd also like to thank Professor Quentin Griette for all the discussions and his careful check to make the thesis better.

Moreover, I would like to thank all my colleagues at the IMB and the members in the group of population dynamics, especially my fellow Ph.D. candidates: Paul, Krisztian, Marco, Edoardo, Jared and so on for all the discussions and company from you. I would specially thank Corentin Prigent for his great help in the numerical simulation and Quentin Richard for his suggestions and corrections in French. I would also like to thank all my Chinese colleagues and friends that I cannot enumerate here for our unforgettable meals together.

I would also like to seize this opportunity to thank my master's supervisor Rong Yuan, Professor Zhihua Liu, and Professor Yunfei Lü for their warm reception during my stay in China as well as the suggestions for my future career. Special thanks go to China Scholarship Council, due to which I could come to France for my Ph.D. study.

I always regard it as a precious chance to do a Ph.D. in a foreign country, which trains me to persevere through each valley and to rejoice in each circumstance. Of course, all of this become possible because of other's companionship and encouragement. I thank my friends for their help in adapting myself to the life here. I thank all my special "family members" here who support me so much, especially John, Betsy, and Xin. You are my family here.

Last but not least, I will never be grateful enough for my parents without whom nothing would be possible.

# Contents

# Résumé

L'objectif principal de cette thèse est de modéliser les interactions dans la co-culture de cellules multi-espèces. Parmi ces interactions, on peut mentionner l'attraction, la répulsion et la ségrégation de cellules, conduisant à la formation de motifs. Nous choisissons une classe d'équations de réaction-diffusion avec advection non-locale. Dans la première partie de la thèse (Chapitres 1 et 2), nous développons principalement le cadre théorique de ces modèles, à savoir le caractère bien posé du problème dans le cas d'une ou de plusieurs espèces. De plus, nous discutons des bifurcations de Turing et de Turing-Hopf ainsi que du comportement asymptotique des solutions.

En ce qui concerne la seconde moitié de cette thèse (Chapitre 3), nous appliquons nos modèles à une expérimentation de co-culture cellulaire. Nous choisissons alors un modèle hyperbolique de Keller-Segel, qui peut être considéré comme une variation du modèle non-local et dont nous établissons également les résultats théoriques. En utilisant les données expérimentales, nous simulons une croissance cellulaire de 6 jours dans une boîte de pétri et nous montrons l'impact de la propriété de ségrégation et des distributions initiales sur les proportions des populations.

## 1 Aperçu de la thèse

Dans ce manuscrit, nous étudions deux types d'équation de réaction-diffusion avec advection non-linéaire et non-locale. Nous considérons d'abord l'équation mono-espèce suivante

$$\partial_t u(t,x) + \operatorname{div}\left(u(t,x)\mathbf{v}(t,x)\right) = D\Delta u(t,x) + f(u(t,x)),\ t>0,\ x\in\Omega\subset\mathbb{R}^N. \tag{1.1}$$

Ici $D \geq 0$ est le paramètre de viscosité. La divergence, le gradient et le laplacien sont pris par rapport à $x$. Le champ de vélocité $\mathbf{v}$ se calcule à partir de la pression $P$ :

$$\mathbf{v}(t,x) = -\nabla P(t,x).$$

**Cas 1:** Nous considérons les solutions de l'équation (1.1) qui sont **périodiques en espace**. Ici, une fonction $u(t,x)$ est dite $2\pi$ **-périodique dans chaque direction** (ou pour simplifier **périodique**) si

$$u(t,x+2k\pi) = u(t,x),\ \forall k\in\mathbb{Z}^N, x\in\mathbb{R}^N.$$

Dans le cas non-local, la pression $P$ est de la forme

$$P(t,x) = \int_{\mathbb{R}^N} \rho(x-y)u(t,y)\mathrm{d}y, \quad t>0, x\in\mathbb{R}^N. \tag{1.2}$$

Le problème ci-dessus peut s'écrire comme l'équation suivante posée sur $\Omega := [0, 2\pi]^N$ avec la condition périodiques aux bords

$$\begin{cases} \partial_t u = D\Delta u + \operatorname{div}\left(u\nabla\left(K \circ u\right)\right) + f(u),\ t > 0,\ x \in \Omega, \\ u(0, x) = u_0(x),\ x \in \Omega, \end{cases}$$

où le noyau $K \in L^1_{\text{per}}(\Omega)$ est défini par

$$K(x) = (2\pi)^N \sum_{k \in \mathbb{Z}^N} \rho(x + 2\pi k),\ x \in \mathbb{R}^N.$$

Ici et dans toute la suite de la thèse, le symbole $\circ$ représente le produit de convolution sur le tore $\Omega = \mathbb{R}^N/(2\pi\mathbb{Z}^N) \simeq [0, 2\pi]^N$, c'est-à-dire

$$\left(\varphi \circ \psi\right)(x) = |\Omega|^{-1} \int_\Omega \varphi(x - y)\psi(y)dy,\ \forall \varphi, \psi \in L^1_{\text{per}}(\Omega). \tag{1.3}$$

Par conséquent, nous réécrivons la pression (1.2) de la manière suivante

$$P(t, x) = |\Omega|^{-1} \int_\Omega K(x - y)u(t, y)\mathrm{d}y.$$

**Cas 2:** Lorsque $\Omega \subset \mathbb{R}^N$ est un ensemble borné, nous imposons la condition aux bords de non-flux et nous définissons

$$P(t, x) = (I - \chi\Delta)^{-1}u(t, x), \quad \nabla P \cdot \nu = 0, \tag{1.4}$$

où $\nu$ est le vecteur normal sortant, $\chi$ est une constante positive représentant le coefficient de détection des cellules et $(I - \chi\Delta)^{-1}$ est la résolvante du Laplacien avec condition de Neumann aux bords.

L'équation (1.4) peut être obtenue formellement comme limite singulière de l'équation parabolique suivante (qui est le cas classique dans l'équation de Keller-Segel [61]) lorsque $\varepsilon$ tend vers 0:

$$\varepsilon\partial_t P(t, x) = \chi\Delta P(t, x) + u(t, x) - P(t, x).$$

Le fait de prendre $\varepsilon \to 0$ correspond à l'hypothèse selon laquelle la dynamique du chimio-repoussant est rapide par rapport à l'évolution de la densité cellulaire.

En fait, l'équation (1.4) peut également être considérée comme une advection non-locale en utilisant la représentation

$$P(t, x) = \int_\Omega \kappa(x, y)u(t, y)dy,$$

où $\kappa$ est un noyau de convolution qui est obtenu par la somme des fonctions propres de l'opérateur $(I - \chi\Delta)^{-1}$ sur $L^2(\Omega)$, coefficientées par leurs valeurs propres.

## 1.1 Bifurcations de Turing et de Turing-Hopf pour une équation de réaction-diffusion avec advection non-locale

Le Chapitre 1 traite du système monospécifique en dimension $N = 1$ avec la condition périodique

$$\frac{\partial u}{\partial t} = \frac{\partial}{\partial x}\left[D\frac{\partial u}{\partial x} + u\frac{\partial}{\partial x}(\rho * u)\right] + f(u),\ t > 0,\ x \in \mathbb{R}.$$

Nous étudions les propriétés de stabilité et de bifurcation de l'équilibre intérieur positif pour une telle équation de réaction-diffusion avec advection non-locale. Sous certaines hypothèses générales sur le noyau non-local, nous étudions d'abord le caractère bien posé du problème dans les espaces de Sobolev d'ordre fractionnaire et nous obtenons des résultats de stabilité pour l'état d'équilibre homogène. Comme cas particuliers, nous montrons que les noyaux "standards" tels que le noyau de Cauchy, de Laplace, Gaussien et triangulaire conduiront à la stabilité de l'équilibre homogène.

Ensuite, nous considérons le modèle dont le noyau est une fonction étagée et nous examinons deux types de bifurcations, à savoir la bifurcation de Turing et de Turing-Hopf. En général, une équation de réaction-diffusion scalaire et locale ne présente pas de formation de motifs, à cause du principe de comparaison. Cependant, en ce qui concerne les interactions non-locales, le principe de comparaison peut ne pas exister et des comportements dynamiques plus complexe peuvent se produire. Dans le Chapitre 1, nous prouvons qu'une équation scalaire avec un noyau non-local ayant la forme d'une fonction étagée, peut induire des bifurcations de Turing et de Turing-Hopf avec le nombre d'ondes dominant aussi grand que souhaité. De plus, des instabilités similaires peuvent également être observées avec un noyau bimodal. Les dynamiques spatio-temporelles sont illustrées par des simulations numériques.

L'opérateur non-linéaire responsable du déplacement des individus, dénoté par $\mathbf{J}(u)$ et défini par

$$\mathbf{J}(u) = \frac{\partial}{\partial x}\left[D\frac{\partial u}{\partial x} + u\frac{\partial}{\partial x}(\rho * u)\right],$$

a été proposé et étudié par plusieurs auteurs dans la littérature. L'opérateur non-linéaire $\mathbf{J}(u)$ a également été introduit dans les dynamiques d'essaimage, nous nous référons à l'article de Bernoff et Topaz [10] ainsi que les références qui y figurent.

Certaines propriétés de l'équation $\partial_t u = \mathbf{J}(u)$ sans viscosité ont été étudiées par exemple dans [17, 68, 91] (voir aussi les références citées). Enfin, nous nous référons à Burger et Di Francesco [18] pour une étude d'une équation légèrement différente incluant la diffusion non-linéaire.

Dans le Chapitre 1, dans le contexte de la dynamique de la population cellulaire, la fonction $f$ modélise le processus de prolifération cellulaire. Au lieu de considérer une terme de réaction de type logistique, nous utiliserons la fonction établie par Ducrot et al. [38]. Nous supposons alors que la fonction $f$ a la forme suivante

$$f(u) = \frac{bu}{1+\gamma u} - \mu u,\ b > 0,\ \mu > 0,\ \gamma > 0.$$

Cette forme spécifique nous permettra d'utiliser des calculs explicites lors de notre analyse et d'utiliser le paramètre $\gamma > 0$ comme un paramètre de bifurcation. Dans le contexte de

la dynamique des populations cellulaires, cette fonction non-linéaire tient compte de la division cellulaire et du taux de sortie par les paramètres $b$ et $\mu$ respectivement. La partie de saturation due au paramètre $\gamma > 0$ reflète la phase de dormance cellulaire. Nous nous référons à [38] pour plus de détails sur la modélisation.

Un exemple de noyau ayant un intérêt particulier est une fonction étagée de la forme

$$\rho(x) = \rho_{\eta,s}(x) = \frac{1}{2\eta}\chi_{[-1,1]}\left(\frac{x-s}{\eta}\right),\ x \in \mathbb{R},$$

pour un paramètre d'échelle $\eta > 0$, un décalage $s \in \mathbb{R}$ et où $\chi_{[-1,1]}$ désigne la fonction caractéristique sur l'intervalle $[-1, 1]$

$$\chi_{[-1,1]}(x) = \begin{cases} 1 & \text{si } x \in [-1,1], \\ 0 & \text{sinon.} \end{cases}$$

Comme nous le verrons au Chapitre 1, ce noyau peut déstabiliser l'état stable homogène, produisant les instabilités de Turing et l'existence d'un état stable spatialement hétérogène. Plus surprenant, il peut également conduire à un régime spatio-temporel via une bifurcation de Turing-Hopf.

En utilisant ce noyau, on peut observer que la solution de (1.1)-(1.2) est – au moins formellement – la solution de l'équation de Burgers non-locale suivante avec viscosité

$$\frac{\partial u}{\partial t} = D\frac{\partial^2 u}{\partial x^2} + \frac{\partial}{\partial x}Q[u] + f(u),\ t > 0,\ x \in \mathbb{R},$$

où $Q$ est un opérateur non-local quadratique

$$Q[u(t,.)](x) = u(t,x)\frac{u(t,x-\eta+s) - u(t,x+\eta+s)}{2\eta},\ x \in \mathbb{R}.$$

Comme nous l'avons mentionné, avec un choix approprié sur les paramètres du modèle et avec un noyau approprié, les bifurcations de Turing et de Turing-Hopf peuvent se produire. De plus, les résultats théoriques sont confirmés par des simulations numériques au Chapitre 1. Nous présentons ici un des scénarios de bifurcation de Turing.

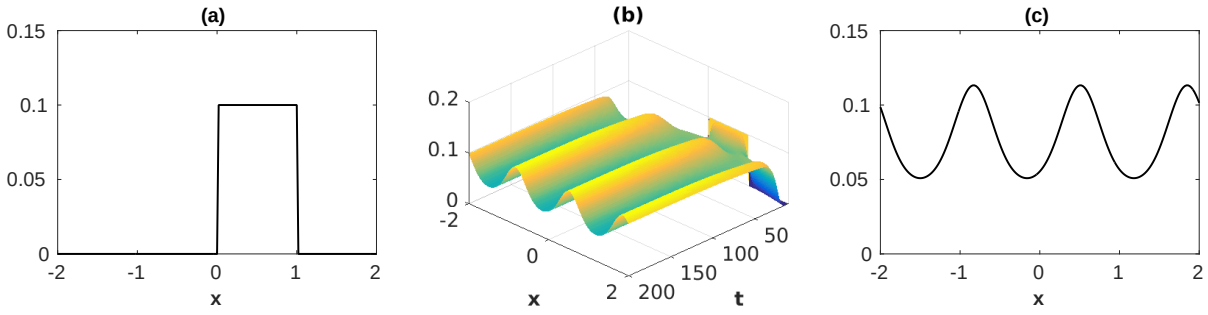


Figure 1: *On considère* $b = 1.5$, $\mu = 1.2$, $\eta = 1$ *et* $(\varepsilon, \gamma) = (0.0056, 3.03)$. *La figure (a) présente la donnée initiale asymétrique, la figure (b) présente l'évolution spatio-temporelle de la solution et la figure (c) présente la solution à* $T = 200$ *quand elle est stabilisée près d'un décalage approprié de l'état stationnaire symétrique. Ici le numéro d'onde est* $n_0 = 3$.

Nous présentons également l'un des scénarios de bifurcation de Turing-Hopf avec le noyau bimodal suivant

$$\rho(x) = \frac{1}{2}\left(e^{-\pi(x+s_1)^2} + e^{-\pi(x-s_2)^2}\right).$$

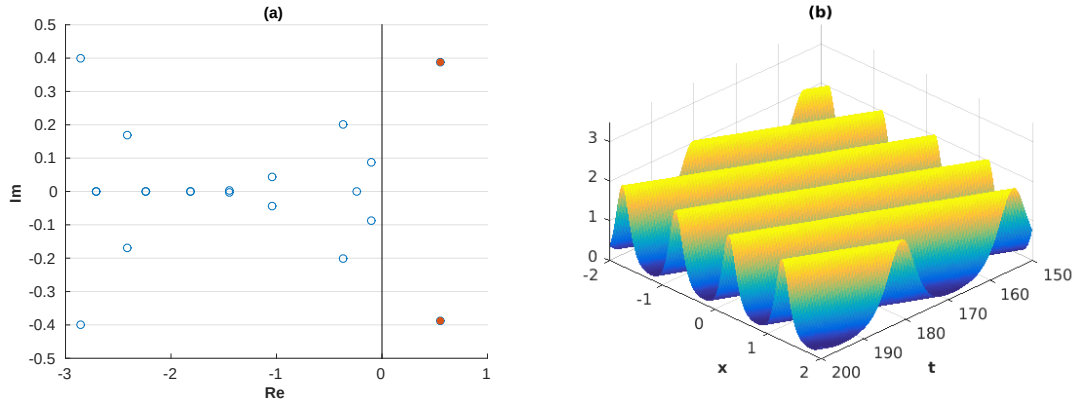


Figure 2: *On fixe* $(\varepsilon, \gamma) = (0.01, 0.2)$, $s_1 = 0.4$, $s_2 = 0.3$. *Dans la figure* $(a)$ *nous traçons les valeurs propres de l'équation linéaire dans le plan complexe pour* $n = -10, -9, \ldots, 9, 10$. *En choisissant les paramètres ci-dessus, il n'y a qu'une seule paire de valeurs propres, à savoir* $\lambda_{\pm 4}$, *avec une partie réelle positive (voir les points solides). On observe une évolution spatio-temporelle des solutions en* $(b)$. *La simulation montre que le noyau bimodal peut également conduire à l'instabilité.*

## 1.2 Comportement asymptotique d'un système d'advection non-local à deux populations

Le Chapitre 2 est inspiré de l'article de Ducrot et Magal [39] où les auteurs traitent du comportement asymptotique d'une équation de réaction-diffusion à une seule espèce avec advection non-locale. Dans le Chapitre 2, nous développons un modèle d'advection non-locale pour deux populations avec conditions aux bords périodiques :

$$\begin{cases} \partial_t u_1(t,x) + \operatorname{div}\big(u_1(t,x)\mathbf{v}(t,x)\big) = u_1(t,x)h_1(u_1(t,x), u_2(t,x)), \\ \partial_t u_2(t,x) + \operatorname{div}\big(u_2(t,x)\mathbf{v}(t,x)\big) = u_2(t,x)h_2(u_1(t,x), u_2(t,x)), \end{cases} \quad t > 0,\ x \in \mathbb{R}^N, \quad (1.5)$$

où le champ de vitesse $\mathbf{v} = -\nabla P$ est établi grâce à la pression

$$P(t,x) := \left(K \circ (u_1 + u_2)(t,.)\right)(x), \quad (1.6)$$

et où $K \circ u$ est défini dans (1.3). Nous supposons que le noyau $K : \mathbb{R}^N \to \mathbb{R}$ est une fonction $\mathbb{T}^N$–périodique de classe $C^m$ sur $\mathbb{R}^N$ pour un entier $m \geq \frac{N+5}{2}$.

Notre motivation pour ce problème vient des expérimentations biologiques pour deux types de cellules avec co-culture monocouche. On peut trouver un exemple d'une telle co-culture dans [88, Figure 1]. Les cellules grandissent et forment des îlots séparés après 7 jours. D'un point de vue plus générale, notre étude est reliée à la ségrégation cellulaire

ainsi qu'à la formation de frontières. Taylor et al. [99] ont conclu que la répulsion hétéro-typique et la cohésion homo-typique peuvent expliquer la ségrégation cellulaire ainsi que la formation de frontières. Nous renvoyons également les lecteurs à Dahmann et al. [34] et aux références qui s'y trouvent pour en savoir plus sur la formation de frontières avec son application en biologie.

La première partie du Chapitre 2 est consacrée à l'existence et l'unicité des solutions et des propriétés de semi-flot associées. Nous utilisons ici la notion de solution intégrée le long des caractéristiques, brièvement expliquée ci-dessous, pour prouver la propriété de ségrégation des solutions. Afin de pallier au manque de compacité de l'orbite positive, nous utilisons la *convergence étroite* dans l'espace des mesures de Young, ce qui nous permet d'obtenir une description du comportement asymptotique des solutions. Nous présentons également quelques simulations numériques, qui vérifient nos résultats théoriques.

Nous précisons la notion de solution. Soit $C^k_{per}\left(\mathbb{R}^N\right)$ l'espace de Banach des fonctions $[0,2\pi]^N$–periodiques de classe $C^k$ de $\mathbb{R}^N$ dans $\mathbb{R}^N$ muni de la norme de la convergence uniforme

$$\|\varphi\|_{C^k} = \sum_{j=0}^{k} \sup_{x\in\mathbb{R}^N} \left|D^j\varphi(x)\right|.$$

Pour chaque $p \in [1,+\infty]$, nous notons $L^p_{per}\left(\mathbb{R}^N\right)$ l'espace des fonctions mesurables et $[0,2\pi]^N$–périodiques de $\mathbb{R}^N$ dans $\mathbb{R}$ telles que

$$\|\varphi\|_{L^p} := \|\varphi\|_{L^p\left((0,2\pi)^N\right)} < +\infty.$$

Ainsi $L^p_{per}\left(\mathbb{R}^N\right)$ muni de la norme $\|\varphi\|_{L^p}$ est un espace Banach. Nous définissons également son cône positif $L^p_{per,+}\left(\mathbb{R}^N\right)$ qui se compose des fonctions en $L^p_{per}\left(\mathbb{R}^N\right)$ qui sont positives presque partout.

Supposons que la solution

$$\mathbf{u} = (u_1,u_2) \in C^1\left([0,\tau]\times\mathbb{R}^N,\mathbb{R}\right)^2 \cap C\left([0,\tau], C^0_{per,+}(\mathbb{R}^N)\right)^2$$

soit une solution classique de (1.5)-(1.6). Nous considérons la solution avec chaque composante $u_i(t,\cdot)$ le long de la courbe caractéristique $\Pi_{\mathbf{v}}(t,0;x)$ respectivement, où les caractéristiques sont solutions d'EDO suivante

$$\begin{cases} \partial_t\Pi_{\mathbf{v}}(t,s;z) = \mathbf{v}(t,\Pi_{\mathbf{v}}(t,s;z)), \text{ pour tout } t,s\in[0,\tau], \\ \Pi_{\mathbf{v}}(s,s;z) = z. \end{cases}$$

On en déduit que pour $i=1,2$,

$$\begin{aligned} \frac{\mathrm{d}}{\mathrm{d}t}\Big(u_i(t,\Pi_{\mathbf{v}}(t,0;z)\Big) &= \partial_t u_i(t,\Pi_{\mathbf{v}}(t,0;z)) + \nabla u_i(t,\Pi_{\mathbf{v}}(t,0;z))\cdot\mathbf{v}(t,\Pi_{\mathbf{v}}(t,0;z)) \\ &= -\mathrm{div}\big(u_1(t,\Pi_{\mathbf{v}}(t,0;z))\mathbf{v}(t,\Pi_{\mathbf{v}}(t,0;z))\big) \\ &\quad + u_i(t,\Pi_{\mathbf{v}}(t,0;z))h_i(u_1(t,\Pi_{\mathbf{v}}(t,0;z)),u_2(t,\Pi_{\mathbf{v}}(t,0;z))) \\ &\quad + \nabla u_i(t,\Pi_{\mathbf{v}}(t,0;z))\cdot\mathbf{v}(t,\Pi_{\mathbf{v}}(t,0;z)) \\ &= u_i(t,\Pi_{\mathbf{v}}(t,0;z))\Big[-\mathrm{div}\,\mathbf{v}(t,\Pi_{\mathbf{v}}(t,0;z)) + h_i(\mathbf{u}(t,\Pi_{\mathbf{v}}(t,0;z))\Big], \end{aligned}$$

où $h_i(\mathbf{u}(t,\Pi_{\mathbf{v}}(t,0;z)) = h_i(u_1(t,\Pi_{\mathbf{v}}(t,0;z),u_2(t,\Pi_{\mathbf{v}}(t,0;z))$. Par conséquent, une solution classique de (1.5)-(1.6) (i.e. de classe $C^1$ en temps et en espace) doit satisfaire

$$u_i(t,\Pi_{\mathbf{v}}(t,0;z)) = \exp\left(\int_0^t h_i\big(\mathbf{u}(l,\Pi_{\mathbf{v}}(l,0;z)) - \operatorname{div}\mathbf{v}(l,\Pi_{\mathbf{v}}(l,0;z))dl\right) u_i\left(0,z\right), i=1,2,$$

ou de manière équivalente

$$u_i(t,z) = \exp\left(\int_0^t h_i\big(\mathbf{u}(l,\Pi_{\mathbf{v}}(l,t;z))\big) - \operatorname{div}\mathbf{v}(l,\Pi_{\mathbf{v}}(l,t;z))dl\right) u_i\left(0,\Pi_{\mathbf{v}}(0,t;z)\right), i=1,2, \tag{1.7}$$

avec

$$\mathbf{v}(t,x) = -\frac{1}{|\mathbb{T}^N|}\int_{\mathbb{T}^N} \nabla K(x-y)(u_1+u_2)(t,y)\mathrm{d}y. \tag{1.8}$$

Les calculs ci-dessus nous amènent à la définition suivante d'une solution.

**Définition 1.1** (Solution intégrée le long des caractéristiques)**.** *Soient* $\mathbf{u}_0 \in L^\infty_{per,+}\left(\mathbb{R}^N\right)^2$ *et* $\tau > 0$. *Une fonction* $\mathbf{u} \in C\left([0,\tau], L^1_{per,+}\left(\mathbb{R}^N\right)\right)^2 \cap L^\infty\left((0,\tau), L^\infty_{per,+}\left(\mathbb{R}^N\right)\right)^2$ *est considérée comme une solution intégrée le long des caractéristiques de* (1.5)-(1.6)*, si* $u_i, i=1,2$ *et* $\mathbf{v}$ *vérifient le système* (1.7)-(1.8).

En résumé, nous pouvons montrer que pour chaque valeur initiale $\mathbf{u}_0$ périodique et bornée, le système (1.5)-(1.6) admet une unique solution intégrée le long des caractéristiques. De plus, le semiflot $\{U(t)\}_{t\geq 0}$ défini par

$$(U(t)\mathbf{u}_0)(x) := \mathbf{u}(t,x) = (u_1(t,x),u_2(t,x)),\ \forall t \geq 0,$$

est continu sur $L^1_{per,+}\times L^1_{per,+}$ et possède les propriétés suivantes

1. toute solution partant d'une condition initiale positive reste positive ;
2. la solution est globale, i.e. $\sup_{t\in[0,\tau]}\|\mathbf{u}(t,\cdot)\|_\infty \leq M(\tau)\|\mathbf{u}_0\|_\infty$ ;
3. si l'on part d'une condition initiale régulière, alors la solution est une solution classique ;
4. loi de conservation : pour tout $A \in \mathcal{B}(\mathbb{T}^N)$

$$\int_{\Pi_{\mathbf{v}}(t,s;A)} u_i(t,x)\mathrm{d}x = \int_A \exp\left[\int_s^t h_i\left(\mathbf{u}\left(l,\Pi_{\mathbf{v}}(l,s;x)\right)\right)\mathrm{d}l\right] u_i(s,x)\mathrm{d}x.$$

Nous pouvons également prouver que les solutions préservent la propriété de ségrégation.

**Théorème 1.1.** *Soit* $\mathbf{u} = \mathbf{u}(t,x)$ *la solution de* (1.5)-(1.6)*. Pour toute condition initiale satisfaisant* $u_1(0,x)u_2(0,x) = 0$ *pour tout* $x \in \mathbb{T}^N$*. Alors* $u_1(t,x)u_2(t,x) = 0$ *pour tout* $t > 0$ *et* $x \in \mathbb{T}^N$.

Nous illustrons la propriété de ségrégation et le comportement asymptotique des solutions par les simulations suivantes.

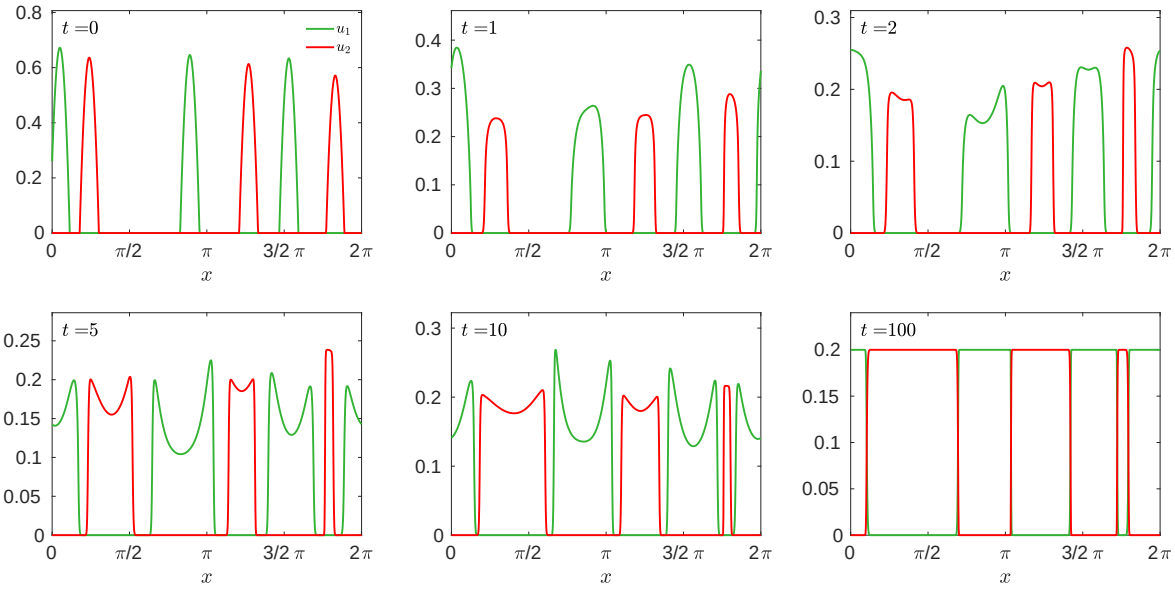


Figure 3: *Les courbes vertes représentent l'espèce $u_1$ et les courbes rouges représentent l'espèce $u_2$. Si les distributions initiales sont séparées pour les deux populations, nous constatons la coexistence des deux espèces et la propriété de ségrégation. Après $t = 100$, la distribution spatiale des deux espèces reste les mêmes.*

## 1.3 Un modèle de répulsion cellulaire par une équation de Keller-Segel hyperbolique

Dans le Chapitre 3, nous proposons un modèle de Keller-Segel hyperbolique à deux populations pour étudier le phénomène de ségrégation dans les expérimentations de co-culture cellulaire (voir (1.9) pour le modèle).

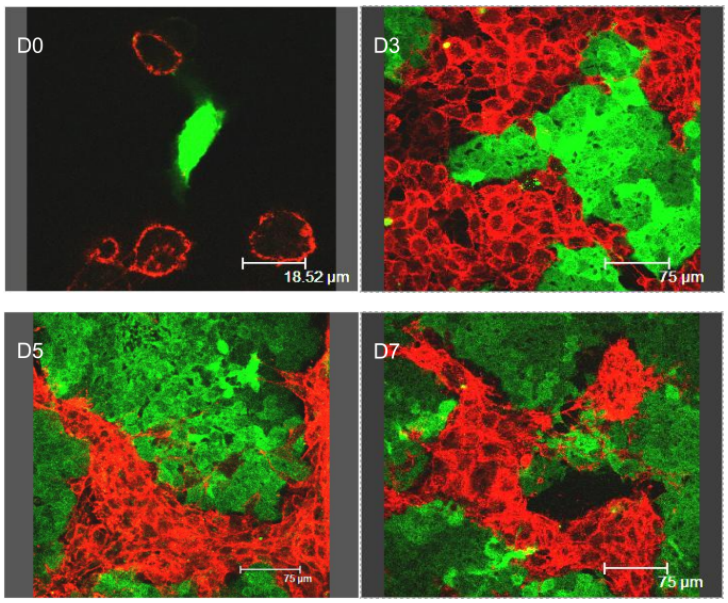


Figure 4: *Immunodétection directe des transferts P-gp dans des co-cultures de variantes sensibles (MCF-7) et résistantes (MCF-7/Doxo) des cellules cancéreuses du sein humain.*

La propriété de ségrégation spatiale entre deux types de cellules a été observée par Pasquier et al. [88]. Ils ont étudié le transfert de protéines entre deux types de cellules cancéreuses du sein humain, à savoir les cellules MCF-7 et MCF-7/Doxo. Au cours d'une co-culture cellulaire de 7 jours, la compétition spatiale a été observée entre ces deux types de cellules et une frontière nette a été établie entre eux (voir Figure 4). Une propriété de ségrégation similaire a également été trouvée dans le motif en mosaïque entre les nécroses et les cadhérines dans les expérimentations de Katsunuma et al. [64].

Nous étudions un modèle de deux espèces sur le disque ouvert unitaire $\Omega \subset \mathbb{R}^2$

$$\begin{cases} \partial_t u_1(t,x) - d_1 \operatorname{div}\big(u_1(t,x)\nabla P(t,x)\big) = u_1(t,x)h_1((u_1,u_2)(t,x)), & \\ \partial_t u_2(t,x) - d_2 \operatorname{div}\big(u_2(t,x)\nabla P(t,x)\big) = u_2(t,x)h_2((u_1,u_2)(t,x)), & (t,x) \in [0,T]\times\Omega \\ \big(I-\chi\Delta\big)P(t,x) = u_1(t,x)+u_2(t,x), & \\ \nabla P(t,x)\cdot\nu(x) = 0, & (t,x)\in[0,T)\times\partial\Omega, \end{cases} \tag{1.9}$$

où $\nu$ est le vecteur normal sortant, $d_i$ est le coefficient de dispersion, $\chi$ est le coefficient de détection. La fonction $h_i$ est de forme

$$h_i(u_1,u_2) = b_i - \delta_i - \sum_{j=1}^{2} a_{ij}u_j, \quad i=1,2,$$

où $b_i > 0$, $i = 1,2$ sont les taux de croissance, $a_{ij} \geq 0$, $i \neq j$ représentent la concurrence mutuelle entre les espèces, $a_{ii}$ est la concurrence au sein d'une même espèce et $\delta_i$ est le taux de mortalité supplémentaire causé par le traitement. Le système (1.9) est complété par la distribution initiale

$$\mathbf{u}_0(\cdot) := (u_1(0,\cdot), u_2(0,\cdot)) \in C^1(\overline{\Omega})^2.$$

Nous considérons un domaine borné bidimensionnel (une boîte de pétri circulaire). Avec la notion de solutions intégrées le long des caractéristiques, nous prouvons l'existence et l'unicité des solutions ainsi que la propriété de ségrégation des deux espèces. Grâce à la condition aux bords appropriée pour l'équation de pression, nous en déduisons que les caractéristiques restent dans le domaine pour tout $t > 0$. La positivité des solutions, la propriété de ségrégation et la loi de conservation sont également déduites pour le modèle (1.9).

Selon [89], les cellules MCF-7 et MCF-7/Doxo sont cultivées séparément avec un nombre initiale de cellules de $10^5$ dans la boîte de pétri de $60 \times 15$ mm avec ou sans le traitement de la doxorubicine.

En utilisant le modèle homogène en espace et les données de croissance cellulaire dans les expérimentations de [89], nous estimons les paramètres $b_i$, $\mu_i$ et $\delta_i$, $i = 1,2$. De plus, nous approchons notre modèle d'EDP avec la méthode des volumes finis pour estimer les paramètres $\chi$ et les coefficients de dispersion $d_i, i = 1,2$.

D'un point de vue numérique, on peut également observer que le modèle admet un principe d'exclusion (les résultats sont différents du modèle d'EDO). Plus important encore, notre modèle montre que la complexité de la distribution cellulaire de co-culture à court terme (6 jours) dépend de la distribution initiale de chaque espèce. Grâce à des

simulations numériques, l'impact de la distribution initiale sur le ratio des populations se situe dans le nombre total initial de cellules et non pas dans la loi de la distribution initiale. Nous constatons également qu'un taux de dispersion rapide donne un avantage à court terme tandis que la dynamique vitale contribue à un avantage à long terme pour la population.

La Figure 5 présente une simulation numérique réalisée du jour 0 au jour 6. Nous traçons également les proportions de chaque type de cellules (voir Figure 5 (f)). La proportion de cellules de l'espèce $i$ est donnée par

$$\frac{U_i(t)}{U_1(t)+U_2(t)} \quad \text{où} \quad U_i(t) := \int_\Omega u_i(t,x)\mathrm{d}x,\ i=1,2.$$

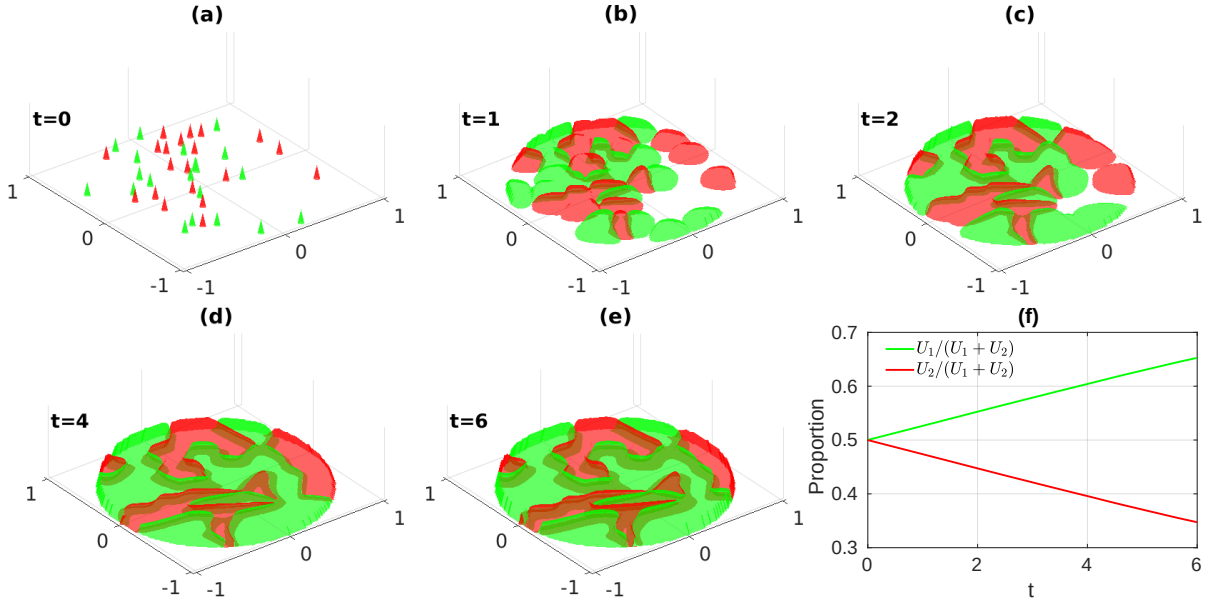


Figure 5: *Évolution spatio-temporelle des deux espèces $u_1$ et $u_2$ et de leurs proportions relatives. Les figures (a)-(e) correspondent à l'évolution de la croissance cellulaire du jour 0 au jour 6 et la figure (f) représente l'évolution des proportions. La distribution initiale suit la distribution uniforme sur un disque avec 20 clusters de cellules initiaux. Le nombre initial de cellules est $U_1 = U_2 = 0,01$ pour chaque espèce et les cellules sont équitablement réparties dans chaque cluster.*

# Introduction

*"C'est avec l'intuition qu'on trouve, c'est avec la logique qu'on prouve." — Henri Poincaré*

Henry Darcy, French engineer born in Dijon, made major contributions to open channel flow research and developed *Darcy's Law* for flow in porous media. His Law is a foundation stone for several fields of study including ground-water hydrology, soil physics, and petroleum engineering. He and his precursor Henri Navier who was also born in Dijon became two of the founders of the science of fluid mechanics.

The idea of generalizing Darcy's law to a nonlocal pressure is relatively recent. As pointed out by Delgoshaie and his collaborators [36] multiscale pathways in porous media can lead to a nonlocal flow model whereby the flow rate at a given point is related to the integral of the pressure difference between that point and every other point in the domain multiplied by a conductivity kernel. We cite the works [33, 34, 62, 93] for nonlocal versions of Darcy's law applied in hydrology. Such nonlocal interactions can also be applied in population dynamics [3, 26, 38, 39, 42, 75]. Over the past couple of decades, a large amount of literature has been devoted to the mathematical modeling of self-organizing populations, based on the concepts of short-range, long-range interactions among different individuals.

The main objective of this thesis is to study the interactions in multi-species cell co-culture. Such interactions can include cell-cell attraction, repulsion, and segregation, leading to pattern formation. We choose a class of reaction-diffusion equations with nonlocal advection. In the first part of the thesis (Chapter 1 and 2), we mainly develop the theoretical framework of these models, namely the well-posedness in both single-species and multi-species cases. Furthermore, we discuss the Turing and Turing-Hopf bifurcations and the asymptotic behavior of solutions.

As far as the second half of this thesis is concerned, we are interested in applying our models to a real-life cell co-culturing experiment. Here we choose a hyperbolic Keller-Segel model, which can be regarded as a variation of the nonlocal model. We also establish theoretical results. Moreover, by analyzing the experimental data, we simulate a 6-day cell growth in a petri dish and discuss the impact of both the segregation property and initial distributions on the population proportions.

# 1 Outline of the thesis

The outline is followed by the modeling part of a nonlinear and nonlocal diffusion equation. Starting from an individual-based model (IBM) with random perturbation, we illustrate the convergence of an IBM to a nonlinear and nonlocal (continuum) equation when the number of particles tends to infinity. After having obtained a general form of the nonlinear and nonlocal diffusion equation, we list a few models that are intimately related to the models studied in this thesis. Furthermore, we resume some previous related works done by other authors. At the end of the Introduction, we present an overview of three different problems treated in this thesis.

Chapter 1 deals with a single-species reaction-diffusion equation with nonlocal advection in the one-dimensional case. We study the well-posedness of the model and investigate the stability and bifurcation properties of the positive interior equilibrium for such an equation. We show that a single scalar equation may display Turing and Turing-Hopf bifurcations with the dominant wavenumber as large as we want. Moreover, similar instabilities exist with a bi-modal kernel. Numerical simulations also confirm the resulting complex spatio-temporal dynamics. This work is from Ducrot, Fu and Magal [40].

In Chapter 2, we consider a nonlocal advection model without the viscosity term for two populations. The first part of the chapter is devoted to the existence and uniqueness of solutions and the associated semi-flow properties. Using the solution integrated along the characteristics, we can prove the segregation property of solutions. To resolve the lack of compactness of the positive orbit, we employ the narrow convergence in the space of Young measures. We also present some numerical simulations, which confirm and complement our theoretical results. This work is from Fu and Magal [48].

In Chapter 3, we propose a two-population hyperbolic Keller-Segel model to study the segregation phenomenon in cell co-culture experiments. We first prove the well-posedness of the model and the segregation property. From a numerical perspective, we can observe that the model admits a competitive exclusion principle (the results are different from the corresponding ODE model). More importantly, our model shows the complexity of the cell distribution depending on the initial values. This work is from Fu and Magal [49].

After that, the main contributions of this thesis are presented as part of the Conclusion, followed by a detailed list of research perspectives. Finally, the Appendix contains some proofs and numerical methods omitted in Chapters 1–3.

# 2 Modeling of a nonlocal and nonlinear diffusion

A classical widespread approach of modeling population dynamics with spatial movement is based on PDE's [60, 75, 80, 81, 83]. The motion of individuals has been described by relevant quantities such as scalar or vector fields. Such kind of models are often called Eulerian models; they describe the evolution of population densities. They are typically (deterministic) nonlinear partial differential equations of the advection-reaction-diffusion type

$$\partial_t u(t,x) + \operatorname{div}\left(u(t,x)\mathbf{v}(t,x)\right) = D\Delta u(t,x) + f(u(t,x)),\ t>0,\ x\in\Omega\subset\mathbb{R}^N, \tag{2.1}$$

where $u$ is the population density, $\mathbf{v}$ is the velocity field and $f(u)$ is a possible additive reaction term which may include birth and death processes. The advection term may describe the interaction mechanisms among individuals (via the velocity $\mathbf{v}$), while the non-advective (diffusive) flux takes into account the spatial spread of the population.

Let us omit, for the moment, the cell dynamics of the population, that is $f(u) \equiv 0$. Suppose the velocity field is composed of two types of interactions in different scales, namely the long-range attractions in *macroscale* and the short-range repulsion in *mesoscale* which comes from the moderate interactions of the particles.

We give a brief description of such an individual-based approximation (*Lagrangian models*). Let us consider $n$ particles interacting in $\mathbb{R}^N$. We denote the spatial location of each particle as $X_k^n(t) \in \mathbb{R}^N$. We assume the position of the $k$–th particle, $X_k^n(t)$, is subject to the specific forces of interaction. Then the law of motion reads

$$\frac{\mathrm{d}X_k^n(t)}{\mathrm{d}t} = h_k^n(X_1^n, \ldots, X_n^n, t), \quad k = 1, \ldots, n, \tag{2.2}$$

Assume individuals interact through a potential $V^n : \mathbb{R}^N \to \mathbb{R}$ (which may include both the attraction and repulsion) and the potential $V^n$ is not subject to a underlying field (i.e., independent of $t$), thus we can suppose that $h_k^n$ follows the form

$$h_k^n(X_1^n, \ldots, X_n^n, t) = \frac{1}{n} \sum_{m=1, m\neq k}^{n} \nabla V^n(X_k^n(t) - X_m^n(t)).$$

If one denotes the empirical measure $\frac{1}{n}\sum_{k=1}^n \delta_{X_k^n(t)}$ as follows

$$\mu_n(t) := \frac{1}{n} \sum_{k=1}^{n} \delta_{X_k^n(t)},$$

where for any measurable set $B \in \mathcal{M}(\mathbb{R}^N)$, $\delta$ is the singular measure defined as follows

$$\delta_{X_k^n(t)}(B) = \begin{cases} 1, & \text{if } X_k^n(t) \in B, \\ 0, & \text{if } X_k^n(t) \notin B. \end{cases}$$

We have

$$\mu_n(t)(B) = \frac{1}{n} \sum_{k=1}^{n} \delta_{X_k^n(t)}(B) = \frac{\#\text{ particles in B at time t}}{n}.$$

By introducing the empirical measure $\mu_n(t)$, we can rewrite the drift term $h_k^n$ as a convolution

$$\begin{aligned} h_k^n(X_1^n, \ldots, X_n^n, t) &= \frac{1}{n} \sum_{m=1, m\neq k}^{n} \nabla V^n(X_k^n(t) - X_m^n(t)) \\ &= \left[\nabla V^n * \mu_n(t)\right](X_k^n(t)). \end{aligned}$$

We express our modeling assumptions by introducing in $V^n$ two additive components : $V_1^n$, responsible of aggregation, and $V_2^n$, responsible of repulsion, such that

$$V^n = V_1^n - V_2^n,$$

where the positive (resp. negative) sign represents a force of attraction (resp. repulsion). Now we rewrite Equation (2.2) as

$$\frac{\mathrm{d}X_k^n(t)}{\mathrm{d}t} = \Big( [\nabla V_1^n * \mu_n(t)]\,(X_k^n(t)) - [\nabla V_2^n * \mu_n(t)]\,(X_k^n(t)) \Big), \quad k = 1, \dots, n. \tag{2.3}$$

We assume that each potential $V_i^n, i = 1, 2$ satisfies the following scaling property

$$V_i^n(x) = n^\beta V_i\left(n^{\frac{\beta}{N}} x\right), \quad i = 1, 2,$$

for some $\beta \in [0, 1]$ and where $V_i$ is a fixed potential. Using this framework, the scaling with $\beta = 0$ (resp. $\beta \in (0, 1)$, resp. $\beta = 1$) corresponds to the so-called *Mckean-Vlasov* (macroscale) limit (resp. mesoscale limit, resp. hydrodynamics limit) (see Oelschläger [85]). Roughly speaking, in one space dimension $N = 1$, the characteristic length between particles corresponds to order $\mathcal{O}(n^{-1})$, while the characteristic length of interaction induced by the potential $V_n$ corresponds to order $\mathcal{O}(n^{-\beta})$. The Mckean-Vlasov framework, namely, $\beta = 0$, corresponds to order $\mathcal{O}(1)$ length of interaction, that is, long range interactions.

We assume that the aggregation and repulsion coexist but act at different scales: the potential $V_1$ satisfies the Vlasov framework ($\beta = 0$), implying the long-range attraction while $V_2$ satisfies the mesoscale framework, implying the short-range repulsion. In fact, in order to obtain the limiting reaction-diffusion equation with nonlocal advection, we need to assume that particles are subject to a random dispersal described by the Brownian motion $\{W_k\}_{k=1}^n$ (a family of independent standard Wiener processes), we rewrite (2.3) as

$$\mathrm{d}X_k^n(t) = \Big( [\nabla V_1^n * \mu_n(t)]\,(X_k^n(t)) - [\nabla V_2^n * \mu_n(t)]\,(X_k^n(t)) \Big)\mathrm{d}t + \sigma_n \mathrm{d}W_k(t), \quad k = 1, \dots, n. \tag{2.4}$$

where $\sigma_n$ defined as the coefficients for the intrinsic stochasticity.

Using the above particle interaction modeling, the corresponding macroscopic law of motion is obtained by investigating the convergence $n \to \infty$ of the empirical measure $\{\mu_n(t)\}_{t\in\mathbb{R}_+}$. Suppose that indeed the empirical $\{\mu_n(t)\}_{t\in\mathbb{R}_+}$ converges, as $n \to \infty$ to a deterministic process $\{\mu(t)\}_{t\in\mathbb{R}_+}$ and furthermore it admits a density $u(t, x)$ with respect to the Lebesgue measure on $\mathbb{R}^N$, such that

$$\begin{aligned} \lim_{n\to\infty} \langle \mu_n(t), \phi(t, \cdot)\rangle &= \langle \mu(t), \phi(t, \cdot)\rangle \\ &= \int_{\mathbb{R}^N} \phi(t, x) u(t, x) \mathrm{d}x, \quad \forall \phi \in C^{1,2}(\mathbb{R}_+ \times \mathbb{R}^N). \end{aligned}$$

Then a formal derivation (see, for example, [77]) of the continuum model from the stochastic system (2.4) can be obtained, that is

$$\begin{aligned} \partial_t u(t, x) &= D\Delta u(t, x) + \mathrm{div}\Big( u(t, x)\nabla u(t, x) - u(t, x)\big[\nabla V_1 * u(t, \cdot)\big](x) \Big) \\ &= D\Delta u(t, x) - \mathrm{div}(u(t, x)\mathbf{v}(t, x)), \quad x \in \mathbb{R}^N, t \geq 0, \\ u(0, x) &= u_0(x), \quad x \in \mathbb{R}^N, \end{aligned} \tag{2.5}$$

where $\mathbf{v}(t, x) := -\nabla u(t, x) + \big[\nabla V_1 * u(t, \cdot)\big](x)$ and $D := \lim_{n\to\infty} \sigma_n/2$ with $\sigma_n$ defined as the mean free path in (2.4). Here we assume that the mean free path of each particle may reduce up to a limiting value that may be zero as the number of particles increases.

**Remark 2.1.** *Here we need to mention that the choice of kernel $V_2$ is critical for the convergence to the nonlinear diffusion* $\operatorname{div}\big(u(t,x)\nabla u(t,x)\big)$ *in the limiting equation (2.5). To simply assume that $V_2$ is symmetric and smooth is not sufficient (see Chapter 1, Figure 1.7 for an illustration), in fact, in order to ensure the interaction of particles is purely repulsive, we give a sufficient condition on the sign of the Fourier coefficients of $V_2$ which will be detailed both analytically and numerically later in Chapter 1.*

A rigorous proof of the convergence of the stochastic evolution system (2.4) for the mean-valued empirical process $\{\mu_n(t)\}_{t\in\mathbb{R}_+}$ to the evolution equation (2.5) for the spatial density of the deterministic mean-valued process $\{\mu(t)\}_{t\in\mathbb{R}_+}$ is presented in the work of Oelschläger [84, 85], Morale, Capasso, and Oelschläger [77], Capasso and Morale [24] and Bodnar and Velazquez [17]. For the comparison of individual-based model with continuum model in this nonlocal diffusion context, we refer to Byrne and Drasdo [20], Motsch and Peurichard [78].

## 2.1 Single species model

Below we focus on several single-species models which are closely related to the problems discussed in this thesis. We always suppose $(t,x) \in \mathbb{R}_+ \times \Omega$ with $\Omega$ as an open set (bounded or unbounded) in $\mathbb{R}^N$.

*The nonlocal model*

We first give the nonlocal reaction-diffusion-advection model as follows

$$u_t + \operatorname{div}(u\nabla(\rho * u)) = D\Delta u + f(u), \tag{M1}$$

where $(\rho * u)(t,x) = \int_{\mathbb{R}^N} \rho(x-y)u(t,y)\mathrm{d}y$ represents the long-range interactions between individuals, $D$ is the linear diffusion coefficient and the nonlinear function $f(u)$ represents the vital dynamics of the population. We emphasize the generality included in the choice kernel. In fact, based on the choice of the kernel $\rho$, it can include a force of attraction/repulsion with finite/infinite range of sensing radius (with compact/non-compact supported kernels), symmetry/asymmetry, etc. Moreover, if the domain $\Omega \subset \mathbb{R}^N$ is bounded, for some $T > 0$, one often considers the non-flux boundary condition

$$(-D\nabla u + u\nabla(\rho * u)) \cdot \nu = 0, \quad (t,x) \text{ on } (0,T] \times \partial\Omega,$$

where $\nu$ is the normal outward vector.

*The Keller-Segel model*

Another model that has been widely studied to describe the attraction and the repulsion of populations is known as *chemotaxis* (Keller-Segel model). Here we only present a prototype of Keller-Segel model with cell dynamics represented by a function $f$

$$\begin{aligned} u_t + \operatorname{div}(u\mathbf{v}) &= D\Delta u + f(u), \\ \mathbf{v} &= \pm\nabla P, \\ \varepsilon\partial_t P &= \Delta P + u - P. \end{aligned} \tag{M2}$$

Here the velocity field $\mathbf{v}$ is the proportional to the gradient of the concentration of the chemical signal $P$. The positive sign in front of $\nabla P$ represents chemoattractant interaction

while the negative sign represents chemorepellent interaction. The scaling coefficient $\varepsilon$ represents the different time scale between the dynamics of the chemotaxis compared to the evolution of the cell dynamics. When the domain $\Omega \subset \mathbb{R}^N$ is bounded, for some $T > 0$, the non-flux boundary condition reads

$$\begin{aligned} (-D\nabla u + u\,\mathbf{v}) \cdot \nu &= 0, \\ \nabla P \cdot \nu &= 0, \end{aligned} \quad (t, x) \text{ on } (0, T] \times \partial\Omega,$$

where $\nu$ is the normal outward vector.

*The nonlinear model*

As we pointed out, under the mesoscale framework, one can deduce a nonlinear diffusion model. Here we give a more general version of the nonlinear diffusion model

$$u_t = D\Delta u^m + f(u), \tag{M3}$$

where $m \geq 1$ and $m - 1$ is the so-called *polytropic exponent* following from the Darcy's law. This equation is known as the *porous medium equation* which describes the flow of an ideal gas through a homogeneous porous medium.

*The nonlinear and nonlocal model*

In a complex dynamical system, a multiple scale approach is often adopted as in the modeling of Equation (2.5). Here we study two versions of nonlinear and nonlocal models,

$$u_t + \operatorname{div}(u\nabla(\rho * u)) = D\Delta u^m. \tag{M4a}$$

As we have mentioned, Model (M4a) is composed of long-range interaction, as measured by $\operatorname{div}(u\nabla(\rho * u))$ and short-range repulsion, as measured by $D\Delta u^m$. Here we set $f \equiv 0$, in such scenario, the model is better studied in an analytical point of view. We also present the following general nonlinear-nonlocal model

$$u_t + \operatorname{div}(g_1(u)\nabla(\rho * g_2(u))) = \Delta A(u) + f(u), \tag{M4b}$$

where $g_1, g_2$ and $A$ are nonlinear functions. Such a model is widely used in studying the pattern formation arising from both attraction and repulsion.

## 2.2 Two species model

*The self-diffusion and cross-diffusion model*

It is worth mentioning a two-species version of nonlinear model (M3). The study of such a model dates back to 1970s by Shigesada et al. [95]

$$\begin{aligned} \partial_t u_1 &= \Delta\big(u_1\,(d_1 + a_{11}u_1 + a_{12}u_2)\,\big) + f_1(u_1, u_2), \\ \partial_t u_2 &= \Delta\big(u_1\,(d_2 + a_{21}u_1 + a_{22}u_2)\,\big) + f_2(u_1, u_2). \end{aligned} \tag{M5}$$

*The nonlocal and nonlinear model*

A two-species nonlocal and nonlinear model can be written as

$$\begin{aligned}\partial_t u_1 + \operatorname{div}(g_{11}(u_1,u_2)\nabla(\rho * g_{12}(u_1,u_2))) &= \Delta\big(u_1\,(d_1 + a_{11}u_1 + a_{12}u_2)\,\big) + f_1(u_1,u_2),\\ \partial_t u_2 + \operatorname{div}(g_{21}(u_1,u_2)\nabla(\rho * g_{22}(u_1,u_2))) &= \Delta\big(u_1\,(d_2 + a_{21}u_1 + a_{22}u_2)\,\big) + f_2(u_1,u_2).\end{aligned} \tag{M6}$$

Due to the complexity of the model, the results for such a model are mainly restricted to the numerical analysis.

# 3 Summary of the models

We briefly summarize the different single-species models in the previous section in the following form:

$$\begin{aligned}u_t(t,x) + \operatorname{div}(g(u(t,x))\mathbf{v}(t,x)) &= \Delta A(u(t,x)) + f(u(t,x)),\\ \mathbf{v}(t,x) &= \pm\nabla P(t,x),\end{aligned}$$

with $P$ satisfying one of the following forms

$$P(t,x) = \int_\Omega \rho(x-y)\phi(u(t,y))\mathrm{d}y, \tag{Nonlocal}$$

$$\varepsilon P_t(t,x) = \Delta P(t,x) + u(t,x) - P(t,x), \tag{Keller-Segel}$$

on the domain $\mathbb{R}_+ \times \Omega$ with prescribed initial data.

| Model | $A(u)$ | $\mathbf{v}$ | $g(u)$ | $f(u)$ | Boundary Condition | Ref. |
|---|---|---|---|---|---|---|
| (M1) | $Du$ | $\nabla\rho * u$ | $u$ | – | $\mathbb{R}^N$ | [10, 12, 13, 52, 75] |
| (M1) | – | $\nabla\rho * u$ | $u$ | ✓ | Periodic B.C. | [39, 48] |
| (M2)* | $Du$ | *Keller-Segel* | $u$ | ✓ | Non-flux B.C. | [21, 57, 61, 82, 90] |
| (M3) | $Du^m$ | – | – | ✓ | $\mathbb{R}^N$ | [5, 35, 37, 51, 104] |
| (M4a) | $Du^m$ | $\nabla\rho * u$ | $u$ | – | Non-flux B.C. | [7, 11] |
| (M4b) | $Du$ | $\nabla\rho * u$ | $u(1-u)$ | ✓ | Periodic B.C. | [3, 79] |
| (M4b) | $Du$ | $\nabla\rho * \phi(u)$ | $u$ | ✓ | Periodic B.C. | [26, 86] |

Table 1: *Summary of various cases for single-species model. In the table, the symbol "–" refers to the absence of the corresponding term while "✓" means that the model includes such a term. We only choose a very limited amount of references in the Ref. column. *For the Keller-Segel model, $P$ satisfies Equation* (Keller-Segel) *with scaling parameter $\varepsilon \geq 0$.*

Kawasaki [65] in 1980s studied the Model (M1) for the stability of the homogeneous steady state

$$u_t + \operatorname{div}(u\nabla(\rho * u)) = D\Delta u + f(u), \tag{M1}$$

Mogilner, Edelstein-Keshet in their work [75] used such a model to study the swarming behavior in the case when $f = 0$. In fact, they used $V * u$ instead of $\nabla(\rho * u)$ to represent the non-local interactions. Based on the same model, Bernoff, Topaz in their review paper [10] used the tools from the calculus of variations to study equilibria of the equation and their stability. Bertozzi et al. [12, 13] studied the finite time blowup of solutions and the well-posednees in $L^p$ theory when $D = 0$ and $f = 0$ in multidimensional space. Ducrot, Magal [39] and Fu, Magal [48] studied the asymptotic behavior of solutions in a periodic setting with the help of Young measures. Hamel and Henderson [52] investigated the existence of the traveling wave solution under a general assumption on the kernel with logistic source $f(u) = u(1 - u)$.

Our second model (M2) is known as chemotaxis (Keller-Segel) model.

$$\begin{aligned} u_t + \operatorname{div}(u\mathbf{v}) &= D\Delta u + f(u), \\ \mathbf{v} &= \pm\nabla P, \\ \varepsilon\partial_t P &= \Delta P + u - P. \end{aligned} \tag{M2}$$

Theoretical and mathematical modeling of chemotaxis began from the pioneering works of Patlak [87] in the 1950s and Keller and Segel [66] in the 1970s. It has become an important model in the description of tumor growth or embryonic development. We refer to the review papers of Horstmann [61] and Hillen, Painter [57] and Calvez, Dolak-Struß [21] for a detailed introduction about the Keller–Segel model. For the traveling wave solutions of Keller-Segel model, we refer to Nadin, Perthame, Ryzhik [82] and the references therein. For the case when the scaling parameter $\varepsilon = 0$ which is so-called hyperbolic Keller–Segel equation, we refer to the work of Perthame, Dalibard [90] and Calvez, Corrias and Ebde [22].

The monograph by Vázquez [104] is devoted to studying the nonlinear model (M3)

$$u_t = D\Delta u^m + f(u), \tag{M3}$$

Gurney and Nisbet [51] considered the model with a Malthusian instead of a Fisher-KPP growth term, that is

$$f(u) = u, \quad m = 2.$$

For the existence of wavefronts using phase-plane analysis, we refer readers to Atkinson et al. [5] and de Pablo and Vázquez [35]. For more recent work, we refer to Du et al. [37].

For Model (M4a), we have

$$u_t + \operatorname{div}(u\nabla(\rho * u)) = D\Delta u^m. \tag{M4a}$$

The well-posedness of the model has been considered by Bertozzi and Slepcev [11] and Bedrossian et al. [7] on a bounded domain $\Omega \subset \mathbb{R}^N$ with non-flux boundary condition.

The study of the two-species self/cross-diffusion model (M5) can date back to 1970s

$$\begin{aligned} \partial_t u_1 &= \Delta\big(u_1\left(d_1 + a_{11}u_1 + a_{12}u_2\right)\big) + f_1(u_1, u_2), \\ \partial_t u_2 &= \Delta\big(u_1\left(d_2 + a_{21}u_1 + a_{22}u_2\right)\big) + f_2(u_1, u_2). \end{aligned} \tag{M5}$$

In the work of Shigesada, Kawasaki and Teramoto [95], such a nonlinear two-species model was intended to study a *segregation property* of solutions which does not exist in single-species model. They found that the spatial segregation acts to stabilize the coexistence of

two similar species, relaxing the competition among different species. Lou and Ni [69, 70] generalized the model and studied the steady state problem for the self/cross-diffusion model. For the nonlinear diffusion model, Bertsch et al. [14] in their work proved the existence of segregated solutions when the reaction term is of Lotka-Volterra type. The same authors also studied the traveling wave solutions of this model [15].

Finally we discuss Model (M4b)

$$u_t + \operatorname{div}(g_1(u)\nabla(\rho * g_2(u))) = \Delta A(u) + f(u), \tag{M4b}$$

and its two-species version (M6)

$$\begin{aligned}\partial_t u_1 + \operatorname{div}(g_{11}(u_1,u_2)\nabla(\rho * g_{12}(u_1,u_2))) &= \Delta\big(u_1\left(d_1 + a_{11}u_1 + a_{12}u_2\right)\big) + f_1(u_1,u_2),\\ \partial_t u_2 + \operatorname{div}(g_{21}(u_1,u_2)\nabla(\rho * g_{22}(u_1,u_2))) &= \Delta\big(u_1\left(d_2 + a_{21}u_1 + a_{22}u_2\right)\big) + f_2(u_1,u_2).\end{aligned} \tag{M6}$$

Armstrong, Painter and Sherratt [3] in their early work proposed a model (APS model) under the principle of a local diffusion plus a nonlocal attraction driven by adhesion forces to describe the phenomenon of cell mixing, full/partial engulfment and complete sorting in the cell sorting problem. Based on the APS model, Murakawa and Togashi [79] thought that the population pressure should come from the cell volume size instead of the linear diffusion. Therefore, they changed the linear diffusion term into a nonlinear diffusion in order to capture the sharp fronts and the segregation in cell co-culture. Carrillo et al. [26] recently proposed a new assumption on the adhesion velocity field and their model showed a good agreement with the experiments in the work of Katsunuma et al. [64]. The idea of long-range attraction and short-range repulsion can also be seen in the work of Leverentz, Topaz and Bernoff [68]. They considered a nonlocal advection model to study the asymptotic behavior of the solution. By choosing a Morse-type kernel which follows the attractive-repulsive interactions, they found that the solution can asymptotically spread, contract (blow-up), or reach a steady-state. Burger, Fetecau and Huang [19] considered a similar nonlocal adhesion model with nonlinear diffusion, they studied the well-posedness of the model and proved the existence of a compactly supported, non-constant steady state. Dyson et al. [42] established the local existence of a classical solution for a nonlocal cell-cell adhesion model in spaces of uniformly continuous functions. We also refer the readers to Mogliner et al. [76], Eftimie et al. [43] and Carillo et al. [25] for more topics about nonlocal advection equations. For the derivation of such models, we refer readers to the work of Bellomo et al. [8] and Morale, Capasso and Oelschläger [77].

We list a few models mentioned in the references above. For the sake of simplicity, we only mention the single-species model (M4b) when $A(u) = u^m$ and its two-species version (M6) is similar. Armstrong, Painter and Sherratt [3] considered the case when

$$g_1(u) = u, \quad g_2(u) = u(1-u), \quad f(u) = u(1-u), \quad m = 1,$$

Painter et al. [86] consider the case when

$$g_1(u) = u(1-u), \quad g_2(u) = u, \quad f(u) = u(1-u), \quad m = 1$$

Murakawa and Togashi [79] consider the case when

$$g_1(u) = u, \quad g_2(u) = u(1-u), \quad f(u) = u(1-u), \quad m = 2$$

Carrillo et al. [26] studied the case when

$$g_1(u) = u(1-u), \quad g_2(u) = u, \quad f(u) = u(1-u), \quad m = 2$$

In Table 1 and the references mentioned above, we only list a limited amount of references. For more detailed references, we refer readers to the introduction of each Chapter and the references therein.

# 4 Overview of the thesis

This thesis deals with two types of reaction-diffusion equation with nonlinear and nonlocal advection. Let us first consider the single-species equation

$$\partial_t u(t,x) + \operatorname{div}\left(u(t,x)\mathbf{v}(t,x)\right) = D\Delta u(t,x) + f(u(t,x)),\ t>0,\ x\in\Omega\subset\mathbb{R}^N. \tag{4.1}$$

Here $D \geq 0$ denotes the viscosity parameter. The divergence, gradient and Laplacian are taken with respect to $x$. The velocity field $\mathbf{v}$ is derived from the pressure $P$, where

$$\mathbf{v}(t,x) = -\nabla P(t,x). \tag{4.2}$$

**Case 1:** We consider solutions of Equation (4.1) which are **periodic in space**. Here a function $u(t,x)$ is said to be $2\pi$**-periodic in each direction** (or for simplicity **periodic**) if

$$u(t,x+2k\pi) = u(t,x),\ \forall k\in\mathbb{Z}^N, x\in\mathbb{R}^N.$$

In the nonlocal case, the pressure $P$ reads

$$P(t,x) = \int_{\mathbb{R}^N} \rho(x-y)u(t,y)\mathrm{d}y, \quad t>0, x\in\mathbb{R}^N. \tag{4.3}$$

The above problem can be rewritten as the following equation posed on $\Omega := [0,2\pi]^N$ with periodic boundary condition

$$\begin{cases} \partial_t u = D\Delta u + \operatorname{div}\left(u\nabla\left(K\circ u\right)\right) + f(u),\ t>0,\ x\in\Omega, \\ u(0,x) = u_0(x),\ x\in\Omega, \end{cases} \tag{4.4}$$

where the kernel $K \in L^1_{\mathrm{per}}(\Omega)$ is defined by

$$K(x) = (2\pi)^N \sum_{k\in\mathbb{Z}^N} \rho(x+2\pi k),\ x\in\mathbb{R}^N.$$

Here and in the sequel of this thesis the symbol $\circ$ denotes the convolution product on the torus $\Omega = \mathbb{R}^N/(2\pi\mathbb{Z}^N) \simeq [0,2\pi]^N$, i.e.,

$$\left(\varphi\circ\psi\right)(x) = |\Omega|^{-1}\int_\Omega \varphi(x-y)\psi(y)dy,\ \forall\varphi,\psi\in L^1_{\mathrm{per}}(\Omega). \tag{4.5}$$

Therefore, we rewrite the pressure (4.3) as

$$P(t,x) = |\Omega|^{-1} \int_\Omega K(x-y)u(t,y)\mathrm{d}y.$$

**Case 2:** When $\Omega \subset \mathbb{R}^N$ is a bounded set, we impose the non-flux boundary condition and define

$$P(t,x) = (I-\chi\Delta)^{-1}u(t,x), \quad \nabla P \cdot \nu = 0, \tag{4.6}$$

where $\nu$ is the normal outward vector, $\chi$ is a positive constant representing the sensing coefficient of cells and $(I-\chi\Delta)^{-1}$ is the resolvent of the Laplacian operator with Neumann boundary condition.

Equation (4.6) can be derived from the following parabolic equation (which is the classical case in the Keller-Segel equation [61]) as $\varepsilon$ goes to 0:

$$\varepsilon\partial_t P(t,x) = \chi\Delta P(t,x) + u(t,x) - P(t,x).$$

The process of letting $\varepsilon \to 0$ corresponds to the assumption that the dynamics of the chemorepellent is fast compared to the evolution of the cell density.

In fact, Equation (4.6) can also be regarded as a nonlocal advection by using the representation

$$P(t,x) = \int_\Omega \kappa(x,y)u(t,y)dy,$$

where $\kappa$ is a convolution kernel which can be represented by the sum of eigenfunctions of the operator $(I-\chi\Delta)^{-1}$ weighted by their eigenvalues in $L^2(\Omega)$.

## 4.1 Turing and Turing-Hopf bifurcations for a reaction diffusion equation with nonlocal advection

Chapter 1 deals with the following single-species system in dimension $N = 1$ with a periodic setting

$$\frac{\partial u}{\partial t} = \frac{\partial}{\partial x}\left[D\frac{\partial u}{\partial x} + u\frac{\partial}{\partial x}(\rho * u)\right] + f(u),\ t>0,\ x\in\mathbb{R}.$$

We study the stability and the bifurcation properties of the positive interior equilibrium for such a reaction-diffusion equation with nonlocal advection. Under some rather general assumptions on the nonlocal kernel, we first study the local well-posedness of the problem in suitable fractional spaces and we obtain stability results for the homogeneous steady state. As a special case, we obtain that "standard" kernels such as Gaussian, Cauchy, Laplace and triangle, lead to stability. Next we specify the model with a given step function kernel and investigate two types of bifurcations, namely Turing bifurcation and Turing-Hopf bifurcation. Roughly speaking, a scalar and local reaction-diffusion equation typically does not exhibit pattern formation, which is the result of suitable comparison arguments. However as far as nonlocal interactions are concerned, the application of comparison arguments may fail and more complex dynamical behaviors may occur. In Chapter

1, we prove that a single scalar equation may display these two types of bifurcations with the dominant wave number as large as we want. Moreover, similar instabilities can also be observed with a bi-modal kernel. The resulting complex spatio-temporal dynamics are illustrated by numerical simulations.

The nonlinear operator responsible for the motion of individuals, denoted by $\mathbf{J}(u)$ and defined by

$$\mathbf{J}(u) = \frac{\partial}{\partial x}\left[D\frac{\partial u}{\partial x} + u\frac{\partial}{\partial x}(\rho * u)\right]$$

was proposed and studied by several authors in the literature. The nonlinear operator $\mathbf{J}(u)$ has also been introduced in swarming dynamics and we refer to the survey paper of Bernoff and Topaz in [10] and the references therein. Some properties of the equation $\partial_t u = \mathbf{J}(u)$ without viscosity term have been studied for instance in [17, 68, 91] (see also the references cited therein). We also refer to Burger and Di Francesco [18] and the references therein for a study of a slightly different equation including nonlinear diffusion.

In Chapter 1, in the context of cell population dynamics, the function $f$ models the process of cell proliferation. Instead of considering the reaction term as logistic type, we shall make use of the function derived by Ducrot et al. in [38]. Hence we use the following specific form for this function $f$

$$f(u) = \frac{bu}{1+\gamma u} - \mu u,\ b > 0,\ \mu > 0,\ \gamma > 0.$$

This specific form allows us to make use of explicit computations in our analysis and to use the parameter $\gamma > 0$ as a bifurcation parameter. In the context of cell population dynamics, this nonlinear function takes account of the cell division and exit rate through the parameter $b$ and $\mu$ respectively. The saturation part due to the parameter $\gamma > 0$ reflects the cell dormant phase. We refer to [38] for more details on the modelling issues.

One type of kernel function that is of particular interest is a step function of the form

$$\rho(x) = \rho_{\eta,s}(x) = \frac{1}{2\eta}\mathbb{1}_{[-1,1]}\left(\frac{x-s}{\eta}\right),\ x \in \mathbb{R},$$

for some scaling parameter $\eta > 0$, a shift $s \in \mathbb{R}$ and where $\mathbb{1}_{[-1,1]}$ denotes the characteristic function of the interval $[-1,1]$, that is

$$\mathbb{1}_{[-1,1]}(x) = \begin{cases} 1, & \text{if } x \in [-1,1], \\ 0, & \text{otherwise.} \end{cases}$$

As it will be seen in Chapter 1, this kernel may destabilize the positive homogeneous steady state yielding Turing instabilities and the existence of a spatially heterogeneous steady state and, more surprisingly, it may also lead to spatio-temporal heterogeneous regime through Turing-Hopf bifurcation.

Using this kernel, one may observe that the solution of (4.1)-(4.3) is – at least formally – solution of the following active nonlocal Burgers' equation with viscosity

$$\frac{\partial u}{\partial t} = D\frac{\partial^2 u}{\partial x^2} + \frac{\partial}{\partial x}Q[u] + f(u),\ t > 0,\ x \in \mathbb{R},$$

where $Q$ denotes the quadratic nonlocal operator

$$Q[u(t,.)](x) = u(t,x)\frac{u(t,x-\eta+s)-u(t,x+\eta+s)}{2\eta},\ x\in\mathbb{R}.$$

As we mentioned, with a suitable choice for the model parameters and with an appropriate kernel function, Turing bifurcation and Turing-Hopf bifurcation can occur and in Chapter 1 we confirm our theoretical results by some numerical experiments. Here we present one of the Turing bifurcation scenarios with one set of parameters.

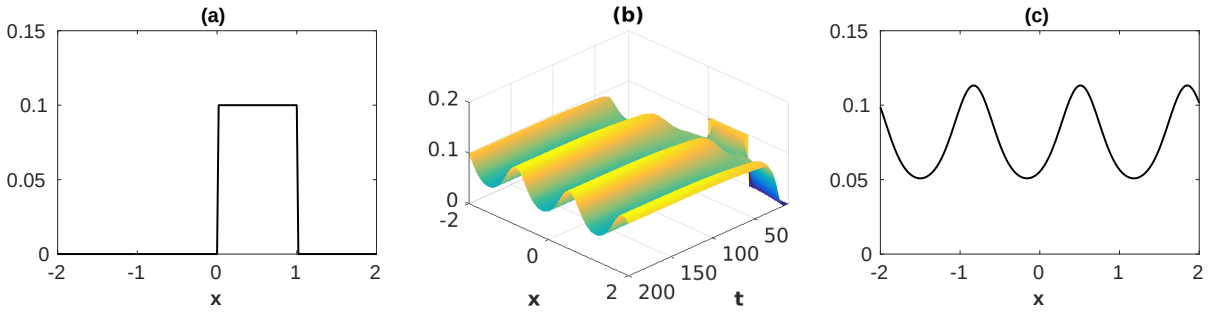


Figure 6: *Choosing parameters values as* $b = 1.5, \mu = 1.2, \eta = 1$ *and* $(\varepsilon,\gamma) = (0.0056, 3.03)$ *we obtain the above figures. Figure (a) presents the given non-symmetric initial value, figure (b) presents the spatio-temporal evolution of the solution and figure (c) presents the solution at a large time* $T = 200$ *when it is mostly stabilized close to a suitable shift of the symmetric stationary state. Here the wave number* $n_0 = 3$.

We also present one of the Turing-Hopf bifurcation scenarios with the following bi-modal kernel

$$\rho(x) = \frac{1}{2}\left(e^{-\pi(x+s_1)^2} + e^{-\pi(x-s_2)^2}\right).$$

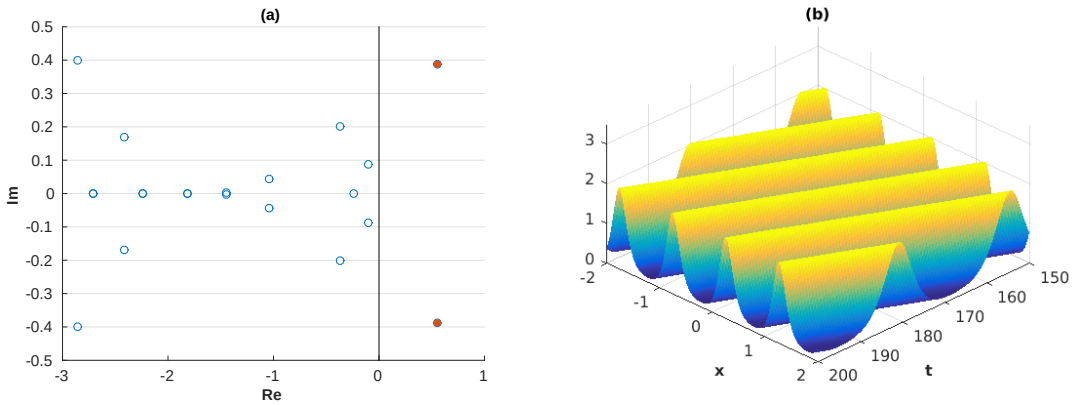


Figure 7: *In this figure we fix the parameter values as in* $(\varepsilon,\gamma) = (0.01, 0.2)$, $s_1 = 0.4$, $s_2 = 0.3$. *In Figure (a) we plot the eigenvalues of the linearized equation in the complex plane for* $n = -10, -9, .., 9, 10$. *By choosing the above parameters, there is only one pair of eigenvalues, namely* $\lambda_{\pm 4}$, *with a positive real part (see the filled dots). We observe a corresponding spatio-temporal evolution of the solutions in (b). The simulation shows the bi-modal kernels can also lead to instability.*

## 4.2 Asymptotic behavior of a nonlocal advection system with two populations

Chapter 2 is inspired by the work Ducrot and Magal [39] where the authors discussed the asymptotic behavior of a single-species reaction-diffusion equation with nonlocal advection. In Chapter 2, we consider a nonlocal advection model for two populations with periodic boundary condition.

$$\begin{cases} \partial_t u_1(t,x) + \operatorname{div}\big(u_1(t,x)\mathbf{v}(t,x)\big) = u_1(t,x)h_1(u_1(t,x),u_2(t,x)), \\ \partial_t u_2(t,x) + \operatorname{div}\big(u_2(t,x)\mathbf{v}(t,x)\big) = u_2(t,x)h_2(u_1(t,x),u_2(t,x)), \end{cases} \quad t>0,\ x\in\mathbb{R}^N, \tag{4.7}$$

and the velocity field $\mathbf{v} = -\nabla P$ is derived from pressure

$$P(t,x) := (K \circ (u_1+u_2)(t,.))(x), \tag{4.8}$$

where $K \circ u$ is defined in (4.5). We assume the kernel $K : \mathbb{R}^N \to \mathbb{R}$ is a $\mathbb{T}^N-$ periodic function ($\mathbb{T}^N \simeq [0,2\pi]^N$) of the class $C^m$ on $\mathbb{R}^N$ for some integer $m \geq \frac{N+5}{2}$.

Our motivation for this problem comes from biological experiments for two types of cells with monolayer co-culture. One can find an example of such a co-culture in [88, Figure 1]. Cells are growing and meanwhile forming segregated islets after 7 days. For a more general perspective, our study is connected to the cell segregation and border formation. Taylor et al. [99] concluded that the heterotypic repulsion and homotypic cohesion can account for cell segregation and border formation. We also refer the readers to Dahmann et al. [34] and the references therein for more about boundary formation with its application in biology.

The first part of Chapter 2 is devoted to the existence and uniqueness of solutions and the associated semi-flow properties. Here we use the notion of solution integrated along the characteristics which will be briefly explained later. Next, using the solution integrated along the characteristics, we can prove a segregation property for solutions. In order to resolve the lack of compactness of the positive orbit, we use the narrow convergence in the space of Young measures and obtain a description of the asymptotic behavior of solutions. We also present some numerical simulations, which confirm our theoretical results.

We precise the notion of solution in this work. Let $C^k_{per}\left(\mathbb{R}^N\right)$ denote the Banach space of functions of the class $C^k$ from $\mathbb{R}^N$ into $\mathbb{R}$ and $[0,2\pi]^N$–periodic endowed with the usual supremum norm

$$\|\varphi\|_{C^k} = \sum_{j=0}^{k} \sup_{x\in\mathbb{R}^N} \left|D^j\varphi(x)\right|.$$

For each $p \in [1,+\infty]$, let us denote by $L^p_{per}\left(\mathbb{R}^N\right)$ the space of measurable and $[0,2\pi]^N-$periodic functions from $\mathbb{R}^N$ to $\mathbb{R}$ such that

$$\|\varphi\|_{L^p} := \|\varphi\|_{L^p\left((0,2\pi)^N\right)} < +\infty.$$

Then $L^p_{per}\left(\mathbb{R}^N\right)$ endowed with the norm $\|\varphi\|_{L^p}$ is a Banach space. We also introduce its positive cone $L^p_{per,+}\left(\mathbb{R}^N\right)$ consisting of function in $L^p_{per}\left(\mathbb{R}^N\right)$ almost everywhere positive.

Assume the solution

$$\mathbf{u} = (u_1, u_2) \in C^1\left([0,\tau]\times\mathbb{R}^N,\mathbb{R}\right)^2 \cap C\left([0,\tau], C^0_{per,+}(\mathbb{R}^N)\right)^2$$

is a classical solution of (4.7)-(4.8). We consider the solution with each component $u_i(t,\cdot)$ along the characteristic curve $\Pi_{\mathbf{v}}(t,0;x)$ respectively, where the characteristics are solutions of the following ODE

$$\begin{cases} \partial_t \Pi_{\mathbf{v}}(t,s;z) = \mathbf{v}(t,\Pi_{\mathbf{v}}(t,s;z)), \text{ for each } t,s\in[0,\tau], \\ \Pi_{\mathbf{v}}(s,s;z) = z. \end{cases}$$

We obtain for $i=1,2$,

$$\begin{aligned} \frac{\mathrm{d}}{\mathrm{d}t}\Big(u_i(t,\Pi_{\mathbf{v}}(t,0;z)\Big) &= \partial_t u_i(t,\Pi_{\mathbf{v}}(t,0;z)) + \nabla u_i(t,\Pi_{\mathbf{v}}(t,0;z))\cdot\mathbf{v}(t,\Pi_{\mathbf{v}}(t,0;z)) \\ &= -\mathrm{div}\big(u_1(t,\Pi_{\mathbf{v}}(t,0;z))\mathbf{v}(t,\Pi_{\mathbf{v}}(t,0;z))\big) \\ &\quad + u_i(t,\Pi_{\mathbf{v}}(t,0;z))h_i(u_1(t,\Pi_{\mathbf{v}}(t,0;z)),u_2(t,\Pi_{\mathbf{v}}(t,0;z))) \\ &\quad + \nabla u_i(t,\Pi_{\mathbf{v}}(t,0;z))\cdot\mathbf{v}(t,\Pi_{\mathbf{v}}(t,0;z)) \\ &= u_i(t,\Pi_{\mathbf{v}}(t,0;z))\Big[-\mathrm{div}\,\mathbf{v}(t,\Pi_{\mathbf{v}}(t,0;z)) + h_i(\mathbf{u}(t,\Pi_{\mathbf{v}}(t,0;z))\Big], \end{aligned}$$

where $h_i(\mathbf{u}(t,\Pi_{\mathbf{v}}(t,0;z)) = h_i(u_1(t,\Pi_{\mathbf{v}}(t,0;z),u_2(t,\Pi_{\mathbf{v}}(t,0;z))$. Hence a classical solution of (4.7)-(4.8) (i.e. $C^1$ in time and space) must satisfy

$$u_i(t,\Pi_{\mathbf{v}}(t,0;z)) = \exp\left(\int_0^t h_i\big(\mathbf{u}(l,\Pi_{\mathbf{v}}(l,0;z)) - \mathrm{div}\,\mathbf{v}(l,\Pi_{\mathbf{v}}(l,0;z))dl\right) u_i\left(0,z\right), i=1,2,$$

or equivalently

$$u_i(t,z) = \exp\left(\int_0^t h_i\big(\mathbf{u}(l,\Pi_{\mathbf{v}}(l,t;z))\big) - \mathrm{div}\,\mathbf{v}(l,\Pi_{\mathbf{v}}(l,t;z))dl\right) u_i\left(0,\Pi_{\mathbf{v}}(0,t;z)\right), i=1,2, \tag{4.9}$$

where

$$\mathbf{v}(t,x) = -\frac{1}{|\mathbb{T}^N|}\int_{\mathbb{T}^N}\nabla K(x-y)(u_1+u_2)(t,y)\mathrm{d}y. \tag{4.10}$$

The above computations lead us to the following definition of solution.

**Definition 4.1** (Solution integrated along the characteristics)**.** *Let* $\mathbf{u}_0 \in L^\infty_{per,+}\left(\mathbb{R}^N\right)^2$, $\tau>0$ *be given. A function* $\mathbf{u}\in C\left([0,\tau], L^1_{per,+}\left(\mathbb{R}^N\right)\right)^2 \cap L^\infty\left((0,\tau), L^\infty_{per,+}\left(\mathbb{R}^N\right)\right)^2$ *is said to be a solution integrated along the characteristics of* (4.7)-(4.8)*, if* $u_i$ *satisfies* (4.9) *for* $i=1,2$*, with* $\mathbf{v}$ *defined in* (4.10)*.*

Briefly speaking, we can prove that for each initial value $\mathbf{u}_0$ which is periodic and bounded, system (4.7)-(4.8) has a unique solution integrated along the characteristics and the corresponding semiflow $\{U(t)\}_{t\geq 0}$ defined by

$$(U(t)\mathbf{u}_0)(x) := \mathbf{u}(t,x) = (u_1(t,x),u_2(t,x)),\ \forall t\geq 0,$$

is a continuous semiflow on $L^1_{per,+}\times L^1_{per,+}$ and has the following properties

1. Any solution starting from a positive initial value remains positive;
2. The solution is globally defined, namely, $\sup_{t\in[0,\tau]} \|\mathbf{u}(t,\cdot)\|_\infty \leq M(\tau)\|\mathbf{u}_0\|_\infty$;
3. If one starts from a smooth initial value, then the solution is a classical solution;
4. Conservation law: for any $A \in \mathcal{B}(\mathbb{T}^N)$

$$\int_{\Pi_{\mathbf{v}}(t,s;A)} u_i(t,x)\mathrm{d}x = \int_A \exp\left[\int_s^t h_i\left(\mathbf{u}\left(l,\Pi_{\mathbf{v}}(l,s;x)\right)\right)\mathrm{d}l\right] u_i(s,x)\mathrm{d}x.$$

We can also prove that solutions preserve the segregation property.

**Theorem 4.2.** *Suppose* $\mathbf{u} = \mathbf{u}(t,x)$ *is the solution of* (4.7)-(4.8). *For any initial distribution with* $u_1(0,x)u_2(0,x) = 0$ *for all* $x \in \mathbb{T}^N$. *Then* $u_1(t,x)u_2(t,x) = 0$ *for any* $t > 0$ *and* $x \in \mathbb{T}^N$.

We illustrate the segregation property and the asymptotic behavior of solutions by the following simulations.

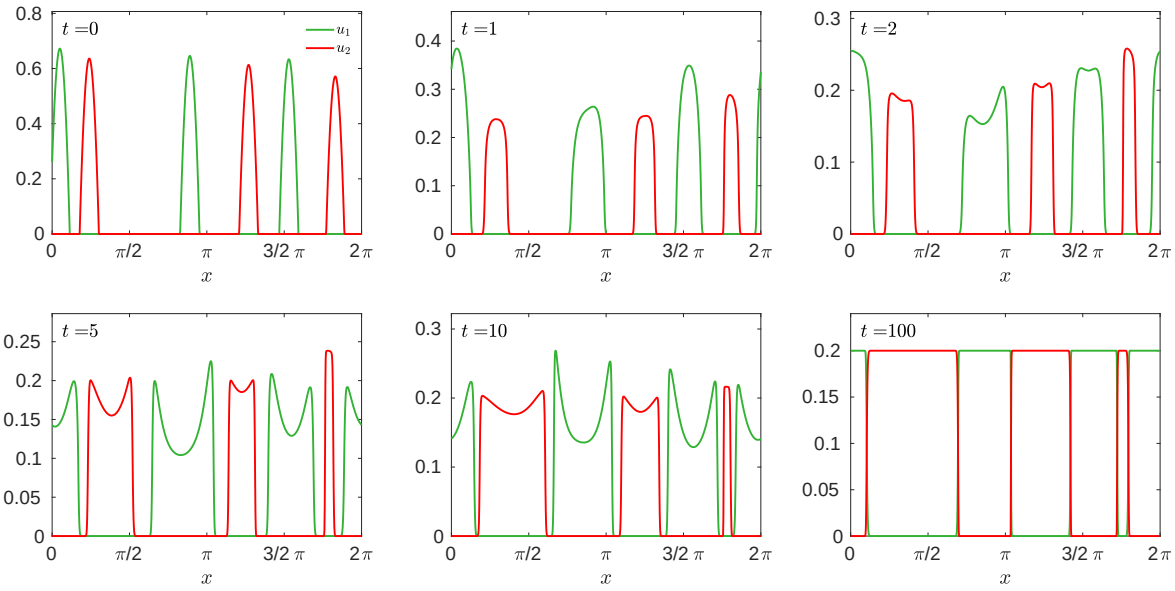


Figure 8: *The green curves represent species* $u_1$, *the red represents species* $u_2$. *Given a segregated initial distribution for two population, we observe the coexistence of the two species and the segregation property. After* $t = 100$ *the distributions of the two species stay the same.*

## 4.3 A cell-cell repulsion model on a hyperbolic Keller-Segel equation

In Chapter 3, we propose a two-population hyperbolic Keller-Segel model to study the segregation phenomenon in cell co-culture experiments (see (4.11) for the model). Spatial segregation property between two types of cells was observed by Pasquier et al. [88].

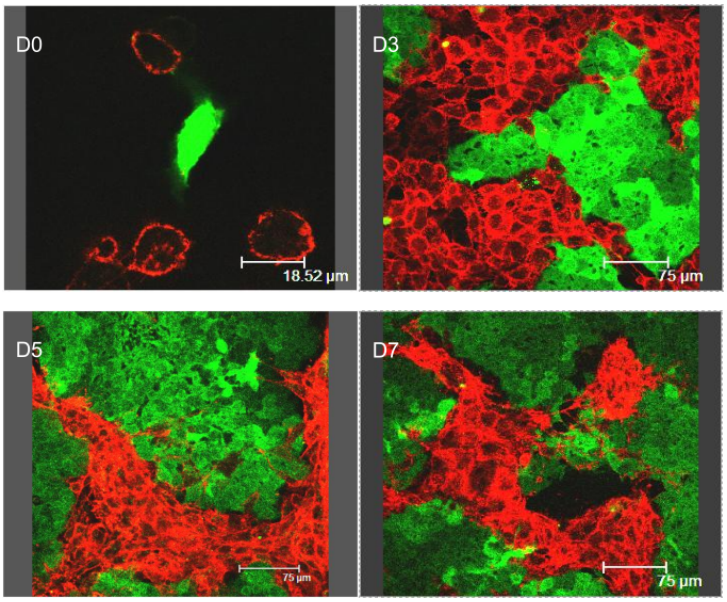


Figure 9: *Direct immunodetection of P-gp transfers in co-cultures of sensitive (MCF-7) and resistant (MCF-7/Doxo) variants of the human breast cancer cell line.*

They studied the protein transfer between two types of human breast cancer cell, namely MCF-7 and MCF-7/Doxo cells. Over a 7-day cell co-culture, the spatial competition was observed between two types of cells and a clear boundary was formed between them on day 7 (see Figure 9). A similar segregation property is also found in the mosaic pattern between nections and cadherins in the experiments of Katsunuma et al. [64].

We study a two species population dynamics model on a unit open disk $\Omega \subset \mathbb{R}^2$ given as follows

$$\begin{cases} \partial_t u_1(t,x) - d_1 \operatorname{div}\big(u_1(t,x)\nabla P(t,x)\big) = u_1(t,x)h_1((u_1,u_2)(t,x)) & \\ \partial_t u_2(t,x) - d_2 \operatorname{div}\big(u_2(t,x)\nabla P(t,x)\big) = u_2(t,x)h_2((u_1,u_2)(t,x)) & \text{in } [0,T]\times\Omega \\ \big(I-\chi\Delta\big)P(t,x) = u_1(t,x)+u_2(t,x) & \\ \nabla P(t,x)\cdot\nu(x) = 0 & \text{on } [0,T)\times\partial\Omega, \end{cases} \tag{4.11}$$

where $\nu$ is the outward normal vector, $d_i$ is the dispersion coefficient, $\chi$ is the sensing coefficient. Recall the function $h_i$ is of form

$$h_i(u_1,u_2) = b_i - \delta_i - \sum_{j=1,2} a_{ij}u_j, \quad i=1,2,$$

where $b_i > 0$, $i = 1,2$ are the growth rates, $a_{ij} \geq 0$, $i \neq j$ represent the mutual competition between the species, $a_{ii}$ is the competition among the same species and $\delta_i$ is the additional mortality rate caused by drug treatment. System (4.11) is supplemented with the initial distribution

$$\mathbf{u}_0(\cdot) := (u_1(0,\cdot), u_2(0,\cdot)) \in C^1(\overline{\Omega})^2.$$

We consider a two-dimensional bounded domain (a flat circular petri dish). With the notion of solution integrated along the characteristics, we prove the existence and uniqueness of the solution and the segregation property of the two species. Thanks to the appropriate

boundary condition of the pressure equation, we deduce that the characteristics stay in the domain for any positive time. The positivity of solutions, the segregation property and the conservation law follow for the model (4.11) as well.

From the work in [89], MCF-7 and MCF-7/Doxo cells are cultured separately at initial cell number $10^5$ in $60 \times 15$ mm cell dish with or without drug (doxorubicine). Given the cell growth data in the experiments in [89], we fit the parameters $b_i$, $\mu_i$, $\delta_i$, $i = 1, 2$, by using the model that is homogeneous in space. Furthermore, we use our PDE model with finite volume method to estimate the parameters $\chi$ and the dispersion coefficients $d_i, i = 1, 2$.

From a numerical perspective, we can also observe that the model admits a competitive exclusion (the results are different from the corresponding ODE model). More importantly, our model shows that the complexity of the short term (6 days) co-cultured cell distribution depends on the initial distribution of each species. Through numerical simulations, the impact of the initial distribution on the population ratio lies in the initial total cell number and our study shows that the population ratio is not impacted by the law of initial distribution. We also find that a fast dispersion rate gives a short-term advantage while the vital dynamic contributes to a long-term population advantage.

We present one numerical simulation in Figure 10 from day 0 to day 6. We also plot the relative cell numbers in Figure 10 (f) where we define the relative cell number for species $i$ as

$$\frac{U_i(t)}{U_1(t) + U_2(t)}, \qquad \text{where } U_i(t) := \int_\Omega u_i(t, x)\mathrm{d}x,\ i = 1, 2.$$

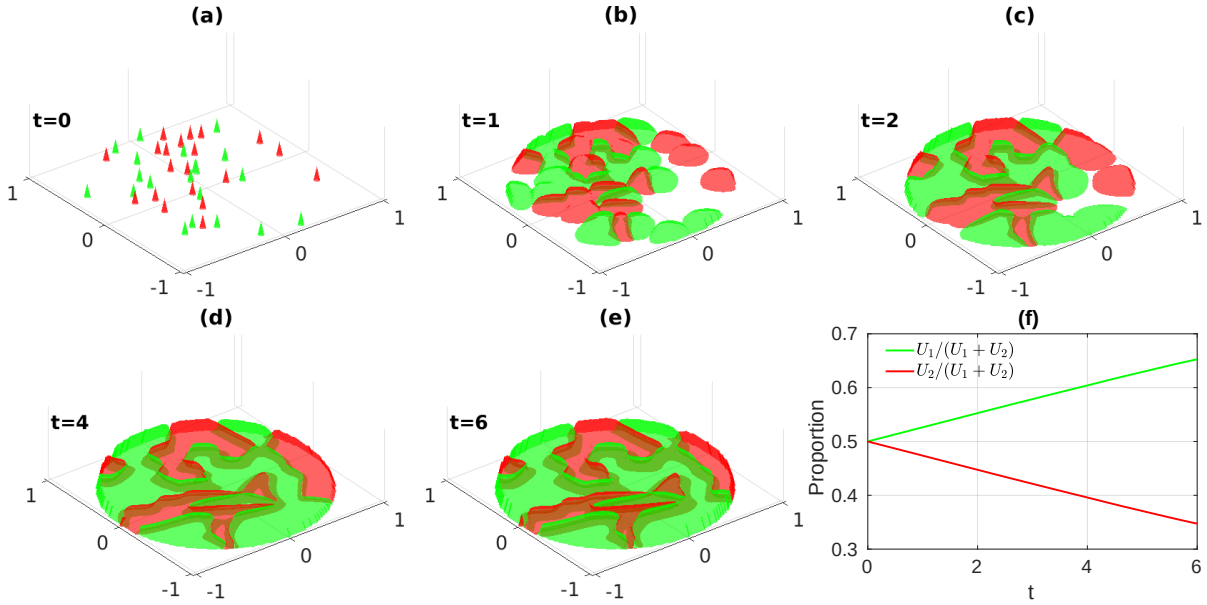


Figure 10: *Spatial-temporal evolution of the two species $u_1$ and $u_2$ and their relative proportions. Figures (a)-(e) correspond to the evolution of cell growth form day 0 to day 6 and Figure (f) is the relative proportion plot from day 0 to day 6. The initial distribution follows the uniform distribution on a disk with 20 initial cell clusters. The initial total cell number is $U_1 = U_2 = 0.01$ for each species and cells are equally distributed in each cluster.*

# Chapter 1

# Turing and Turing-Hopf bifurcations for a reaction diffusion equation with nonlocal advection

## Contents

# 1 Introduction

In this work we consider the following one-dimensional nonlocal reaction-diffusion-advection equation

$$\frac{\partial u}{\partial t} = \varepsilon \frac{\partial^2 u}{\partial x^2} - \frac{\partial}{\partial x}(u\mathbf{v}) + f(u),\ t > 0,\ x \in \mathbb{R}. \tag{1.1}$$

Here $\varepsilon \geq 0$ denotes the viscosity parameter. The velocity field $\mathbf{v}$ is derived from pressure $P$, where

$$\mathbf{v} = -\frac{\partial P}{\partial x} \text{ with } P(t,x) = (\rho * u(t,.))(x) = \int_{\mathbb{R}} \rho(x-y)u(t,y)dy. \tag{1.2}$$

In the above equation we assume that the pressure $P$ follows nonlocal Darcy law with the kernel $\rho \in L^1(\mathbb{R})$ and the symbol $*$ denotes the convolution product on $\mathbb{R}$. Hence with this closure equation, (1.1) reads as a reaction-diffusion problem with a nonlocal advection term.

In this Chapter Problem (1.1)-(1.2) is supplemented with an initial data $u(0,x) = u_0(x)$ that is assumed to be $2L-$periodic with some given and fixed value $L > 0$. In that periodic setting, we rewrite the above problem as the following equation posed on $(-L, L)$ with periodic boundary conditions

$$\begin{cases} \dfrac{\partial u}{\partial t} = \varepsilon \dfrac{\partial^2 u}{\partial x^2} + \dfrac{\partial}{\partial x}\left(u \dfrac{\partial}{\partial x}(K \circ u)\right) + f(u),\ t > 0,\ x \in (-L, L), \\ \\ u(0,x) = u_0(x),\ x \in (-L, L), \end{cases} \tag{1.3}$$

wherein the kernel $K \in L^1_{\text{per}}(-L, L)$ is defined by

$$K(x) = 2L \sum_{k \in \mathbb{Z}} \rho(x + 2Lk),\ x \in \mathbb{R}. \tag{1.4}$$

Here and in the sequel of this Chapter the symbol $\circ$ denotes the convolution product on the torus $\mathbb{R}/(2L\mathbb{Z})$ i.e.,

$$(g \circ h)(x) = \frac{1}{2L} \int_{-L}^{L} g(x-y)h(y)dy,\ \forall g, h \in L^1_{\text{per}}(-L, L),$$

while for any $p \in [1, \infty]$, we shall also make use of the notation $L^p_{\text{per}}(-L, L)$ to denote the usual Lebesgue spaces of $2L-$periodic functions on $\mathbb{R}$.

System (1.1)-(1.2) (or the periodic equation (1.3)) appears in the mathematical modeling of cell population dynamics. It allows to model the motion of cells by taking into account interactions through cell-cell communication, but also the proliferation of cells and cell cycle through the active part of the equation, namely the function $f = f(u)$.

The nonlinear operator responsible for the motion of cells, denoted by $M(u)$ and defined by

$$M(u) = \frac{\partial}{\partial x}\left[\varepsilon \frac{\partial u}{\partial x} + u \frac{\partial}{\partial x}(\rho * u)\right]$$

was proposed and studied by several authors in the literature. With zero viscosity term $\varepsilon = 0$, this operator has been obtained by Oelschläger in [85] as a suitable limit of interacting system of particles. We also refer to Morale, Capasso and Oelschläger [77] for the derivation of the above operator with a viscosity term. The nonlinear operator $M(u)$ has also been introduced in crowd dynamics and we refer to the survey paper of Bernoff and Topaz in [10] and the references therein.

Some properties of the equation $\dfrac{\partial u}{\partial t} = M(u)$ without viscosity has been studied for instance in [17, 68, 91] (see also the references cited therein). We also refer to Burger and Di Francesco [18] and the references therein for a study of a slightly different equation including nonlinear diffusion.

The nonlinear equation (1.1) has been considered by Ducrot and Magal in [39] with the zero viscosity $\varepsilon = 0$. The authors mostly considered the case of logistic nonlinearity function $f = f(u)$, and most importantly, they considered a specific class of kernel function $\rho$. More specifically, the aforementioned work deals with the global asymptotic behavior of the problem for kernels with positive Fourier transform. In this work, this situation roughly corresponds to the stability case (see Remark 2.10 below).

As already mentioned, in the context of cell population dynamics, the function $f$ models the process of cell proliferation. Instead of considering the reaction term as logistic type, we shall make use of the function derived by Ducrot et al. in [38]. Hence throughout this Chapter we use the following specific form for this function $f$

$$f(u) = \frac{bu}{1+\gamma u} - \mu u,\ b > 0,\ \mu > 0,\ \gamma > 0. \tag{1.5}$$

This specific form will allow us to make use of explicit computations in our analysis and to use the parameter $\gamma > 0$ as a bifurcation parameter. In the context of cell population dynamics, this nonlinear function takes account of the cell division and exit rate through the parameter $b$ and $\mu$ respectively. The saturation part due to the parameter $\gamma > 0$ reflects the cell cycle and more precisely the dormant phase. We refer to [38] for more details on the modeling issues.

The aim of this Chapter is to study stability and pattern formation for Problem (1.1)-(1.2) or more specifically for its $2L-$periodic counterpart (1.3) through bifurcation analysis methods. Roughly speaking, a scalar and local reaction-diffusion equation typically does not exhibit pattern formation, which is the result of suitable comparison arguments. However as far as nonlocal interaction are concerned, the application of comparison arguments may fail and more complex dynamical behaviors may occur.

Oscillations due to nonlocal interactions has already been observed and studied. We refer for instance to Fiedler and Polácik [46] for a nice work in this direction. Here, we shall discuss the existence of complex asymptotic behavior of the solutions of (1.1)-(1.2) (or (1.3)) close to the positive homogeneous stationary state and, our discussion will be strongly related with some properties (expressed in term of Fourier transform) of the kernel function $\rho$ arising in the nonlocal advection term.

One type of kernel function that is of particular interest is a step function of the form

$$\rho(x) = \rho_{\eta,s}(x) = \frac{1}{2\eta}\chi_{[-1,1]}\left(\frac{x-s}{\eta}\right),\ x \in \mathbb{R}, \tag{1.6}$$

for some scaling parameter $\eta > 0$, a shift $s \in \mathbb{R}$ and where $\chi_{[-1,1]}$ denotes the characteristic function of the interval $[-1, 1]$, that is

$$\chi_{[-1,1]}(x) = \begin{cases} 1, \text{ if } x \in [-1, 1], \\ 0, \text{ otherwise.} \end{cases}$$

As it will be seen in this Chapter, this kernel may destabilize the positive homogeneous steady-state yielding Turing instabilities and the existence of spatially heterogeneous steady-state and, more surprisingly, it may also lead to spatio-temporal regime through Turing-Hopf bifurcation.

Using this kernel, one may observe that the solution of (1.1)-(1.2) is – at least formally – solution of the following active nonlocal Burgers' equation with viscosity

$$\frac{\partial u}{\partial t} = \varepsilon \frac{\partial^2 u}{\partial x^2} + \frac{\partial}{\partial x} Q[u] + f(u),\ t > 0,\ x \in \mathbb{R},$$

wherein $Q$ denotes the quadratic nonlocal operator

$$Q[u(t,.)](x) = u(t,x) \frac{u(t, x - \eta + s) - u(t, x + \eta + s)}{2\eta},\ x \in \mathbb{R}.$$

As already mentioned above our goal in this Chapter is to study the stability of the positive homogeneous equilibrium for Problem (1.3) and to provide a bifurcation analysis when it destabilizes. The stability condition is studied using a rather general and possibly non smooth kernel function $\rho$. Our bifurcation analysis is performed using the more specific kernel $\rho$ proposed in (1.6) above involving the two parameters $\eta > 0$ and $s \in \mathbb{R}$. Here, this specific choice of the kernel $\rho$ is used to compute explicitly the bifurcation property of the system.

This work is organized as follows. In Section 2 we reformulate (1.3) as an abstract parabolic Cauchy problem. From this we are able to study the local well posedness of Problem (1.3) and to study the stability properties of equilibrium state through spectral analysis. In Section 3 we study bifurcations at the positive equilibrium when it becomes spectrally unstable. Moreover, we prove, using the kernel $\rho$ proposed in (1.6), that Turing and Turing-Hopf bifurcations may occur yielding complex spatio-temporal dynamics. We conclude this Chapter by a short discussion on (1.3) without vital dynamics, namely $f(u) = 0$ and its connection with the porous medium equation.

# 2 Semiflow and stability

## 2.1 Spectral analysis

In this section, we consider Problem (1.3). We assume that $\varepsilon > 0$, $L > 0$ are given and fixed. Next recalling the definition of the function $f$ in (1.5) we assume that

$$\gamma > 0,\ b > 0,\ \mu > 0 \text{ and } b - \mu > 0.$$

In that case Problem (1.3) has a unique positive homogeneous steady state given by

$$u_e := \frac{b-\mu}{\gamma\mu} > 0. \tag{2.1}$$

In this section we first study some spectral properties of the – formally – linearized problem at the above positive equilibrium. Then we turn to the stability analysis. The linearized problem in the state space $L^2_{\text{per}}(-L,L)$ reads

$$\begin{cases} \dfrac{\partial v}{\partial t}(t,x) = \dfrac{\partial^2}{\partial x^2}\left(\varepsilon v + u_e(K\circ v(t,\cdot))(x)\right) + f'(u_e)v(t,x), & t>0, x\in(-L,L), \\ v(t,-L) = v(t,L),\ \partial_x v(t,-L) = \partial_x v(t,L), & t>0, \end{cases}$$

where

$$f'(u_e) = \frac{\mu(\mu-b)}{b} < 0.$$

To handle this problem we define the linear operator $\mathcal{A} : D(\mathcal{A}) \subset L^2_{\text{per}}(-L,L) \to L^2_{\text{per}}(-L,L)$ as follows

$$\begin{cases} D(\mathcal{A}) = H^2_{\text{per}}(-L,L), \\ \mathcal{A}\phi = \varepsilon\phi'' + u_e\left(K\circ\phi''\right). \end{cases} \tag{2.2}$$

Here recall that the kernel $K \in L^1_{\text{per}}(-L,L)$. To analyze this operator we shall make use of Fourier analysis. To that aim we shall also use of the notation $\langle .,. \rangle$ to denote the inner product in $L^2_{\text{per}}(-L,L;\mathbb{C})$ defined by

$$\langle f,g\rangle = \frac{1}{2L}\int_{-L}^{L} \overline{f(x)}g(x)dx,\ \forall f,g\in L^2_{\text{per}}(-L,L).$$

The corresponding norm on $L^2_{\text{per}}(-L,L)$ is denoted by $\|\cdot\|_0$.

We also introduce the Hilbert basis $\left\{e_n : x\to e^{i\pi\frac{nx}{L}}\right\}_{n\in\mathbb{Z}}$ on $L^2_{\text{per}}(-L,L)$ as well as, for each function $\varphi\in L^1_{\text{per}}(-L,L;\mathbb{C})$, its Fourier coefficients $\{c_n(\varphi)\}_{n\in\mathbb{Z}}\subset\mathbb{C}$ defined by

$$c_n(\varphi) = \langle e_n,\varphi\rangle = \frac{1}{2L}\int_{-L}^{L}\varphi(x)e^{-i\pi\frac{nx}{L}}dx,\ \text{for any } n\in\mathbb{Z}.$$

Recall that using the above notation, the map $\varphi\mapsto\{c_n(\varphi)\}_{n\in\mathbb{Z}}$ is an isometry from $L^2_{\text{per}}(-L,L;\mathbb{C})$ – endowed with the norm $\|\cdot\|_0$ – onto $l^2(\mathbb{Z};\mathbb{C})$.

We now describe the spectrum of the operator $\mathcal{A}$ defined above.

**Proposition 2.1.** *Recalling that $K\in L^1_{\text{per}}(-L,L)$, the spectrum of the linear operator $\mathcal{A}$, denoted by $\sigma(\mathcal{A})$, consists in point spectrum and one has*

$$\sigma(\mathcal{A}) = \left\{\lambda_n := -\left(\frac{n\pi}{L}\right)^2\left[\varepsilon + u_e c_n(K)\right],\ n\in\mathbb{Z}\right\},$$

*and the corresponding eigenvectors are given by $\mathcal{A}e_n = \lambda_n e_n$ for all $n\in\mathbb{Z}$.*

*In addition, for each $\lambda\in\rho(\mathcal{A}) := \mathbb{C}\setminus\sigma(\mathcal{A})$, the resolvent set of $\mathcal{A}$, and each $f\in L^2_{\text{per}}(-L,L)$, one has*

$$(\lambda-\mathcal{A})^{-1}f = \sum_{n\in\mathbb{Z}}\frac{c_n(f)}{\lambda-\lambda_n}e_n.$$

**Remark 2.2.** *The key observation in the above lemma is the fact that since* $K \in L^1_{\text{per}}(-L, L)$ *we have by the Riemann-Lebesgue lemma*

$$\lim_{|n|\to+\infty} c_n(K) = 0.$$

*Therefore the results for purely diffusive systems (i.e. whenever* $K = 0$*) can be extended to the above class of linear operators. Recalling the definition of the kernel* $K$ *in* (1.4)*, one may notice that the Fourier coefficients* $c_n(K)$ *can be expressed using the Fourier transform of the kernel* $\rho$ *in the original model* (1.3)*. In the one dimensional setting, this relationship reads as follows*

$$c_n(K) = \widehat{\rho}\left(\frac{n}{2L}\right),\ n \in \mathbb{Z} \text{ where } \widehat{\rho}(\xi) = \int_{\mathbb{R}} \rho(x) e^{-2i\pi x\xi} dx. \tag{2.3}$$

*Proof.* Let us first observe that for each $n \in \mathbb{Z}$ one has:

$$\left(\mathcal{A}e_n\right)(x) = -\left(\frac{n\pi}{L}\right)^2 \left[\varepsilon + \frac{u_e}{2L}\int_{-L}^{L} K(y) e^{-\frac{in\pi}{L}y} dy\right] e_n(x).$$

As a consequence one obtains $\mathcal{A}e_n = \lambda_n e_n$ for all $n \in \mathbb{Z}$, that is $\{\lambda_n, n \in \mathbb{Z}\} \subset \sigma_p(\mathcal{A})$, the point spectrum of $\mathcal{A}$.

Now we claim that:

**Claim 2.3.** *Let* $\lambda \in \mathbb{C} \setminus \{\lambda_n,\ n \in \mathbb{Z}\}$ *be given. Then for each* $f \in L^2_{\text{per}}(-L, L)$ *there exists a unique* $u_f \in H^2_{\text{per}}(-L, L)$ *such that*

$$(\lambda - \mathcal{A})\, u_f = f,$$

*and that the linear map* $f \mapsto u_f$ *is continuous on* $L^2_{\text{per}}(-L, L)$ *into* $H^2_{\text{per}}(-L, L)$ *and it is given by*

$$u_f = \sum_{n\in\mathbb{Z}} \frac{c_n(f)}{\lambda - \lambda_n} e_n.$$

Note that this claim ensures that

$$\mathbb{C} \setminus \{\lambda_n,\ n \in \mathbb{Z}\} \subset \rho(\mathcal{A}),$$

which implies

$$\sigma_p(\mathcal{A}) \subset \sigma(\mathcal{A}) \subset \{\lambda_n,\ n \in \mathbb{Z}\},$$

and this completes the first part of the proposition. Note also that the explicit formula for the resolvent operator also follows from the above claim.

To prove this claim recall that the space $H^2_{\text{per}}(-L, L)$ can be re-written using the Fourier coefficients as follows:

$$H^2_{\text{per}}(-L, L) = \left\{\varphi \in L^2_{\text{per}}(-L, L) : \sum_{n\in\mathbb{Z}} \left(1 + n^2\right)^2 |c_n(\varphi)|^2 < \infty\right\},$$

and the norm $\|.\|_2$ on $H^2_{\text{per}}(-L,L)$, defined by:

$$\|\varphi\|_2^2 = \sum_{n\in\mathbb{Z}} \left(1+n^2\right)^2 |c_n(\varphi)|^2, \ \forall \varphi \in H^2_{\text{per}}(-L,L),$$

is equivalent to the usual $H^2_{\text{per}}(-L,L)-$norm. Using this characterization we are now able to complete the proof of the above claim.

*Proof of Claim 2.3:* Let $\lambda \in \mathbb{C} \setminus \{\lambda_n,\, n\in\mathbb{Z}\}$ be given. Let $f \in L^2_{\text{per}}(-L,L)$ be given. Assume first that there exists $u = u_f \in D(\mathcal{A})$ such that

$$(\lambda - \mathcal{A})u = f.$$

Then we get

$$\langle e_n, (\lambda-\mathcal{A})u\rangle = \langle e_n, f\rangle, \ \forall n\in\mathbb{Z}.$$

However, since for each $n\in\mathbb{Z}$, one has

$$\langle e_n, (\lambda-\mathcal{A})u\rangle = (\lambda-\lambda_n)\, c_n(u),$$

one obtains that

$$c_n(u) = \frac{c_n(f)}{\lambda-\lambda_n}, \ \forall n\in\mathbb{Z}.$$

As a consequence, the solution is unique as long as it exists.

On the other hand consider the sequence $\left\{F_n(\lambda) := \frac{c_n(f)}{\lambda-\lambda_n}\right\}_{n\in\mathbb{Z}}$, that is well defined since $\lambda \neq \lambda_n$ for all $n\in\mathbb{Z}$. Since $K \in L^1_{\text{per}}(-L,L)$, one can use the Riemann-Lebesgue lemma to get that $c_n(K)\to 0$ as $|n|\to\infty$, so that

$$\lambda_n \sim -\varepsilon\left(\frac{n\pi}{L}\right)^2 \text{ as } |n|\to+\infty.$$

Hence the sequence $\left\{\frac{1+n^2}{\lambda-\lambda_n}\right\}_{n\in\mathbb{Z}}$ is bounded. As a consequence one gets

$$\sum_{n=-\infty}^{\infty} \left|1+n^2\right|^2 |F_n(\lambda)|^2 \leq \sup_{n\in\mathbb{Z}}\left|\frac{1+n^2}{\lambda-\lambda_n}\right|^2 \sum_{n=-\infty}^{\infty} |c_n(f)|^2 \leq \sup_{n\in\mathbb{Z}}\left|\frac{1+n^2}{\lambda-\lambda_n}\right|^2 \|f\|_0^2. \tag{2.4}$$

As a consequence the function $u = u_f$ defined by

$$u_f = \sum_{n\in\mathbb{Z}} F_n(\lambda) e_n,$$

satisfies:

$$u_f \in H^2_{\text{per}}(-L,L) \text{ and } (\lambda-\mathcal{A})u_f = f.$$

Summarizing the above arguments we have obtained that for each $f\in L^2_{\text{per}}(-L,L)$ the function $u_f \in H^2_{\text{per}}(-L,L)$ is the unique solution of $(\lambda-\mathcal{A})u_f = f$. Furthermore (2.4) ensures that

$$\left\|(\lambda-\mathcal{A})^{-1} f\right\|_2^2 \leq \sup_{n\in\mathbb{Z}}\left|\frac{1+n^2}{\lambda-\lambda_n}\right|^2 \|f\|_0^2, \ \forall f\in L^2_{\text{per}}(-L,L),$$

that completes the proof of the claim. □

**Remark 2.4.** *As a corollary of the above proposition and more precisely of the resolvent formula, one obtains the following estimate:*
*For each $\lambda \in \rho(\mathcal{A})$ one has:*

$$\|(\lambda - \mathcal{A})^{-1}\|_{\mathcal{L}(L^2_{\text{per}}(-L,L))} \leq \sup_{n\in\mathbb{Z}} \frac{1}{|\lambda - \lambda_n|}. \tag{2.5}$$

*Now observe that, since $c_n(K) \to 0$ as $|n| \to \infty$, one has*

$$\lim_{|n|\to+\infty} \frac{\text{Im}\lambda_n}{\text{Re}\lambda_n} = \lim_{|n|\to+\infty} \frac{u_e \text{Im}\{c_n(K)\}}{\epsilon + u_e \text{Re}\{c_n(K)\}} = 0.$$

*Hence, since $|\lambda_n|$ is bounded from above, for each $a > 0$ large enough there exists $\phi_a \in \left(0, \frac{\pi}{2}\right)$ and $0 < k_a < a$ large enough such that $\{\lambda_n\}_{n\in\mathbb{Z}} \subset \overline{\Sigma_a}$ wherein $\Sigma_a \subset \mathbb{C}$ is defined by*

$$\Sigma_a = \left\{ z = a + re^{i\theta} \in \mathbb{C} : \, r > k_a \text{ and } |\pi - \theta| < \phi_a \right\}.$$

*One concludes from the above estimate that the linear operator $\mathcal{A}$ is a sectorial operator in $L^2_{\text{per}}(-L, L)$.*

Using the above proposition we now focus on the stability analysis of the homogeneous steady state $u_e$ (defined in (2.1)) of Problem (1.3). To that aim we need to strengthen our assumption for the kernel $K \in L^1_{\text{per}}(-L, L)$. More precisely we assume that
**Assumption 2.5.** *There exists $\nu \in (0, 1]$ such that the convolution kernel $K \in L^1_{\text{per}}(-L, L)$ satisfies*

$$\sup_{n\in\mathbb{Z}} \left(|n|^\nu \, |c_n(K)|\right) < \infty.$$

Using the above assumption we shall rewrite (1.3) as an abstract Cauchy problem involving a sectorial operator and suitable fractional spaces. To reach this goal, let us introduce the scale of Hilbert spaces $H^s_{per}$ for $s \in \mathbb{R}$ by

$$H^s_{per}(-L, L) = \left\{ \varphi \in L^2_{\text{per}}(-L, L) : \sum_{n\in\mathbb{Z}} \left(1 + |n|^2\right)^s |c_n(\varphi)|^2 < \infty \right\}.$$

These spaces are endowed with the inner product $\langle ., . \rangle_s$ defined by

$$\langle \varphi, \psi \rangle_s = \sum_{n\in\mathbb{Z}} \left(1 + |n|^2\right)^s \overline{c_n(\varphi)} c_n(\psi).$$

We denote by $\|\varphi\|_s := \sqrt{\langle \varphi, \varphi \rangle_s}$ the corresponding norm. Beside, we denote that

$$L^2_{\text{per}}(-L, L) = L^2_{\text{per}}$$

and with norm $\|\cdot\|_0$.

Now define the sectorial operator $A : D(A) \subset L^2_{\text{per}} \to L^2_{\text{per}}$ by

$$D(A) = H^2_{\text{per}}(-L, L) \text{ and } A = -I + \varepsilon \frac{\partial^2}{\partial x^2}.$$

Next observe (see [55, 105]) that for all $s \in \mathbb{R}$ one has

$$(-A)^s = \sum_{n=-\infty}^{\infty} \left[1 + \varepsilon \left(\frac{n\pi}{L}\right)^2\right]^s c_n(.)e_n,$$

so that $H^{2s}_{\text{per}} = D\left((-A)^s\right)$ and the norm $\|.\|_{2s}$ is equivalent to the graph norm $\|(-A)^s.\|$ on $H^{2s}_{\text{per}}$. Moreover, noticing the norm of $D((-A)^s) = H^{2s}_{\text{per}}$ is equivalent to the norm on $H^s(-L, L)$ (See [100, p.50]). Thus, for the simplicity of notation, we denote $H^s := H^s_{\text{per}}(-L, L)$ for any $s > 0$ and we choose $H^{2-\nu}$ as our state space, therefore $H^{2-\nu} \hookrightarrow C_{\text{per}}([-L, L])$ is a continuous embedding if $0 < \nu \leq 1$ where $C_{\text{per}}([-L, L])$ denotes the space of the continuous $2L$-periodic functions endowed with the uniform norm $\|\cdot\|_\infty$. In the sequel we shall also use the notation $H^0$ to denote $L^2_{\text{per}}$.

## 2.2 Existence of the semiflow in a fractional space

In this section we shall rewrite Problem (1.3) as an abstract Cauchy problem involving a sectorial linear operator and prove that it generates a maximal semiflow in a suitable fractional space, namely $H^{2-\nu}$ where the parameter $\nu \in (0, 1]$ is defined in Assumption 2.5. To that aim we first need to prove the following lemma.

**Lemma 2.6.** *Let Assumption 2.5 be satisfied. Then the bilinear map*

$$B : (\varphi, \psi) \mapsto \frac{d}{dx}\left(\varphi \frac{d}{dx} K \circ \psi\right),$$

*is continuous from $H^1 \times H^{2-\nu}$ to $L^2_{\text{per}}$.*

*Proof.* Let $\varphi$ and $\psi$ be two $2L-$periodic smooth functions. Then one has

$$B(\varphi, \psi) = \varphi'\left(K \circ \psi'\right) + \varphi\left(K \circ \psi''\right).$$

Hence we get

$$\begin{aligned}\|B(\varphi, \psi)\|_0 &\leq \|\varphi'\|_0 \|K \circ \psi'\|_0 + \|\varphi\|_{L^\infty} \|K \circ \psi''\|_0 \\ &\leq \|\varphi'\|_0 \|K\|_{L^1} \|\psi'\|_0 + \|\varphi\|_{L^\infty} \|K \circ \psi''\|_0.\end{aligned}$$

Recalling that $N = 1$, due to Sobolev embedding one has $H^1 \hookrightarrow L^\infty$ and, there exists some constant $C_1 > 0$ (that does not depend on $\varphi$ and $\psi$) such that

$$\|B(\varphi, \psi)\|_0 \leq \|\varphi\|_1 \|K\|_{L^1} \|\psi\|_1 + C_1 \|\varphi\|_1 \|K \circ \psi''\|_0.$$

It remains to estimate the last term. To that aim note that

$$\begin{aligned}\|K \circ \psi''\|_0^2 &= \sum_{n=-\infty}^{\infty} \left(\frac{n\pi}{L}\right)^4 |c_n(K)|^2 |c_n(\psi)|^2 \\ &= \left(\frac{\pi}{L}\right)^4 \sum_{n=-\infty}^{\infty} |n|^{2\nu} |c_n(K)|^2 \left(|n|^{2-\nu}\right)^2 |c_n(\psi)|^2 \\ &\leq \left(\frac{\pi}{L}\right)^4 \left(\sup_{n\in\mathbb{Z}} |n|^\nu |c_n(K)|\right)^2 \sum_{n=-\infty}^{\infty} \left(1 + |n|^{2-\nu}\right)^2 |c_n(\psi)|^2 \\ &\leq C_2^2 \|\psi\|_{2-\nu}^2 \text{ with } C_2 = \left(\frac{\pi}{L}\right)^2 \left(\sup_{n\in\mathbb{Z}} |n|^\nu |c_n(K)|\right).\end{aligned}$$

As a consequence of the above estimates and since $\nu \in (0,1]$, so that $H^{2-\nu} \subset H^1$, one obtains that for any smooth periodic functions

$$\|B(\varphi,\psi)\|_0 \leq [\|K\|_{L^1} + C_1C_2]\,\|\varphi\|_1\|\psi\|_{2-\nu}.$$

This completes the proof of the lemma using a usual density argument. □

Using the above lemma we can rewrite (1.3) as an abstract Cauchy problem. Recall that $H^{2-\nu} \subset H^1 \subset C_{\text{per}}([-L,L])$ with continuous embedding. We also modify the reaction term $f$ on the negative real line. We consider $\tilde{f}(u)$ that coincide with the formula (1.5) when $u \geq 0$ and $\tilde{f}$ is $C^\infty$ on $\mathbb{R}$. Hence the map $F : H^{2-\nu} \to L^2_{\text{per}}$ defined by

$$F(\varphi)(x) = B(\varphi,\varphi)(x) + \tilde{f}(\varphi(x)) + \varphi(x),\ \forall x \in (-L,L),$$

is smooth. We rewrite Problem (1.3) in the space $H^{2-\nu}$ as the following abstract Cauchy problem:

$$\begin{cases} \dfrac{du(t)}{dt} = Au(t) + F(u(t)),\ \text{for } t \geq 0, \\ u(0) = u_0 \in H^{2-\nu}. \end{cases} \tag{2.6}$$

A function $u \in C([0,\tau], H^{2-\nu})$ is called a *mild solution* of the equation (2.6) on $[0,\tau]$, if

$$u(t) = e^{At}u(0) + \int_0^t e^{A(t-s)}F(u(s))ds, \forall t \in [0,\tau].$$

Before going further, let us recall the following definition.

**Definition 2.7.** *Let $\tau$ (maximal time of existence) be a map from a Banach space $X$ into $(0,+\infty]$ and let $U$ be a map from $D_\tau := \{(t,u) \in [0,+\infty) \times X : 0 \leq t < \tau(u)\}$ into $X$. Set $U(t)u := U(t,u), \forall (t,u) \in D_\tau$. We say that $(U,\tau)$ is a maximal semiflow on $X$ if the following properties are satisfied:*

(i) *$U(t)U(s)u = U(t+s)u, \forall t,s \in [0,\tau(u))$ with $t+s < \tau(u)$ and $u \in X$ ;*

(ii) *$U(0)u = u$ for all $u \in X$;*

(iii) *$\tau(U(s)u) = s + \tau(u)$ for any $u \in X$ and $s \in [0,\tau(u))$;*

(iv) *if $\tau(u) < \infty$ then*

$$\lim_{t \nearrow \tau(u)} \|U(t)u\|_X = \infty.$$

The existence of a maximal semiflow for (2.6) is based on the fact that the map $F : H^{2-\nu} \to L^2_{\text{per}}$ is smooth enough and Lipschitz continuous on bounded sets and the following estimate

$$\sup_{t\in[0,T]} \| \int_0^t e^{A(t-s)}\varphi(s)ds\|_{2-\nu} \leq CT^{\nu/2} \sup_{t\in[0,T]} \|\varphi(t)\|_{L^2_{\text{per}}},$$

for any $\varphi \in C([0,T], L^2_{\text{per}})$ where $C$ is some constant.

By using the above estimation we follow the same idea as in Cazenave and Haraux [28, Chapter 5], Lunardi [71, Theorem 7.1.3 (i) p.260 and Proposition 7.1.9 (i) p.267] and Magal and Ruan [72, 73] to derive the following theorem.

**Theorem 2.8** (**Existence of the unique maximal semiflow**). *The abstract Cauchy problem (2.6) generates a unique maximal semiflow on $H^{2-\nu}$. This means for each $u_0 \in H^{2-\nu}$, we can find a map $\tau : H^{2-\nu} \to (0, +\infty]$ (maximal time of existence) and a map $U : D_\tau \to H^{2-\nu}$ where*

$$D_\tau := \{(t, u_0) \in [0, +\infty) \times H^{2-\nu} : 0 \leq t < \tau(u_0)\}.$$

*such that there exists a unique mild solution $U(\cdot)u_0 \in C([0, \tau(u_0)), H^{2-\nu})$. Moreover, for every $\hat{\tau} < \tau(u_0)$, there exist two constants $r > 0$ and $K > 0$ such that if $\|u_0 - \widehat{u}_0\|_{2-\nu} \leq r$, then $\tau(\widehat{u}_0) > \hat{\tau}$ and*

$$\|U(t)u_0 - U(t)\widehat{u}_0\|_{2-\nu} \leq K\|u_0 - \widehat{u}_0\|_{2-\nu}, \forall t \in [0, \hat{\tau}].$$

## 2.3 Stability and instability of the equilibria

In this section we discuss the linear stability and instability of the stationary state $u_e$ by using the abstract Cauchy problem formulation described in the previous section. Towards that purpose, we shall make use of Theorem 5.1.2 and 5.1.3 in the monograph of Henry [55] to deal with the stability and instability of the stationary state $u_e$. Within this framework the – local – stability and instability of $u_e$ relies on the spectrum of the linear operator $A + F'(u_e)$ that reads as $\mathcal{A} + f'(u_e)$. The spectrum of this linear operator has been fully described in Section 2 and one has:

$$\sigma\left(A + F'(u_e)\right) = \left\{ -\left(\frac{n\pi}{L}\right)^2 [\varepsilon + u_e c_n(K)] - \frac{\mu(b-\mu)}{b},\ n \in \mathbb{Z} \right\}. \tag{2.7}$$

As a consequence one obtains the following result:

**Theorem 2.9.** *Suppose Assumption 2.5 is satisfied. Then the following statements hold true:*

*(i) If*

$$-\left(\frac{n\pi}{L}\right)^2 [\varepsilon + u_e \operatorname{Re}(c_n(K))] - \frac{\mu(b-\mu)}{b} < 0,\ \forall n \in \mathbb{Z},$$

*then $u_e$ is a locally – exponentially – stable homogeneous steady state of (2.6) in a neighbourhood of $u_e$ in $H^{2-\nu}$. Here $c_n(K)$ is the Fourier coefficient defined by (2.3).*

*(ii) If there exists $n \in \mathbb{Z}$ such that*

$$-\left(\frac{n\pi}{L}\right)^2 [\varepsilon + u_e \operatorname{Re}(c_n(K))] - \frac{\mu(b-\mu)}{b} > 0,$$

*then $u_e$ is an unstable stationary state of (2.6) in $H^{2-\nu}$.*

**Remark 2.10.** *Using the first statement $(i)$ in the above result, note that if $\operatorname{Re}(c_n(K)) \geq 0$ for all $n \in \mathbb{Z} \setminus \{0\}$, then the spectrum is contained in the left complex half plane and $u_e$ is locally stable.*

Due to the above remark and by using the explicit computations of the Fourier transform coupled with Remark 2.2, one obtains the following corollary showing that "standard" kernels lead to stability.

**Corollary 2.11** (**Local stability for "standard" kernels**). *Standard kernel functions, $\rho$, such as Gaussian, Cauchy, Laplace and triangle law respectively defined by the following forms*

$$x \mapsto e^{-\pi x^2},\ x \mapsto \frac{2}{1+4\pi^2 x^2},\ x \mapsto \pi e^{-2\pi|x|} \text{ and } x \mapsto \rho_{\text{triangle}}(x),$$

*lead to the local stability of the interior equilibrium $u_e$. Here the function $\rho_{\text{triangle}}$ is defined by*

$$\rho_{\text{triangle}}(x) = \begin{cases} 1+x, & x \in [-1,0), \\ 1-x, & x \in [0,1], \\ 0 & \text{otherwise.} \end{cases}$$

The next lemma shows that the positive equilibrium is locally exponentially stable whenever the parameter $\gamma > 0$ is large enough.

**Theorem 2.12** (**Local stability for $\gamma \gg 1$**). *Let Assumption 2.5 be satisfied. Let $\varepsilon > 0$, with $b > \mu \geq 0$. Then there exists $\gamma_0 = \gamma_0(\varepsilon, b, \mu) > 0$ such that when $\gamma \geq \gamma_0$ the homogeneous steady state $u_e = (b-\mu)/(\gamma\mu)$ of the equation (2.6) is locally exponentially stable. i.e.,*

$$\operatorname{Re}(\lambda_n + f'(u_e)) = -\left(\frac{n\pi}{L}\right)^2 [\varepsilon + u_e \operatorname{Re}(c_n(K))] - \frac{\mu(b-\mu)}{b} < 0,\ \forall n \in \mathbb{Z}.$$

*Proof.* We denote $u_e$ as $u_e(\gamma)$ indicating $u_e$ is dependent on the parameter $\gamma$. For the moment, we choose $\gamma \geq \bar{\gamma}$ for a fixed $\bar{\gamma} > 0$, therefore $u_e(\gamma)$ is bounded above. For any $K$ satisfy the Assumption 2.5, we have $c_n(K) \to 0$ as $|n| \to \infty$. Therefore, for any $\varepsilon > 0$ fixed, there exists a $n_0$ such that

$$\inf_{n \geq n_0} \{\varepsilon + u_e(\gamma) \operatorname{Re}(c_n(K))\} \geq 0. \tag{2.8}$$

Notice if we increase $\gamma$, the equation (2.8) still holds. Thus for the finite set $\{0, 1, \ldots, n_0\}$ one can easily deduce

$$\lim_{\gamma \to \infty} \max_{n \in \{0,1,\ldots,n_0\}} \left\{ -\left(\frac{n\pi}{L}\right)^2 [\varepsilon + u_e(\gamma) \operatorname{Re}(c_n(K))] \right\} < 0.$$

The result follows. □

# 3 Bifurcation analysis

In this section we investigate pattern formation for Problem (1.3). Our study is based on bifurcation analysis and we will show that with a suitable choice for the model parameters and with an appropriate kernel function, Turing bifurcation and Turing-Hopf bifurcation can occur.

In this section, we always fix a specific kernel function $\rho = \rho_{\eta,s}$ as in (1.6). The corresponding $2L-$periodic kernel (see (1.4)) is denoted by $K = K_{\eta,s}$. This choice of the

above kernel function is motivated by Remark 2.10. Indeed the Fourier coefficients of $K_{\eta,s}$ can be explicitly computed and they read as follows (see Remark 2.2):

$$c_n\left(K_{\eta,s}\right) = \widehat{\rho_{\eta,s}}\left(\frac{n}{2L}\right) = \frac{\sin\left(n\eta\pi/L\right)}{n\eta\pi/L} e^{-i\frac{n\pi s}{L}}, \ \forall n \in \mathbb{Z}. \tag{3.1}$$

As we can see, the real part of the Fourier coefficients that changes signs will lead to the instability of the system. Note also that, with such kernel, namely (1.6), Assumption 2.5 is satisfied so that the results of the previous section holds true with such a choice.

## 3.1 Turing bifurcation

Throughout this subsection we consider Problem (1.3) with the kernel $\rho_{\eta,0}$ defined above in (1.6) with $s = 0$. We shall focus on the existence of Turing bifurcation for this problem.

We denote by $\mathcal{A}_\eta$ the linear operator defined in (2.2) with the kernel $K = K_{\eta,0}$ associated to the step function $\rho_{\eta,0}$ (see definition (1.4)). Next lemma describes that a proper choice of parameters can lead to spectral Turing bifurcation singularities.

**Lemma 3.1.** *Let $k_0 \in \mathbb{N}\backslash\{0\}$ and $\eta_0 > 0$ such that $L/(2\eta_0) \in \mathbb{N}$. Then there exists a pair of parameters $\varepsilon_0 > 0$ and $\gamma_0 > 0$, such that the eigenvalues $\lambda_n + f'(u_e) =: \widehat{\lambda}_n$ of the linear operator $\mathcal{A}_{\eta_0} + f'(u_e)$ satisfy*

$$\widehat{\lambda}_{\pm n_0} = 0, \ \widehat{\lambda}_n < 0, \ \text{for any } n \in \mathbb{Z}\backslash\{\pm n_0\},$$

*with $n_0 = \frac{L}{2\eta_0}(-1 + 4k_0) \in \mathbb{N} \setminus \{0\}$. In other words one can choose $k_0$ as large as we want, and set*

$$\varepsilon_0 = \frac{4\mu(b-\mu)}{b}\left(\frac{\eta_0}{-\pi + 4k_0\pi}\right)^2, \qquad \gamma_0 = \frac{b}{4(\mu\eta_0)^2}(-\pi + 4k_0\pi)$$

*such that $\widehat{\lambda}_{n_0}(= \widehat{\lambda}_{-n_0})$ is the only zero eigenvalue of multiplicity two while the other eigenvalues are negative.*

**Remark 3.2.** *Note that since the kernel $\rho_{\eta,0}$ is symmetric (hence is $K_{\eta,0}$) then $c_n(K_{\eta,0}) = c_{-n}(K_{\eta,0})$ for all $n \in \mathbb{Z}$. As a consequence $\widehat{\lambda}_n = \widehat{\lambda}_{-n}$ for all $n \in \mathbb{Z}$ and, with the notations of the above lemma one has*

$$\ker\left(\widehat{\lambda}_{n_0} - \mathcal{A}_{\eta_0}\right) = \text{span}\left(x \mapsto \cos\left(\frac{n_0\pi x}{L}\right), x \mapsto \sin\left(\frac{n_0\pi x}{L}\right)\right).$$

*Proof.* Our proof is divided in two steps. We first provide parameter conditions that ensure the existence of a unique pair (due to symmetry) of dominant eigenvalues and then we describe conditions for the dominant eigenvalue to be zero.

**First step:** Existence and uniqueness of a pair of dominant eigenvalues:

Set $u_e(\gamma) = \frac{b-\mu}{\gamma\mu}$. Then the eigenvalues of $\mathcal{A}_\eta + f'(u_e(\gamma))$ reads as follows (recall here that $s = 0$ in this subsection)

$$\widehat{\lambda}_n = -\left(\frac{n\pi}{L}\right)^2\left[\varepsilon + u_e(\gamma)\frac{\sin(n\eta\pi/L)}{n\eta\pi/L}\right] - \frac{\mu(b-\mu)}{b}, \forall n \in \mathbb{Z},$$

Due to symmetry we only consider $n \in \mathbb{N}$ and we set $\alpha = \varepsilon/\eta^2$, $\beta = (b-\mu)/(\gamma\mu\eta^2)$ and

$$\phi(x) := -\alpha x^2 - \beta x \sin x.$$

By using the above notations, we can rewrite the eigenvalues $\widehat{\lambda}_n$ as

$$\widehat{\lambda}_n = \phi(\frac{n\eta\pi}{L}) - \frac{\mu(b-\mu)}{b}. \tag{3.2}$$

The function $\phi$ is of transcendental type and it is not easy to consider the maximum directly. Thus we rewrite $\phi(x)$ as follows

$$\phi(x) = -\alpha\left(x + \frac{\beta \sin x}{2\alpha}\right)^2 + \frac{\beta^2 \sin^2 x}{4\alpha} \leq \frac{\beta^2}{4\alpha},$$

and $\phi$ reaches its maximum $\frac{\beta^2}{4\alpha}$ if and only if

$$x = -\frac{\beta}{2\alpha}\sin x, \ \sin^2 x = 1. \tag{3.3}$$

If we assume $x > 0$, the above equation has an unique solution which satisfies

$$x = \frac{\beta}{2\alpha}, \quad \sin x = -1.$$

Therefore, fix $k_0 \in \mathbb{N}\backslash\{0\}$ arbitrarily large and we choose $\gamma$ and $\varepsilon$ such that the product $\gamma\varepsilon$ satisfies

$$\frac{\beta}{2\alpha} \equiv \frac{b-\mu}{2\mu(\gamma\varepsilon)} = -\frac{\pi}{2} + 2k_0\pi. \tag{3.4}$$

With such a choice, (3.3) is satisfied and thus $\phi(\frac{b-\mu}{2\gamma\mu\varepsilon}) = \sup_{x\geq 0}\phi(x)$. Next note that

$$\frac{n\eta\pi}{L} = -\frac{\pi}{2} + 2k_0\pi \Longleftrightarrow n = L/(2\eta)(-1+4k_0).$$

Hence choosing $n_0 = L/(2\eta_0)(-1+4k_0) \in \mathbb{N}\setminus\{0\}$ one has

$$\frac{n_0\eta_0\pi}{L} = \frac{b-\mu}{2\gamma\mu\varepsilon} = -\frac{\pi}{2} + 2k_0\pi \Longleftrightarrow n_0 = \frac{L}{2\eta_0}(-1+4k_0). \tag{3.5}$$

By (3.2) and (3.5) one deduces

$$\widehat{\lambda}_{n_0} = \phi(\frac{n_0\eta_0\pi}{L}) - \frac{\mu(b-\mu)}{b} \text{ and } \widehat{\lambda}_{n_0} > \max_{n\in\mathbb{N}\backslash\{n_0\}}\widehat{\lambda}_n.$$

**Second step:** The dominant eigenvalue is zero.

To complete the proof of the lemma we have to fix $\varepsilon$ and $\gamma$ such $\widehat{\lambda}_{n_0} = 0$ keeping in mind that the product $\varepsilon\gamma$ is already fixed by (3.4).

In order to ensure that $\widehat{\lambda}_{n_0} = 0$ is the unique zero eigenvalue we fix $\gamma_0 > 0$ such that

$$\frac{b-\mu}{2\gamma_0\mu\eta_0^2}\left(-\frac{\pi}{2} + 2k_0\pi\right) \equiv \phi(\frac{n_0\eta\pi}{L}) = \frac{\mu(b-\mu)}{b}.$$

Hence $\varepsilon_0 > 0$ is fixed by (3.4) and we obtain that $\widehat{\lambda}_{n_0} = 0$ and $\widehat{\lambda}_n < 0$, for any $n \in \mathbb{N}\backslash\{n_0\}$. This completes the proof of the lemma. □

Now we will show the configuration of the parameters described above induces a Turing bifurcation using $\gamma$ as a bifurcation parameter, that will lead to the existence of a spatially heterogeneous stationary state. To that aim we fix $k_0 \in \mathbb{N}\setminus\{0\}$, $\eta_0 > 0$, $\varepsilon_0 > 0$ and $\gamma_0 > 0$ as in Lemma 3.1 as such that $n_0 \in \mathbb{N} \setminus \{0\}$. Next we rewrite the stationary equation associated to (2.6) by shifting the positive homogeneous steady state to 0. By setting $w := u - u_e(\gamma)$ we obtain the following stationary equation

$$0 = \mathcal{H}(w, \gamma) := Aw + \tilde{F}(w, \gamma), \quad w \in H^2, \tag{3.6}$$

where $A : D(A) \to L^2_{\text{per}}$ is the sectorial operator defined by

$$Aw = -w + \varepsilon_0 w'', \tag{3.7}$$

while $\tilde{F} : H^{2-\nu} \times (0, +\infty) \to L^2_{\text{per}}$ is defined by

$$\tilde{F}(w, \gamma) = \frac{b-\mu}{\gamma\mu} (K_{\eta_0} \circ w)'' + B(w, w) + \left( \frac{\mu^2}{b + \gamma\mu w} - \mu \right) w + w. \tag{3.8}$$

Therefore $\tilde{F}(0, \gamma) = 0$ for any $\gamma \in (0, +\infty)$ and

$$\partial_w \tilde{F}(0, \gamma) \cdot \tilde{w} = \frac{b-\mu}{\gamma\mu} (K_{\eta_0} \circ \tilde{w})'' - \frac{\mu(b-\mu)}{b} \tilde{w} + \tilde{w}.$$

Next the linear operator $\partial_w \mathcal{H}(0, \gamma) = \mathcal{A}_{\eta_0} + f'(u_e(\gamma))$ and its spectrum is given by

$$\sigma\left(\partial_w \mathcal{H}(0, \gamma)\right) = \left\{ \widehat{\lambda}_n(\gamma) = -\left(\frac{n\pi}{L}\right)^2 \left[ \varepsilon_0 + \frac{b-\mu}{\gamma\mu} c_n\left(K_{\eta_0}\right) \right] - \frac{\mu(b-\mu)}{b}, n \in \mathbb{Z} \right\}.$$

Due to Lemma 3.1 and the choice of the parameters we know that

$$\widehat{\lambda}_{\pm n_0}(\gamma_0) = 0 \text{ and } \widehat{\lambda}_n(\gamma_0) < 0, \, \forall n \neq \pm n_0. \tag{3.9}$$

Furthermore by the continuity of the eigenvalues with respect to the parameter $\gamma$, there exists $\delta_0 > 0$ small enough such that

$$\widehat{\lambda}_n(\gamma) < -\delta_0 < 0 : n \neq \pm n_0, \, \forall \gamma \in (\gamma_0 - \delta_0, \gamma_0 + \delta_0), \tag{3.10}$$

together with

$$\frac{d\widehat{\lambda}_{n_0}(\gamma_0)}{d\gamma} = \left(\frac{n_0\pi}{L}\right)^2 \frac{b-\mu}{\gamma_0^2\mu} c_{n_0}(K_{\eta_0}) < 0. \tag{3.11}$$

Now in order to investigate the existence of non trivial branch of solutions for (3.6) and provide a simple proof, we shall overcome the difficulty coming from the zero eigenvalue of multiplicity two (see Remark 3.2) by working on the close subspace of symmetric functions. To that aim let us consider for $s \in \mathbb{R}$, the closed subspace $H^s_\sharp$ defined by

$$H^s_\sharp = \{\varphi \in H^s : \varphi(-x) = \varphi(x), \, a.e. \, x \in (-L, L)\}.$$

Note that the above spaces can also be characterized using the symmetry of the Fourier coefficients as follows:

$$H^s_\sharp = \{\varphi \in H^s : c_n(\varphi) = c_{-n}(\varphi), \, \forall n \in \mathbb{Z}\}.$$

Using the above set of notations, we now state our Turing bifurcation result.

**Theorem 3.3** (**Turing bifurcation**). *Suppose $\eta_0, \varepsilon_0, \gamma_0$ and $n_0 \in \mathbb{N}$ are given as in Lemma 3.1 such that (3.9), (3.10) and (3.11) are satisfied. Then $(0, \gamma_0)$ is a bifurcation point for the stationary equation $\mathcal{H}(w, \gamma) = 0$ with $w \in H^2_\sharp$ in the sense that there exist $\sigma_0 > 0$ and a unique $C^1-$curve $(\gamma, \psi) : (-\sigma_0, \sigma_0) \to \mathbb{R} \times Z_\sharp$ such that*

$$\begin{cases} \mathcal{H}\left(\sigma \cos\left(\frac{n_0\pi\cdot}{L}\right) + \psi(\sigma), \gamma(\sigma)\right) = 0, \\ \gamma(0) = \gamma_0, \psi(0) = \psi'(0) = 0, \end{cases} \qquad \forall \sigma \in (-\sigma_0, \sigma_0).$$

*Herein $Z_\sharp \subset H^2_\sharp$ denotes the closed subspace defined by*

$$Z_\sharp = \{\varphi \in H^2_\sharp : \int_{-L}^{L} \varphi(x) \cos\left(\frac{n_0\pi x}{L}\right) dx = 0\}.$$

*Furthermore, there is a neighbourhood $\mathcal{V}$ of $(0, \gamma_0)$ in $H^2_\sharp \times (0, \infty)$ such that*

$$\mathcal{H}^{-1}(0) \cap \mathcal{V} = \{(0, \gamma) : \gamma \in (\mu, \infty)\} \cup \{(se_{n_0} + \psi(s), \gamma(s)) : |s| < \delta_0\}.$$

The proof of this theorem given below is based on the implicit function theorem. The idea of the proof goes back to Crandall and Rabinowitz [29]. Here we closely follow the proof of Theorem 13.4 of the monograph of Smoller [96].

**Remark 3.4.** *One can observe that, due to the translation invariance of (1.3), the above result allows us to obtain a non-symmetric family of heterogeneous stationary states for the equation $\mathcal{H}(w, \gamma) = 0$ in a neighbourhood of $(0, \gamma_0)$. Indeed, with the notations of the above theorem, for each $\sigma \in (-\sigma_0, \sigma_0)$ and each $\tau \in \mathbb{R}$ one has*

$$\mathcal{H}\left(w_\sigma(\cdot + \tau, \gamma(\sigma)\right) = 0,$$

*wherein we have set $w_\sigma(x) = \cos\left(\frac{n_0\pi}{L}x\right) + \psi(\sigma)(x)$, $x \in [-L, L]$. Furthermore from the numerical experiments provided in Figure 1.3, for each $\sigma$, the family $\{w_\sigma(\cdot + \tau)\}_{\tau \in \mathbb{R}}$ seems to be orbitally stable.*

*Proof.* To prove this result, we shall apply the implicit function theorem on a space of symmetric function such that the eigenspace associated to the zero eigenvalue is one dimensional. To that aim we consider the map

$$\begin{aligned} \mathcal{G}(\sigma, z, \gamma) &:= \mathcal{H}\left(\sigma \cos\left(\frac{n_0\pi\cdot}{L}\right) + \sigma z, \gamma\right) \\ &= A\left(\sigma \cos\left(\frac{n_0\pi\cdot}{L}\right) + \sigma z\right) + \tilde{F}\left(\sigma \cos\left(\frac{n_0\pi\cdot}{L}\right) + \sigma z, \gamma\right), \end{aligned}$$

that is of class $C^2$ and is defined on a small neighbourhood of $(0, 0, \gamma_0) \in \mathbb{R} \times Z \times (0, +\infty)$. Here $Z := \{\varphi \in H^2 : \int_{-L}^{L} \varphi(x) \cos\left(\frac{n_0\pi x}{L}\right) dx = 0\}$. As a consequence we fix $r > 0$ small enough and we consider the map $\mathcal{G}$ as defined from $(-r, r) \times B_Z(0, r) \times (\gamma_0 - r, \gamma_0 + r)$ with value in $H^0$. Here $B_Z(0, r) \subset H^2$ denotes the open ball in the Banach space $Z$ with center 0 and radius $r$ small enough. Now observe that, since the kernel $K_{\eta_0,0}$, is symmetric with respect to 0, the nonlinear operator $\mathcal{G}$ satisfies

$$\mathcal{G}(\sigma, \varphi, \gamma) \in H^0_\sharp, \text{ for all } |\sigma| < r, \varphi \in B_Z(0, r) \cap H^2_\sharp \text{ and } |\gamma_0 - \gamma| < r.$$

As a consequence we consider the map $\mathcal{G}_\sharp(\sigma,z,\gamma)=\mathcal{G}(\sigma,z,\gamma)$ defined from $(-r,r)\times B_{Z_\sharp}(0,r)\times(\gamma_0-r,\gamma_0+r)$ with values in $H^0_\sharp$ with $B_{Z_\sharp}(0,r)=B_Z(0,r)\cap H^2_\sharp$. As already mentioned it is a smooth map, namely of class $C^2$, on this open set and it furthermore satisfies

$$\mathcal{G}_\sharp(0,z,\gamma)=0,\ \forall(\gamma,z)\in(\gamma_0-r,\gamma_0+r)\times B_{Z_\sharp}(0,r).$$

Now to prove our result we consider the $C^1$ map $\mathcal{F}_\sharp$ defined from $(-r,r)\times B_{Z_\sharp}(0,r)\times(\gamma_0-r,\gamma_0+r)$ into $H^0_\sharp$ by

$$\mathcal{F}(\sigma,z,\gamma)=\begin{cases}\frac{1}{\sigma}\mathcal{G}_\sharp\left(\sigma,z,\gamma\right) & \text{if } \sigma\neq 0\\ \\ \partial_\sigma\mathcal{G}_\sharp\left(0,z,\gamma\right) & \text{if } \sigma=0.\end{cases}$$

Let us observe that one has

$$\mathcal{F}(0,0,\gamma_0)=\partial_\sigma\mathcal{G}_\sharp(0,0,\gamma_0)=\partial_w\mathcal{H}(0,\gamma_0)\cdot\mathrm{Re}\left(e_{n_0}\right)=\mathrm{Re}\left(\widehat{\lambda}_{n_0}(\gamma_0)e_{n_0}\right)=0.$$

Hence to prove our result we shall apply the implicit function theorem for the $C^1-$function $\mathcal{F}$ in the neighbourhood of the point $(\sigma,z,\gamma)=(0,0,\gamma_0)$. Thus to complete the proof of the theorem, it is sufficient to prove that the partial derivative operator $\partial_{(z,\gamma)}\mathcal{F}(0,0,\gamma_0)$ is a linear isomorphism from $Z_\sharp\times\mathbb{R}$ onto $H^0_\sharp$. To check the invertibility of $\partial_{(z,\gamma)}\mathcal{F}(0,0,\gamma_0)$ first note that one has

$$\partial_{(z,\gamma)}\mathcal{F}(0,0,\gamma_0)\cdot(z,\gamma)=\partial_w\mathcal{H}(0,\gamma_0)\cdot z+\gamma\widehat{\lambda}'_{n_0}(\gamma_0)\mathrm{Re}\ \left(e_{n_0}\right).$$

Let $h\in H^0_\sharp$ be given and let us solve the equation

$$\text{Find } (z,\gamma)\in Z_\sharp\times\mathbb{R} \text{ such that } \partial_{(z,\gamma)}\mathcal{F}(0,0,\gamma_0)\cdot(z,\gamma)=h.$$

However writing $h=\sum_{n\in\mathbb{Z}}h_ne_n$ with $(h_n)\in l^2(\mathbb{Z};\mathbb{C})$ and $h_n=h_{-n}$ for all $n\in\mathbb{Z}$ and projecting the above equation on the Hilbert basis $(e_n)$ the above equation reads as follows:

$$\begin{cases}\widehat{\lambda}_n(\gamma_0)z_n=h_n\,\forall n\in\mathbb{Z}\setminus\{\pm n_0\},\\ \gamma\widehat{\lambda}'_{\pm n_0}(\gamma_0)=h_{\pm n_0}.\end{cases}$$

Herein $z_n\in\mathbb{C}$ denotes the projection of $z$ on $e_n$. Since $\widehat{\lambda}'_{n_0}(\gamma_0)\neq 0$, $\widehat{\lambda}_n(\gamma)=\widehat{\lambda}_{-n}(\gamma)$ and $h_n=h_{-n}$ this yields

$$\begin{aligned}&z_n=z_{-n},\ \forall n\in\mathbb{Z}\backslash\{\pm n_0\},\\ &z_n=\frac{h_n}{\widehat{\lambda}_n(\gamma_0)}\,\forall n\in\mathbb{N}\setminus\{n_0\}\text{ and }\gamma=\frac{h_{n_0}}{\widehat{\lambda}'_{n_0}(\gamma_0)}.\end{aligned}$$

Hence the above equation has at most one solution in $Z_\sharp\times\mathbb{R}$. Furthermore since $\widehat{\lambda}_n(\gamma_0)\sim-n^2\frac{\pi^2\varepsilon_0}{L^2}$ as $|n|\to\infty$, the vector $(z,\gamma)$ defined by

$$z=\sum_{n\in\mathbb{Z}\backslash\{\pm n_0\}}\frac{h_n}{\widehat{\lambda}_n(\gamma_0)}e_n,\ \gamma=\frac{h_{n_0}}{\widehat{\lambda}'_{n_0}(\gamma_0)},$$

satisfies $z \in Z_\sharp$ and $\gamma \in \mathbb{R}$ as well as $\partial_{(z,\gamma)}\mathcal{F}(0,0,\gamma_0)\cdot(z,\gamma) = h$. Hence $\partial_{(z,\gamma)}\mathcal{F}(0,0,\gamma_0)$ is invertible from $Z_\sharp \times \mathbb{R}$ into $H^0_\sharp$. As a consequence, the implicit function theorem ensures the existence of a $C^1-$map $\sigma \mapsto (\phi(\sigma), \gamma(\sigma)) \in Z_\sharp \times \mathbb{R}$ defined in some neighbourhood of $\sigma = 0$, denoted by $(-\sigma_0, \sigma_0)$ for some $\sigma_0 > 0$, such that

$$\gamma(0) = \gamma_0 \text{ and } \phi(0) = 0,$$

and for all $\sigma \in (-\sigma_0, \sigma_0)$,

$$\begin{cases} z \in Z_\sharp, \quad \|z\|_{H^2} \le r, \quad |\gamma - \gamma_0| \le r, \\ \mathcal{G}(\sigma, z, \gamma) = 0 \end{cases} \Leftrightarrow z = \phi(\sigma) \text{ and } \gamma = \gamma(\sigma).$$

This completes the proof of the theorem by setting $\psi(\sigma) = \sigma\phi(\sigma) \in Z_\sharp$. □

We complete this section by the following stability result for the symmetric and spatially heterogeneous bifurcation branch. Let us notice that since the kernel $K_{\eta_0,0}$ is symmetric, the nonlinear maximal semiflow provided in Theorem 2.8 leaves the space $H^{2-\nu}_\sharp$ invariant. We denote the semiflow restricted on $H^{2-\nu}_\sharp$ by $U_\sharp(t)(\cdot)$. Next by using the results in [55, Theorem 6.3.2 p.178] and incorporating (3.9), (3.10) and (3.11), we obtain the following stability results of the bifurcated solution.

**Theorem 3.5.** *Let $\eta_0$, $\varepsilon_0$, $\gamma_0$ and $n_0$ be parameters as in Lemma 3.1 such that (3.9), (3.10) and (3.11) are satisfied. Then there exists $r > 0$ small enough and a nontrivial equilibrium $u_\gamma = u_\gamma(x) \in H^2_\sharp$ for $\gamma \in (\gamma_0 - r, \gamma_0 + r)$ such that it is unstable with respect to $U_\sharp$ (in $H^{2-\nu}_\sharp$) if $\gamma > \gamma_0$ but asymptotically stable for $\gamma < \gamma_0$.*

**Remark 3.6.** *As the Lemma 3.1 shows, $\phi(x) - \frac{\mu(b-\mu)}{b} = 0$ will be the curve above which the bifurcation occurs. Re-writing it explicitly reads as follows*

$$-\frac{\varepsilon}{\eta^2}x^2 - \frac{b-\mu}{\gamma\mu\eta^2}x\sin x = \frac{\mu(b-\mu)}{b}.$$

*Therefore, for any fixed $b$, $\mu$, $\eta_0$ and $L$ with $\frac{L}{2\eta_0} \in \mathbb{N}$. For $n \ge 0$, regarding $\varepsilon$ as a function of $\gamma^{-1}$, the curves*

$$\epsilon = -\frac{b-\mu}{\mu}\frac{\sin(n\eta\pi/L)}{n\eta\pi/L}\gamma^{-1} - \left(\frac{n\pi}{L}\right)^{-2}\frac{\mu(b-\mu)}{b} =: H_n(\gamma^{-1}),$$

*determines the stability region of the system. In fact, the spatially homogeneous steady state $u_e = u_e(\gamma)$ is locally stable in the region above all the curves $H_n(\gamma^{-1})$ for $n = \frac{L}{2\eta_0}(-1+4k)$ with $k \in \mathbb{N}\setminus\{0\}$.*

We continue this section with numerical experiments of (1.3) with the kernel $\rho_{\eta_0,0}$ (as defined in (1.6)). To that aim we fix the parameter values

$$L = 2,\ b = 1.5,\ \mu = 1.2 \text{ and } \eta = 1. \tag{3.12}$$

Note that $\frac{L}{2\eta} = 1$ so that the condition $\frac{L}{2\eta} \in \mathbb{N}$ is satisfied.

Figure 1.1 depicts the stability region and the different bifurcation curves corresponding to different $k = 1, 2, ..., 10$.

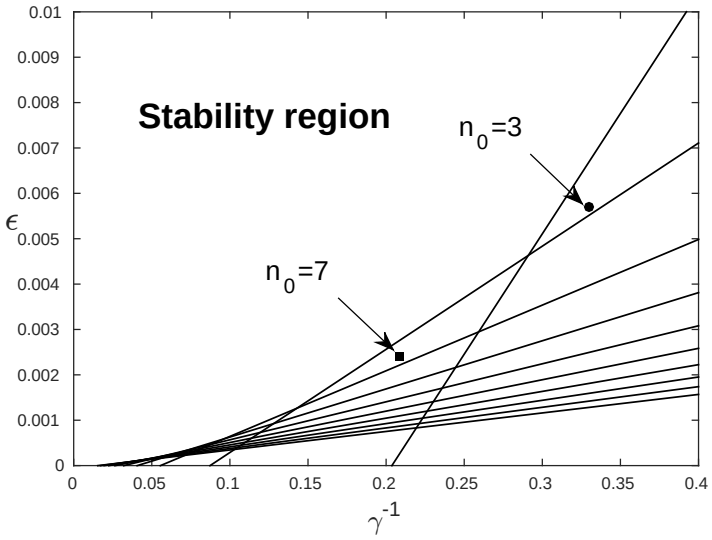


Figure 1.1: *Plots of the curves* $\varepsilon = H_n(\gamma^{-1})$ *with* $n = -1 + 4k$ *and* $k = 1, 2, \ldots, 10$. *They are straight lines and their slopes is decreasing with respect to* $n$, *hence to* $k$. *The stability region of the homogeneous steady state is above all these curves.*

Our numerical experiments are concerned with the behaviour of the nonlinear system (1.3) with the parameter (3.12). The choice of the parameter $\varepsilon$ and $\gamma$ are given in Table 3.14. These choices of parameters are presented in Figure 1.1 by the circle and square dots respectively. Both situations correspond to the instability of the homogeneous steady state and more deeply, both of these situations correspond to a unique pair of unstable eigenvalues $\widehat{\lambda}_{\pm n_0}$ for $n_0 = 3$ and 7 respectively. The results of the simulations are presented in Figure 1.2. Here we use the following Gaussian type function

$$u_0(x) = \frac{0.05}{\sqrt{2\pi\sigma^2}} e^{-\frac{x^2}{(2\sigma^2)}},\ x \in [-2, 2], \tag{3.13}$$

with $\sigma = 0.2$ as initial distribution. The simulations show that the instability of the homogeneous stationary state will give rise to a stable symmetric stationary pattern solutions. As we can observe from Figure 1.2, the dominant wave number of the solutions of the nonlinear equation (1.3) is exactly in accordance with the index $n_0$ where $\widehat{\lambda}_{\pm n_0}$ is the unique pair positive eigenvalues of the linear operator $\mathcal{A} + f'(u_e)$.

$$\begin{aligned} &\text{First configuration:} \quad (\varepsilon, \gamma) = (0.0056,\ 3.03)\,, \\ &\text{Second configuration:} \quad (\varepsilon, \gamma) = (0.0023,\ 4.80)\,. \end{aligned} \tag{3.14}$$

As we have mentioned in Remark 3.4, the symmetric heterogeneous steady state is translation invariant. Therefore, given a non-symmetric initial profile, we present the spatio-temporal evolution of the solution as in Figure 1.3 and the simulation indicates the solution will converge to a non-symmetric heterogeneous steady state. Therefore the family of steady states $\{w_\sigma(\cdot + \tau)\}_{\tau \in \mathbb{R}}$ should be orbitally stable.

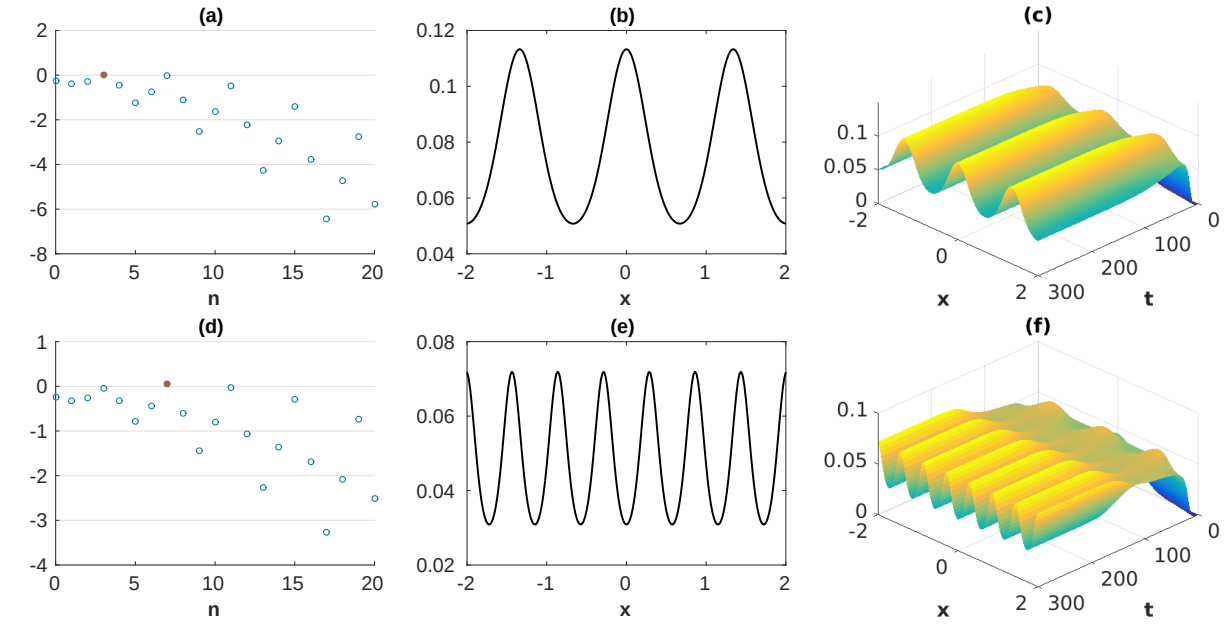


Figure 1.2: *Simulations* (1.3) *with parameters values* (3.12) *and* (3.14). *The upper row corresponds to* $(\varepsilon, \gamma) = (0.0056, 3.03)$ *while the bottom row to* $(\varepsilon, \gamma) = (0.0023, 4.80)$. *Figure* $(a), (d)$ *describe the spectrum of the linearized equation at the homogeneous steady state;* $(b), (e)$ *present the spatial distributions of the solution at a given large time* $T = 300$*; and,* $(c), (f)$ *present the spatio-temporal evolution of the solutions. The initial distribution is given in* (3.13) *with* $\sigma = 0.2$.

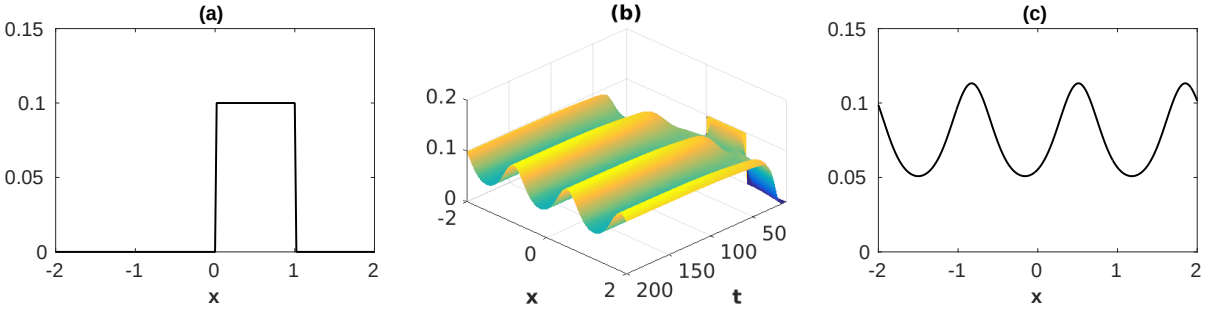


Figure 1.3: *Choosing parameters values as in* (3.12) *and the first configuration in* (3.14) *we obtain the above figures. Figure (a) presents the given non-symmetric initial value, figure (b) presents the spatio-temporal evolution of the solution and figure (c) presents the solution at a large time* $T = 200$ *when it is mostly stabilized close to a suitable shift of the symmetric stationary state. The other parameters are the same as in Figure 1.2 for the wave number* $n_0 = 3$.

## 3.2 Turing-Hopf bifurcation

In this section we continue the bifurcation analysis of Problem (1.3) by using the kernel function $\rho_{\eta,s}$ defined in (1.6). Here we shall vary the shift parameter $s \in \mathbb{R}$ which will lead us to what we call Turing-Hopf bifurcation and the existence of spatially heterogeneous time periodic solutions.

The reason that we call it Turing-Hopf bifurcation is based on the fact that by choosing the parameters of the system properly, it admits a Hopf bifurcation such that:
(i). We can find some mode $n_0$, as large as we want, such that the periodic orbit is tangent to the eigenfunction $e_{n_0}$;
(ii). It consists in the first Hopf bifurcation, which means that the equilibrium is passing from a stable to an unstable situation, by playing on the Hopf bifurcation parameter.

Let us mention that the first bifurcation is of particular interest in practice since this is the bifurcation that can be observed numerically.

As already mentioned that we will work on Problem (1.3) with the kernel $K_{\eta,s}$, the corresponding $2L-$periodic kernel associated to $\rho_{\eta,s}$ in (1.6), for some well chosen parameter $\eta > 0$ and $s \in (0, L]$. The corresponding linearized operator at the equilibrium $u_e = u_e(\gamma)$ is denoted by $\mathcal{A}_{\eta,s} + f'(u_e(\gamma))$.

Note that introducing the shift parameter $s$ implies that the step function is no longer symmetric so that the eigenvalues of $\mathcal{A}_{\eta,s}+f'(u_e(\gamma))$ can take complex – non real – values. In the next lemma we shall prove a result rather similar to the one stated in Lemma 3.1 with complex 'dominant' eigenvalues. More precisely, choosing the shifting parameter $s = \eta$, we shall prove that one can choose a mode $n_0 \geq 1$ such that the eigenvalues $\widehat{\lambda}_{n_0}$ and $\widehat{\lambda}_{-n_0}$ are a unique pair of purely imaginary eigenvalues satisfying the transversality condition with respect to the bifurcation parameter $\gamma$ while the other eigenvalues have negative real part.

**Lemma 3.7.** *Let $k_0 \in \mathbb{N}\backslash\{0\}$ be given and fix $s = \eta_0$ with $L/(4\eta_0) \in \mathbb{N}$. Let us denote by $\widehat{\lambda}_n(\gamma)$ the sequence of eigenvalues of $\mathcal{A}_{\eta_0,\eta_0} + f'(u_e(\gamma))$. Then there exist $\varepsilon_0 > 0$ and $\gamma_0 > 0$ such that*

$$\overline{\widehat{\lambda}_{n_0}(\gamma_0)} = \widehat{\lambda}_{-n_0}(\gamma_0),$$
$$\mathrm{Re}(\widehat{\lambda}_{\pm n_0}(\gamma_0)) = 0,\ \mathrm{Im}(\widehat{\lambda}_{n_0}(\gamma_0)) > 0,\quad \frac{d\mathrm{Re}(\widehat{\lambda}_{n_0})(\gamma_0)}{d\gamma} \neq 0,$$

*and*

$$\sigma\left(\mathcal{A}_{\eta_0,\eta_0} + f'(u_e(\gamma_0))\right) \cap i\mathbb{R} = \left\{\widehat{\lambda}_{n_0}(\gamma_0), \widehat{\lambda}_{-n_0}(\gamma_0)\right\},$$

*with $n_0 = \frac{L}{4\eta_0}(-1 + 4k_0) \in \mathbb{N}\backslash\{0\}$. Moreover, we have*

$$\mathrm{Re}(\widehat{\lambda}_n(\gamma_0)) < 0,\ \textit{for any } n \in \mathbb{Z}\backslash\{\pm n_0\}.$$

*Proof.* As mentioned above we set $s = \eta$. Hence recalling (3.1), the eigenvalues of $\mathcal{A}_{\eta,\eta} + f'(u_e(\gamma))$ take the following form, for any $n \in \mathbb{Z}$,

$$\mathrm{Re}(\widehat{\lambda}_n(\gamma)) = -\left(\frac{n\pi}{L}\right)^2\left(\varepsilon + u_e(\gamma)\frac{\sin(2n\eta\pi/L)}{2n\eta\pi/L}\right) - \frac{\mu(b-\mu)}{b},$$
$$\mathrm{Im}(\widehat{\lambda}_n(\gamma)) = \left(\frac{n\pi}{L}\right)^2\frac{\sin^2(n\eta\pi/L)}{n\eta\pi/L}u_e(\gamma).$$

Note that one has

$$\overline{\widehat{\lambda}_n(\gamma)} = \widehat{\lambda}_{-n}(\gamma),\ \forall n \in \mathbb{Z},\ \gamma > 0.$$

Let $k_0 \geq 1$ and $\eta_0 > 0$ such that $L(4\eta_0)^{-1} \in \mathbb{N}$ be given. Then using the same arguments as the ones in the proof of Lemma 3.1 one can find $\varepsilon_0 > 0$ and $\gamma_0 > 0$ such that

$$\begin{aligned} &\mathrm{Re}(\widehat{\lambda}_{\pm n_0}(\gamma_0)) = 0, \quad \frac{d\mathrm{Re}(\widehat{\lambda}_{n_0})(\gamma_0)}{d\gamma} \neq 0, \\ &\mathrm{Re}(\widehat{\lambda}_n(\gamma_0)) < 0, \text{ for any } n \in \mathbb{Z}\backslash\{\pm n_0\}, \end{aligned}$$

with $n_0 = \frac{L}{4\eta_0}(-1 + 4k_0)$, that is

$$\frac{2n_0\eta_0\pi}{L} \equiv \frac{b-\mu}{2\mu\gamma_0\varepsilon_0} = -\frac{\pi}{2} + 2k_0\pi.$$

To complete the proof of the lemma, it remains to check that $\mathrm{Im}(\widehat{\lambda}_{n_0}(\gamma_0)) > 0$. However simple computations yield

$$\mathrm{Im}(\widehat{\lambda}_{n_0}(\gamma_0)) = \left(\frac{n_0\pi}{L}\right)^2 \frac{\sin^2(-\frac{\pi}{4} + k_0\pi)}{n_0\eta_0\pi/L} u_e(\gamma_0) = \left(\frac{n_0\pi}{L}\right) \frac{1}{2\eta_0} u_e(\gamma_0) > 0.$$

And, this complete the proof of the lemma. □

The spectral configuration discussed in the above lemma will allow us to state the following Hopf bifurcation result for the evolution problem

$$\frac{dw(t)}{dt} = Aw(t) + \tilde{F}(w(t), \gamma),$$

wherein we have set, as in the previous subsection, $w(t) = u(t) - u_e(\gamma)$, the linear operator $A$ and the function $\tilde{F}$ are defined in (3.7) and (3.8) respectively.

In order to discuss our Hopf bifurcation theorem we first discuss the existence of a center manifold reduction for the above problem. To that aim, we fix $k_0 \geq 1$ and $\eta_0 > 0$ as in the previous lemma and let $\varepsilon_0 > 0$, $\gamma_0 > 0$ and $n_0 \geq 1$ be the parameter provided by this lemma. Next we include the parameter $\gamma$ into the state space and we consider the the following problem

$$\frac{d}{dt}\begin{pmatrix} w(t) \\ \gamma(t) \end{pmatrix} = L\begin{pmatrix} w(t) \\ \gamma(t) \end{pmatrix} + R\begin{pmatrix} w(t) \\ \gamma(t) \end{pmatrix},$$

wherein we have set

$$L = \begin{pmatrix} \left(A + \partial_w\tilde{F}(0,\gamma_0)\right) & 0 \\ 0 & 0 \end{pmatrix} \in \mathcal{L}\left(H^2 \times \mathbb{R}, H^0 \times \mathbb{R}\right),$$

and

$$R\begin{pmatrix} w \\ \gamma \end{pmatrix} = \begin{pmatrix} \tilde{F}(w,\gamma) - \partial_w\tilde{F}(0,\gamma_0)w \\ 0 \end{pmatrix}.$$

The function $R$ is defined and of class $C^\infty$ from a neighbourhood $\mathcal{V} \subset H^2 \times \mathbb{R}$ of $(w, \gamma) = (0, \gamma_0)$ into $H^0 \times \mathbb{R}$. Note also that $R$ satisfies $R\begin{pmatrix} 0 \\ \gamma_0 \end{pmatrix} = 0$ and $DR\begin{pmatrix} 0 \\ \gamma_0 \end{pmatrix} = 0$.

Next, the spectral configuration described in Lemma 3.7 ensures that

$$\sigma(L) \cap i\mathbb{R} = \left\{0, \widehat{\lambda}_{n_0}(\gamma_0), \overline{\widehat{\lambda}_{n_0}(\gamma_0)}\right\},$$

while $\sigma(L) \cap \{z \in \mathbb{C} : \operatorname{Re} z > 0\} = \emptyset$.
Note that the center space $\mathcal{E}_c$ is generated by $(e_{n_0}, 0)$, $(e_{-n_0}, 0)$ and $(0, 1)$.
Moreover because of the resolvent estimate (2.5) and due to the spectral configuration described in Lemma 3.7, there exist $\omega_0 > 0$ and $M > 0$ such that

$$\left\|(i\omega - L)^{-1}\right\|_{\mathcal{L}(H^0 \times \mathbb{R})} \leq \frac{M}{|\omega|}, \text{ for all } \omega \in \mathbb{R} \text{ such that } |\omega| > \omega_0,$$

Now since $H^2 \times \mathbb{R}$ and $H^0 \times \mathbb{R}$ are both Hilbert spaces, Theorem 2.20 in [53] applies and ensures the existence of smooth center manifold. Applying Hopf bifurcation theorem (see for instance [54]), this center manifold reduction allows us to obtain the Hopf bifurcation result.

**Theorem 3.8** (**Hopf Bifurcation**). *Let $k_0 \geq 1$ and $\eta_0 > 0$ be given such that $L/(4\eta_0) \in \mathbb{N}$. Let $\varepsilon_0 > 0$ and $\gamma_0 > 0$ be the parameters provided by Lemma 3.7. There exist $\sigma^* > 0$, two smooth functions $\sigma \mapsto \gamma(\sigma)$ and $\sigma \mapsto \omega(\sigma)$ defined on $(0, \sigma^*)$ such that for all $\sigma \in (0, \sigma^*)$ the equation*

$$\frac{dw(t)}{dt} = Aw(t) + \tilde{F}\left(w(t), \gamma(\sigma)\right), \ t \in \mathbb{R},$$

*has a non trivial $\omega(\sigma)-$time periodic solution $w(t)$. Furthermore one has*

$$\gamma(\sigma) = \gamma_0 + O(\sigma^2), \quad \omega(\sigma) = \frac{2\pi}{\operatorname{Im} \widehat{\lambda}_{n_0}(\gamma_0)} + O(\sigma^2) \text{ as } \sigma \to 0.$$

**Remark 3.9.** *The stability of the bifurcated periodic solution is studied in Appendix A by using the center manifold reduction and the study of the normal form. The stability of the Turing bifurcation presented in the previous section can also be investigated by using similar computations.*

**Remark 3.10.** *Another proof for the existence of the Hopf Bifurcation in our case can be found in the work by Crandall and Rabinowitz [30] by using the implicit function theorem. In fact, in our case the sectorial operator $A_{\eta_0,\eta_0} + \partial_w \tilde{F}(0, \gamma_0)$ satisfies $\sigma\left(A_{\eta_0,\eta_0} + \partial_w \tilde{F}(0, \gamma_0)\right) \cap i\mathbb{R} = \left\{\widehat{\lambda}_{n_0}(\gamma_0), \widehat{\lambda}_{-n_0}(\gamma_0)\right\}$ and the eigenvalues are simple. Moreover, the operator*

$$(\lambda - (A_{\eta_0,\eta_0} + \partial_w \tilde{F}(0, \gamma_0)))^{-1} : H^0 \to H^0$$

*is compact for any $\lambda$ in the resolvent set. Therefore, the hypothesis $(HL), (Hf)$ and $(H\beta)$ in [30] are satisfied and Theorem 1.11 in this aforementioned work ensures the existence and uniqueness of the Hopf bifurcation in a small neighbourhood of $(0, \gamma_0) \in H^{2-\nu} \times \mathbb{R}_+$.*

We continue this section by numerical experiments for System (1.3) with the kernel (1.6). To that aim, we fix the following parameter sets

$$b = 1.5,\ \mu = 1.2,\ L = 2,\ \eta = \eta_0 = s = 0.5. \tag{3.15}$$

Note that one has $L/(4\eta_0) = 1 \in \mathbb{N}$.

We consider two situations, close to the Turing-Hopf bifurcation point described above, that correspond to the parameters

$$\begin{aligned} &\text{First configuration:} \quad (\varepsilon, \gamma) = (0.0023,\ 4.8)\,, \\ &\text{Second configuration:} \quad (\varepsilon, \gamma) = (0.00084,\ 8.4)\,. \end{aligned} \tag{3.16}$$

With such choices the spectrum configuration reads as follows: $\widehat{\lambda}_{\pm n_0}$ are the only eigenvalues with positive real part and all the other eigenvalues have negative real parts. Moreover $\mathrm{Re}\,(\widehat{\lambda}_{\pm n_0})$ is close to zero and $\mathrm{Im}(\widehat{\lambda}_{\pm n_0}) \neq 0$. This holds true for $n_0 = 7$ and $n_0 = 11$ respectively for the two parameter sets $(\varepsilon, \gamma)$ mentioned above.

With the parameters described above and equipped with the same initial data as the one use in Figure 1.2 (see (3.13)), the spatio-temporal evolution for the solutions of (1.3) is presented in Figure 1.4 for the two parameter configurations in (3.16).

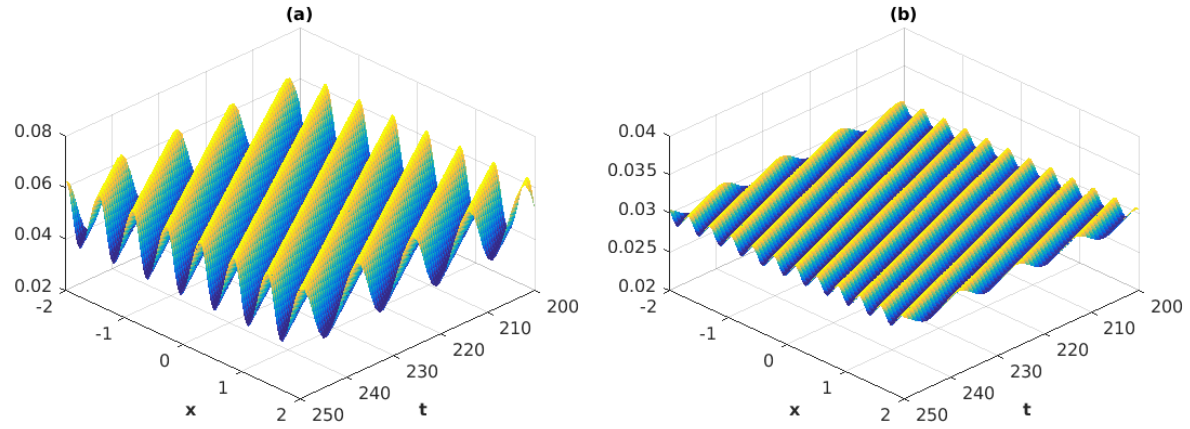


Figure 1.4: *In this figure we fix the parameter values as in* (3.15) *and* (3.16). *We observe a spatio-temporal evolution of the solutions corresponding in* (*a*) *(respectively in* (*b*)*) to the first configuration (respectively the second configuration) of the parameters in* (3.16).

These simulations show that the solutions takes the form of a periodic wave train solution. Heuristically the first order approximation of the bifurcated solutions take the form

$$\begin{aligned} u(t,x) &\approx u_e + \mathrm{Re}\left(a(\gamma)e^{i\omega t}e_{n_0}(x)\right) + h.o.t, \quad \text{for some constant } a(\gamma) \in \mathbb{C}\setminus\{0\} \\ &= u_e + |a(\gamma)|\cos\left(\omega t + \frac{n_0\pi}{L}x + \varphi\right) + h.o.t, \end{aligned} \tag{3.17}$$

where $\omega \approx \mathrm{Im}(\widehat{\lambda}_{n_0})$ and $\varphi \in \mathbb{R}$ is a phase number while the amplitude $|a(\gamma)|$ of the oscillating solution depends on the bifurcation parameter $\gamma$. Moreover from the normal

form reduction provided in Appendix 5.1 we have $|a(\gamma)| \sim a_* \sqrt{|\gamma - \gamma_0|}$ for some constant $a_*$ when $0 < \gamma - \gamma_0 \ll 1$ or $0 < \gamma_0 - \gamma \ll 1$ depending on the nature (supercritical or subcritical) of the Hopf bifurcation. Therefore, the expression in (3.17) roughly explains the spatio-temporal pattern observed in Figure 1.4. Moreover the numerical comparison of the wave lengths of the solutions in Figure 1.4 and the above expression are in accordance.

We continue this section by exploring an other type of kernel function $\rho$. And we show that instabilities, and more precisely Turing-Hopf bifurcation, may also occur for some bi-modal kernel. Here as an example, we consider two identical Gaussian functions, one shifted to the left and one shifted to the right, namely

$$\rho_2(x) = \frac{1}{2}\left(G(x+s_1) + G(x-s_2)\right), \text{ with } G(x) := e^{-\pi x^2},$$

and wherein $s_1$ and $s_2$ are two positive parameters. Here we restrict ourselves to a numerical exploration of Problem (1.1)-(1.2) with such a kernel function. However similar analytical results as the ones presented above can be obtained for this bi-modal example (see Remark 3.11 below). Note also that such a choice of multi-modal kernel is biologically relevant when we consider the preferred sensing radius of a certain type of cell.
When kernel $\rho_2$ is considered, the Fourier transform of this kernel can be calculated explicitly and we have

$$\widehat{\rho_2}(\xi) = \frac{1}{2} e^{-\pi\xi^2}\left[e^{2i\pi s_1 \xi} + e^{-2i\pi s_2 \xi}\right]. \tag{3.18}$$

Therefore, according to (2.7), the real part and imaginary part of the eigenvalues for the system (1.3) are given as follows

$$\begin{aligned} \mathrm{Re}(\lambda_n) &= -\left(\frac{n\pi}{L}\right)^2 \left[\epsilon + u_e \mathrm{Re}\left(\widehat{\rho_2}\left(\frac{n}{2L}\right)\right)\right] - \frac{\mu(b-\mu)}{b}, \\ \mathrm{Im}(\lambda_n) &= -\left(\frac{n\pi}{L}\right)^2 u_e \,\mathrm{Im}\left(\widehat{\rho_2}\left(\frac{n}{2L}\right)\right), \; n \in \mathbb{Z}. \end{aligned} \tag{3.19}$$

In the following simulation, we fix parameters $b, \mu$ and $L$ as in (3.15) while we take

$$(\varepsilon, \gamma) = (0.01,\, 0.2), \quad s_1 = 0.4,\, s_2 = 0.3. \tag{3.20}$$

By choosing the above parameters one can check that when $n = \pm 4$, $\lambda_n$ is the only pair of eigenvalues which has positive real part and we plot the distribution of the eigenvalues on the complex plane in Figure 1.5 (a). Using the same initial distribution in Figure 1.2, the numerical simulation of (1.3) with kernel $\rho_2$ is presented in Figure 1.5 (b).

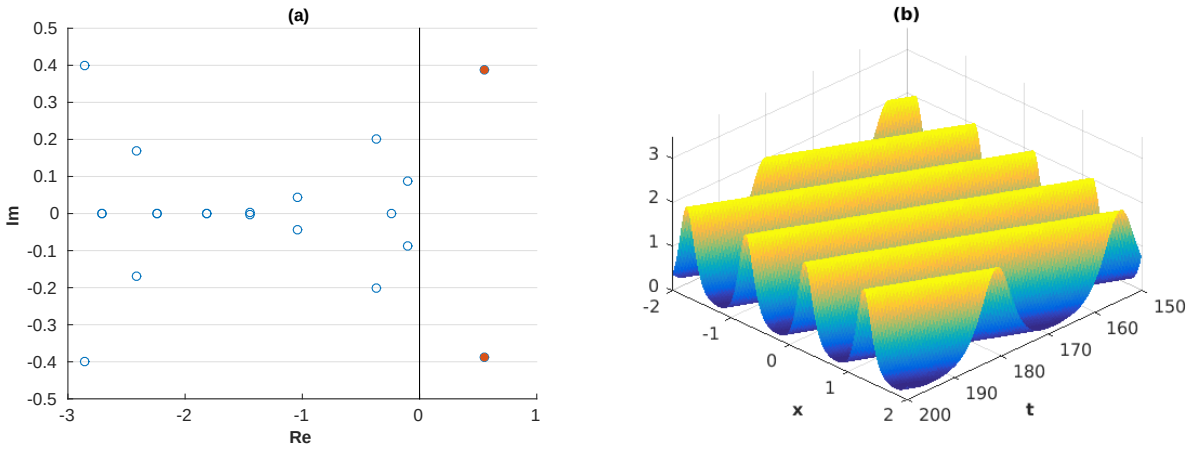


Figure 1.5: *In this figure we fix the parameter values as in* (3.16) *and* (3.20). *In Figure* (*a*) *we plot the eigenvalues of the linearized equation by* (3.19) *in the complex plane for* $n = -10, -9, .., 9, 10$. *By choosing the parameters in configuration* (3.20), *there is only one pair of eigenvalues, namely* $\lambda_{\pm 4}$, *with a positive real part (see the solid points). We observe a corresponding spatio-temporal evolution of the solutions in* (*b*). *The simulation shows the bi-modal kernels can also lead to instability.*

**Remark 3.11.** *If we take* $\gamma$ *as a bifurcation parameter and choose appropriate parameters* $\varepsilon$, $s_1$ *and* $s_2$, *a similar spectral analysis as in Lemma 3.7 for the linearized equation with kernel* $\rho_2$ *can be performed by using the explicit formula in* (3.18) *and* (3.19). *And one may use similar arguments as the ones developed for the proof of Theorem 3.8 to prove the existence of a Hopf bifurcation for the bi-modal case.*

# 4 Conclusion and discussion

In this Chapter we discussed some dynamical properties of Problem (1.3). Depending on the kernel function $\rho$, we are able first to discuss the stability and instability of the unique homogeneous positive steady state. A bifurcation analysis has been performed to understand emerging complex patterns when the positive homogeneous steady state becomes unstable. With a symmetric step function kernel, Turing bifurcation of equilibrium may occur. As a result we obtain the existence of a stable branch of spatially heterogeneous steady states. More surprisingly when this symmetry is broken by shifting the step function, the homogeneous steady state may undergo what we have called Turing-Hopf bifurcation yielding the existence of a branch of spatially heterogeneous and time periodic solutions.

It is also interesting to recognize the complexity raised by the nonlinear and nonlocal diffusion compare to nonlinear but local diffusion equation. As we can see from our bifurcation analysis, when $\varepsilon$ goes to 0, rich dynamical behaviors emerge from the model (1.3). This is also true without vital dynamic term, *i.e.* whenever $f = 0$.

The case of zero viscosity, i.e., $\varepsilon = 0$, is also of particular interest. From the spectral analysis of the operator $\mathcal{A}$ with kernel $\rho_{\eta,s}$, we can expect that the frequencies of oscillating solutions will become higher if the viscosity coefficient becomes small. This may be due

to the increasing number of positive eigenvalues in such case. Moreover, we point out other kernels with their Fourier transform changing signs will present the similar complex dynamics as the one observed for the step function kernel when $\varepsilon \ll 1$ is small enough. To illustrate this issue we consider the $C^\infty$ kernel

$$\rho_\sharp(x) = c_0 e^{\frac{1}{x^2-1}} \chi_{(-1,1)}(x), \tag{4.1}$$

where the constant $c_0$ is defined by $c_0 := 1/\int_{-1}^{1} \rho_\sharp(x)dx$. We furthermore denote by $\rho_{\eta,\sharp}(x) := \frac{1}{\eta}\rho_\sharp(\frac{x}{\eta})$ the function $\rho_\sharp$ with scaling parameter $\eta > 0$. However, unlike the step kernel, the Fourier coefficient of $\rho_{\eta,\sharp}$ does not have an explicit form, here we give in Figure 1.6 a numerical illustration of the following map

$$n \longmapsto -\left(\frac{n\pi}{L}\right)^2 \widehat{\rho}\left(\frac{n}{2L}\right), \ n \in \mathbb{Z}$$

for step function kernel $\rho = \rho_{\eta,0}$ and $\rho = \rho_{\eta,\sharp}$. Note that $\widehat{\rho}_\eta\left(\frac{n}{2L}\right) = \widehat{\rho}\left(\frac{n\eta}{2L}\right)$. These numerical illustrations are performed with the fixed values $L = 4$ and $\eta = 0.8$. By the symmetry of Fourier coefficients, here we plot these maps for $n = 0, 1, 2, \ldots, 50$.

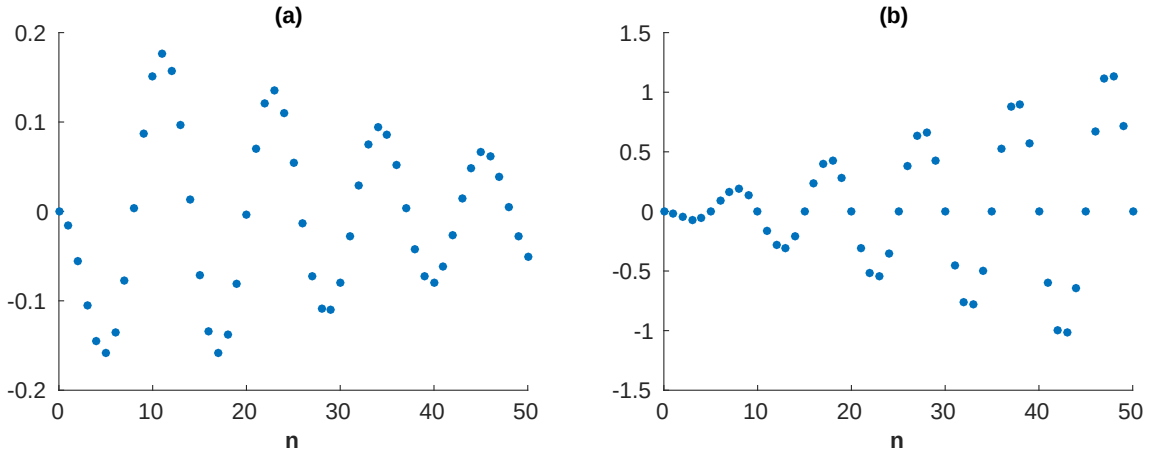


Figure 1.6: *In this figure we plot of* $n \mapsto -\left(\frac{n\pi}{L}\right)^2 \widehat{\rho}\left(\frac{n\eta}{2L}\right)$ *(with* $n = 0, 1, \ldots, 50$*). The Figure* $(a)$ *and* $(b)$ *correspond respectively to the smooth function* $\rho = \rho_{\eta,\sharp}$ *defined in* (4.1) *and to the step function* $\rho = \rho_{\eta,0}$ *defined in* (1.6)*. In both cases we fix* $L = 4$ *and* $\eta = 0.8$*. The blue dots corresponds to the eigenvalues of the linear operator* $\mathcal{A}$ *whenever* $\varepsilon = 0$*.*

As we can see in Figure 1.6 $(a)$ a smooth kernel can also leads to an infinite number of positive eigenvalues. Also the Figure (b) should be compared to the Figure 1.3 $(a)$ and $(d)$ in which $\varepsilon > 0$ plays an crucial role to get only one positive eigenvalue. The existence of positive Fourier coefficients will result in the essential difference between nonlinear diffusion and nonlocal diffusion. Notice when $\eta$ is small, we have , at least formally, $\partial_x(\rho_\eta * u(t,\cdot)) \approx \partial_x u(t,\cdot)$ so that (1.3) with $f(u) = 0$, with $\varepsilon \ll 1$ and $\eta \ll 1$ should be a good approximation of porous medium equation

$$\partial_t u(t,x) = \partial_x \left(u \partial_x u(t,x)\right), \quad x \in \mathbb{R}, \quad t > 0. \tag{4.2}$$

To explore numerically the connection between (1.3) with $f(u) = 0$ and (4.2) we consider the so-called Barenblatt solution to equation (4.2) that is defined as

$$u_{\mathbf{B}}(t,x,C) = t^{-1/3} \max(C - k|x|^2 t^{-2/3}, 0),$$

where $C > 0$ denotes any positive constant (see for instance [104]). In the numerical experiments below we fix $C = 0.1$ and we fix the scaling parameter for the kernel function $\eta = 0.8$. In the sequel we shall make use of the notation $\rho_0$ and $\rho_\sharp$ to denote $\rho_{\eta,0}$ and $\rho_{\eta,\sharp}$ respectively. To go further we also introduce the viscosity threshold associated to the kernel $\rho$

$$\varepsilon_0 := -u^* \min_{n\in\mathbb{N}} \left\{ \widehat{\rho}(\frac{n\eta}{2L}) \right\},$$

wherein we have set $u^* = \frac{1}{2L}\int_{-L}^{L} u_0(x)dx$, the total mass of $u_0$ in $[-L, L]$.

Next we select the initial distribution $u_0(x) := u_{\mathbf{B}}(T_1, x, 0.1)$ for $T_1 = 3$ and $x \in [-4, 4]$. The simulation starts from time $T_1$ to time $T_2 = 5, 10$ and 50 respectively. With such an initial data one has $u^* = 0.0258$ while, we can obtain the threshold values for two kernels

$$\varepsilon_0 = \begin{cases} 0.0025 \text{ for } \rho = \rho_0, \\ 0.0056 \text{ for } \rho = \rho_\sharp. \end{cases}$$

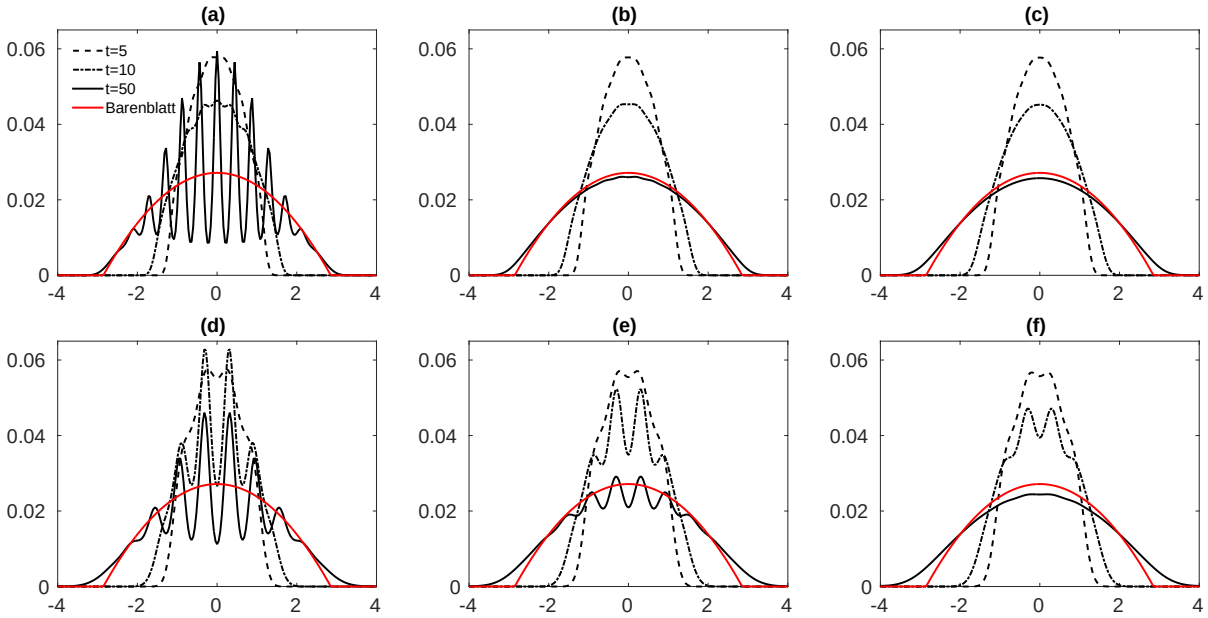


Figure 1.7: *Numerical simulations of* (1.3) *for the two kernels* $\rho_\sharp$ *and* $\rho_0$ *with initial data* $u_0(x) := u_{\boldsymbol{B}}(3, x, 0.1)$ *and without reaction term (i.e.* $f = 0$*). We plot the solutions at time* $T_2 = 5, 10, 50$ *in each sub-figure and we compare the simulation at the final time* $T = 50$ *with Barenblatt solution* $u_{\boldsymbol{B}}(50, x, 0.1)$ *(red curves). Figures (a)-(c) on the top correspond to the solutions with kernel* $\rho_\sharp$ *and viscosity coefficient* $\varepsilon = 0.0015, 0.0025$ *and* $0.0035$ *respectively; while figures (d)-(f) in the bottom correspond to the kernel* $\rho_0$ *and the viscosity* $\varepsilon = 0.0046, 0.0056$ *and* $0.0066$ *respectively.*

**Remark 4.1.** *The numerical experiments in Figure 1.7 are performed so that the space step* $\Delta x$ *is chosen rather small in order to overcome some difficulties linked with the high concentration of the kernel (due to the scaling parameter* $\eta$*). We choose* $\Delta x \leq 0.1\eta$ *so that we set a mesh with more than 20 points in the interval* $[-\eta, \eta]$*. The numerical method is discussed in the appendix.*

As we can see from Figure 1.7, when $\eta$ and $\varepsilon$ are small, the nonlocal model (1.3) with the above two kernels does not provide a good approximation of the solution of the nonlinear diffusion (4.2). As we can see from the Figure 1.7, when $\varepsilon = \varepsilon_0 - 10^{-3}$, the solutions with both kernels $\rho_\sharp$ and $\rho_0$ in Figure (a) and (d) differ remarkably from the Barenblatt solution of the porous medium equation. While when we set $\varepsilon = \varepsilon_0 + 10^{-3}$, the simulations (c) and (f) at time $t = 50$ are relatively good approximation of Barenblatt solution.

# Chapter 2

# Asymptotic behavior of a nonlocal advection system with two populations

## Contents

# 1 Introduction

In this work, we study a two-species model with nonlocal advection

$$\begin{cases} \partial_t u_1(t,x) + \operatorname{div}\left(u_1(t,x)\mathbf{v}(t,x)\right) = u_1(t,x)h_1(u_1(t,x),u_2(t,x)), \\ \partial_t u_2(t,x) + \operatorname{div}\left(u_2(t,x)\mathbf{v}(t,x)\right) = u_2(t,x)h_2(u_1(t,x),u_2(t,x)), \end{cases} \quad t>0,\ x\in\mathbb{R}^N, \tag{1.1}$$

and the velocity field $\mathbf{v} = -\nabla P$ is derived from pressure $P$

$$P(t,x) := \left(\rho * (u_1+u_2)(t,\cdot)\right)(x),$$

where $*$ is the convolution in $\mathbb{R}^N$. Suppose system (1.1) is supplemented with a periodic initial distribution

$$\mathbf{u}_0(x) := \begin{pmatrix} u_1(0,x) \\ u_2(0,x) \end{pmatrix} \in \mathbb{R}^2_+ \text{ where } \mathbf{u}_0 \text{ is a } 2\pi\text{–periodic function in each direction.} \tag{1.2}$$

We consider the solutions of system (1.1) which are **periodic in space**. Here a function $u(x)$ is said to be $2\pi$**-periodic in each direction** (or for simplicity **periodic**) if

$$u(x+2k\pi) = u(x),\ \forall k\in\mathbb{Z}^N, x\in\mathbb{R}^N.$$

When $u(x)$ is periodic, we can reduce the convolution to the $N$–dimensional torus $\mathbb{T}^N := \mathbb{R}^N/2\pi\mathbb{Z}^N$ by the following observations

$$\begin{aligned} \left(\rho * u\right)(x) &= \int_{\mathbb{R}^N} \rho(x-y)u(y)\mathrm{d}y \\ &= \sum_{k\in\mathbb{Z}^N}\int_{[0,2\pi]^N} \rho(x-(y+2k\pi))u(y+2k\pi)\mathrm{d}y \\ &= \sum_{k\in\mathbb{Z}^N}\int_{[0,2\pi]^N} \rho(x-y-2k\pi)u(y)\mathrm{d}y. \end{aligned}$$

Hence we can reformulate as

$$\left(\rho * u\right)(x) = \frac{1}{(2\pi)^N}\int_{[0,2\pi]^N} K(x-y)u(y)\mathrm{d}y,$$

where $K$ is again $2\pi$–periodic in each direction and defined by

$$K(x) = (2\pi)^N \sum_{k\in\mathbb{Z}^N} \rho(x+2\pi k),\ x\in\mathbb{R}^N.$$

The fast decay of $\rho$ is necessary to ensure the convergence of the above series (see Remark 1.3 for details). Now we can rewrite the velocity field $\mathbf{v}$ as follows:

$$\mathbf{v}(t,x) = -\nabla\left[K\circ(u_1+u_2)(t,\cdot)\right](x), \tag{1.3}$$

where $\circ$ denotes the convolution operator on the $N$–dimensional torus $\mathbb{T}^N := \mathbb{R}^N/2\pi\mathbb{Z}^N \simeq [0,2\pi]^N$ defined for each $2\pi$-periodic in each direction and measurable functions $\varphi$ and $\psi$ by

$$\left(\varphi\circ\psi\right)(x) = |\mathbb{T}^N|^{-1}\int_{\mathbb{T}^N}\varphi(x-y)\psi(y)\mathrm{d}y.$$

Our motivation for this problem comes from a cell monolayer co-culture experiment in the study of human breast cancer cells. In [88, Figure 1], two types of cells grow meanwhile form segregated islets over 7 days and the growth stops when they are locally saturated.

In this work, we model this mechanism by using a nonlocal advection system with contact inhibition. As we will see, our model captures the finite propagating speed in cell co-culture. In the context of cell sorting, the impact of cell adhesion and repulsion on the cell movement and pattern formation has been studied by many authors. We refer to the work of Armstrong, Painter and Sherratt [3] and Painter et al. [86]. From a more general perspective, our study is connected to cell segregation and border formation. Taylor et al. [99] concluded the heterotypic repulsion and homotypic cohesion can account for cell segregation and border formation. We also refer the readers to Dahmann et al. [34] and the references therein for more about boundary formation with its application in biology. These observations and results in biological experiments lead us to consider a nonlocal advection system which is able to explain the phenomena such as cell finite propagation speed and segregation. The segregation property was brought up in the 80's by using cross diffusion by Shigesada, Kawasaki and Teramoto [95] and Mimura and Kawasaki [74]. Since then, the cross diffusion has been widely studied and we refer to Lou and Ni [69, 70] for more results about this subject.

The well-posedness of the nonlocal advection model with nonlinear diffusion has been considered by Bertozzi and Slepcev [11] and Bedrossian et al. [7] on a bounded domain $\Omega \subset \mathbb{R}^N$ with non-flux boundary condition. Bertozzi et al. [12, 13] studied the finite time blowup of solutions and the well-posednees in $L^p$ theory of such nonlocal advection equations in multidimensional space. For the studies of the long-time asymptotics of nonlocal equations, we refer to Bodnar and Velazquez [17] and Raoul [91]. The traveling wave solution of such nonlocal equations with or without linear diffusion were considered by many authors, we refer the readers to [9, 68, 75] for a connection with swarming models. Hamel and Henderson [52] investigated the existence of the traveling wave solution under a general assumption on the kernel with logistic source $f(u) = u(1-u)$. We also mention that system (1.1) is also related to hyperbolic Keller-Segel equation (see Perthame and Dalibard [90]).

The single species model of equation (1.1) has been studied by Ducrot and Magal in [39] (see the derivation of the model therein). Compared to the work in [39], one of the technical difficulties in this work is that we do not have the $L^2$ uniform boundedness of the solution a priori. This is because we allow nonlinear function $h$ to be more general (see Assumption 1.1 and 4.1). This difficulty obliges us to find another method to prove the $L^\infty$ uniform boundedness of solutions (see Lemma 4.9, Remark 4.11 and Theorem 4.10). Moreover, we prove the segregation property for two species by using the notion of solution integrated along the characteristics. Assumption 4.4 on the positivity of Fourier coefficients enables to construct a decreasing energy functional, this condition has also been considered in [9] and [39]. Using this important property, we can prove the $L^\infty$ convergence of the sum of the two species when the initial distribution is strictly positive (see Corollary 4.12). Furthermore, the segregation property preserves when $t$ tends to infinity in the sense of narrow convergence (see Lemma 5.15). In Section 7, by using numerical simulations, we obtain some results which are not proved theoretically.

**Assumption 1.1.** *For $i = 1, 2$, suppose $h_i : \mathbb{R}^2_+ \to \mathbb{R}$ are of class $C^1$ satisfying*

$$\sup_{u_1,u_2\geq 0} h_i(u_1, u_2) < \infty, \qquad \sup_{u_1,u_2\geq 0} \partial_{u_j} h_i(u_1, u_2) < \infty, \quad j = 1, 2.$$

An example of function $h_i$ is the following function

$$h_i(u_1, u_2) = \lambda_i(1 - (u_1 + u_2)).$$

Therefore, the reaction term $u_i\, h_i(u_1, u_2)$ is of Lotka-Volterra type.

Motivated by the model derived from Ducrot et al. in [38] which describes the contact inhibition (i.e. cells stop growing when they are locally saturated), we would like to use the following non-linear function.

$$h_i(u_1, u_2) = \frac{b_i}{1 + \gamma_i\,(u_1 + u_2)} - \mu_i,$$

where $b_i > 0$ is the division rate, $\mu_i > 0$ is the mortality rate and $\gamma_i > 0$ is the coefficient representing the dormant phase of cells (see [38] for details). In such a case the map $h_i$ is bounded from below therefore we can not apply the same arguments as in [39] to obtain an $L^\infty$ bound for the solution. This shows that our results can be applied to a larger class of nonlinearity than [39].

**Assumption 1.2.** *The kernel $K : \mathbb{R}^N \to \mathbb{R}$ is a $\mathbb{T}^N-$ periodic function of class $C^m$ on $\mathbb{R}^N$ for some integer $m \geq \frac{N+5}{2}$.*

**Remark 1.3.** *The above regularity Assumption 1.2 can be reduced to $m \geq 3$ in proving the existence and uniqueness of solutions. The higher regularity is crucial for Lemma 4.9. For the dimension $N \leq 3$, the regularity condition in Assumption 1.2 is always satisfied whenever $K \in C^4$. For the choice of $\rho$ in (1.1), it suffice to choose $\rho \in C^m(\mathbb{R}^N)$ satisfying for any $\varepsilon > 0$ and multi-index $\alpha$ with $|\alpha| \leq m$, there exists $M > 0$ such that for any $|x| \geq M$*

$$|D^\alpha \rho(x)| \leq C/|x|^{N+\varepsilon},$$

*where $C$ is a positive constant. For each multi-index $\alpha$ with $|\alpha| \leq m$, the series*

$$x \longmapsto \sum_{k\in\mathbb{Z}^N} D^\alpha \rho(x + 2\pi k)$$

*is uniformly converging on $\mathbb{T}^N$. Hence, $K$ satisfies Assumption 1.2.*

The plan of this work is the following. In Section 2, we investigate the existence and uniqueness of solutions integrated along the characteristics. In Section 3, we study the segregation property. In Sections 4 and 5, the asymptotic behavior of segregated solutions is studied by Young measures (a generalization of $L^\infty$ weak $*$–convergence). Section 6 is devoted to numerical simulations where we explore some further results that are not proved analytically, these numerical simulations complement our theoretical part.

## 2 Solution integrated along the characteristics

In this section we study the existence and uniqueness of solution for (1.1)-(1.3) with initial data $\mathbf{u}_0 \in L^\infty_{per}\left(\mathbb{R}^N\right)^2$.

Before going further, let us introduce some notations that will be used in the following. For each $k \in \mathbb{N}$, let us denote by $C^k_{per}\left(\mathbb{R}^N\right)$ the Banach space of functions of class $C^k$ from $\mathbb{R}^N$ into $\mathbb{R}$ and $[0,2\pi]^N$–periodic endowed with the usual supremum norm

$$\|\varphi\|_{C^k} = \sum_{p=0}^{k} \sup_{x\in\mathbb{R}^N} \left|D^p\varphi(x)\right|.$$

For each $p \in [1,+\infty]$, let us denote by $L^p_{per}\left(\mathbb{R}^N\right)$ the space of measurable and $[0,2\pi]^N$–periodic functions from $\mathbb{R}^N$ to $\mathbb{R}$ such that

$$\|\varphi\|_{L^p} := \|\varphi\|_{L^p\left((0,2\pi)^N\right)} < +\infty.$$

Then $L^p_{per}\left(\mathbb{R}^N\right)$ endowed with the norm $\|\varphi\|_{L^p}$ is a Banach space. We also introduce its positive cone $L^p_{per,+}\left(\mathbb{R}^N\right)$ consisting of all the functions in $L^p_{per}\left(\mathbb{R}^N\right)$ that are almost everywhere positive.

**Remark 2.1.** *When we study the product space $C^k_{per}\left(\mathbb{R}^N\right)^n, L^p_{per}\left(\mathbb{R}^N\right)^n$ when $n \in \mathbb{N}$, for simplicity, we use the same notation $\|\cdot\|_{C^k}$ and $\|\cdot\|_{L^p}$ for the norm in product space.*

We first investigate the characteristic curves of the problem.

**Lemma 2.2.** *Let Assumption 1.2 be satisfied. Let $u_i \in C\left([0,\tau], L^1_{per}\left(\mathbb{R}^N\right)\right), i = 1,2$ be given. Then by setting $\mathbf{v}(t,x) = -\nabla\left[K \circ (u_1+u_2)(t,\cdot)\right](x)$, the following non-autonomous system for each $s \in [0,\tau]$ and each $z \in \mathbb{R}^N$:*

$$\begin{cases} \partial_t \Pi_{\mathbf{v}}(t,s;z) = \mathbf{v}(t,\Pi_{\mathbf{v}}(t,s;z)), \text{ for each } t \in [0,\tau], \\ \Pi_{\mathbf{v}}(s,s;z) = z, \end{cases}$$

*generates a unique non-autonomous continuous flow $\{\Pi_{\mathbf{v}}(t,s)\}_{t,s\in[0,\tau]}$, that is to say,*

$$\Pi_{\mathbf{v}}(t,r;\Pi_{\mathbf{v}}(r,s;z)) = \Pi_{\mathbf{v}}(t,s;z), \forall t,s,r \in [0,\tau], \text{ and } \Pi_{\mathbf{v}}(s,s;.) = I$$

*and the map $(t,s,z) \to \Pi_{\mathbf{v}}(t,s;z)$ is continuous. Moreover for each $t,s \in [0,\tau]$, we have*

$$\Pi_{\mathbf{v}}(t,s;z+2\pi k) = \Pi_{\mathbf{v}}(t,s;z) + 2\pi k, \forall z \in \mathbb{R}^{\mathbb{N}}, k \in \mathbb{Z}^N,$$

*the map $z \to \Pi_{\mathbf{v}}(t,s;z)$ is continuously differentiable and one has the determinant of Jacobi matrix:*

$$\det(\partial_z \Pi_{\mathbf{v}}(t,s;z)) = \exp\left(\int_s^t \mathrm{div}\mathbf{v}(l,\Pi_{\mathbf{v}}(l,s;z))dl\right). \tag{2.1}$$

*Proof.* By the assumption, we have

$$\mathbf{v}(t,x) \in C\left([0,\tau], C^1_{per}\left(\mathbb{R}^N\right)^N\right),$$

and we have the following estimations

$$\begin{aligned}\|\mathbf{v}(t,\cdot)\|_{C^0} &\leq \|\nabla K\|_{C^0}\,\|(u_1+u_2)(t,\cdot)\|_{L^1}\,,\\ \|\operatorname{div}\mathbf{v}(t,\cdot)\|_{C^0} &\leq \|\Delta K\|_{C^0}\,\|(u_1+u_2)(t,\cdot)\|_{L^1}\,.\end{aligned}$$

Therefore, the first part of the results follows by using classical arguments on ordinary differential equations. For the proof of (2.1), note that

$$\begin{cases}\partial_t\partial_z\Pi_{\mathbf{v}}(t,s;z)=\partial_x\mathbf{v}(t,\Pi_{\mathbf{v}}(t,s;z))\partial_z\Pi_{\mathbf{v}}(t,s;z),\ t\in[0,\tau]\,,\\ \partial_z\Pi_{\mathbf{v}}(s,s;z)=I.\end{cases}$$

For any matrix-valued $C^1$ function $A:t\mapsto A(t)$, the Jacobi's formula reads as follows

$$\frac{\mathrm{d}}{\mathrm{d}t}\det A(t)=\det A(t)\mathrm{tr}\left(A^{-1}(t)\frac{d}{dt}A(t)\right).$$

Hence we obtain

$$\frac{\mathrm{d}}{\mathrm{d}t}\det\partial_z\Pi_{\mathbf{v}}(t,s;z)=\det\partial_z\Pi_{\mathbf{v}}(t,s;z)\times\mathrm{tr}\left(\partial_x\mathbf{v}(t,\Pi_{\mathbf{v}}(t,s;z))\right)$$

and since $\mathrm{tr}\left(\partial_x\mathbf{v}(t,\Pi_{\mathbf{v}}(t,s;z))\right)=\operatorname{div}\mathbf{v}(t,\Pi_{\mathbf{v}}(t,s;z))$ therefore the result follows. □

In order to precise the notion of solution in this work, assume first that

$$\mathbf{u}=(u_1,u_2)\in C^1\left([0,\tau]\times\mathbb{R}^N,\mathbb{R}\right)^2\cap C\left([0,\tau],C^0_{per,+}(\mathbb{R}^N)\right)^2$$

is a classical solution of (1.1)-(1.3). We consider the solution with each component $u_i(t,\cdot)$ along the characteristic curve $\Pi_{\mathbf{v}}(t,0;x)$ respectively, we obtain for $i=1,2$,

$$\begin{aligned}\frac{\mathrm{d}}{\mathrm{d}t}\Big(u_i(t,\Pi_{\mathbf{v}}(t,0;z)\Big)&=\partial_t u_i(t,\Pi_{\mathbf{v}}(t,0;z))+\nabla u_i(t,\Pi_{\mathbf{v}}(t,0;z))\cdot\mathbf{v}(t,\Pi_{\mathbf{v}}(t,0;z))\\ &=u_i(t,\Pi_{\mathbf{v}}(t,0;z))\Big[-\operatorname{div}\mathbf{v}(t,\Pi_{\mathbf{v}}(t,0;z))+h_i(\mathbf{u}(t,\Pi_{\mathbf{v}}(t,0;z))\Big],\end{aligned}$$

where $h_i(\mathbf{u}(t,\Pi_{\mathbf{v}}(t,0;z))=h_i(u_1(t,\Pi_{\mathbf{v}}(t,0;z),u_2(t,\Pi_{\mathbf{v}}(t,0;z))$. Hence a classical solution of (1.1)-(1.3) (i.e. $C^1$ in time and space) must satisfy

$$u_i(t,\Pi_{\mathbf{v}}(t,0;z))=\exp\left(\int_0^t h_i\big(\mathbf{u}(l,\Pi_{\mathbf{v}}(l,0;z))-\operatorname{div}\mathbf{v}(l,\Pi_{\mathbf{v}}(l,0;z))dl\right)u_i\left(0,z\right),i=1,2,\tag{2.2}$$

or equivalently

$$u_i(t,z)=\exp\left(\int_0^t h_i\big(\mathbf{u}(l,\Pi_{\mathbf{v}}(l,t;z))\big)-\operatorname{div}\mathbf{v}(l,\Pi_{\mathbf{v}}(l,t;z))dl\right)u_i\left(0,\Pi_{\mathbf{v}}(0,t;z)\right),i=1,2,\tag{2.3}$$

where

$$\mathbf{v}(t,x)=-\frac{1}{|\mathbb{T}^N|}\int_{\mathbb{T}^N}\nabla K(x-y)(u_1+u_2)(t,y)\mathrm{d}y.\tag{2.4}$$

The above computations lead us to the following definition of solution.

**Definition 2.3** (Solution along the characteristics). *Let* $\mathbf{u}_0 \in L^\infty_{per,+}\left(\mathbb{R}^N\right)^2$, $\tau > 0$ *be given. A function* $\mathbf{u} \in C\left([0,\tau], L^1_{per,+}\left(\mathbb{R}^N\right)\right)^2 \cap L^\infty\left((0,\tau), L^\infty_{per,+}\left(\mathbb{R}^N\right)\right)^2$ *is said to be a solution integrated along the characteristics of* (1.1)-(1.3)*, if* $u_i$ *satisfies* (2.3) *for* $i = 1, 2$*, with* $\mathbf{v}$ *defined in* (2.4).

We will use a fixed point theorem to prove the existence and uniqueness of the solutions integrated along the characteristics. Consider

$$\mathbf{w} = (w_1, w_2), \quad w_i(t,x) := u_i(t, \Pi_{\mathbf{v}}(t,0;x)),\ i = 1,2, \tag{2.5}$$

and we will construct a fixed point problem for the pair $(\mathbf{w}, \mathbf{v})$.

If there exists a solution integrated along the characteristics, then by (2.2) we have

$$w_i(t,x) = \exp\left(\int_0^t h_i\big(\mathbf{w}(l,x)\big) - \operatorname{div}\mathbf{v}(l, \Pi_{\mathbf{v}}(l,0;x))dl\right) u_i(0,x),\ i = 1,2, \tag{2.6}$$

where $h_i(\mathbf{w}(t,x)) = h_i(w_1(t,x), w_2(t,x))$ for $i = 1,2$. By the definition of $\mathbf{v}$ we obtain

$$\begin{aligned}
\mathbf{v}(t,x) &= -\frac{1}{|\mathbb{T}^N|}\int_{\mathbb{T}^N} \nabla K(x-y)(u_1+u_2)(t,y)\mathrm{d}y \\
&= -\int_{\mathbb{R}^N} \nabla\rho(x-y)(u_1+u_2)(t,y)\mathrm{d}y \\
&= -\int_{\mathbb{R}^N} \nabla\rho\left(x - \Pi_{\mathbf{v}}(t,0;z)\right) \sum_{i=1,2} u_i(t, \Pi_{\mathbf{v}}(t,0;z))\ \det\partial_z(\Pi_{\mathbf{v}}(t,0;z))\mathrm{d}z \\
&= -\int_{\mathbb{R}^N} \nabla\rho\left(x - \Pi_{\mathbf{v}}(t,0;z)\right) \sum_{i=1,2} w_i(t,z)\ \det\partial_z(\Pi_{\mathbf{v}}(t,0;z))\mathrm{d}z,
\end{aligned} \tag{2.7}$$

where we have used the change of variable $y = \Pi_{\mathbf{v}}(t,0;z)$. By using the determinant of Jacobi matrix in (2.1) and (2.6) we deduce that

$$w_i(t,z)\det\ \partial_z(\Pi_{\mathbf{v}}(t,0;z)) = e^{\int_0^t h_i(\mathbf{w}(l,z))\mathrm{d}l} u_i\left(0,z\right),\ i = 1,2,$$

thus equation (2.7) becomes

$$\begin{aligned}
\mathbf{v}(t,x) &= -\int_{\mathbb{R}^N} \nabla\rho\left(x - \Pi_{\mathbf{v}}(t,0;z)\right) \sum_{i=1,2} e^{\int_0^t h_i(\mathbf{w}(l,z))dl} u_i\left(0,z\right) dz \\
&= -\frac{1}{|\mathbb{T}^N|}\int_{\mathbb{T}^N} \nabla K\left(x - \Pi_{\mathbf{v}}(t,0;z)\right) \sum_{i=1,2} e^{\int_0^t h_i(\mathbf{w}(l,z))dl} u_i\left(0,z\right) dz.
\end{aligned} \tag{2.8}$$

Therefore incorporating equations (2.6) and (2.8) leads us to find the solution of the following problem

$$\begin{cases}
w_i(t,x) = \exp\left(\displaystyle\int_0^t h_i\big(\mathbf{w}(l,x)\big) - \operatorname{div}\mathbf{v}(l, \Pi_{\mathbf{v}}(l,0;x))dl\right) u_i\left(0,x\right),\ i = 1,2, \\
\mathbf{v}(t,x) = -\dfrac{1}{|\mathbb{T}^N|}\displaystyle\int_{\mathbb{T}^N} \nabla K\left(x - \Pi_{\mathbf{v}}(t,0;z)\right) \sum_{i=1,2} e^{\int_0^t h_i\left(\mathbf{w}(l,z)\right)dl} u_i\left(0,z\right) dz.
\end{cases} \tag{2.9}$$

In order to choose a proper space for $(\mathbf{w}, \mathbf{v})$, we observe the following estimation

$$\left\| \int_0^t h_i\big(\mathbf{w}(l,x)\big) - \operatorname{div} \mathbf{v}(l, \Pi_{\mathbf{v}}(l,0;x))dl \right\|_{L^\infty} \leq t\left(\bar{h} + \|\mathbf{v}\|_{C^1}\right),\ i = 1,2,$$

where $\bar{h} := \sup_{u_1,u_2\geq 0} \sum_{i=1,2} h_i(u_1,u_2)$. Hence we can choose the following spaces

$$\mathbf{w} = (w_1, w_2) \in C\left([0,\tau], L^\infty_{per,+}\left(\mathbb{R}^N\right)\right)^2, \quad \mathbf{v} \in C([0,\tau], C^1_{per}(\mathbb{R}^N)^N).$$

We write our fixed point problem as follows

$$\begin{pmatrix} \mathbf{w} \\ \mathbf{v} \end{pmatrix} \in \begin{pmatrix} C\left([0,\tau], L^\infty_{per,+}\left(\mathbb{R}^N\right)\right)^2 \\ C([0,\tau], C^1_{per}(\mathbb{R}^N)^N) \end{pmatrix} \quad \text{and} \quad \mathcal{T}\begin{pmatrix} \mathbf{w} \\ \mathbf{v} \end{pmatrix} = \begin{pmatrix} \mathbf{w^1} \\ \mathbf{v^1} \end{pmatrix},$$

wherein $\mathbf{w^1}$ and $\mathbf{v^1}$ are defined by

$$\begin{aligned} \mathbf{w^1}(t,x) &= \begin{pmatrix} \exp\left(\int_0^t h_1\big(\mathbf{w}(l,x)\big) - \operatorname{div} \mathbf{v^1}(l, \Pi_{\mathbf{v}}(l,0;x))dl\right) u_1(0,x) \\ \exp\left(\int_0^t h_2\big(\mathbf{w}(l,x)\big) - \operatorname{div} \mathbf{v^1}(l, \Pi_{\mathbf{v}}(l,0;x))dl\right) u_2(0,x) \end{pmatrix}, \\ \mathbf{v^1}(t,x) &= -\frac{1}{|\mathbb{T}^N|} \int_{\mathbb{T}^N} \nabla K(x - \Pi_{\mathbf{v}}(t,0;z)) \sum_{i=1,2} e^{\int_0^t h_i\left(\mathbf{w}(l,z)\right)dl} u_i(0,z)\,\mathrm{d}z. \end{aligned} \tag{2.10}$$

**Theorem 2.4.** *Let Assumption 1.1 and Assumption 1.2 be satisfied. For each $\mathbf{u}_0 \in L^\infty_{per,+}\left(\mathbb{R}^N\right)^2$, system (1.1)-(1.2) has a unique solution integrated along the characteristics*

$$t \mapsto U(t)\mathbf{u}_0 \text{ in } C\left([0,+\infty), L^1_{per,+}\left(\mathbb{R}^N\right)\right)^2 \cap L^\infty_{loc}\left([0,\infty), L^\infty_{per,+}\left(\mathbb{R}^N\right)\right)^2.$$

*Moreover $\{U(t)\}_{t\geq 0}$ is a continuous semiflow on $L^1_{per,+}\left(\mathbb{R}^N\right)^2$, that is to say*

(i) *$U(t)U(s) = U(t+s), \forall t,s \geq 0$ and $U(0) = I$;*

(ii) *The map $(t,\mathbf{u}_0) \to U(t)\mathbf{u}_0$ maps every bounded set of $[0,+\infty) \times L^\infty_{per,+}\left(\mathbb{R}^N\right)^2$ into a bounded set of $L^\infty_{per,+}\left(\mathbb{R}^N\right)^2$;*

(iii) *If $\{t_n\}_{n\in\mathbb{N}} (\subset [0,+\infty)) \to t < +\infty$ and $\{\mathbf{u}_0^n\}_{n\in\mathbb{N}}$ is bounded sequence in $L^\infty_{per,+}\left(\mathbb{R}^N\right)^2$ such that $\|\mathbf{u}_0^n - \mathbf{u}_0\|_{L^1} \to 0$ as $n \to +\infty$, then*

$$\|U(t_n)\mathbf{u}_0^n - U(t)\mathbf{u}_0\|_{L^1} \to 0 \text{ as } n \to +\infty,$$

*where the norm is the product norm of $L^1_{per,+}\left(\mathbb{R}^N\right)^2$ (see Remark 2.1). The semiflow $U$ also satisfies the two following properties*

$$U(t)\mathbf{u}_0 \geq 0, \forall \mathbf{u}_0 \geq 0, \forall t \geq 0, \tag{2.11}$$

$$\|U(t)\mathbf{u}_0\|_{L^1} \leq e^{t\bar{h}} \|\mathbf{u}_0\|_{L^1}, \forall t \geq 0, \tag{2.12}$$

*where we define*

$$\bar{h} := \sup_{u_1,u_2\geq 0} \sum_{i=1,2} h_i(u_1,u_2). \tag{2.13}$$

We need the following lemma before we prove Theorem 2.4.

**Lemma 2.5.** *Suppose* $\mathbf{v}, \tilde{\mathbf{v}} \in C([0,\tau], C^1_{per}(\mathbb{R}^N)^N)$. *Then for any* $\tau > 0$, *we have*

$$\sup_{t\in[0,\tau]} \|\Pi_{\mathbf{v}}(t,0;\cdot) - \Pi_{\tilde{\mathbf{v}}}(t,0;\cdot)\|_{L^\infty} \le \tau \sup_{t\in[0,\tau]} \|\mathbf{v}(t,\cdot) - \tilde{\mathbf{v}}(t,\cdot)\|_{L^\infty} e^{\tau \sup_{t\in[0,\tau]} \|\mathbf{v}(t,\cdot)\|_{C^1}}.$$

*Proof.* For any fixed $t \in [0,\tau]$,

$$\partial_t \left(\Pi_{\mathbf{v}}(t,0;x) - \Pi_{\tilde{\mathbf{v}}}(t,0;x)\right) = \mathbf{v}(t,\Pi_{\mathbf{v}}(t,0;x)) - \tilde{\mathbf{v}}(t,\Pi_{\tilde{\mathbf{v}}}(t,0;x)).$$

Hence we have

$$\begin{aligned}
&\|\Pi_{\mathbf{v}}(t,0;\cdot) - \Pi_{\tilde{\mathbf{v}}}(t,0;\cdot)\|_{L^\infty} \\
&= \left\| \int_0^t \mathbf{v}(t,\Pi_{\tilde{\mathbf{v}}}(l,0;\cdot)) - \tilde{\mathbf{v}}(t,\Pi_{\tilde{\mathbf{v}}}(l,0;\cdot)) + \mathbf{v}(l,\Pi_{\mathbf{v}}(l,0;\cdot)) - \mathbf{v}(t,\Pi_{\tilde{\mathbf{v}}}(l,0;\cdot)) \mathrm{d}l \right\|_{L^\infty} \\
&\le t\|\mathbf{v}(t,\cdot) - \tilde{\mathbf{v}}(t,\cdot)\|_{L^\infty} + \int_0^t \|\mathbf{v}(t,\cdot)\|_{C^1} \|\Pi_{\mathbf{v}}(l,0;\cdot) - \Pi_{\tilde{\mathbf{v}}}(l,0;\cdot)\|_{L^\infty} \mathrm{d}l.
\end{aligned}$$

By Gronwall inequality, we obtain

$$\sup_{t\in[0,\tau]} \|\Pi_{\mathbf{v}}(t,0;\cdot) - \Pi_{\tilde{\mathbf{v}}}(t,0;\cdot)\|_{L^\infty} \le \tau \sup_{t\in[0,\tau]} \|\mathbf{v}(t,\cdot) - \tilde{\mathbf{v}}(t,\cdot)\|_{L^\infty} e^{\tau \sup_{t\in[0,\tau]} \|\mathbf{v}(t,\cdot)\|_{C^1}}.$$

The result follows. □

*Proof of Theorem 2.4.* We prove this theorem by showing that the contraction mapping theorem applies for $\mathcal{T}$ as long as $\tau > 0$ is small enough. This ensures the local existence and uniqueness of solutions. To that aim, we fix $\tau > 0$ which will be chosen later and we define Banach space $Z$ by $Z := X \times Y$ where

$$X := C\left([0,\tau], L^\infty_{per}\left(\mathbb{R}^N\right)\right)^2, \quad Y := C([0,\tau], C^1_{per}(\mathbb{R}^N)^N)$$

endowed with the norm:

$$\left\| \begin{pmatrix} \mathbf{w} \\ \mathbf{v} \end{pmatrix} \right\|_Z = \|\mathbf{w}\|_X + \|\mathbf{v}\|_Y,$$

where

$$\|\mathbf{w}\|_X = \|w_1\|_{C\left([0,\tau], L^\infty_{per}(\mathbb{R}^N)\right)} + \|w_2\|_{C\left([0,\tau], L^\infty_{per}(\mathbb{R}^N)\right)}.$$

We also introduce the closed subset $X_+ \subset X$ defined by:

$$X_+ = C\left([0,\tau], L^\infty_{per,+}\left(\mathbb{R}^N\right)\right)^2,$$

and define $Z_+ = X_+ \times Y$. Note that due to (2.10) one has

$$\mathcal{T}(Z_+) \subset Z_+. \tag{2.14}$$

For each given $\begin{pmatrix} \mathbf{w} \\ \mathbf{v} \end{pmatrix} \in X$ and $\kappa > 0$, let $\overline{B}_Z \left( \begin{pmatrix} \mathbf{w} \\ \mathbf{v} \end{pmatrix}, \kappa \right)$ be the closed ball in $Z$ of center $\begin{pmatrix} \mathbf{w} \\ \mathbf{v} \end{pmatrix}$ and radius $\kappa$. Now for any $\kappa > 0$ and any initial distribution

$$\mathbf{u}_0 = (u_1(0,\cdot), u_2(0,\cdot)) \in X_+ \text{ and } \mathbf{v}_0 = -\nabla K \circ ((u_1+u_2)(0,\cdot)).$$

We claim that there exists $\widehat{\tau} > 0$ such that for each $\tau \in (0, \widehat{\tau})$:

$$\mathcal{T}\left(Z_+ \cap \overline{B}_Z\left(\begin{pmatrix}\mathbf{u}_0\\ \mathbf{v}_0\end{pmatrix}, \kappa\right)\right) \subset Z_+ \cap \overline{B}_Z\left(\begin{pmatrix}\mathbf{u}_0\\ \mathbf{v}_0\end{pmatrix}, \kappa\right). \tag{2.15}$$

To prove this claim, for any $\begin{pmatrix}\mathbf{w}\\ \mathbf{v}\end{pmatrix} \in Z_+ \cap \overline{B}_Z\left(\begin{pmatrix}\mathbf{u}_0\\ \mathbf{v}_0\end{pmatrix}, \kappa\right)$, we estimate component $\mathbf{w}, \mathbf{v}$ separately. Recalling the definition of $\mathbf{w}$ in (2.10), one obtains

$$\begin{aligned}
&\|\mathbf{w}^1(t,\cdot) - \mathbf{u}_0(\cdot)\|_{L^\infty}\\
=& \left\|\exp\left(\int_0^t h_1\big(\mathbf{w}(l,\cdot)\big) - \operatorname{div}\mathbf{v}^{\mathbf{1}}(l, \Pi_{\mathbf{v}}(l,0;\cdot))dl\right) u_1(0,\cdot) - u_1(0,\cdot)\right\|_{L^\infty}\\
&+ \left\|\exp\left(\int_0^t h_2\big(\mathbf{w}(l,\cdot)\big) - \operatorname{div}\mathbf{v}^{\mathbf{1}}(l, \Pi_{\mathbf{v}}(l,0;\cdot))dl\right) u_2(0,\cdot) - u_2(0,\cdot)\right\|_{L^\infty}\\
\le& \|\mathbf{u}_0\|_{L^\infty} \sum_{i=1,2} \left\|\exp\left(\int_0^t h_i\big(\mathbf{w}(l,\cdot)\big) - \operatorname{div}\mathbf{v}^{\mathbf{1}}(l, \Pi_{\mathbf{v}}(l,0;\cdot))dl\right) - 1\right\|_{L^\infty}.
\end{aligned}$$

Note that by the classic inequality $|e^x - 1| \le |x|e^{|x|}$ for any $x \in \mathbb{R}$, we can deduce

$$\sup_{t\in[0,\tau]} \|\mathbf{w}^1(t,\cdot) - \mathbf{u}_0(\cdot)\|_{L^\infty} \le \|\mathbf{u}_0\|_{L^\infty}\theta(\tau)e^{\theta(\tau)}, \tag{2.16}$$

here $\theta(\tau)$ is defined by

$$\begin{aligned}
\theta(\tau) &= \sum_{i=1}^{2}\int_0^\tau \|h_i\big(\mathbf{w}(l,x)\big) - \operatorname{div}\mathbf{v}(l, \Pi_{\mathbf{v}}(l,0;\cdot))\|_{L^\infty}\mathrm{d}l\\
&\le \tau\left(h_\kappa + \|\mathbf{v}\|_Y\right)\\
&\le \tau(h_\kappa + \kappa + \|\mathbf{v}_0\|_Y),
\end{aligned}$$

where we set

$$h_\kappa := \sup_{0\le u_1,u_2\le \kappa + \|\mathbf{u}_0\|_{L^\infty}} \sum_{i=1,2} |h_i(u_1,u_2)|. \tag{2.17}$$

On the other hand,

$$\begin{aligned}
&\sup_{t\in[0,\tau]} \|\mathbf{v}^{\mathbf{1}}(t,\cdot) - \mathbf{v}_0(\cdot)\|_{C^1}\\
\le& \|\mathbf{u}_0\|_{L^\infty}\frac{1}{|\mathbb{T}^N|}\sup_{t\in[0,\tau]}\left\|\int_{\mathbb{T}^N} \nabla K(\cdot - \Pi_{\mathbf{v}}(t,0;z)) \sum_{i=1,2} e^{\int_0^t h_i(\mathbf{w}(l,z))\mathrm{d}l} - \nabla K(\cdot - z)dz\right\|_{C^1}\\
\le& \|\mathbf{u}_0\|_{L^\infty}\frac{1}{|\mathbb{T}^N|}\sup_{t\in[0,\tau]}\Big\| \int_{\mathbb{T}^N} \nabla K(\cdot - \Pi_{\mathbf{v}}(t,0;z)) \sum_{i=1,2} e^{\int_0^t h_i(\mathbf{w}(l,z))\mathrm{d}l} - \nabla K(\cdot - \Pi_{\mathbf{v}}(t,0;z))\\
&+ \nabla K(\cdot - \Pi_{\mathbf{v}}(t,0;z)) - \nabla K(\cdot - z)dz\Big\|_{C^1}\\
\le& \|\mathbf{u}_0\|_{L^\infty}\left\{\left(\|K\|_{C^1} + \|K\|_{C^2}\right)|e^{\tau h_\kappa} - 1| + \left(\|K\|_{C^2} + \|K\|_{C^3}\right)\sup_{t\in[0,\tau]}\|\Pi_{\mathbf{v}}(t,0;\cdot) - \cdot\|_{L^\infty}\right\}
\end{aligned}$$

$$\leq 2\|\mathbf{u}_0\|_{L^\infty}\|K\|_{C^3}\Big\{|e^{\tau h_\kappa}-1|+\sup_{t\in[0,\tau]}\|\Pi_{\mathbf{v}}(t,0;\cdot)-\Pi_{\mathbf{v}_0}(t,0;\cdot)\|_{L^\infty}$$

$$+\sup_{t\in[0,\tau]}\|\Pi_{\mathbf{v}_0}(t,0;\cdot)-\cdot\|_{L^\infty}\Big\}. \tag{2.18}$$

Recalling Lemma 2.5, we have

$$\begin{aligned}\sup_{t\in[0,\tau]}\|\Pi_{\mathbf{v}}(t,0;\cdot)-\Pi_{\mathbf{v}_0}(t,0;\cdot)\|_{L^\infty}&\leq\tau\sup_{t\in[0,\tau]}\|\mathbf{v}(t,\cdot)-\mathbf{v}_0(t,\cdot)\|_{L^\infty}e^{\tau\sup_{t\in[0,\tau]}\|\mathbf{v}(t,\cdot)\|_{C^1}}\\&\leq\tau\kappa e^{\tau(\kappa+\|\mathbf{v}_0\|_Y)}.\end{aligned}$$

Therefore, equation (2.18) becomes

$$\begin{aligned}&\sup_{t\in[0,\tau]}\|\mathbf{v^1}(t,\cdot)-\mathbf{v}_0(\cdot)\|_{C^1}\\&\leq 2\|\mathbf{u}_0\|_{L^\infty}\|K\|_{C^3}\left\{|e^{\tau h_\kappa}-1|+\tau\kappa e^{\tau(\kappa+\|\mathbf{v}_0\|_Y)}+\sup_{t\in[0,\tau]}\|\Pi_{\mathbf{v}_0}(t,0;\cdot)-\cdot\|_{L^\infty}\right\}.\end{aligned}$$

Since we have

$$\sup_{t\in[0,\tau]}\|\Pi_{\mathbf{v}_0}(t,0;\cdot)-\cdot\|_{L^\infty}\leq\int_0^\tau\|\mathbf{v}_0(l,\Pi_{\mathbf{v}_0}(l,0;\cdot))\|_{L^\infty}\mathrm{d}l\to 0,\quad\text{as }\tau\to 0.$$

Incorporating (2.16), (2.18) and (2.14), then the above estimations complete the proof of (2.15) by choosing a $\hat{\tau}$ small enough.

We now claim that for any

$$\begin{pmatrix}\mathbf{w}\\\mathbf{v}\end{pmatrix},\begin{pmatrix}\tilde{\mathbf{w}}\\\tilde{\mathbf{v}}\end{pmatrix}\in Z_+\cap\overline{B}_Z\left(\begin{pmatrix}\mathbf{u}_0\\\mathbf{v}_0\end{pmatrix},\kappa\right),$$

where

$$\mathbf{w}(t,x)=\mathbf{u}(t,\Pi_{\mathbf{v}}(t,0;x)),\ \tilde{\mathbf{w}}(t,x)=\tilde{\mathbf{u}}(t,\Pi_{\tilde{\mathbf{v}}}(t,0;x)),$$

there exists $\tau^*\in(0,\widehat{\tau})$ such that for each $\tau\in(0,\tau^*)$ we can find a $L(\tau)\in(0,1)$ such that

$$\left\|\mathcal{T}\begin{pmatrix}\mathbf{w}\\\mathbf{v}\end{pmatrix}-\mathcal{T}\begin{pmatrix}\tilde{\mathbf{w}}\\\tilde{\mathbf{v}}\end{pmatrix}\right\|_Z\leq L(\tau)\left\|\begin{pmatrix}\mathbf{w}\\\mathbf{v}\end{pmatrix}-\begin{pmatrix}\tilde{\mathbf{w}}\\\tilde{\mathbf{v}}\end{pmatrix}\right\|_Z. \tag{2.19}$$

To prove this claim, as before we estimate each component separately. For any given $\tau\in(0,\tau^*)$

$$\begin{aligned}&\sup_{t\in[0,\tau]}\left\|\mathbf{w^1}(t,\cdot)-\widetilde{\mathbf{w}}^{\mathbf{1}}(t,\cdot)\right\|_{L^\infty}\\&=\sum_{i=1}^{2}\|\mathbf{u}_0\|_{L^\infty}\sup_{t\in[0,\tau]}\|e^{\int_0^t h_i(\mathbf{w}(l,\cdot))-\operatorname{div}\mathbf{v}(l,\Pi_{\mathbf{v}}(l,0;\cdot))\mathrm{d}l}-e^{\int_0^t h_i(\tilde{\mathbf{w}}(l,\cdot))-\operatorname{div}\tilde{\mathbf{v}}(l,\Pi_{\tilde{\mathbf{v}}}(l,0;\cdot))\mathrm{d}l}\|_{L^\infty}\end{aligned}$$

$$\leq \|\mathbf{u}_0\|_{L^\infty}\Big(e^{\tau(\kappa+\|\mathbf{v}_0\|_Y)}\underbrace{\sum_{i=1}^{2}\sup_{t\in[0,\tau]}\|e^{\int_0^t h_i(\mathbf{w}(l,\cdot))\mathrm{d}l}-e^{\int_0^t h_i(\tilde{\mathbf{w}}(l,\cdot))\mathrm{d}l}\|_{L^\infty}}_{\mathrm{I}}$$
$$+\,e^{\tau h_\kappa}\underbrace{\sup_{t\in[0,\tau]}\|e^{-\int_0^t \operatorname{div}\mathbf{v}(l,\Pi_{\mathbf{v}}(l,0;\cdot))\mathrm{d}l}-e^{-\int_0^t \operatorname{div}\tilde{\mathbf{v}}(l,\Pi_{\tilde{\mathbf{v}}}(l,0;\cdot))\mathrm{d}l}\|_{L^\infty}}_{\mathrm{II}}\Big).$$

*Estimation for I:* We estimate the first term. Since for any $x, y \in \mathbb{R}$, we have $|e^x - e^y| \leq e^{\max\{|x|,|y|\}}|x-y|$. Thus

$$\begin{aligned}
&\sum_{i=1}^{2}\sup_{t\in[0,\tau]}\Big\|e^{\int_0^t h_i(\mathbf{w}(l,\cdot))\mathrm{d}l}-e^{\int_0^t h_i(\tilde{\mathbf{w}}(l,\cdot))\mathrm{d}l}\Big\|_{L^\infty}\\
&\leq e^{\tau h_\kappa}\sum_{i=1}^{2}\Big\|\int_0^t h_i\big(\mathbf{w}(l,\cdot)\big)-h_i\big(\tilde{\mathbf{w}}(l,\cdot)\big)\mathrm{d}l\Big\|_{L^\infty}\\
&\leq \tau e^{\tau h_\kappa}|\nabla h_\kappa|\|\mathbf{w}-\tilde{\mathbf{w}}\|_X,
\end{aligned}\tag{2.20}$$

where $|\nabla h_\kappa| = \sum_{i=1}^2 \sup_{u_1,u_2\in[0,\|\mathbf{u}_0\|_{L^\infty}+\kappa]}|\nabla h_i(u_1,u_2)|$ and $h_\kappa$ is defined in (2.17).

*Estimation for II:* For the second term, we obtain

$$\begin{aligned}
&\sup_{t\in[0,\tau]}\|e^{-\int_0^t \operatorname{div}\mathbf{v}(l,\Pi_{\mathbf{v}}(l,0;\cdot))\mathrm{d}l}-e^{-\int_0^t \operatorname{div}\tilde{\mathbf{v}}(l,\Pi_{\tilde{\mathbf{v}}}(l,0;\cdot))\mathrm{d}l}\|_{L^\infty}\\
&\leq \tau e^{\tau(\kappa+\|\mathbf{v}_0\|_Y)}\sup_{t\in[0,\tau]}\|\operatorname{div}\mathbf{v}(t,\Pi_{\mathbf{v}}(t,0;\cdot))-\operatorname{div}\tilde{\mathbf{v}}(t,\Pi_{\tilde{\mathbf{v}}}(t,0;\cdot))\|_{L^\infty},
\end{aligned}$$

while due to (2.8) we can estimate the last term as follows

$$\begin{aligned}
&\sup_{t\in[0,\tau]}\|\operatorname{div}\mathbf{v}(t,\Pi_{\mathbf{v}}(t,0;\cdot))-\operatorname{div}\tilde{\mathbf{v}}(t,\Pi_{\tilde{\mathbf{v}}}(t,0;\cdot))\|_{L^\infty}\\
&\leq \frac{1}{|\mathbb{T}^N|}\sum_{i=1}^{2}\sup_{t\in[0,\tau]}\Big\|\int_{\mathbb{T}^N}\Delta K(\Pi_{\mathbf{v}}(t,0;\cdot)-\Pi_{\mathbf{v}}(t,0;z))e^{\int_0^t h_i(\mathbf{w}(l,z))\mathrm{d}l}\\
&\quad-\Delta K(\Pi_{\tilde{\mathbf{v}}}(t,0;\cdot)-\Pi_{\tilde{\mathbf{v}}}(t,0;z))e^{\int_0^t h_i(\tilde{\mathbf{w}}(l,z))\mathrm{d}l}\mathrm{d}z\Big\|_{L^\infty}\|\mathbf{u}_0\|_{L^\infty}\\
&\leq \|\mathbf{u}_0\|_{L^\infty}\Big\{\|K\|_{C^2}\sum_{i=1}^{2}\sup_{t\in[0,\tau]}\Big\|e^{\int_0^t h_i(\mathbf{w}(l,\cdot))\mathrm{d}l}-e^{\int_0^t h_i(\tilde{\mathbf{w}}(l,\cdot))\mathrm{d}l}\Big\|_{L^\infty}\\
&\quad+2e^{\tau h_\kappa}\|K\|_{C^3}\sup_{t\in[0,\tau]}\|\Pi_{\mathbf{v}}(t,0;\cdot)-\Pi_{\tilde{\mathbf{v}}}(t,0;\cdot)\|_{L^\infty}\Big\},
\end{aligned}$$

where the first part can be estimated by (2.20). Recalling Lemma 2.5 and since $\mathbf{v}, \tilde{\mathbf{v}} \in \overline{B}_Y(\mathbf{v}_0,\kappa)$ we have

$$\sup_{t\in[0,\tau]}\|\Pi_{\mathbf{v}}(t,0;\cdot)-\Pi_{\tilde{\mathbf{v}}}(t,0;\cdot)\|_{L^\infty}\leq\tau\sup_{t\in[0,\tau]}\|\mathbf{v}(t,\cdot)-\tilde{\mathbf{v}}(t,\cdot)\|_{L^\infty}e^{\tau(\kappa+\|\mathbf{v}_0\|_Y)}.\tag{2.21}$$

Incorporating the estimation in (2.20) leads us to the following estimation

$$\big\|\mathbf{w}^{\mathbf{1}}-\widetilde{\mathbf{w}}^{\mathbf{1}}\big\|_X\leq L_1(\tau)\big(\|\mathbf{w}-\tilde{\mathbf{w}}\|_X+\|\mathbf{v}-\tilde{\mathbf{v}}\|_Y\big)\tag{2.22}$$

with $L_1(\tau) \to 0$ as $\tau \to 0$.

To complete the proof of (2.19), let us notice

$$\begin{aligned}
\left\|\mathbf{v^1} - \widetilde{\mathbf{v}}^{\mathbf{1}}\right\|_Y &= \sup_{t\in[0,\tau]} \left\|\mathbf{v^1}(t,\cdot) - \widetilde{\mathbf{v}}^{\mathbf{1}}(t,\cdot)\right\|_{C^1} \\
&= \frac{1}{|\mathbb{T}^N|} \sup_{t\in[0,\tau]} \| \int_{\mathbb{T}^N} \nabla K(\cdot - \Pi_{\mathbf{v}}(t,0;z)) \sum_{i=1,2} e^{\int_0^t h_i(\mathbf{w}(l,z))\mathrm{d}l} u_i(0,z)\mathrm{d}z \\
&\quad - \int_{\mathbb{T}^N} \nabla K(\cdot - \Pi_{\tilde{\mathbf{v}}}(t,0;z)) \sum_{i=1,2} e^{\int_0^t h_i(\tilde{\mathbf{w}}(l,z))\mathrm{d}l} u_i(0,z)dz\|_{C^1} \\
&\le \|\mathbf{u}_0\|_{L^\infty} \Big\{ 2e^{\tau h_\kappa} \left(\|K\|_{C^2} + \|K\|_{C^3}\right) \sup_{t\in[0,\tau]} \|\Pi_{\mathbf{v}}(t,0;\cdot) - \Pi_{\tilde{\mathbf{v}}}(t,0;\cdot)\|_{L^\infty} \\
&\quad + \left(\|K\|_{C^1} + \|K\|_{C^2}\right) \sum_{i=1}^{2} \sup_{t\in[0,\tau]} \|e^{\int_0^t h_i(\mathbf{w}(l,\cdot))\mathrm{d}l} - e^{\int_0^t h_i(\tilde{\mathbf{w}}(l,\cdot))\mathrm{d}l}\|_{L^\infty} \Big\} \\
&\le L_2(\tau)\big(\|\mathbf{w} - \tilde{\mathbf{w}}\|_X + \|\mathbf{v} - \tilde{\mathbf{v}}\|_Y\big),
\end{aligned} \tag{2.23}$$

and by using (2.20) and (2.21) we have $L^2(\tau)$ satisfying

$$\lim_{\tau\to 0} L_2(\tau) = 0.$$

Let $L(\tau) := L_1(\tau) + L_2(\tau)$ and together with (2.22) and (2.23) we complete the proof of (2.19).

Finally one concludes from (2.15) and (2.19) that for $\tau$ small enough, the contraction mapping theorem applies to operator $\mathcal{T}$. Hence the operator $\mathcal{T}$ has a unique fixed point in $Z_+ \cap \overline{B}_Z \left( \begin{pmatrix} \mathbf{u}_0 \\ \mathbf{v}_0 \end{pmatrix}, \kappa \right)$. Recalling (2.5), this ensures the existence and uniqueness of the local solution integrated along the characteristic of (1.1). The positivity property (2.11) follows from the same arguments. The semiflow property in Theorem 2.4-(i) follows by a standard uniqueness argument. Next we show that the semiflow is globally defined and the properties (ii) and (iii) of the semiflow. In fact, one can see that

$$u_i(t,x) = \exp\left(\int_0^t h_i\big(\mathbf{u}(l,\Pi_{\mathbf{v}}(l,t;x))\big) - \operatorname{div}\mathbf{v}(l,\Pi_{\mathbf{v}}(l,t;x))\mathrm{d}l\right) u_i\left(0,\Pi_{\mathbf{v}}(0,t;x)\right). \tag{2.24}$$

Therefore, one has

$$u_i(t,x) \le \exp\left(t\bar{h}\right) \exp\left(\int_0^t -\operatorname{div}\mathbf{v}(l,\Pi_{\mathbf{v}}(l,t;x))\mathrm{d}l\right) u_i\left(0,\Pi_{\mathbf{v}}(0,t;x)\right), i = 1,2,$$

then we integrate over $\mathbb{T}^N$, using the change of variable $x = \Pi_{\mathbf{v}}(t,0,z)$ to right hand side, which completes the estimation of $u$ in $L^1$ norm (2.12), i.e.,

$$\|u_i(t,\cdot)\|_{L^1} \le e^{t\bar{h}} \|u_i(0,\cdot)\|_{L^1},\ i = 1,2, \forall t \ge 0. \tag{2.25}$$

Moreover, recall the definition $\bar{h}$ in (2.13) we have

$$\sup_{t\in[0,\tau]} \|\mathbf{u}(t,\cdot)\|_{L^\infty} \le e^{\tau\left(\bar{h} + \|\Delta K\|_{L^\infty} e^{\tau\bar{h}} \|\mathbf{u}_0\|_{L^\infty}\right)} \|\mathbf{u}_0\|_\infty,\ \forall \tau \ge 0. \tag{2.26}$$

The result (ii) follows. In the last part of the proof we study the $L^1$ continuity of the semiflow. For any $0 \le s \le t$,

$$\begin{aligned}&\|U(t)\mathbf{u}_0 - U(s)\mathbf{u}_0\|_{L^1} \le e^{s\bar{h}}\|U(t-s)\mathbf{u}_0 - \mathbf{u}_0\|_{L^1}\\ &= e^{s\bar{h}}\sum_{i=1}^{2}\|e^{\int_0^{t-s} h_i(\mathbf{u}(l,\Pi_{\mathbf{v}}(l,t-s;\cdot)))-\operatorname{div}\mathbf{v}(l,\Pi_{\mathbf{v}}(l,t-s;\cdot))\mathrm{d}l}u_i(0,\Pi_{\mathbf{v}}(0,t-s;\cdot)) - u_i(0,\cdot)\|_{L^1},\end{aligned} \tag{2.27}$$

since

$$\sum_{i=1}^{2}\|\int_0^{t-s} h_i(\mathbf{u}(l,\Pi_{\mathbf{v}}(l,t-s;\cdot))) - \operatorname{div}\mathbf{v}(l,\Pi_{\mathbf{v}}(l,t-s;\cdot))\mathrm{d}l\|_{L^\infty} \le J(t-s),$$

where

$$J(\tau) := \tau\left(\bar{h} + \|\Delta K\|_{C^0}e^{\tau\bar{h}}\|\mathbf{u}_0\|_{L^\infty}\right).$$

Then from (2.27) we have

$$\begin{aligned}&\|U(t)\mathbf{u}_0 - U(s)\mathbf{u}_0\|_{L^1}\\ &\le e^{s\bar{h}}\|\mathbf{u}_0(\Pi_{\mathbf{v}}(0,t-s;\cdot)) - \mathbf{u}_0\|_{L^1}e^{J(t-s)} + e^{s\bar{h}}\|\mathbf{u}_0\|_{L^1}\left|e^{J(t-s)} - 1\right| \to 0, \quad s \to t.\end{aligned} \tag{2.28}$$

If $\{\mathbf{u}_0^n\}_{n\in\mathbb{N}}$ is bounded sequence in $L^\infty_{per,+}\left(\mathbb{R}^N\right)$ such that $\|\mathbf{u}_0^n - \mathbf{u}_0\|_1 \to 0$ as $n \to +\infty$, then by (2.25), we have

$$\|U(t)\mathbf{u}_0^n - U(t)\mathbf{u}_0\|_{L^1} \to 0, \quad n \to +\infty,$$

together with (2.28), we have proved the continuity of the semiflow in (iii). □

**Theorem 2.6.** *Let Assumption 1.1 and Assumption 1.2 be satisfied. In addition,* $\mathbf{u}_0 \in W^1_{per}\left(\mathbb{R}^N\right)^2$, *then* $U(\cdot)\mathbf{u}_0 \in C^1\left([0,+\infty), L^1_{per}\left(\mathbb{R}^N\right)\right)^2$. *Moreover, if* $\mathbf{u}_0 \in C^1_{per}\left(\mathbb{R}^N\right)^2$ *then* $\mathbf{u}(t,x) = U(t)\mathbf{u}_0(x)$ *belongs to* $C^1\left([0,+\infty)\times\mathbb{R}^N\right)^2$ *and* $u(t,x)$ *is a classical solution of system* (1.1)-(1.3).

*Sketch of the proof.* If $\mathbf{u}_0 \in W^1_{per}(\mathbb{R}^N)^2$, we claim $U(\cdot)\mathbf{u}_0 \in C^1([0,\infty), L^1_{per}(\mathbb{R}^N))^2$. In fact, we define for $i = 1, 2$,

$$w_i(t,x) = e^{\int_0^t h_i(\mathbf{w}(l,x))-\operatorname{div}\mathbf{v}(l,\Pi_{\mathbf{v}}(l,0;x))\mathrm{d}l}u_i(0,x) =: e^{\int_0^t h_i(\mathbf{w}(l,x))\mathrm{d}l}B_i(t,x), \tag{2.29}$$

where $B_i(t,x) := e^{\int_0^t -\operatorname{div}\mathbf{v}(l,\Pi_{\mathbf{v}}(l,0;x))\mathrm{d}l}u_i(0,x)$ is $C([0,\tau], W^1_{per}(\mathbb{R}^N))$ by our assumption. Define the formal derivative $\tilde{w}_i(t,\cdot) = \nabla_x w_i(t,\cdot)$, solving the following fixed point problem

$$\mathcal{T}\begin{pmatrix}\tilde{w}_1(t,x)\\ \tilde{w}_2(t,x)\\ \mathbf{v}\end{pmatrix} = \begin{pmatrix}\left(\int_0^t\sum_{j=1}^2\partial_{u_j}h_1(\mathbf{w}(l,x))\tilde{w}_j(l,x)\mathrm{d}l\, B_1(t,x) + \nabla_x B_1(t,x)\right)e^{\int_0^t h_1(\mathbf{w}(l,x))\mathrm{d}l}\\ \left(\int_0^t\sum_{j=1}^2\partial_{u_j}h_2(\mathbf{w}(l,x))\tilde{w}_j(l,x)\mathrm{d}l\, B_2(t,x) + \nabla_x B_2(t,x)\right)e^{\int_0^t h_2(\mathbf{w}(l,x))\mathrm{d}l}\\ -\frac{1}{|\mathbb{T}^N|}\int_{\mathbb{T}^N}\nabla K(x-\Pi_{\mathbf{v}}(t,0;z))\sum_{i=1,2}e^{\int_0^t h_i\left(\mathbf{w}(l,z)\right)\mathrm{d}l}u_i(0,z)\,\mathrm{d}z\end{pmatrix},$$

on space $C([0,\tau], L^\infty_{per}(\mathbb{R}^N)^N)^2 \times C([0,\tau], C^1_{per}(\mathbb{R}^N)^N)$ where $\partial_{u_j}h_i(u_1,u_2)$ is the partial derivative of $h_i$. Similarly, one can show the mapping $\mathcal{T}$ is from $C([0,\tau], L^\infty_{per}(\mathbb{R}^N)^N)^2 \times C([0,\tau], C^1_{per}(\mathbb{R}^N)^N)$ to itself and is a contraction if $\tau$ is small. Therefore,

$$\tilde{w}_i(t,x) = \left(\int_0^t\sum_{j=1}^2\partial_{u_j}h_i(\mathbf{w}(l,x))\tilde{w}_j(l,x)\mathrm{d}l\, B_i(t,x) + \nabla_x B_i(t,x)\right)e^{\int_0^t h_i(\mathbf{w}(l,x))\mathrm{d}l}, i = 1, 2,$$

on $[0,\tau]$, since by our assumption

$$\sup_{u_1,u_2\geq 0}\partial_{u_j}h_i(u_1,u_2)<\infty,\quad i=1,2,\ j=1,2,$$

applying Gronwall inequality we have $\tilde{\mathbf{w}}\in C([0,\infty),L^1_{per}(\mathbb{R}^N)^N)^2$ for any positive time.

Since we have for $i=1,2$, $w_i(t,\Pi_{\mathbf{v}}(0,t;x))=u_i(t,x)$, and

$$\partial_t u_i(t,x)=\partial_t w_i(t,\Pi_{\mathbf{v}}(0,t;x))+\tilde{w}_i(t,x)\cdot\partial_t\Pi_{\mathbf{v}}(0,t;x)\in C([0,\infty);L^1_{per}(\mathbb{R}^N)).$$

If $\mathbf{u}_0\in C^1(\mathbb{R}^N)^2$, then $B_i(t,x)\in C^1\left([0,+\infty)\times\mathbb{R}^N\right)$ and by (2.29), we have $\mathbf{w}\in C^1([0,\infty)\times\mathbb{R}^N)^2$ therefore $u$ is a classical solution. □

**Remark 2.7** (Conservation law)**.** *The above computations lead us to the following conservation law: for each Borel set $A\subset\mathbb{T}^N$ and each $0\leq s\leq t$:*

$$\int_{\Pi_{\mathbf{v}}(t,s;A)}u_i(t,x)\mathrm{d}x=\int_A\exp\left[\int_s^t h_i\left(\mathbf{u}\left(l,\Pi_{\mathbf{v}}(l,s;z)\right)\right)\mathrm{d}l\right]u_i(s,z)\mathrm{d}z,i=1,2.$$

# 3 Segregation property

From the mono-layer cell populations co-culture experiments, we can see that the spreading speed of cell propagation is finite. Moreover, once the two cell populations confront each other, they stop growing and form segregated islets. Our next theorem will show that the solution along the characteristics can easily explain the segregation property.

**Theorem 3.1.** *Suppose $\mathbf{u}=\mathbf{u}(t,x)$ is the solution of (1.1)-(1.3) provided by Theorem 2.4. For any initial distribution with $u_1(0,x)u_2(0,x)=0$ for all $x\in\mathbb{T}^N$. Then $u_1(t,x)u_2(t,x)=0$ for any $t>0$ and $x\in\mathbb{T}^N$.*

*Proof.* We argue by contradiction, assume there exist $t_1>0,x_1\in\mathbb{T}^N$ such that

$$u_1(t_1,x_1)u_2(t_1,x_1)>0.$$

Since $z\to\Pi_{\mathbf{v}}(t,s;z)$ is invertible from $\mathbb{R}^N\to\mathbb{R}^N$, then there exists some $x_0\in\mathbb{R}^N$ such that $\Pi_{\mathbf{v}}(t_1,0;x_0)=x_1$. Denote $x_0=\tilde{x}_0+2\pi k_0$ for some $\tilde{x}_0\in\mathbb{T}^N$ and $k_0\in\mathbb{Z}^N$, thus by Lemma 2.2 we have

$$0<u_i(t_1,\Pi_{\mathbf{v}}(t_1,0;x_0))=u_i(t_1,\Pi_{\mathbf{v}}(t_1,0;\tilde{x}_0)+2\pi k_0)=u_i(t_1,\Pi_{\mathbf{v}}(t_1,0;\tilde{x}_0)).$$

Thus, for any $i=1,2$,

$$u_i(t_1,\Pi_{\mathbf{v}}(t_1,0;\tilde{x}_0))=\exp\left(\int_0^{t_1}h_i\big(\mathbf{u}(l,\Pi_{\mathbf{v}}(l,0;\tilde{x}_0))-\operatorname{div}\mathbf{v}(l,\Pi_{\mathbf{v}}(l,0;\tilde{x}_0))\mathrm{d}l\right)u_i\left(0,\tilde{x}_0\right)>0,$$

which implies

$$u_i\left(0,\tilde{x}_0\right)>0,\ \forall i=1,2.$$

This is a contradiction. □

**Remark 3.2.** *Suppose the dimension $N = 1$ and $u_1, u_2$ are classical solutions, we give an illustration (see Figure 2.1) of the segregation for the solutions integrated along the characteristics $u_i(t, \Pi_{\mathbf{v}}(t, 0; x))$ for $i = 1, 2$. In fact, if there exists for some $x_0$ such that $u_i(0, x_0) = 0$ for $i = 1, 2$. Then from equation (2.2) we obtain*

$$u_1(t, \Pi_{\mathbf{v}}(t, 0; x_0)) = 0 = u_2(t, \Pi_{\mathbf{v}}(t, 0; x_0)), \forall t > 0.$$

*Therefore, the characteristics $t \mapsto \Pi_{\mathbf{v}}(t, 0; x_0)$ forms a segregation barrier for the two cell populations.*

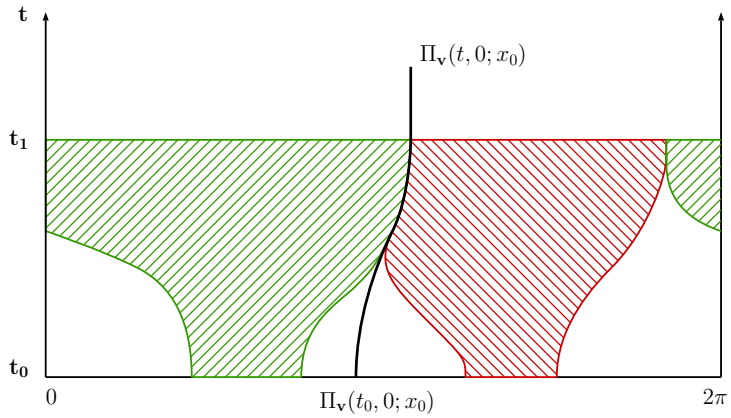


Figure 2.1: *The shaded areas represent the supports of two populations (red and green) evolving along the time. Notice that if one starts with two separated supports and choose $x_0$ where $u_i(0, x_0) = 0$ for $i = 1, 2$, then the characteristics $t \mapsto \Pi_{\mathbf{v}}(t, 0; x_0)$ forms a segregation "wall" between the two cell populations, which indicates no matter how close they are, they will keep separated.*

# 4 Asymptotic behavior

In the rest of the work, we always assume the initial distributions for the two populations are separated.

**Assumption 4.1.** *For initial value $\mathbf{u}_0 \in L^\infty_{per,+}\left(\mathbb{R}^N\right)^2$, we assume*

$$u_1(0, x)u_2(0, x) = 0, \forall x \in \mathbb{T}^N.$$

*Furthermore, we suppose $h_i$ in equation (1.1) has the following form*

$$h_i(u_1, u_2) = h_i(u_1 + u_2),\ i = 1, 2,$$

*with $h_i(r_i) = 0$ for some $r_i > 0$, $i = 1, 2$, and*

$$h_i(u) > 0,\ \forall u \in [0, r_i), \quad h_i(u) < 0,\ \forall u > r_i, \quad \limsup_{u\to\infty} h_i(u) < 0,\ i = 1, 2.$$

*Moreover, $u \longmapsto uh_i(u)$ is a concave function for $i = 1, 2$.*

**Remark 4.2.** *Notice that segregation property in Theorem 3.1 implies the following equality:*

$$u_i(t, x)h_i(u_1(t, x) + u_2(t, x)) = u_i(t, x)h_i(u_i(t, x)),\ i = 1, 2,\ \forall (t, x) \in [0, \infty) \times \mathbb{T}^N. \quad (4.1)$$

**Lemma 4.3.** *Let Assumptions 1.1, 1.2 and 4.1 be satisfied. Suppose* $\mathbf{u} = \mathbf{u}(t,x)$ *is the solution of* (1.1)-(1.3). *Then we have*

(i) $\sup_{t\geq 0} \|u_i(t,\cdot)\|_{L^1} \leq \max\{\|u_i(0,\cdot)\|_{L^1}, |\mathbb{T}^N|\}$, $i = 1,2$.

(ii) $\mathbf{v}(t,x) := (\nabla K \circ (u_1+u_2)(t,\cdot))(x)$ *satisfies* $\mathbf{v} \in L^\infty((0,\infty), W^{1,\infty}_{per}(\mathbb{R}^N))^N$ *and*

$$\|\mathbf{v}(t,\cdot)\|_{C^1} \leq 2\|K\|_{C^2} \max\{\|u_1(0,\cdot)\|_{L^1}, \|u_2(0,\cdot)\|_{L^1}, |\mathbb{T}^N|\}.$$

*Proof.* To prove the above estimate, we first deal with classical solution. By the equation (4.1) due to segregation, the equation (1.1) can be rewritten as

$$\partial_t u_i + \operatorname{div}\left(u_i \mathbf{v}\right) = u_i h_i(u_i),\ i = 1,2. \tag{4.2}$$

By Assumption 4.1 the function $f_i(u) = uh_i(u)$ is concave for each $i$, integrating (4.2) over $\mathbb{T}^N$ and using Jensen's inequality, we have for classical solution

$$\frac{\mathrm{d}}{\mathrm{d}t}\|u_i(t,\cdot)\|_1 = \|f(u_i(t,\cdot))\|_1 \leq f\left(\|u_i(t,\cdot)\|_{L^1}\right).$$

Then the results follows using the usual ordinary differential arguments with Assumption 4.1, where we can prove

$$\sup_{t\geq 0} \|u_i(t,\cdot)\|_{L^1} \leq \max\{\|u_i(0,\cdot)\|_{L^1}, |\mathbb{T}^N|\},\ i = 1,2.$$

Let $\mathbf{u}_0 \in L^\infty_{per,+}\left(\mathbb{R}^N\right)^2$ be given and $\mathbf{u}$ be the corresponding solution integrated along the characteristics. Consider a sequence $\{\mathbf{u}_0^n\}_{n\geq 0}$ in $C^1_{per,+}(\mathbb{R}^N)^2$ such that $\|\mathbf{u}_0^n - \mathbf{u}_0\|_{L^1} \to 0$ as $n \to +\infty$. Then denote $\mathbf{u}^n$ the solutions corresponding to $\mathbf{u}_0^n$, from Theorem 2.4 we have $\|\mathbf{u}^n(t,\cdot) - \mathbf{u}(t,\cdot)\|_{L^1} \to 0$ and $\mathbf{u}(t,\cdot) \in L^\infty_{per,+}\left(\mathbb{R}^N\right)^2$. Therefore, by using the Lebesgue convergence theorem, the result (i) follows. Then result (ii) is a direct consequence of (i). □

## 4.1 Energy functional

In order to prove that our energy functional is decreasing, we make the following assumption on kernel $K$.

**Assumption 4.4.** *The Fourier's coefficients of function* $K$ *on* $\mathbb{T}^N$ *denoted by* $\{c_n[K]\}_{n\in\mathbb{Z}^N}$ *satisfy* $c_n[K] > 0$, $\forall n \in \mathbb{Z}^N \setminus \{0\}$. *Here the Fourier coefficients are defined by*

$$c_n[K] = |\mathbb{T}^N|^{-1} \int_{\mathbb{T}^N} e^{-in\cdot x} K(x)\mathrm{d}x, \quad \forall n \in \mathbb{Z}^N.$$

**Remark 4.5.** *If* $\rho$ *in system* (1.1) *satisfies that the Fourier transformation* $\widehat{\rho}(\xi) > 0$ *for all* $\xi \in \mathbb{R}^N$, *then for the kernel* $K$, *we have* $c_n[K] > 0$ *for all* $n \in \mathbb{Z}^N$. *This implies that Assumption 4.4 is satisfied.*

We construct the functional for $u_i, i = 1,2$, as

$$E_i[u_i(t,\cdot)] = \frac{1}{|\mathbb{T}^N|}\int_{\mathbb{T}^N} G_i(u_i(t,x))\mathrm{d}x,$$

where $G_i : [0,\infty) \to [0,\infty)$ is defined by

$$G_i(u) := u \ln\left(\frac{u}{r_i}\right) - u + r_i. \tag{4.3}$$

Notice that $G_i'(u) = \ln(u/r_i)$ for $u > 0$ and we define the energy functional as

$$E[(u_1,u_2)(t,\cdot)] := \sum_{i=1,2} E_i[u_i(t,\cdot)]. \tag{4.4}$$

**Theorem 4.6.** *Let Assumptions 1.1, 1.2, 4.1 and 4.4 be satisfied. Suppose $\mathbf{u} = \mathbf{u}(t,x)$ is the solution of (1.1)-(1.3). Then for any $t,\tau > 0$ set $u := u_1 + u_2$ we have*

$$\begin{aligned} &E[(u_1,u_2)(t+\tau,\cdot)] - E[(u_1,u_2)(t,\cdot)] \\ &= -\int_t^{t+\tau} \sum_{k\in\mathbb{Z}^N} |k|^2 c_k[K]\,|c_k[u(s,\cdot)]|^2\,\mathrm{d}s - \frac{1}{|\mathbb{T}^N|}\int_t^{t+\tau}\int_{\mathbb{T}^N} \sum_{i=1,2} u_i \left| h_i(u_i)\ln\left(\frac{u_i}{r_i}\right)\right| \mathrm{d}x\mathrm{d}s. \end{aligned} \tag{4.5}$$

*Proof.* For any $\delta > 0$, as before we first suppose $\mathbf{u} = (u_1,u_2)$ to be the classical solution. Setting $u = u_1 + u_2 \geq 0$, recall the property in (4.1) we have

$$\begin{aligned} \frac{\mathrm{d}}{\mathrm{d}t} E_i[(u_i+\delta)(t,\cdot)] &= \frac{1}{|\mathbb{T}^N|}\int_{\mathbb{T}^N} \ln\left(\frac{u_i+\delta}{r_i}\right)\partial_t u_i \mathrm{d}x \\ &= \frac{1}{|\mathbb{T}^N|}\int_{\mathbb{T}^N} \ln\left(\frac{u_i+\delta}{r_i}\right)\Big[\mathrm{div}\,[u_i\nabla(K\circ u)] + u_i h_i(u_i)\Big]\mathrm{d}x \\ &= \frac{1}{|\mathbb{T}^N|}\int_{\mathbb{T}^N} \frac{u_i^2}{u_i+\delta}\Delta(K\circ u) + u_i\nabla K\circ u\cdot\nabla\left(\frac{u_i}{u_i+\delta}\right)\mathrm{d}x \\ &\quad + \frac{1}{|\mathbb{T}^N|}\int_{\mathbb{T}^N} u_i h_i(u_i)\ln\left(\frac{u_i+\delta}{r_i}\right)\mathrm{d}x. \end{aligned}$$

Therefore, for any $t,\tau > 0$ we obtain

$$\begin{aligned} &E_i[(u_i+\delta)(t+\tau,\cdot)] - E_i[(u_i+\delta)(t,\cdot)] \\ &= \frac{1}{|\mathbb{T}^N|}\int_t^{t+\tau}\int_{\mathbb{T}^N} \frac{u_i^2}{u_i+\delta}\Delta(K\circ u) + u_i\nabla K\circ u\cdot\nabla\left(\frac{u_i}{u_i+\delta}\right)\mathrm{d}x\mathrm{d}s \\ &\quad + \frac{1}{|\mathbb{T}^N|}\int_t^{t+\tau}\int_{\mathbb{T}^N} u_i h_i(u_i)\ln\left(\frac{u_i+\delta}{r_i}\right)\mathrm{d}x\mathrm{d}s. \end{aligned}$$

Now by letting $\delta \to 0$ we can see that

$$\begin{aligned} &E_i[u_i(t+\tau,\cdot)] - E_i[u_i(t,\cdot)] \\ &= \frac{1}{|\mathbb{T}^N|}\int_t^{t+\tau}\int_{\mathbb{T}^N} u_i\Delta(K\circ u)\mathrm{d}x\mathrm{d}s + \frac{1}{|\mathbb{T}^N|}\int_t^{t+\tau}\int_{\mathbb{T}^N} u_i h_i(u_i)\ln\left(\frac{u_i}{r_i}\right)\mathrm{d}x\mathrm{d}s. \end{aligned}$$

By summing the two functional $E_i, i = 1,2$, we obtain

$$\begin{aligned} &E[(u_1,u_2)(t+\tau,\cdot)] - E[(u_1,u_2)(t,\cdot)] \\ &= \frac{1}{|\mathbb{T}^N|}\int_t^{t+\tau}\int_{\mathbb{T}^N} u\Delta(K\circ u)\mathrm{d}x\mathrm{d}s + \frac{1}{|\mathbb{T}^N|}\int_t^{t+\tau}\int_{\mathbb{T}^N} \sum_{i=1,2} u_i h_i(u_i)\ln\left(\frac{u_i}{r_i}\right)\mathrm{d}x\mathrm{d}s. \end{aligned}$$

On the other hand, for each $\phi \in L^2_{per}(\mathbb{R}^N)$, one has $\phi(x) = \sum_{k\in\mathbb{Z}^N} \overline{c_k[\phi]} e^{in\cdot x}$ almost everywhere, thus

$$\begin{aligned}\frac{1}{|\mathbb{T}^N|}\int_{\mathbb{T}^N} \phi\Delta(K\circ\ \phi)\mathrm{d}x &= \sum_{k\in\mathbb{Z}^N} \frac{1}{|\mathbb{T}^N|}\int_{\mathbb{T}^N} \overline{c_k[\phi]} e^{in\cdot x}\Delta(K\circ\ \phi)\mathrm{d}x\\ &= \sum_{k\in\mathbb{Z}^N} \overline{c_k[\phi]} c_k[\Delta K\circ\ \phi]\\ &= -\sum_{k\in\mathbb{Z}^N} |k|^2 c_k[K]c_k[\phi]^2.\end{aligned}$$

Therefore, by the above calculation and by the fact that $h_i(u)\ln(u/r_i) < 0, i = 1, 2$, we have

$$\begin{aligned}&E[u(t+\tau,\cdot)] - E[u(t,\cdot)]\\ &= -\int_t^{t+\tau}\sum_{k\in\mathbb{Z}^N} |k|^2 c_k[K]\left|c_k[u(s,\cdot)]\right|^2 \mathrm{d}s - \frac{1}{|\mathbb{T}^N|}\int_t^{t+\tau}\int_{\mathbb{T}^N}\sum_{i=1,2} u_i\left|h_i(u_i)\ln\left(\frac{u_i}{r_i}\right)\right|\mathrm{d}x\mathrm{d}s.\end{aligned}$$

The usual limiting procedure as in Lemma 4.3 allows us to extend the estimation to solutions integrated along the characteristics. □

**Remark 4.7.** *By the above theorem, we can see the energy functional $E$ is non-negative and is decreasing along the trajectories of (1.1), by letting $t \to +\infty$ we deduce from (4.5) that*

$$\lim_{t\to+\infty}\int_t^{t+\tau}\sum_{k\in\mathbb{Z}^N} |k|^2 c_k[K]\left|c_k[u(s,\cdot)]\right|^2 \mathrm{d}s = 0, \tag{4.6}$$

*and*

$$\lim_{t\to+\infty}\int_t^{t+\tau}\int_{\mathbb{T}^N} u_i\left|h_i(u_i)\ln\left(\frac{u_i}{r_i}\right)\right|\mathrm{d}x\mathrm{d}s = 0,\ i = 1, 2. \tag{4.7}$$

Before we prove the $L^\infty$ boundedness of the solution for all $t \geq 0$, i.e.,

$$\sup_{t\geq 0}\|u_i(t,\cdot)\|_{L^\infty} < \infty$$

for $i = 1, 2$, we need following lemmas.

**Lemma 4.8.** *Let Assumptions 1.1, 1.2, 4.1 and 4.4 be satisfied. Suppose $\mathbf{u} = \mathbf{u}(t, x)$ is the solution of (1.1)-(1.3). Then for any $k \in \mathbb{Z}^N$ and for each $i = 1, 2$, the mapping*

$$t \longmapsto c_k[u_i(t,\cdot)]$$

*is a $C^1$ function. Here $c_k[u_i(t,\cdot)]$, $k \in \mathbb{Z}^N$ are the Fourier coefficients. Moreover,*

$$\sup_{t\geq 0}\left|\frac{\mathrm{d}}{\mathrm{d}t}c_k[u_i(t,\cdot)]\right| < \infty.$$

*Proof.* For any $k \in \mathbb{Z}^N$, suppose $\mathbf{u} = (u_1, u_2)$ is the classical solution then we have

$$\frac{\mathrm{d}}{\mathrm{d}t}c_k[u_i(t,\cdot)] = \frac{1}{|\mathbb{T}^N|}\int_{\mathbb{T}^N} e^{-ik\cdot x}\left[-\mathrm{div}\,(u_i\mathbf{v}) + u_i h_i(u_i)\right]\mathrm{d}x$$

$$= \frac{1}{|\mathbb{T}^N|}\int_{\mathbb{T}^N} u_i \nabla\left(e^{-ik\cdot x}\right)\cdot \mathbf{v} + e^{-ik\cdot x}u_i h_i(u_i)\mathrm{d}x.$$

Therefore, by using the Jensen's inequality for $f_i(u) = uh_i(u)$ again, we derive

$$\left|\frac{\mathrm{d}}{\mathrm{d}t}c_k[u_i(t,\cdot)]\right| \leq |k|\|u_i(t,\cdot)\|_1\|\mathbf{v}(t,\cdot)\|_{C^0} + f(\|u_i(t,\cdot)\|_{L^1}),$$

the result follows by Lemma 4.3. The case of the solution integrated along the characteristics can be proved by applying a classical regularization procedure. □

The regularity condition for kernel $K$ defined in Assumption 1.2 serves mainly for the following result.

**Lemma 4.9.** *Let Assumptions 1.1, 1.2, 4.1 and 4.4 be satisfied. Suppose* $\mathbf{u} = \mathbf{u}(t,x)$ *is the solution of* (1.1)-(1.3) *and define* $u := u_1 + u_2$. *Then for* $\mathbf{v}(t,x) = (\nabla K \circ u(t,\cdot))(x)$ *we have*

$$\lim_{t\to+\infty}\|\mathrm{div}\,\mathbf{v}(t,\cdot)\|_{C^0} = 0.$$

*Proof.* By Assumption 1.2 $K \in C^m_{per}(\mathbb{R}^N)$ with $m \geq \frac{N+5}{2}$, therefore by Temam [100, page. 50]

$$\sum_{k\in\mathbb{Z}^N}(1+|k|^2)^{\frac{N+5}{2}}c_k[K]^2 < \infty. \tag{4.8}$$

Moreover, we can deduce from (4.6) that for each $k \in \mathbb{Z}^N\backslash\{0\}$

$$\lim_{t\to+\infty}\int_t^{t+\tau}|c_k[u(s,\cdot)]|^2\,\mathrm{d}s = \lim_{t\to+\infty}\int_0^{\tau}|c_k[u(s+t,\cdot)]|^2\mathrm{d}s = 0.$$

The last equality together with the results in Lemma 4.8, we can deduce

$$\lim_{t\to+\infty}c_k[u(t,\cdot)] = 0, \quad k\in\mathbb{Z}^N\backslash\{0\}. \tag{4.9}$$

We can compute that

$$\begin{aligned}
\mathrm{div}\,\mathbf{v}(t,x) &= -\frac{1}{|\mathbb{T}^N|}\int_{\mathbb{T}^N}\Delta K(x-y)u(t,y)\mathrm{d}y\\
&= -\frac{1}{|\mathbb{T}^N|}\int_{\mathbb{T}^N}\Delta K(x-y)\sum_{k\in\mathbb{Z}^N}e^{-ik\cdot y}c_k[u(t,\cdot)]\mathrm{d}y\\
&= -\frac{1}{|\mathbb{T}^N|}\int_{\mathbb{T}^N}\sum_{k\in\mathbb{Z}^N}\Delta K(z)e^{ik\cdot(z-x)}c_k[u(t,\cdot)]\mathrm{d}z\\
&= \sum_{k\in\mathbb{Z}^N}|k|^2c_k[K]c_k[u(t,\cdot)]e^{-ik\cdot x},
\end{aligned}$$

where the last series converges due to (4.8). In fact, by Lemma 4.3, we can find a constant $M > 0$ such that for each $k \in \mathbb{Z}^N$ we have

$$|c_k[u(t,\cdot)]| < \|u(t,\cdot)\|_{L^1} \leq M,\ \forall t \geq 0.$$

Therefore,

$$\begin{aligned}\|\operatorname{div}\mathbf{v}(t,x)\|_{C^0} &= \left\|\sum_{k\in\mathbb{Z}^N}|k|^2c_k[K]c_k[u(t,\cdot)]e^{-ik\cdot x}\right\|_{C^0}\\ &\le M\sum_{k\in\mathbb{Z}^N}|k|^2c_k[K] = M\sum_{k\in\mathbb{Z}^N\setminus\{0\}}|k|^{-\frac{N+1}{2}}|k|^{2+\frac{N+1}{2}}c_k[K]\\ &\le M\left(\sum_{k\in\mathbb{Z}^N\setminus\{0\}}\frac{1}{|k|^{N+1}}\right)^{\frac12}\left(\sum_{k\in\mathbb{Z}^N\setminus\{0\}}|k|^{N+5}c_k[K]^2\right)^{\frac12},\end{aligned}$$

and due to (4.8), this last series converges. Therefore, by Lebesgue dominated convergence theorem and (4.9) we have

$$\limsup_{t\to+\infty}\|\operatorname{div}\mathbf{v}(t,x)\|_{C^0} \le \limsup_{t\to+\infty}\sum_{k\in\mathbb{Z}^N}|k|^2c_k[K]|c_k[u(t,\cdot)]| = 0.$$

The result follows. □

As a consequence of Lemma 4.9, we obtain Theorem 4.10 and Corollary 4.12 which are the main results of this section.

**Theorem 4.10.** *Let Assumptions 1.1, 1.2, 4.1 and 4.4 be satisfied. Suppose* $\mathbf{u}=\mathbf{u}(t,x)$ *is the solution of* (1.1)-(1.3). *Then we have for each* $i=1,2$,

$$\sup_{t\ge0}\|u_i(t,\cdot)\|_{L^\infty} < +\infty,$$

*and more precisely we have*

$$\limsup_{t\to+\infty}\|u_i(t,\cdot)\|_{L^\infty} \le r_i.$$

*Moreover, for any* $x\in\mathbb{R}^N$ *such that* $u_i(0,x)>0$. *Then the solution integrated along the characteristics converges point-wisely to the positive equilibrium* $r_i$ *for* $i=1,2$. *That is, for any* $x\in\mathcal{U}_i$ *where* $\mathcal{U}_i=\{x\in\mathbb{R}^N : u_i(0,x)>0\}$

$$\lim_{t\to\infty}u_i(t,\Pi_{\mathbf{v}}(t,0;x)) = r_i.$$

*Or equivalently, for any* $x\in\mathbb{R}^N$ *we have*

$$u_i(t,\Pi_{\mathbf{v}}(t,0;x)) \xrightarrow{p.w.} r_i\mathbb{1}_{\mathcal{U}_i}(x), \qquad \text{as } t\to\infty.$$

**Remark 4.11.** *Notice from the above theorem, we obtain the following* $L^2$ *uniform boundedness of the solution* $u=u_1+u_2$, *that is*

$$\sup_{t\ge0}\|u(t,\cdot)\|_{L^2} < \infty.$$

*Moreover for any sequence* $\{t_n\}_{n\ge0}$ *which tends to infinity, since for Fourier coefficients, one has*

$$\lim_{n\to\infty}c_k[u(t_n,\cdot)] = 0, \quad \forall k\in\mathbb{Z}^N\setminus\{0\},$$

*therefore by Banach-Alaoglu-Bourbaki theorem, we deduce that there exists a subsequence* $\{t_{n_l}\}_{l\geq 0}$ *such that*

$$u(t_{n_l},\cdot) \rightharpoonup c \text{ in } L^2,$$

*where* $c$ *is a constant which depends on the choice of the subsequence. With the above argument we can deduce*

$$\lim_{t\to\infty} \|\mathbf{v}(t,\cdot)\|_{C^0} = 0. \tag{4.10}$$

*In fact, for any sequence* $\{t_n\}_{n\geq 0}$ *with* $t_n \to \infty$ *as* $n \to \infty$*, we can find a subsequence such that*

$$\mathbf{v}(t_{n_l},x) = \int_{\mathbb{T}^N} \nabla K(x-y)u(t_{n_l},y)dy \to c\int_{\mathbb{T}^N} \nabla K(x-y)dy = 0,$$

*where the last equation is follows since* $K$ *is periodic. Thus, equation* (4.10) *follows.*

*Proof.* Suppose $\mathbf{u} = (u_1, u_2)$ the classical solution. The usual limiting procedure allows us to extend the estimation to solutions integrated along the characteristics. We recall the notation in (2.5) where $w_i(t,x) := u_i(t,\Pi_{\mathbf{v}}(t,0;x))$, $i = 1,2$, and for any $x \in \mathbb{R}^N$ we have

$$\begin{aligned}\frac{\mathrm{d}w_i(t,x)}{\mathrm{d}t} &= w_i(t,x)\left[-\operatorname{div}\mathbf{v}(t,\Pi_{\mathbf{v}}(t,0;x)) + h_i((w_1+w_2)(t,x))\right]\\ &= w_i(t,x)\left[-\operatorname{div}\mathbf{v}(t,\Pi_{\mathbf{v}}(t,0;x)) + h_i(w_i(t,x))\right],\end{aligned}$$

where the second equation is due to segregation. Now we compare the solution along the characteristics with the solution of the following ordinary differential equation. For any $\tau > 0$, let $\overline{w}_i(t)$ to be the solution of the following Cauchy problem

$$\begin{cases}\dfrac{\mathrm{d}\overline{w}_i(t)}{\mathrm{d}t} &= \overline{w}_i(t)\left[\sup\limits_{t\geq\tau}\|\operatorname{div}\mathbf{v}(t,\cdot)\|_{C^0} + h_i(\overline{w}_i(t))\right] \quad t>\tau,\\ \overline{w}_i(\tau) &= \|w_i(\tau,\cdot)\|_{L^\infty}.\end{cases}$$

Then we note that

$$\limsup_{t\to+\infty}\overline{w}_i(t) \leq \overline{\Phi}_i(\tau) := \inf\{z > r_i : \sup_{t\geq\tau}\|\operatorname{div}\mathbf{v}(t,\cdot)\|_{C^0} + h_i(y) \leq 0,\ \forall y \geq z\}.$$

If the set is empty, then $\overline{\Phi}_i(\tau) = +\infty$. By comparison principle, for any $\tau > 0$ we have

$$\limsup_{t\to+\infty}\|w_i(t,\cdot)\|_{L^\infty} \leq \limsup_{t\to+\infty}\overline{w}_i(t) \leq \overline{\Phi}_i(\tau),$$

while due to Assumption 4.1 where $h_i(u) < 0$ for any $u > r_i$ and $\limsup_{u\to\infty} h_i(u) < 0$ and Lemma 4.9, we have $\lim_{\tau\to+\infty}\overline{\Phi}_i(\tau) = r_i$ thus we have

$$\limsup_{t\to+\infty}\|u_i(t,\Pi_{\mathbf{v}}(t,0;\cdot))\|_{L^\infty} \leq r_i. \tag{4.11}$$

Since $x \mapsto \Pi_{\mathbf{v}}(t,0;x)$ is invertible on $\mathbb{R}^N$, we have

$$\limsup_{t\to+\infty}\|u_i(t,\cdot)\|_{L^\infty} \leq r_i.$$

Together with the $L^\infty$ estimation of $\mathbf{u}$ in finite time in (2.26) , we can see that

$$\sup_{t\geq 0}\|u_i(t,\cdot)\|_{L^\infty} < \infty.$$

Now we prove the second part of the theorem. For any fixed $x \in \mathbb{R}^N$ with $u_i(0,x) > 0$, we can see from the definition of the solution integrated along the characteristics (2.9) that

$$w_i(t,x) = u_i(t, \Pi_{\mathbf{v}}(t,0;x)) > 0, \ \forall t > 0.$$

For any $\tau > 0$, define the solution $\underline{w}_i(t)$ to be the solution of the following Cauchy problem

$$\begin{cases} \dfrac{\mathrm{d}\underline{w}_i(t)}{\mathrm{d}t} & = \underline{w}_i(t) \left[ -\sup\limits_{t \geq \tau} \|\mathrm{div}\, \mathbf{v}(t,\cdot)\|_{C^0} + h_i(\underline{w}_i(t)) \right], \\ \underline{w}_i(\tau) & = w_i(\tau, x) > 0. \end{cases}$$

Then we note that

$$\liminf_{t \to +\infty} \underline{w}_i(t) \geq \underline{\Phi}_i(\tau) := \sup\{z > 0 : -\sup_{t \geq \tau} \|\mathrm{div}\, \mathbf{v}(t,\cdot)\|_{C^0} + h_i(y) \geq 0, \forall y \leq z\}.$$

If the set is empty, then $\underline{\Phi}_i(\tau) = -\infty$. As before we use the comparison principle, for any $\tau > 0$ and any $x \in \{x \in \mathbb{R}^N : u_i(0,x) > 0\}$ we have

$$\liminf_{t \to +\infty} w_i(t,x) \geq \liminf_{t \to +\infty} \underline{w}_i(t) \geq \underline{\Phi}_i(\tau).$$

Due to Assumption 4.1 where $h_i(u) > 0$ for any $u \in [0, r_i)$, we have $\lim_{\tau \to +\infty} \underline{\Phi}_i(\tau) = r_i$ thus we have for any $x \in \{x \in \mathbb{R}^N : u_i(0,x) > 0\}$,

$$\liminf_{t \to +\infty} u_i(t, \Pi_{\mathbf{v}}(t,0;x)) \geq r_i,$$

together with (4.11) the result follows. □

Next corollary is a consequence of Theorem 4.10.

**Corollary 4.12.** *Let Assumptions 1.1, 1.2, 4.1 and 4.4 be satisfied. Suppose* $\mathbf{u} = \mathbf{u}(t,x)$ *is the solution of* (1.1)-(1.3). *If for some constant* $\delta > 0$ *and* $u(0,x) = \sum_{i=1,2} u_i(0,x) \geq \delta > 0$ *for a.e.* $x \in \mathbb{T}^N$. *Moreover, we assume* $r_1 = r_2 =: r$ *in Assumption 4.1. Then*

$$\lim_{t \to \infty} \|u(t,\cdot) - r\|_{L^\infty} = 0.$$

*Proof.* Here again we only prove the convergence when $\mathbf{u} = (u_1, u_2)$ is the classical solution. We use the same notations as in Theorem 4.10 and define

$$w(t,x) := w_1(t,x) + w_2(t,x).$$

Due to estimation (4.11) in Theorem 4.10 and segregation property, we have

$$\limsup_{t \to +\infty} \sup_{x \in \mathbb{R}^N} w(t,x) \leq r. \tag{4.12}$$

Moreover, we can obtain

$$\frac{\mathrm{d}w(t,x)}{\mathrm{d}t} = -w(t,x)\mathrm{div}\, \mathbf{v}(t, \Pi_{\mathbf{v}}(t,0;x)) + \sum_{i=1}^{2} w_i h_i(w_i).$$

In order to use comparison principle, we set $\underline{h}(u) = \min_{u\geq 0}\{h_1(u), h_2(u)\}$ and by the separation property in Theorem 3.1 we have

$$w_1 h_1(w_1) + w_2 h(w_2) \geq w_1 \underline{h}(w_1) + w_2 \underline{h}(w_2) = (w_1 + w_2)\underline{h}(w_1 + w_2).$$

Hence,

$$\frac{\mathrm{d}w(t,x)}{\mathrm{d}t} \geq w(t,x)\left[-\sup_{t\geq\tau}\|\mathrm{div}\,\mathbf{v}(t,\cdot)\|_{C^0} + \underline{h}(w(t,x))\right],\ t \geq \tau.$$

For any $\tau > 0$, we have $\inf_{x\in\mathbb{R}^N} w(\tau, x) > 0$. In fact, by our assumption, $u(0,x) \geq \delta > 0$ on $\mathbb{T}^N$, thus $u(0,x) \geq \delta > 0$ on $\mathbb{R}^N$ and by equation (2.9) we have $w(\tau,x) > 0$ for any $x \in \mathbb{R}^N$ and since $w(t, x+2\pi) = w(t,x)$ for any $x \in \mathbb{R}^N$, we have $\inf_{x\in\mathbb{R}^N} w(\tau,x) \geq \tilde{\delta} > 0$ for some positive $\tilde{\delta}$. Thus, for any $\tau > 0$, we define $\underline{w}(t)$ to be the solution of the following ordinary differential equation

$$\begin{cases} \dfrac{\mathrm{d}\underline{w}(t)}{\mathrm{d}t} &= \underline{w}(t)\left[-\sup\limits_{t\geq\tau}\|\mathrm{div}\,\mathbf{v}(t,\cdot)\|_{C^0} + \underline{h}(\underline{w}(t))\right], \\ \underline{w}(\tau) &= \inf_{x\in\mathbb{R}^N} w(\tau,x) > 0. \end{cases}$$

By the similar argument as in Theorem 4.10, we can see that

$$\liminf_{t\to+\infty}\inf_{x\in\mathbb{R}^N} w(t,x) \geq \liminf_{t\to+\infty}\underline{w}(t) \geq r.$$

Together with (4.12), we have

$$\lim_{t\to\infty}\|w(t,\cdot) - r\|_{L^\infty} = 0.$$

Since for any $t > 0$, the mapping $t \mapsto \Pi_{\mathbf{v}}(t,0;\cdot)$ is a bijection, we have

$$\|w(t,\cdot) - r\|_{L^\infty} = \|u(t,\Pi_{\mathbf{v}}(t,0;\cdot)) - r\|_{L^\infty} = \|u(t,\cdot) - r\|_{L^\infty}.$$

Thus, we obtain

$$\lim_{t\to\infty}\|u(t,\cdot) - r\|_{L^\infty} = 0.$$

The result follows. □

**Remark 4.13.** *Note that the result in the corollary, we only assume the roots of two different reaction functions $h_1, h_2$ to be the same to obtain the convergence in $L^\infty$.*

# 5 Young measure

We first introduce the notion of Young measures. The basic idea of Young measure is to replace the map $(t,x) \to u(t,x) = u_1(t,x) + u_2(t,x)$ by the map

$$(t,x) \to \delta_{u(t,x)}$$

from $[0,\infty)\times\mathbb{T}^N$ into a probability space. Namely, for fixed $t$ and $x$, the Dirac mass $\delta_{u(t,x)}$ is regarded as an element of the dual space the continuous functions $C([0,\gamma],\mathbb{R})$ (where $\gamma := \|u\|_{L^\infty([0,\infty)\times\mathbb{T}^N)}$) by using the following mapping

$$f \longmapsto \int_{[0,\gamma]} f(\lambda)\delta_{u(t,x)}(\mathrm{d}\lambda) = f(u(t,x)).$$

This means that the map $(t,x) \to \delta_{u(t,x)}$ is identified to an element of

$$L^\infty\left([0,\infty)\times\mathbb{T}^N, C([0,\gamma],\mathbb{R})^\star\right).$$

The goal of this procedure is to use the weak star topology to regard Young measure as an element the dual space of

$$L^1\left([0,\infty)\times\mathbb{T}^N, C([0,\gamma],\mathbb{R})\right).$$

The space of Young measures in our specific context is nothing but $L^\infty\left([0,\infty)\times\mathbb{T}^N, \mathbb{P}\left([0,\gamma]\right)\right)$ (where $\mathbb{P}\left([0,\gamma]\right)$ is the space of probabilities on $[0,\gamma]$) endowed with the weak star topology.

In Corollary 4.12, we have the $L^\infty$ convergence of the solution $u(=u_1+u_2)$ when the initial distribution is strictly positive. Then one would like to know about the convergence of the solution when the initial distribution admits zero values. To answer this question, we prove the following result.

**Theorem 5.1.** *Let Assumptions 1.1, 1.2, 4.1 and 4.4 be satisfied. Suppose* $\mathbf{u}=\mathbf{u}(t,x)$ *is the solution of (1.1)-(1.3) provided by Theorem 2.4. Let us denote by* $\gamma$ *as in (5.1). Furthermore, suppose we have*

$$r_1 = r_2 = r,$$

*in Assumption 4.1 and define*

$$E_\infty := \lim_{t\to\infty} E[(u_1,u_2)(t,\cdot)],$$

*where* $E[(u_1,u_2)(t,\cdot)]$ *is the energy functional defined in (4.4).*

*Then for each* $i=1,2$ *and each* $t\geq 0$ *the Dirac measure* $\delta_{(u_1+u_2)(t,x)}$ *belongs to the space of Young measures* $Y\left(\mathbb{T}^N;[0,\gamma]\right)$ *which means*

$$(u_1+u_2)(t,x)\in[0,\gamma],\ \forall t\geq 0 \text{ and almost every } x\in\mathbb{R}^N,$$

$$\int_{A\times[0,\gamma]}\eta(\lambda)\delta_{(u_1+u_2)(t,x)}(\mathrm{d}\lambda)\mathrm{d}x = \int_A \eta((u_1+u_2)(t,x))\mathrm{d}x,\ \forall\, A\in\mathcal{B}(\mathbb{T}^N),\ \forall\eta\in C([0,\gamma],\mathbb{R}).$$

*Moreover, we obtain*

$$r\leq E_\infty\leq 2r$$

*and*

$$\lim_{t\to\infty}\delta_{(u_1+u_2)(t,x)} = (E_\infty/r-1)\delta_0 + (2-E_\infty/r)\delta_r,$$

*in the sense of the narrow convergence topology of* $Y(\mathbb{T}^N;[0,\gamma])$. *This means that for each continuous function* $\eta:[0,\gamma]\to\mathbb{R}$ *and for any* $A\in\mathcal{B}(\mathbb{T}^N)$

$$\lim_{t\to\infty}\int_A \eta((u_1+u_2)(t,x))\mathrm{d}x = \int_A (E_\infty/r-1)\eta(0) + (2-E_\infty/r)\eta(r)\mathrm{d}x.$$

**Remark 5.2.** *Under the same assumptions as in Theorem 5.1, let* $\{t_n\}_{n\geq 0}$ *be any sequence tending to* $\infty$ *as* $n\to\infty$. *Then the sequence* $\{(u_1+u_2)(t_n,\cdot)\}_{n\geq 0}\subset L^\infty_{per}(\mathbb{R}^N)$ *is relatively compact in* $L^1_{per}(\mathbb{R}^N)$ *if and only if*

$$E_\infty = r \quad \text{or} \quad E_\infty = 2r.$$

*The above result is a direct consequence of Young measure properties (see [27, Corollary 3.1.5]), which says if the sequence of Young measures* $\{\delta_{(u_1+u_2)(t_n,x)}\}_{n\geq 0}$ *converges in the narrow sense to a Young measure* $\nu(x,\cdot)$ *and* $\nu(x,\cdot)$ *is a single Dirac measure* $\delta_{\phi(x)}(\cdot)$ *for almost all* $x \in \mathbb{T}^N$*. Then we have*

$$(u_1+u_2)(t_n,x) \xrightarrow{L^1} \phi(x), \quad n \to \infty.$$

*In our case, when* $E_\infty = r$ *(resp.* $= 2r$*), then*

$$(u_1+u_2)(t_n,x) \xrightarrow{L^1} r \text{ (resp. } 0), \quad n \to \infty.$$

**Remark 5.3.** *When* $E_\infty$ *lies strictly in the interval* $(r,2r)$*, then* $\delta_{(u_1+u_2)(t,x)}$ *converges to two Dirac measures as* $t \to \infty$*. To illustrate the notion of narrow convergence to two Dirac measures, one may consider the following example. For each* $n \in \mathbb{N}$*,*

$$u_n(x) = \begin{cases} 1, & x \in \Delta x\,[j, j+p), \\ 0, & x \in \Delta x\,[j+p, j+1). \end{cases}, \quad j = 0,1,\ldots,n, \quad p \in (0,1),\ \Delta x = \frac{2\pi}{n+1}.$$

*Then one can prove that*

$$\lim_{n\to\infty} \delta_{u_n(x)} = p\delta_1 + (1-p)\delta_0$$

*in the sense of narrow convergence. Indeed, for any* $\eta \in C_b([0,1])$ *and* $\varphi \in L^1(0,2\pi)$ *one has*

$$\int_{[0,2\pi]} \varphi(x) \int_{[0,1]} \eta(\lambda)\delta_{u_n(x)}(d\lambda)dx = \int_{[0,2\pi]} \varphi(x)\eta(u_n(x))\mathrm{d}x$$
$$= \sum_{j=0}^{n} \int_{\Delta x[j,j+p)} \varphi(x)\eta(1)dx + \int_{\Delta x[j+p,j+1)} \varphi(x)\eta(0)\mathrm{d}x,$$

*and the result follows when* $n \to \infty$*.*

Next, we introduce the notion of Young measure and the notion of narrow convergence topology in a general case.

**Definition 5.4** (Young measure)**.** *Let* $(\mathcal{S},d)$ *be a separable metric space and let* $\mathbb{P}(\mathcal{S})$ *be the set of probability measures on* $(\mathcal{S},d)$*. Let* $(\Omega,\mathcal{A},\mu)$ *be a finite measure space endowed with* $\sigma-$*algebra* $\mathcal{A}$ *(in practice* $\mu$ *will be a Lebesgue measure in our case). A map* $\nu : \Omega \to \mathbb{P}(\mathcal{S})$ *(i.e. the map* $\nu$ *maps each* $x \in \Omega$ *to a probability* $B \to \nu(x,B)$ *on* $\mathcal{S}$*) is said to be a* ***Young measure*** *if for each Borel set* $B \in \mathcal{B}(\mathcal{S})$ *the function* $x \mapsto \nu(x,B)$ *is measurable from* $(\Omega,\mathcal{A})$ *into* $[0,1]$*. The set of all Young measures from* $(\Omega,\mathcal{A})$ *into* $\mathcal{S}$ *is denoted by* $Y(\Omega,\mathcal{A};\mathcal{S})$*.*

**Definition 5.5** (Narrow convergence topology)**.** *The set* $Y(\Omega,\mathcal{A};\mathcal{S})$ *is endowed with narrow convergence topology which is the weakest topology on* $Y(\Omega,\mathcal{A};\mathcal{S})$ *such that all the functionals from* $Y(\Omega,\mathcal{A};\mathcal{S})$ *into* $\mathbb{R}$ *defined by*

$$\nu \longmapsto \int_A \int_{\mathcal{S}} \eta(\lambda)\nu(x,\mathrm{d}\lambda)\mu(\mathrm{d}x)$$

*is continuous whenever* $A \in \mathcal{A}$ *and* $\eta \in C_b(\mathcal{S};\mathbb{R})$*.*

**Remark 5.6.** *Note that a sequence* $\{\nu^n\}_{n\in\mathbb{N}} \subset Y(\Omega,\mathcal{A};\mathcal{S})$ *narrowly converges to* $\nu \in Y(\Omega,\mathcal{A};\mathcal{S})$ *if and only if for any* $\eta \in C_b(\mathcal{S};\mathbb{R})$ *and* $A \in \mathcal{A}$

$$\lim_{n\to\infty}\int_A\int_{\mathcal{S}}\eta(\lambda)\nu^n(x,\mathrm{d}\lambda)\mu(\mathrm{d}x) = \int_A\int_{\mathcal{S}}\eta(\lambda)\nu(x,\mathrm{d}\lambda)\mu(\mathrm{d}x).$$

*For the sake of simplicity, we use* $Y(\Omega;\mathcal{S})$ *to denote* $Y(\Omega,\mathcal{A};\mathcal{S})$ *if* $\mathcal{A}=\mathcal{B}(\Omega)$.

Since the time variable $t$ is in a unbounded domain, we introduce the local narrow convergence topology.

**Definition 5.7** (Local narrow convergence topology)**.** *Let* $(\mathcal{S},d)$ *be a separable metric space and let* $(\Omega,\mathcal{A},\mu)$ *be a finite measure space (in practice* $\mu$ *will be a Lebesgue measure in our case). The set* $Y\left(\mathbb{R}\times\Omega,\mathcal{B}(\mathbb{R})\otimes\mathcal{A};\mathcal{S}\right)$ *is endowed with the local narrow convergence topology denoted by* $\mathcal{T}_{loc}$ *which is defined as the weakest topology on* $Y\left(\mathbb{R}\times\Omega,\mathcal{B}(\mathbb{R})\otimes\mathcal{A};\mathcal{S}\right)$ *such that all the functionals from* $Y(\Omega,\mathcal{A};\mathcal{S})$ *into* $\mathbb{R}$ *defined by*

$$\nu \longmapsto \int_{I\times A}\left(\int_{\mathcal{S}}\eta(\lambda)\nu(t,x,\mathrm{d}\lambda)\right)(\mathrm{d}t\otimes\mu(\mathrm{d}x)),$$

*is continuous for each bounded interval* $I\subset\mathbb{R}$, $A\in\mathcal{A}$ *and* $\eta\in C_b(\mathcal{S};\mathbb{R})$.

For our case, we consider $\Omega=\mathbb{T}^N$, $\mathcal{A}=\mathcal{B}\left(\mathbb{T}^N\right)$ is the Borel $\sigma-$ algebra and $\mu$ is the Lebegues measure. By setting

$$\gamma := \sup_{t\geq 0}\sum_{i=1,2}\|u_i(t,\cdot)\|_{L^\infty} < \infty, \tag{5.1}$$

the set $\mathcal{S}=[0,\gamma]$ ($\gamma$ here corresponds to the $L^\infty$ bound of $u_1+u_2$) endowed with Euclidean norm. To simplify the notations, we set

$$Y(\mathbb{T}^N;[0,\gamma]) := Y(\mathbb{T}^N,\mathcal{B}(\mathbb{T}^N);[0,\gamma]).$$

We define $Y_{loc}\left(\mathbb{R}\times\mathbb{T}^N;[0,\gamma]\right)$ to be the topological space $Y\left(\mathbb{R}\times\mathbb{T}^N;[0,\gamma]\right)$ endowed with the local narrow convergence topology $\mathcal{T}_{loc}$.

Furthermore, let us consider the probability space $\mathbb{P}\left(\mathbb{T}^N\times[0,\gamma]\right)$ and let us recall that the usual weak $*-$topology on $\mathbb{P}\left(\mathbb{T}^N\times[0,\gamma]\right)$ is metrizable by using the so-called bounded dual Lipschitz metric (Wasserstein metric $W_p$ when $p=1$) defined for each $\mu,\nu\in\mathbb{P}\left(\mathbb{T}^N\times[0,\gamma]\right)$ by

$$\Theta(\mu,\nu) = \sup\left\{\left|\int_{\mathbb{T}^N\times[0,\gamma]} f(x,\lambda)\,(\mu-\nu)(\mathrm{d}x,\mathrm{d}\lambda)\right| \; f\in \mathrm{Lip}\left(\mathbb{T}^N\times[0,\gamma]\right),\ \|f\|_{\mathrm{Lip}}\leq 1\right\}.$$

Recall that the Lipschitz norm for metric space $(X,d)$ is defined as follows

$$\|f\|_{\mathrm{Lip}} = \sup_{x\in X}|f(x)| + \sup_{(x,y)\in X^2,\,x\neq y}\frac{|f(x)-f(y)|}{d(x,y)},\ \forall f\in\mathrm{Lip}(X).$$

We refer to Dudley [41, Theorem 18] for the equivalence between the weak $*-$topology on $\mathbb{P}\left(\mathbb{T}^N\times[0,\gamma]\right)$ and the topology induced by $\Theta(\cdot,\cdot)$. In the sequel the probability space $\mathbb{P}\left(\mathbb{T}^N\times[0,\gamma]\right)$ is always endowed with the metric topology induced by $\Theta$ without further precision.
Let $\{t_n\}_{n\geq 0}$ be a given increasing sequence tending to $\infty$ as $n\to\infty$. Using the above definition, we can prove the following lemma.

**Lemma 5.8.** *Let Assumptions 1.1, 1.2, 4.1 and 4.4 be satisfied. Let $T > 0$ and $i = 1, 2$ be given. The sequence of maps $\left\{t \longmapsto \mu_{i,t}^n\right\}_{n\in\mathbb{N}}$ from $[-T, T]$ to $\mathbb{P}\left(\mathbb{T}^N \times [0, \gamma]\right)$ (endowed with the above metric $\Theta$) and defined by*

$$\int_{\mathbb{T}^N\times[0,\gamma]} g(x, y)\mu_{i,t}^n(\mathrm{d}x, \mathrm{d}y) = |\mathbb{T}^N|^{-1} \int_{\mathbb{T}^N} g\left(x, u_i(t + t_n, x)\right) \mathrm{d}x, \forall g \in C\left(\mathbb{T}^N \times [0, \gamma]; \mathbb{R}\right),$$

*is relatively compact in $C\left([-T, T]; \mathbb{P}\left(\mathbb{T}^N \times [0, \gamma]\right)\right)$.*

**Remark 5.9.** *In the following, we will use the notation*

$$\mu_{i,t}^n(\mathrm{d}x, \mathrm{d}y) = |\mathbb{T}^N|^{-1}\mathrm{d}x \otimes \delta_{u_i(t+t_n,x)}(\mathrm{d}y).$$

*Proof.* Let us first consider the classical solution. For each $g \in C^1(\mathbb{T}^N \times \mathbb{R})$

$$\int_{\mathbb{T}^N} g(x, u_i(t, x))\mathrm{d}x - \int_{\mathbb{T}^N} g(x, u_i(s, x))\mathrm{d}x = \int_s^t \frac{\mathrm{d}}{\mathrm{d}l} \int_{\mathbb{T}^N} g(x, u_i(l, x))\mathrm{d}x\mathrm{d}l.$$

Since $u_i$ is bounded, we have

$$\begin{aligned}
\frac{\mathrm{d}}{\mathrm{d}t} \int_{\mathbb{T}^N} g(x, u_i(t, x))\mathrm{d}x &= \int_{\mathbb{T}^N} \partial_u g(x, u_i(t, x))\partial_t u_i(t, x)\mathrm{d}x \\
&= \int_{\mathbb{T}^N} \partial_u g(x, u_i(t, x)) \left(-\mathrm{div}(u_i\mathbf{v}) + u_i h_i(u_i)\right) \mathrm{d}x \\
&= \int_{\mathbb{T}^N} u_i \nabla_x \left[\partial_u g(x, u_i(t, x))\right] \cdot \mathbf{v} + \partial_u g(x, u_i(t, x))u_i h_i(u_i)\mathrm{d}x,
\end{aligned} \tag{5.2}$$

where the last equality is obtained by applying the Green's formula together with periodic boundary condition. We can see that

$$u_i(t, x)\nabla_x \left[\partial_u g(x, u_i(t, x))\right] = \nabla_x \left[u_i(t, x)\partial_u g(x, u_i(t, x)) - g(x, u_i(t, x))\right] + \mathbf{p}(x, u_i(t, x)),$$

where $\mathbf{p}(x, u) = \nabla_x g(x, u)$.

By substituting the last formula into (5.2) and by using again the periodicity we derive that

$$\begin{aligned}
\frac{\mathrm{d}}{\mathrm{d}t} \int_{\mathbb{T}^N} g(x, u_i(t, x))\mathrm{d}x = &- \int_{\mathbb{T}^N} \left[u_i(t, x)\partial_u g(x, u_i(t, x)) - g(x, u_i(t, x))\right] \mathrm{div}\, \mathbf{v}(t, x)\mathrm{d}x \\
&+ \int_{\mathbb{T}^N} \mathbf{p}(x, u_i(t, x)) \cdot \mathbf{v}(t, x)\mathrm{d}x \\
&+ \int_{\mathbb{T}^N} \partial_u g(x, u_i(t, x))u_i(t, x)h_i(u_i(t, x))\mathrm{d}x.
\end{aligned} \tag{5.3}$$

The formula (5.2) extends to the solution integrated along the characteristics by usual density arguments. Incorporating the estimation of $\sup_{t\geq 0} \|u(t, \cdot)\|_{L^\infty}$ in Theorem 4.10, the estimation of $\mathbf{v}$ in Lemma 4.3, and the above equality (5.3), we deduce that there exists a constant $M > 0$ such that

$$\left| \int_{\mathbb{R}^N} g(x, u_i(t, x))\mathrm{d}x - \int_{\mathbb{R}^N} g(x, u_i(s, x))\mathrm{d}x \right| \leq M\|g\|_{\mathrm{Lip}(\mathbb{T}^N\times[0,\gamma])}|t - s|.$$

From the definition of the metric on $\Theta(\mu,\nu)$, we can see that

$$\Theta\left(\mu_{i,t}^n,\mu_{i,s}^n\right)\leq M|t-s|.$$

From this we observe that each map $t\to\mu_{i,t}^n$ is continuous from $[-T,T]$ to $\mathbb{P}\left(\mathbb{T}^N\times[0,\gamma]\right)$. By Prohorov's compactness theorem [16, Theorem 5.1], the space $\mathbb{P}\left(\mathbb{T}^N\times[0,\gamma]\right)$ endowed with the metric $\Theta$ is a compact metric space. Therefore we can apply Arzela-Ascoli theorem and the result follows. □

Since $u$ is uniformly bounded, one can deduce the following compact result for Young measures (see [94, Theorem 9.15]).

**Lemma 5.10.** *The sequence* $\left\{\delta_{u_i(t+t_n,x)}\right\}_{n\geq 0}$ *is relatively compact for the local narrow convergence topology of* $Y_{loc}\left(\mathbb{R}\times\mathbb{T}^N;[0,\gamma]\right)$.

Using the above Lemma 5.8 and Lemma 5.10, up to a subsequence, one can assume that there exists a Young measure $\nu\equiv\nu_{i,t}(x,\cdot)\in Y\left(\mathbb{R}\times\mathbb{T}^N;[0,\gamma]\right)$ such that

$$\lim_{n\to\infty}\delta_{u_i(t+t_n,x)}=\nu_{i,t}(x,\cdot)\text{ in the topology of }Y_{loc}\left(\mathbb{R}\times\mathbb{T}^N;[0,\gamma]\right). \tag{5.4}$$

and

$$\lim_{n\to\infty}\mu_{i,t}^n=\mu_{i,t}^\infty \tag{5.5}$$

where the limit holds to the locally uniform continuous topology of $C\left(\mathbb{R};\mathbb{P}\left(\mathbb{T}^N\times[0,\gamma]\right)\right)$. Here we would like to recall that the limits $\mu_{i,t}^\infty$ and $\nu_{i,t}(x,\cdot)$ depend on the choice of subsequence.
Next, by definition one has for each continuous function $f\in C\left(\mathbb{T}^N\times[0,\gamma];\mathbb{R}\right)$ and each $n\geq 0$:

$$\int_{\mathbb{T}^N\times[0,\gamma]}f(x,y)\mu_{i,t}^n(\mathrm{d}x,\mathrm{d}y)=|\mathbb{T}^N|^{-1}\int_{\mathbb{T}^N}\int_{[0,\gamma]}f(x,y)\,\delta_{u_i(t+t_n,x)}(\mathrm{d}y)\,\mathrm{d}x.$$

From (5.4) and (5.5), passing to the limit $n\to\infty$ yields to

$$\int_{\mathbb{T}^N\times[0,\gamma]}f(x,y)\mu_{i,t}^\infty(\mathrm{d}x,\mathrm{d}y)=|\mathbb{T}^N|^{-1}\int_{\mathbb{T}^N}\int_{[0,\gamma]}f(x,y)\,\nu_{i,t}(x,\mathrm{d}y)\,\mathrm{d}x.$$

Thus, we can rewrite $\mu_{i,t}^\infty$ as

$$\mu_{i,t}^\infty(\mathrm{d}x,\mathrm{d}y)=|\mathbb{T}^N|^{-1}\mathrm{d}x\otimes\nu_{i,t}(x,\mathrm{d}y).$$

The aim of the following lemmas is to identify the family of measures $\nu_{i,t}(x,\cdot)$. Our next result describes the support of $\nu_{i,t}(x,\cdot)$.

**Lemma 5.11.** *Under the same assumptions of Lemma 5.8, for* $i=1,2$, *there exist measurable maps* $a_i:\mathbb{R}\times\mathbb{T}^N\to\mathbb{R}$ *such that* $0\leq a_i(t,x)\leq 1$ *a.e.* $(t,x)\in\mathbb{R}\times\mathbb{T}^N$ *and*

$$\nu_{i,t}(x,\cdot)=(1-a_i(t,x))\,\delta_0(.)+a_i(t,x)\delta_{r_i}(.),\ \text{a.e.}\,(t,x)\in\mathbb{R}\times\mathbb{T}^N.$$

*Proof.* Let us reconsider $F_i(u) := u\,|h_i(u)\ln(u/r_i)|$ for $u \in [0,\infty)$ and recall that from equation (4.7) we have for any $\tau > 0$

$$\lim_{t\to+\infty}\int_t^{t+\tau}\int_{\mathbb{T}^N} F_i(u_i(s,x))\mathrm{d}x\mathrm{d}s = 0,\ i = 1,2.$$

Therefore, for $i = 1,2$ and from equation (5.5)

$$\begin{aligned} 0 &= \lim_{n\to\infty}\int_0^{\tau}\int_{\mathbb{T}^N} F_i(u_i(t+t_n,x))\mathrm{d}x\mathrm{d}t \\ &= \lim_{n\to\infty}|\mathbb{T}^N|\int_0^{\tau}\int_{\mathbb{T}^N\times[0,\gamma]} F_i(\lambda)\mu_{i,t}^n(\mathrm{d}x,\mathrm{d}\lambda)\mathrm{d}t \\ &= \int_0^{\tau}\int_{\mathbb{T}^N\times[0,\gamma]} F_i(\lambda)\nu_{i,t}(x,\mathrm{d}\lambda)\mathrm{d}x\mathrm{d}t. \end{aligned}$$

Since the map $u \mapsto F_i(u)$ is non-negative and only vanishes at $u = 0$ and $u = r_i$ one obtains that

$$\operatorname{supp}\nu_{i,t}(x,\cdot) \subset \{0\}\cup\{r_i\},\ \ a.e.\,(t,x) \in \mathbb{R}\times\mathbb{T}^N.$$

The above characterization of the support allows us to rewrite

$$\nu_{i,t}(x,\cdot) = \nu_{i,t}\left(x,\{0\}\right)\delta_0(.) + \nu_{i,t}\left(x,\{r_i\}\right)\delta_{r_i}(.),\ a.e.\,(t,x) \in \mathbb{R}\times\mathbb{T}^N.$$

Finally set $a_i(t,x) \equiv \nu_{i,t}(x,\{r_i\})$. Recalling that $(t,x) \mapsto \nu_{i,t}(x,\cdot)$ is measurable with value as a probability measure, thus $\nu_{i,t}\left(x,\{0\}\right) = 1 - \nu_{i,t}\left(x,\{r_i\}\right)$ and $(t,x) \mapsto a(t,x)$ is measurable, the result follows. □

Our next result shows the measurable function $a_i(t,x)$ is independent of the time variable $t$.

**Lemma 5.12.** *Under the same assumptions of Lemma 5.8, there exists a measurable map $c_i : \mathbb{T}^N \to \mathbb{T}^N$ such that $a_i \equiv a^i(t,x)$ provided by Lemma 5.11 is independent of $t$ and satisfies for any $t \in \mathbb{R}$,*

$$a_i(t,x) \equiv c_i(x),\ \ a.e.\ x \in \mathbb{T}^N,\ i = 1,2.$$

*Moreover, for any $t \in \mathbb{R}$,*

$$\nu_{i,t}(x,\cdot) = (1 - c_i(x))\delta_0(.) + c_i(x)\delta_{r_i}(.),\ \ a.e.\ x \in \mathbb{T}^N,\ i = 1,2,$$

*for some measurable functions $c_i : \mathbb{T}^N \to \mathbb{T}^N$, $i = 1,2$.*

*Furthermore, we have*

$$\lim_{n\to\infty}\delta_{u_i(t+t_n,x)} = (1 - c_i(x))\delta_0 + c_i(x)\delta_{r_i}, \tag{5.6}$$

*in the sense of the narrow convergence and where the limit depends on the choice of subsequence.*

*Proof.* Suppose $\mathbf{u} = (u_1, u_2)$ the classical solution. For any $\{t_n\}_{n\geq 0}$ with $t_n \to \infty$ as $n \to 0$ and any $\phi \in C_c^1(\mathbb{T}^N)$,

$$\begin{aligned}&\int_{\mathbb{T}^N} \phi(x)\partial_t u_i(t+t_n,x)\mathrm{d}x + \int_{\mathbb{T}^N} \phi(x)\mathrm{div}(u(t+t_n,x)\mathbf{v}(t+t_n,x))\mathrm{d}x\\ =&\int_{\mathbb{T}^N} \phi(x)u_i(t+t_n,x)h_i(u_i(t+t_n,x))\mathrm{d}x.\end{aligned}$$

Since $\phi$ has compact support, we have

$$\begin{aligned}&\int_{\mathbb{T}^N} \phi(x)\partial_t u_i(t+t_n,x)\mathrm{d}x\\ =&\int_{\mathbb{T}^N} \nabla\phi(x)\cdot\mathbf{v}(t+t_n,x)u(t+t_n,x)\mathrm{d}x + \int_{\mathbb{T}^N} \phi(x)u_i(t+t_n,x)h_i(u_i(t+t_n,x))\mathrm{d}x.\end{aligned}$$

Let $T \in \mathbb{R}$ and $\delta > 0$ be given. Integrating the both sides over $(T, T+\delta)$ leads to

$$\begin{aligned}&\int_{\mathbb{T}^N} \phi(x)\big(u_i(T+\delta+t_n,x) - u_i(T+t_n,x)\big)\mathrm{d}x\\ =&\int_T^{T+\delta}\int_{\mathbb{T}^N} \nabla\phi(x)\cdot\mathbf{v}(t+t_n,x)u(t+t_n,x)\mathrm{d}x\mathrm{d}t\\ &+\int_T^{T+\delta}\int_{\mathbb{T}^N} \phi(x)u_i(t+t_n,x)h_i(u_i(t+t_n,x))\mathrm{d}x\mathrm{d}t.\end{aligned} \tag{5.7}$$

Now equation (5.7) is also true for the solution integrated along the characteristics. In fact, we can apply Theorem 2.4 (iii), by choosing a sequence of initial distribution $\{\varphi_i^n\}_{n\geq 0} \subset C^1(\mathbb{T}^N)$ with

$$\varphi_i^n \xrightarrow{L^1(\mathbb{T}^N)} \varphi_i \in L^\infty(\mathbb{T}^N),$$

since the semiflow is continuous in $L^1$ norm, that is, for any $t \in [T, T+\delta]$,

$$\|u_i(t,x;\varphi_i^n) - u_i(t,x;\varphi_i)\|_{L^1} \to 0, \quad \text{as } n \to \infty,$$

we can pass the limit to both sides of (5.7). For the right-hand-side of (5.7), by (4.10) in Remark 4.11 that $\lim_{t\to\infty}\|\mathbf{v}(t,\cdot)\|_{C^0} = 0$ we have for the first term

$$\begin{aligned}&\lim_{n\to\infty}\left|\int_T^{T+\delta}\int_{\mathbb{T}^N} \nabla\phi(x)\cdot\mathbf{v}(t+t_n,x)u(t+t_n,x)\mathrm{d}x\mathrm{d}t\right|\\ \leq&\lim_{n\to\infty}\delta|\mathbb{T}^N|\|\phi\|_{C^1}\sup_{t\geq 0}\|u_i(t,\cdot)\|_{L^\infty}\|\mathbf{v}(t+t_n,\cdot)\|_{C^0} = 0.\end{aligned} \tag{5.8}$$

and the second term

$$\begin{aligned}&\int_T^{T+\delta}\int_{\mathbb{T}^N} \phi(x)u_i(t+t_n,x)h_i(u_i(t+t_n,x))\mathrm{d}x\mathrm{d}t\\ =&\int_T^{T+\delta}\int_{\mathbb{T}^N} \phi(x)\left[\int_{[0,\gamma]} \lambda h_i(\lambda)\,\delta_{u_i(t+t_n,x)}(\mathrm{d}\lambda)\right]\mathrm{d}x\mathrm{d}t.\end{aligned}$$

Letting $n \to \infty$, we have

$$\begin{aligned}&\lim_{n\to\infty}\int_T^{T+\delta}\int_{\mathbb{T}^N}\phi(x)u_i(t+t_n,x)h_i(u_i(t+t_n,x))\mathrm{d}x\mathrm{d}t\\&=\int_T^{T+\delta}\int_{\mathbb{T}^N}\phi(x)\left[\int_{[0,\gamma]}\lambda h_i\left(\lambda\right)\left[\left(1-a_i(t,x)\right)\delta_0+a_i(t,x)\delta_{r_i}\right]\left(\mathrm{d}\lambda\right)\right]\mathrm{d}x\mathrm{d}t=0.\end{aligned}\tag{5.9}$$

Therefore, by (5.8) and (5.9) we deduce the left-hand-side of (5.7)

$$\begin{aligned}&\lim_{n\to\infty}\int_{\mathbb{T}^N}\phi(x)\big(u_i(T+\delta+t_n,x)-u_i(T+t_n,x)\big)\mathrm{d}x\\&=r_i\int_{\mathbb{T}^N}\phi(x)\big(a_i(T+\delta,x)-a_i(T,x)\big)\mathrm{d}x=0.\end{aligned}$$

Hence we have

$$\int_{\mathbb{T}^N}\phi(x)\big(a_i(T+\delta,x)-a_i(T,x)\big)\mathrm{d}x=0,\ \forall\phi(x)\in C_c^1(\mathbb{T}^N).$$

Since $T\in\mathbb{R}$ and $\delta>0$ is arbitrary, we deduce for any $t\in\mathbb{R}$

$$a_i(t,x)=c_i(x),\ a.e.\,x\in\mathbb{T}^N,\tag{5.10}$$

where $c_i:\mathbb{T}^N\to\mathbb{T}^N$ is a measurable function. The last part of the lemma now follows by the above equation (5.10), (5.4) and Lemma 5.12. □

Next, we study the narrow convergence of the measure $\delta_{(u_1+u_2)(t+t_n,x)}$ as $n\to\infty$.

**Corollary 5.13.** *Let $\{t_n\}_{n\geq 0}$ be a given increasing sequence tending to $\infty$ as $n\to\infty$. Then, up to a subsequence, we have two measurable functions $c_i(x)\in[0,1]$ for $i=1,2$, such that for any $t\geq 0$,*

$$\lim_{n\to\infty}\delta_{(u_1+u_2)(t+t_n,x)}=\left(1-\sum_{i=1,2}c_i(x)\right)\delta_0+\sum_{i=1,2}c_i(x)\delta_{r_i}$$

*in the sense of narrow convergence.*

*Proof.* From segregation property in Theorem 3.1, we have for any $\eta\in C([0,\gamma])$ that

$$\eta\left(u_1(t,x)+u_2(t,x)\right)+\eta(0)=\eta(u_1(t,x))+\eta(u_2(t,x)),\quad\forall(t,x)\in\mathbb{R}_+\times\mathbb{T}^N,$$

which is equivalent to say that

$$\delta_0+\delta_{(u_1+u_2)(t,x)}=\delta_{u_1(t,x)}+\delta_{u_2(t,x)}.$$

Therefore, for any $\varphi\in L^1(\mathbb{T}^N)$, we have

$$\begin{aligned}&\lim_{n\to\infty}\int_{\mathbb{T}^N}\varphi(x)\int_{[0,\gamma]}\eta(\lambda)\left(\delta_0+\delta_{(u_1+u_2)(t+t_n,x)}\right)\left(\mathrm{d}\lambda\right)\mathrm{d}x\\&=\lim_{n\to\infty}\int_{\mathbb{T}^N}\varphi(x)\int_{[0,\gamma]}\eta(\lambda)\left(\delta_{u_1(t+t_n,x)}+\delta_{u_2(t+t_n,x)}\right)\left(\mathrm{d}\lambda\right)\mathrm{d}x\\&=\int_{\mathbb{T}^N}\varphi(x)\int_{[0,\gamma]}\eta(\lambda)\left(\left(2-\sum_{i=1,2}c_i(x)\right)\delta_0+\sum_{i=1,2}c_i(x)\delta_{r_i}\right)\left(\mathrm{d}\lambda\right)\mathrm{d}x.\end{aligned}$$

By subtracting the term $\delta_0$ from each side, we deduce that

$$\lim_{n\to\infty} \delta_{(u_1+u_2)(t+t_n,x)} = \left(1 - \sum_{i=1,2} c_i(x)\right)\delta_0 + \sum_{i=1,2} c_i(x)\delta_{r_i} \tag{5.11}$$

in the sense of the narrow convergence topology of $Y(\mathbb{T}^N;[0,\gamma])$. Here we recall that the limit depends on the choice of subsequence. □

**Lemma 5.14.** *Under the same assumptions as in Lemma 5.8, the following equality holds true:*

$$r_1c_1(x) + r_2c_2(x) \equiv r_1 + r_2 - E_\infty, \text{ a.e. } x \in \mathbb{T}^N,$$

*where* $E_\infty := \lim_{t\to\infty} E\left[(u_1,u_2)(t,\cdot)\right]$ *in* (4.4).

*Proof.* Recall equation (4.3) where we have $G_i(0) = r_i, G(r_i) = 0$, we can see that

$$\begin{aligned}
\lim_{n\to\infty} E_i\left[u_i(t+t_n,\cdot)\right] &= \lim_{n\to\infty} \frac{1}{|\mathbb{T}^N|}\int_{\mathbb{T}^N} G_i(u_i(t+t_n,x))\mathrm{d}x \\
&= \lim_{n\to\infty} \frac{1}{|\mathbb{T}^N|}\int_{\mathbb{T}^N\times[0,\gamma]} G_i(\lambda)\delta_{u_i(t+t_n,x)}(\mathrm{d}\lambda)\mathrm{d}x \\
&= \lim_{n\to\infty} \frac{1}{|\mathbb{T}^N|}\int_{\mathbb{T}^N\times[0,\gamma]} G_i(0)(1-c_i(x)) + G_i(r_i)c_i(x)\mathrm{d}x \\
&= r_i - \frac{1}{|\mathbb{T}^N|}\int_{\mathbb{T}^N} r_ic_i(x)\mathrm{d}x.
\end{aligned} \tag{5.12}$$

Meanwhile, from (4.9) the Fourier coefficients satisfy

$$\lim_{t\to\infty} c_k\left[(u_1+u_2)(t,\cdot)\right] = 0, \quad \forall k \in \mathbb{Z}^N\backslash\{0\}.$$

On the other hand, we have for all $k \in \mathbb{Z}^N\backslash\{0\}$

$$\begin{aligned}
\lim_{n\to\infty} c_k\left[(u_1+u_2)(t+t_n,\cdot)\right] &= \lim_{n\to\infty} \frac{1}{|\mathbb{T}^N|}\int_{\mathbb{T}^N} e^{-ikx}(u_1+u_2)(t+t_n,x)\mathrm{d}x \\
&= \lim_{n\to\infty} \frac{1}{|\mathbb{T}^N|}\int_{\mathbb{T}^N\times[0\times\gamma]} e^{-ikx}\lambda\left(\delta_{u_1(t+t_n,x)} + \delta_{u_1(t+t_n,x)}\right)(\mathrm{d}\lambda)\mathrm{d}x \\
&= \frac{1}{|\mathbb{T}^N|}\int_{\mathbb{T}^N} e^{-ikx}(r_1c_1(x) + r_2c_2(x))\mathrm{d}x.
\end{aligned}$$

Since $c_1, c_2 \in L^\infty(\mathbb{T}^N) \subset L^2(\mathbb{T}^N)$ and $\{e^{-ikx}\}_{k\in\mathbb{Z}}$ is a basis of $L^2(\mathbb{T}^N)$. This implies that $r_1c_1(x) + r_2c_2(x)$ is a constant function. Recall that

$$E_\infty = \lim_{n\to\infty}\sum_{i=1,2} E_i\left[u_i(t+t_n,\cdot)\right] = r_1 + r_2 - \frac{1}{|\mathbb{T}^N|}\int_{\mathbb{T}^N}\sum_{i=1,2} r_ic_i(x)dx,$$

thus the result follows. □

**Lemma 5.15** (Segregation at $t = \infty$)**.** *Under the same assumptions as in Lemma 5.8, the following equation holds*

$$c_1(x)c_2(x) = 0, \quad \text{a.e., } x \in \mathbb{T}^N.$$

*Moreover when* $r_1 = r_2 = r$*, then*

$$r \le E_\infty \le 2r.$$

*Proof.* By using the segregation property in Theorem 3.1, we can see that, for any $\eta \in C_b([0,\gamma])$,

$$\eta\big( (u_1(t,x)+u_2(t,x))^2 \big) = \eta\big(u_1^2(t,x)+u_2^2(t,x)\big),\ \forall\, t\in\mathbb{R}_+,\ a.e.\, x\in\mathbb{T}^N.$$

Therefore, for any Borel set $A\in\mathcal{B}(\mathbb{T}^N)$, we deduce the following equation

$$\begin{aligned}&\int_{A\times[0,\gamma]} \eta(\lambda^2)\delta_{(u_1+u_2)(t+t_n,x)}(\mathrm{d}\lambda)\mathrm{d}x\\ =&\int_{A\times[0,\gamma]^2} \eta(\lambda_1^2+\lambda_2^2)\delta_{u_1(t+t_n,x)}(\mathrm{d}\lambda_1)\delta_{u_2(t+t_n,x)}(\mathrm{d}\lambda_2)\mathrm{d}x.\end{aligned} \tag{5.13}$$

By equation (5.6) and (5.11), we let $n\to\infty$, then for the left-hand-side (L.H.S.) of equation (5.13)

$$\begin{aligned}\lim_{n\to\infty}\text{L.H.S.} &= \int_{A\times[0,\gamma]} \eta(\lambda^2)\left[\left(1-\sum_{i=1,2}c_i(x)\right)\delta_0(\mathrm{d}\lambda)+\sum_{i=1,2}c_i(x)\delta_{r_i}(\mathrm{d}\lambda)\right]\\ &= \int_A \eta(0)\left(1-\sum_{i=1,2}c_i(x)\right)+\sum_{i=1,2}\eta(r_i^2)c_i(x)\mathrm{d}x.\end{aligned}$$

Then for the right-hand-side (R.H.S.) of equation (5.13)

$$\begin{aligned}\lim_{n\to\infty}\text{R.H.S.} &= \int_{A\times[0,\gamma]^2}\eta(\lambda_1^2+\lambda_2^2)\prod_{i=1,2}\left[(1-c_i(x))\,\delta_0(\mathrm{d}\lambda_i)+c_i(x)\delta_{r_i}(\mathrm{d}\lambda_i)\right]\mathrm{d}x\\ &= \int_A\Big(\eta(0)\prod_{i=1,2}(1-c_i(x))+\eta(r_1^2)c_1(x)(1-c_2(x))\\ &\quad+\eta(r_2^2)c_2(x)(1-c_1(x))+\eta(r_1^2+r_2^2)c_1(x)c_2(x)\Big)\mathrm{d}x.\end{aligned}$$

Comparing the two limits and noticing that $A\in\mathcal{B}(\mathbb{T}^N)$ is arbitrary, we conclude that

$$c_1(x)c_2(x)\Big[\eta(0)+\eta(r_1^2+r_2^2)-\eta(r_1^2)-\eta(r_2^2)\Big]=0,\ \text{for a.e. } x\in\mathbb{T}^N.$$

Furthermore, since $\eta\in C_b([0,\gamma])$ is any given function, we can choose an $\eta$ such that

$$\eta(0)+\eta(r_1^2+r_2^2)-\eta(r_1^2)-\eta(r_2^2)\neq 0,$$

thus

$$c_1(x)c_2(x)=0,\quad a.e.,\ x\in\mathbb{T}^N. \tag{5.14}$$

Since by Lemma 5.11 and 5.12, one has $0\le c_i(x)\le 1$ for any $x\in\mathbb{T}^N$. Hence, one can deduce from Lemma 5.14

$$0\le E_\infty\le r_1+r_2.$$

Moreover, one can deduce from (5.14) that

$$\min\{r_1,r_2\}\le E_\infty\le r_1+r_2.$$

If we assume $r_1=r_2=r$, then

$$r\le E_\infty\le 2r.$$

□

*Proof of Theorem 5.1.* By Lemma 5.10, the sequence $\{\delta_{u_i(t+t_n,x)}\}_{n\geq 0}$ is relatively compact in $Y_{loc}\left(\mathbb{R}\times\mathbb{T}^N;[0,\gamma]\right)$ with locally narrow topology, thus, up to a sequence, we have

$$\lim_{n\to\infty}\delta_{u_i(t+t_n,x)}=\nu_{i,t}(x,\cdot)\text{ in the topology of }Y_{loc}\left(\mathbb{R}\times\mathbb{T}^N;[0,\gamma]\right).$$

The key arguments of the proof lies in the two consequences of the decreasing energy functional, namely, equation (4.6) and equation (4.7). Lemma 5.11 is a consequence of the first equation (4.6) by which we can determine the support of $\nu_{i,t}(x,\cdot)$, i.e., there exists measurable functions $a_i(t,x)$ such that

$$\nu_{i,t}(x,\cdot)=(1-a_i(t,x))\delta_0(.)+a_i(t,x)\delta_{r_i}(.),\ \ a.e.\ x\in\mathbb{T}^N,\ i=1,2.$$

Moreover, Lemma 5.8 and Lemma 5.12 enable us to write $a_i(t,x)\equiv c_i(x)$, $i=1,2$. Thus, we have

$$\lim_{n\to\infty}\delta_{u_i(t+t_n,x)}=(1-c_i(x))\delta_0+c_i(x)\delta_{r_i}\text{ in the topology of }Y_{loc}\left(\mathbb{R}\times\mathbb{T}^N;[0,\gamma]\right)$$

Applying the segregation property, we have

$$\delta_0+\delta_{(u_1+u_2)(t,x)}=\delta_{u_1(t,x)}+\delta_{u_2(t,x)},$$

hence by Corollary 4.12,

$$\lim_{n\to\infty}\delta_{(u_1+u_2)(t+t_n,x)}=\left(1-\sum_{i=1,2}c_i(x)\right)\delta_0+\sum_{i=1,2}c_i(x)\delta_{r_i}\tag{5.15}$$

If in addition, we assume that $r_1=r_2=r$, we apply Lemma 5.14 where we used the decaying of Fourier coefficients in equation (4.7), which yields

$$\sum_{i=1}^{2}c_i(x)=2-\frac{E_\infty}{r}.$$

together with equation (5.15) we obtain

$$\lim_{n\to\infty}\delta_{(u_1+u_2)(t+t_n,x)}=(E_\infty/r-1)\delta_0+(2-E_\infty/r)\delta_r,$$

in the sense of the narrow convergence topology of $Y(\mathbb{T}^N;[0,\gamma])$ and by Lemma 5.15 we have $E_\infty\in[r,2r]$. Now the limit does not depend on $t$ and the choice of the subsequence. Since $\{t_n\}_{n\geq 0}$ is any given sequence that tends to infinity and $\left(\mathbb{T}^N,\mathcal{B}(\mathbb{T}^N)\right)$ is a countably generated $\sigma-$algebra then the topology $Y(\mathbb{T}^N;[0,\gamma])$ is metrizable (see for instance [102, Theorem 1] or the monograph [27]), therefore we can conclude that

$$\lim_{t\to\infty}\delta_{(u_1+u_2)(t,x)}=(E_\infty/r-1)\delta_0+(2-E_\infty/r)\delta_r.$$

Thus, Theorem 5.1 follows. □

# 6 Discussion and numerical simulations

In this section we will study the system (1.1) numerically for the one dimensional case. Our original motivation is coming from two species of cell growing in a petri dish. The two dimensional case will be considered in some future work.

Here we will focus on the coexistence and the exclusion principle for two species. From Theorem 5.1, we deduce

$$\lim_{t\to\infty} \delta_{(u_1+u_2)(t,x)} = (E_\infty/r - 1)\delta_0 + (2 - E_\infty/r)\delta_r, \text{ in the sense of narrow convergence.}$$

Therefore the limit $E_\infty := \lim_{t\to\infty} E[(u_1, u_2)(t, \cdot)]$ is an important index to determine whether solution $u_1+u_2$ converges to a Young measure in the sense of narrow convergence or to a constant in $L^1$ norm (see Remark 5.2). To that aim, we trace the curve $t \longmapsto E[(u_1, u_2)(t, \cdot)]$ in numerical simulations, which has been analytically proved decreasing in Theorem 4.6. Moreover, we also plot the curve $t \longmapsto E_i[u_i(t, \cdot)]$, $i = 1, 2$, respectively. This will help us to understand the limit for each species $u_i$.

In the numerical simulations, we focus on the convergence of the energy functional which implies the convergence of the total number for each species. In fact, by using (5.6) we obtain

$$\lim_{t\to\infty} \frac{1}{|\mathbb{T}|}\int_{\mathbb{T}} u_i(t,x)dx = \lim_{t\to\infty} \frac{1}{|\mathbb{T}|}\int_{\mathbb{T}}\int_{[0,\gamma]} \lambda\delta_{u_i(t,x)}(d\lambda)dx = \frac{r_i}{|\mathbb{T}|}\int_{\mathbb{T}}\int_{[0,\gamma]} c_i(x)dx.$$

Hence by using (5.12) one has

$$\lim_{t\to\infty} E_i[u_i(t,\cdot)] = r_i\left(1 - \frac{1}{|\mathbb{T}|}\int_{\mathbb{T}} c_i(x)dx\right) = r_i - \lim_{t\to\infty}\frac{1}{|\mathbb{T}|}\int_{\mathbb{T}} u_i(t,x)dx. \tag{6.1}$$

That is to say that the energy functional inform us about the asymptotic number of individuals for each species.

In this section, we will investigate numerically the following properties.

**Coexistence:** If $r_1 = r_2 = r$, then $c_1(x), c_2(x) \in (0, 1)$, *a.e.*, $x \in \mathbb{T}^N$. For each species, the following limits exist

$$\lim_{t\to\infty} \|u_i(t,\cdot)\|_{L^1} = r\int_{\mathbb{T}^N} c_i(x)dx \in (0, r),\ i = 1, 2.$$

We will see that the relative location of each species influences the asymptotic number in each species. Moreover, we have

$$(u_1 + u_2)(t, x) \xrightarrow{L^1} r,\ t \to \infty.$$

**Exclusion Principle:** If $r_1 > r_2$ (resp. $r_1 < r_2$) then $c_1(x) = 1$, $c_2(x) = 0$ (resp. $c_1(x) = 0$, $c_2(x) = 1$) *a.e.*, $x \in \mathbb{T}^N$ , which implies

$$u_1(t,x) \xrightarrow{L^1} r_1, \quad u_2(t,x) \xrightarrow{L^1} 0,\ (resp.\, u_1(t,x) \xrightarrow{L^1} 0, \quad u_2(t,x) \xrightarrow{L^1} r_2),$$

and

$$(u_1 + u_2)(t, x) \xrightarrow{L^1} \max\{r_1, r_2\},\ t \to \infty.$$

## 6.1 The case $r_1 = r_2$ implies the coexistence

Our first scenario is to present the results in Theorem 5.1. It is interesting to notice that in Theorem 5.1, we only assume the equilibrium of the corresponding ODE system for each species to be the same without imposing any other condition on $h$, which means that the dynamics for these two species can be different. Hence, we will use the following two different reaction functions for different species

$$u_1 h_1(u_1+u_2) = u_1\left(\frac{b_1}{1+\gamma(u_1+u_2)} - \mu\right), \quad u_2 h_2(u_1+u_2) = b_2 u_2\left(1 - \frac{u_1+u_2}{K}\right). \tag{6.2}$$

One can verify that $h_i$ satisfies Assumption 1.1 and Assumption 4.1 with their roots (i.e., $h_i(r_i) = 0$, $i = 1, 2$) as

$$r_1 := \frac{b_1 - \mu}{\gamma\mu}, \quad r_2 = K.$$

Our kernel $\rho$ in the simulation is chosen as

$$\rho(\mathbf{x}) = e^{-\pi|\mathbf{x}|^2}, \quad \mathbf{x} \in \mathbb{R}^N, \tag{6.3}$$

which is the Gaussian kernel and we consider the dimension $N = 1$ in this section. Therefore, due to Remark 1.3 and Remark 4.5, Assumption 1.2 and Assumption 4.4 are satisfied.

We set the initial distribution for two species to be of compact supports and separated. From Theorem 3.1, we shall observe the segregation property of two species as time evolves. Our parameters in system (1.1) are given as

$$b_1 = b_2 = 1.2,\ \mu = 1,\ \gamma = 1,\ K = 0.2, \tag{6.4}$$

therefore one can calculate

$$r_1 = r_2 = 0.2.$$

Now we trace the curve $t \longmapsto E[(u_1, u_2)(t, \cdot)]$ in numerical simulation, which has been analytically proved decreasing in Theorem 5.1. We also plot the curve $t \longmapsto E_i[u_i(t, \cdot)]$, $i = 1, 2$, respectively. Moreover, we plot the variation of the mean value of the total number of individuals for each species, that is

$$t \longmapsto \frac{1}{2\pi}\int_0^{2\pi} u_i(t, x)dx, \quad i = 1, 2.$$

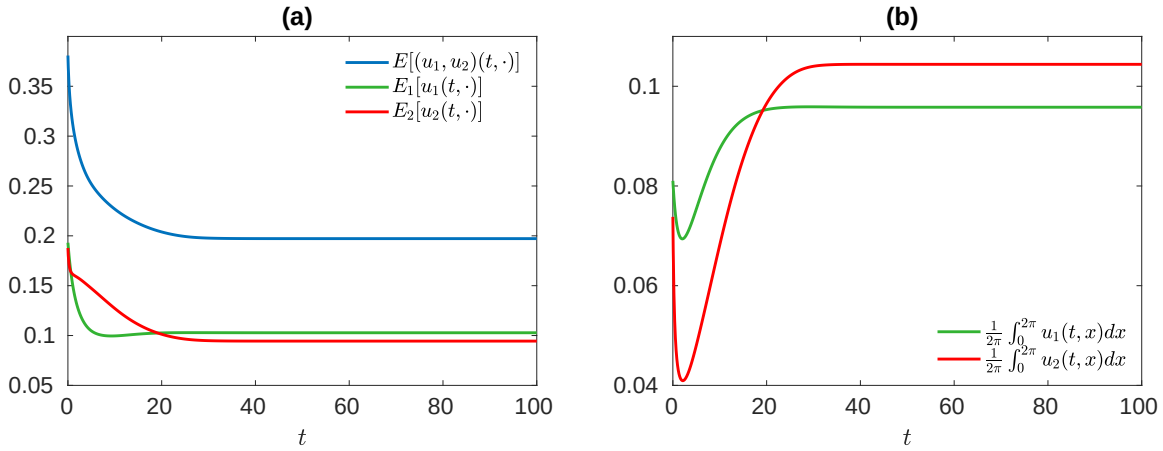


Figure 2.2: *Figure (a) is the plot of the curves* $t \longmapsto E_i[u_i(t,\cdot)]$, $i = 1, 2$, *(green and red curves respectively) and* $t \longmapsto E[u_1, u_2)(t,\cdot)]$ *(blue curve) under system (1.1) with reaction functions as (6.2) and kernel* $\rho$ *as Gaussian in (6.3). We set our parameters as in (6.4). Thus, one has* $r_1 = r_2 = 0.2$. *We trace the curve* $t \longmapsto E[(u_1, u_2)(t,\cdot)]$ *which is decreasing. We can see that the curve* $t \longmapsto E_1[u_1(t,\cdot)]$ *is not monotone decreasing while* $t \longmapsto E_2[u_2(t,\cdot)]$ *is monotone decreasing and they converge when* $t \to \infty$. *Figure (b) is the plot of total number of individuals for each species.*

From Figure 2.2, we can see that the limit $E_\infty$ exists and equals to $r = 0.2$. From Theorem 5.1 and Remark 5.2, the limit $E_\infty = r$ implies

$$(u_1 + u_2)(t,x) \xrightarrow{L^1} r, \quad t \to \infty.$$

Moreover, from the simulation we note that each limit $E_{i,\infty} := \lim_{t\to\infty} E_i[u_i(t,\cdot)]$ exists for $i = 1, 2$. From (6.1) we have

$$E_{i,\infty} = r\left(1 - \frac{1}{|\mathbb{T}|}\int_{\mathbb{T}} c_i(x)dx\right), \quad i = 1, 2. \tag{6.5}$$

By our simulation, we can see that $E_{1,\infty}, E_{2,\infty} \in (0, r)$ while $E_{1,\infty} + E_{2,\infty} = r$, together with equation (6.5) we can deduce $c_1(x), c_2(x) \in (0, 1)$, $c_1(x) + c_2(x) = 1$. Notice that $c_1(x), c_2(x) \in (0, 1)$ implies the limits

$$\lim_{n\to\infty} \delta_{u_i(t_n,x)} = (1 - c_i(x))\delta_0 + c_i(x)\delta_r, \quad i = 1, 2,$$

is not a single Dirac measure. Therefore, using Young measure and the weak compactness in $Y(\mathbb{T}; [0, \gamma])$ helps us to understand the limit of the solution.

Now we plot the evolution of the two populations under system (1.1) in Figure 2.3.

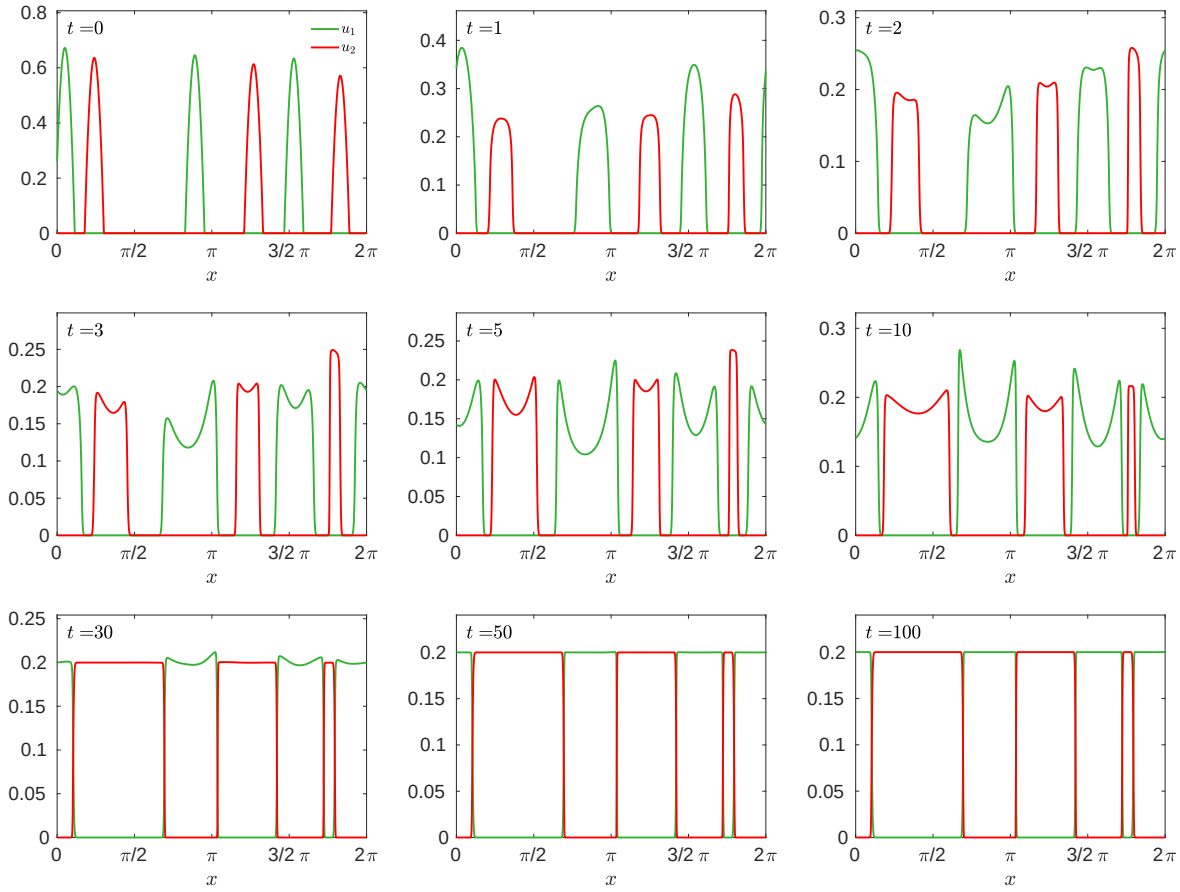


Figure 2.3: *The simulation of system* (1.1) *with reaction functions as* (6.2) *and kernel* $\rho$ *as Gaussian in* (6.3). *The green curves represent species* $u_1$, *the red represents species* $u_2$. *We set our parameters as in* (6.4). *Thus, one has* $r_1 = r_2 = 0.2$. *As we have* $r_1 = r_2$, *we observe the coexistence of the two species and the segregation property and after* $t = 100$ *the distributions of the two species stay the same.*

For the asymptotic behavior of the population, we can see from Figure 2.3 that the sum of two species $u_1 + u_2$ reaches a steady state at $t = 100$. From the pattern at each moment $t$, we can see two species keep segregated in stead of being mixed (in the case with linear diffusion). This result is due to our nonlocal advection term which ensures that the propagation speed is finite, which captures the "islets" phenomenon in the real biological experiments in dimension two (see Figure 1. in [88]).

## 6.2 Initial location matters

Consider two different initial distributions $\mathbf{u_0} = (u_1(0,x), u_2(0,x))$ and $\tilde{\mathbf{u}}_\mathbf{0} = (\tilde{u}_1(0,x), \tilde{u}_2(0,x))$ and assume their $L^1$ norms are the same, that is

$$\int_{\mathbb{T}} u_i(0,x)dx = \int_{\mathbb{T}} \tilde{u}_i(0,x)dx, \quad i = 1, 2.$$

Under the same set of parameters, one may ask whether the limits

$$U_{i,\infty} := \lim_{t\to\infty} \frac{1}{|\mathbb{T}|}\int_{\mathbb{T}} u_i(t,x)dx, \quad \tilde{U}_{i,\infty} := \lim_{t\to\infty} \frac{1}{|\mathbb{T}|}\int_{\mathbb{T}} \tilde{u}_i(t,x)dx, \quad i=1,2. \tag{6.6}$$

for each species $i = 1, 2$ will be the same or not.

In the real biological experiments, this situation corresponds to the case where the researchers use the same quantity of cells for each species for two separate petri dishes. Supposing the intrinsic mechanisms of cell population for these two groups are the same, the only difference is the initial cell distributions in two petri dishes. We are interested in whether the final total mass for each population are the same. Before our simulation, we give two different initial distributions as in Figure 2.4.

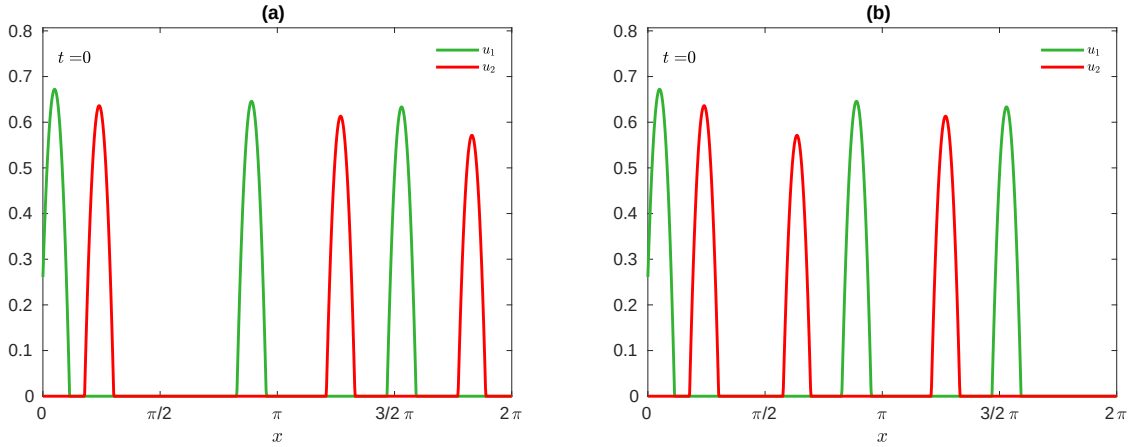


Figure 2.4: *Figures (a) and (b) correspond respectively to the initial distributions* $\mathbf{u_0}$ *and* $\tilde{\mathbf{u}}_\mathbf{0}$. *In Figure (a), we shift the population of* $u_2$ *(red curve) at position in between* $3/2\pi$ *and* $2\pi$ *to position in between* $\pi/2$ *to* $\pi$. *Therefore, the number individuals for each species is conserved.*

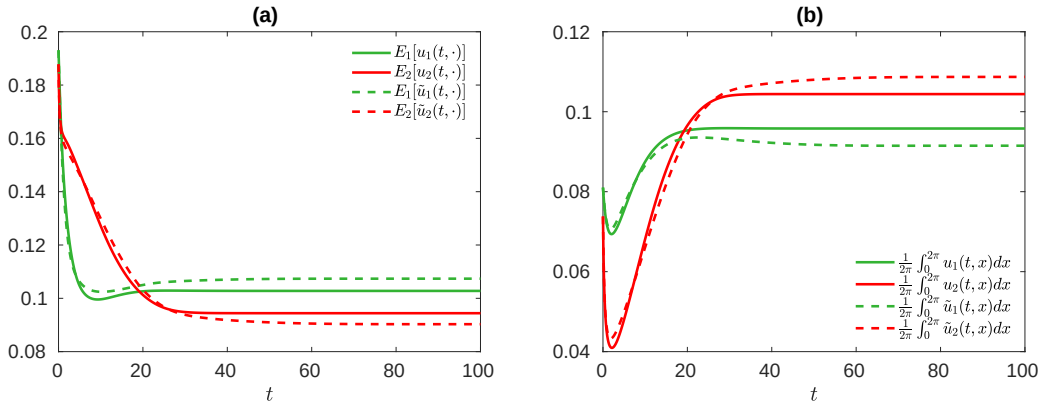


Figure 2.5: *In this figure we plot the energy functional (see Figure (a)) and the mean value of individuals (see Figure (b)) corresponding to two sets of different initial distributions in Figure 2.4. The dashed lines correspond to the simulation with initial distribution as in Figure 2.4 (a) and solid lines correspond to initial distribution as in Figure 2.4 (b). The parameters are the same as in (6.4).*

In Figure 2.5, we plot the energy functional and the number of individuals corresponding to each initial distribution in Figure 2.4. Since the limits $U_{i,\infty}$ and $\tilde{U}_{i,\infty}$ have a significant difference from Figure 2.5 (b), thus we conclude the final total mass depends on the position of the initial value.

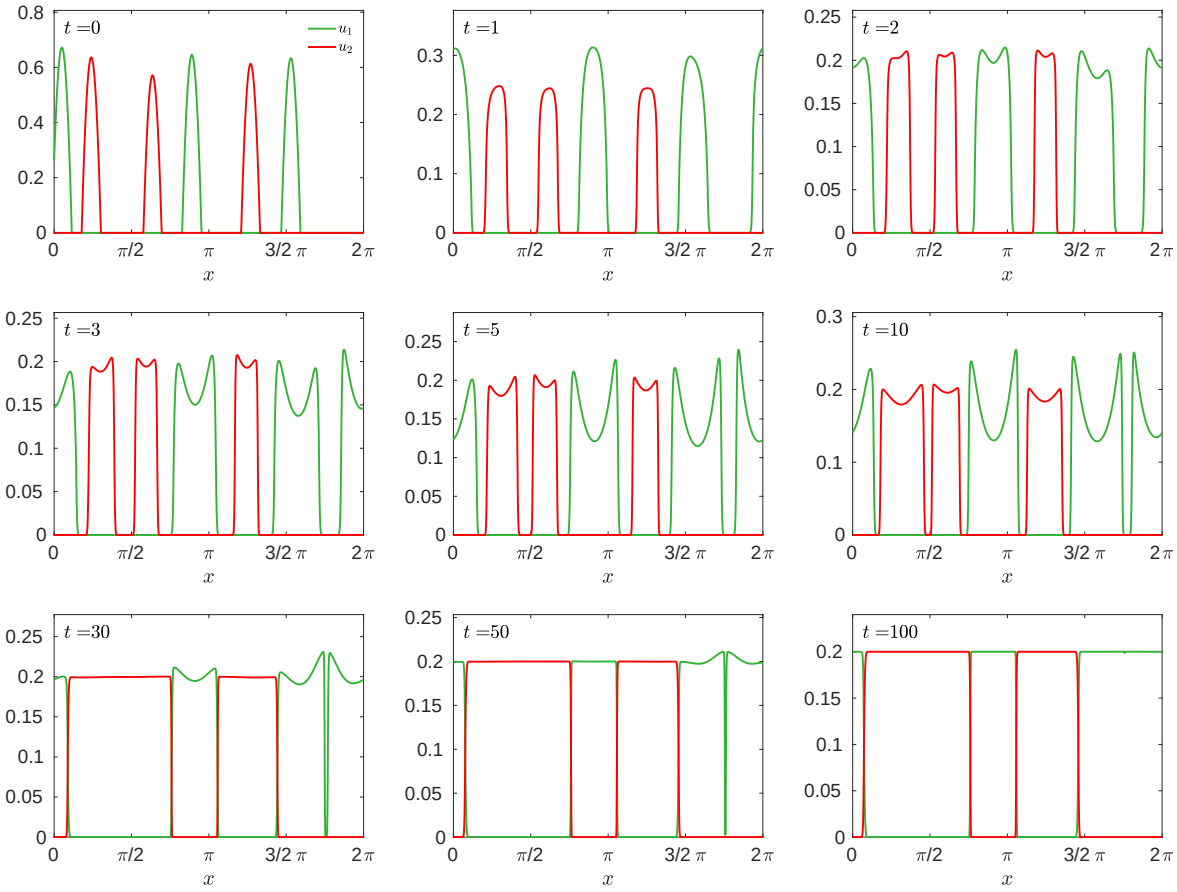


Figure 2.6: *The simulation of system* (1.1) *with reaction functions as* (6.2) *and kernel* $\rho$ *as Gaussian in* (6.3). *The green curves represent species* $u_1$, *the red represents species* $u_2$. *We set our parameters as in* (6.4). *Thus, one has* $r_1 = r_2 = 0.2$ *which implies the coexistence of the two species and after* $t = 100$ *the distributions of the two species stay the same.*

Now we give the evolution of the two populations under system (1.1). As for the simulation in Figure 2.6, we can see the same coexistence as in Figure 2.3 and the sum of the two populations

$$(u_1 + u_2)(t, x) \xrightarrow{L^1} r, \quad t \to \infty.$$

However, the final patterns of two species at $t = 100$ in Figure 2.6. (i) and Figure 2.3. (i) are evidently different.

## 6.3 The case $r_1 \neq r_2$ implies the competitive exclusion

Our second scenario complements the results in Theorem 5.1, without loss of generality we allow $r_1 > r_2$. This means species $u_1$ is favored in the environment. We call this

scenario the exclusion principle. Our parameters for the reaction functions (6.2) are given as

$$b_1 = 1.5,\ b_2 = 1.2,\ \mu = 1,\ \gamma = 1,\ K = 0.2. \tag{6.7}$$

therefore we can calculate

$$r_1 = 0.5 > r_2 = 0.2.$$

As before, we trace the curve $t \longmapsto E[(u_1, u_2)(t, \cdot)]$ in numerical simulation and we also plot the curve $t \longmapsto E_i[u_i(t, \cdot)]$, $i = 1, 2$, respectively. Moreover, we plot the variation of the mean value of the total number of individuals for each species.

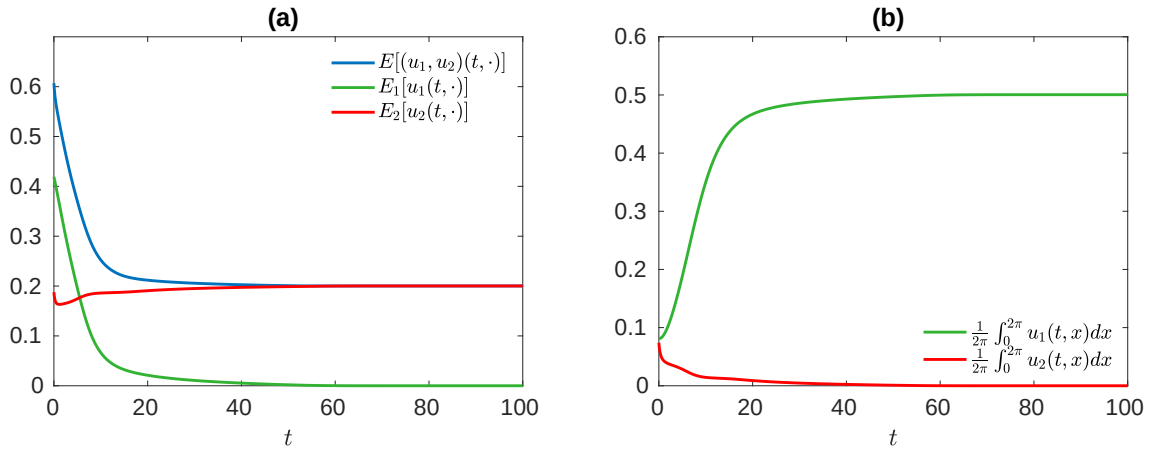


Figure 2.7: *Figure (a) is the plot of the curves $t \longmapsto E_i[u_i(t, \cdot)]$, $i = 1, 2$, (green and red curves respectively) and $t \longmapsto E[u_1, u_2)(t, \cdot)]$ (blue curve) under system (1.1) with reaction functions as (6.2) and kernel $\rho$ as Gaussian in (6.3). We set our parameters as in (6.7). Thus, one has $r_1 = 0.5 > r_2 = 0.2$. We trace the curve $t \longmapsto E[(u_1, u_2)(t, \cdot)]$ which is decreasing. We can also see the curve $t \longmapsto E_1[u_1(t, \cdot)]$ is decreasing while $t \longmapsto E_2[u_2(t, \cdot)]$ is not monotone decreasing and their limits exist. Figure (b) is the plot of mean value of individuals for each species.*

By tracing the curve $t \longmapsto E[(u_1, u_2)(t, \cdot)]$, we can see from Figure 2.7 that it is strictly decreasing and it confirms again the result which has been proved in Theorem 4.6. We can also see that the curve $t \longmapsto E_1[u_1(t, \cdot)]$ is decreasing while $t \longmapsto E_2[u_2(t, \cdot)]$ is not monotone decreasing and their limits are

$$\lim_{t\to\infty} E_1[u_1(t, \cdot)] = 0, \quad \lim_{t\to\infty} E_2[u_1(t, \cdot)] = r_2.$$

If we have $E_{1,\infty} = 0, E_{2,\infty} = r_2$, since $c_i(x) \in [0, 1]$, $a.e.\, x \in \mathbb{T}$ for $i = 1, 2$ and by equation (6.5) one obtains $c_1(x) = 1$, $c_2(x) = 0$. Therefore, we have $c_1(x) + c_2(x) = 1$, $a.e.\, x \in \mathbb{T}$ and the convergence in Theorem 5.1 is in the sense of $L^1$ (see Remark 5.2)

$$u_1(t, x) \xrightarrow{L^1} r_1, \quad u_2(t, x) \xrightarrow{L^1} 0,\ t \to \infty,$$

and

$$(u_1 + u_2)(t, x) \xrightarrow{L^1} r_1,\ t \to \infty.$$

This means if $r_1 > r_2$ (resp. $r_2 > r_1$), the species $u_1$ will exclude $u_2$ (resp. $u_2$ will exclude $u_1$) when $t$ tends to infinity. Therefore, we can conclude the exclusion principle as in the beginning of this section. We plot the evolution of the solution as follows.

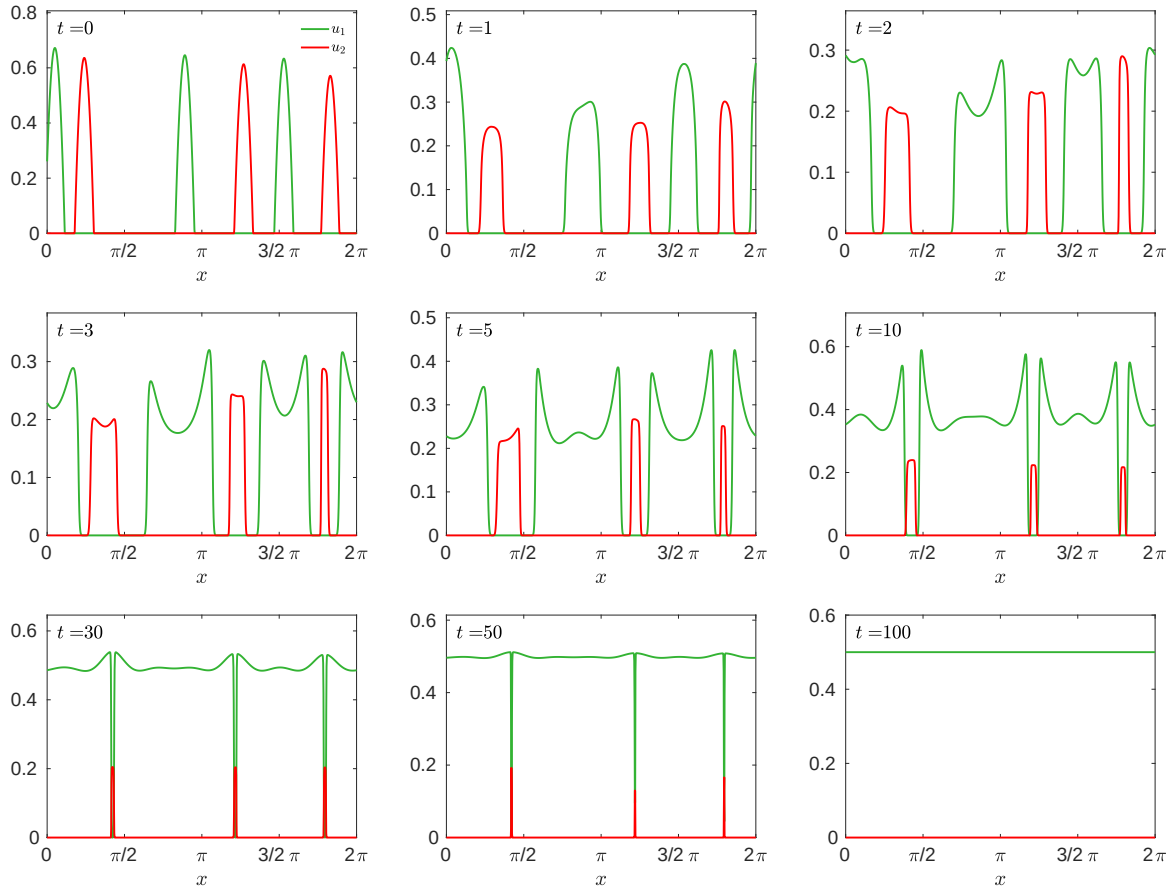


Figure 2.8: *The simulation of system* (1.1) *with kernel* $\rho$ *as in* (6.3). *The green curves represent species* $u_1$, *the red represents species* $u_2$. *We set our parameters as in* (6.7). *Thus, one has* $r_1 = 0.5 > r_2 = 0.2$. *As we have* $r_1 > r_2$, *we observe the principle of exclusion of the two species and the populations maintain the segregation property as time evolves and after* $t = 100$ *the distributions of the two species stay the same.*

In the simulation of Figure 2.8, species $u_1$ shows its dominance over $u_2$ when $t = 5$. As for asymptotic behavior, in the last figure when $t = 100$, we can see species $u_1$ crowd out species $u_2$ completely.

# Chapter 3

# A cell-cell repulsion model on a hyperbolic Keller-Segel equation

## Contents

# 1 Introduction

In many recent biological experiments, the co-culture of multiple types of cells has been used for a better understanding of cell-cell interactions. This is a typical case in the context of studying cancer cells where the interaction between cancer cells and normal cells plays a crucial role in tumor development as well as in the resistance of cells to chemotherapeutic drugs. The goal of this work is to introduce a mathematical model taking care of the cell growth together with the spatial segregation property between two types of cells. Such a phenomenon was observed by Pasquier et al. [88]. They studied the protein transfer between two types of human breast cancer cell. Over a 7-day cell co-culture, the spatial competition was observed between these two types of cells and a clear boundary was formed between them on day 7 (see Figure 3.1). Segregation property in cell co-culture was also studied recently by Taylor et al. [99]. They compared the experimental results with an individual-based model. They found the heterotypic repulsion and homotypic cohesion can account for the cell segregation and the border formation. A similar segregation property is also found in the mosaic pattern between nections and cadherins in the experiments of Katsunuma et al. [64].

The early attempts to explain the segregation property by continuum equations date back to 1970s. Shigesada, Kawasaki and Teramoto [95] studied segregation with a nonlinear diffusion model and they found the spatial segregation acts to stabilize the coexistence of two similar species, relaxing the competition among different species. Lou and Ni [69] generalized the model and studied the steady state problem for the self/cross-diffusion model. For the nonlinear diffusion model, Bertsch et al. [14] in their work proved the existence of segregated solutions when the reaction term is of Lotka-Volterra type.

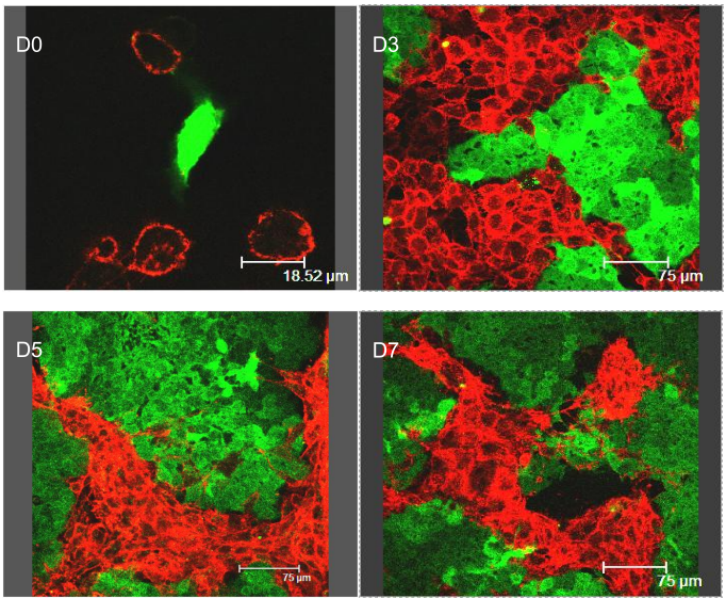


Figure 3.1: *Direct immunodetection of P-gp transfers in co-cultures of sensitive (MCF-7) and resistant (MCF-7/Doxo) variants of the human breast cancer cell line.*

Here instead of using nonlinear diffusion models, we will focus on a (hyperbolic) Keller-Segel model. Such models have been used to describe the attraction and the repulsion of

cell populations known as chemotaxis models. Theoretical and mathematical modeling of chemotaxis can date to the pioneering works of Patlak [87] in the 1950s and Keller and Segel [66] in the 1970s. It has become an important model in the description of tumor growth or embryonic development. We refer to the review papers of Horstmann [61] and Hillen and Painter [57] for a detailed introduction about the Keller–Segel model. To our best knowledge a model taking care of segregation property and cell-cell repulsion of Keller-Segel type has not been studied.

As we will explain in this work, our model can also be regarded as a nonlocal advection model. Recently, implementing nonlocal advection models for the study of cell-cell adhesion and repulsion has attracted a lot of attention. As pointed out by many biologists, cell-cell interactions do not only exist in a local scope, but a long-range interaction should be taken into account to guide the mathematical modeling. Armstrong, Painter and Sherratt [3] in their early work purposed a model (APS model) under the principle of the local diffusion plus the nonlocal attraction driven by the adhesion forces to describe the phenomenon of cell mixing, full/partial engulfment and complete sorting in the cell sorting problem. Based on the APS model, Murakawa and Togashi [79] thought that the population pressure should come from the cell volume size instead of the linear diffusion. Therefore, they changed the linear diffusion term into a nonlinear diffusion in order to capture the sharp fronts and the segregation in cell co-culture. Carrillo et al. [26] recently purposed a new assumption on the adhesion velocity field and their model showed a good agreement in the experiments in the work of Katsunuma et al. [64]. The idea of the long-range attraction and short-range repulsion can also be seen in the work of Leverentz, Topaz and Bernoff [68]. They considered a nonlocal advection model to study the asymptotic behavior of the solution. By choosing a Morse-type kernel which follows the attractive-repulsive interactions, they found the solution can asymptotically spread, contract (blow-up), or reach a steady-state. Burger, Fetecau and Huang [19] considered a similar nonlocal adhesion model with nonlinear diffusion, they studied the well-posedness of the model and proved the existence of a compact supported, non-constant steady state. Dyson et al. [42] established the local existence of a classical solution for a nonlocal cell-cell adhesion model in spaces of uniformly continuous functions. For Turing and Turing-Hopf bifurcation due to the nonlocal effect, we refer to Ducrot et al. [40] and Song et al. [97]. We also refer the readers to Mogliner et al. [76], Eftimie et al. [43], Ducrot and Magal [39], Fu and Magal [48] for more topics about nonlocal advection equations. For the derivation of such models, readers can refer to the work of Bellomo et al. [8] and Morale, Capasso and Oelschläger [77].

In this work, we consider a two-dimensional bounded domain (a flat circular petri dish). We use the notion of solution integrated along the characteristics. Thanks to the appropriate boundary condition of the pressure equation (see Equation (2.2)), we deduce that the characteristics stay in the domain for any positive time. The positivity of solutions, the segregation property and a conservation law follow from the notion of solutions as well. The main goal in this work is to investigate the complexity of the short-term (6 days) co-cultured cell distribution depending on the initial distribution of each species. Through the numerical simulations, we investigate the impact of the initial population number (as well as the law of initial distributions) on the population ratio. In the above mentioned literature, the numerical simulation are restricted to a rectangular domain with periodic boundary conditions. It is worth mentioning that here the domain

is circular with no flux boundary condition for the pressure which requires a finite volume method (see Appendix B).

The plan of the work is the following. In Section 2, we present the model for the single-species case and we prove the local existence and uniqueness of solutions as well as the conservation law by considering the solution integrated along the characteristics. Section 3 is devoted to the numerical analysis of the model. In Section 3.1, we consider the model homogeneous in space which corresponds to an ODE model that has been previously studied by Zeeman [106]. In Section 3.2, we investigated the competitive exclusion principle and the impact of the initial distribution on population ratio. The spatial competition due to the dispersion coefficients and cell kinetics is considered in Section 3.3. Section 4 is devoted to discussion and conclusion and further theoretical analysis are presented in the Appendix.

# 2 Mathematical modeling

## 2.1 Single species model

Let us consider the following one-species model

$$\begin{cases} \partial_t u(t,x) - d\,\mathrm{div}\,\big(u(t,x)\nabla P(t,x)\big) = u(t,x)h(u(t,x)) & \text{in } (0,T]\times\Omega \\ u(0,x) = u_0(x) & \text{on } \overline{\Omega}, \end{cases} \tag{2.1}$$

where $P$ satisfies the following elliptic equation

$$\begin{cases} \big(I-\chi\Delta\big)P(t,x) = u(t,x) & \text{in } (0,T]\times\Omega \\ \nabla P(t,x)\cdot\nu(x) = 0 & \text{on } [0,T]\times\partial\Omega, \end{cases} \tag{2.2}$$

We denote $\Omega \subset \mathbb{R}^2$ to be the unit open disk centered at $\mathbf{0} = (0,0)$ with radius $r = 1$, i.e., $\Omega = B_{\mathbb{R}^2}(\mathbf{0},1)$. Here $\nu$ is the outward normal vector, $d$ is the dispersion coefficient, $\chi$ is the sensing coefficient. The divergence, gradient and Laplacian are taken with respect to $x$. System (2.1)-(2.2) can be regarded as a hyperbolic Keller-Segel equation (with chemotactic repulsion) on a bounded domain.

**Remark 2.1.** *Equation (2.2) can be derived from the following parabolic equation (which is the classical case in the Keller-Segel equation [61]) as $\varepsilon$ goes to 0:*

$$\varepsilon\partial_t P(t,x) = \chi\Delta P(t,x) + u(t,x) - P(t,x). \tag{2.3}$$

*The process of letting $\varepsilon \to 0$ corresponds to the assumption that the dynamics of the chemorepellent is fast compared to the evolution of the cell density. In the case of chemoattractant a variant of such a model was considered by Perthame and Dalibard [90], Calvez and Dolak-Struß [21].*

**Remark 2.2.** *As we mentioned in the introduction, Equation (2.2) can be regarded as a nonlocal integral equation by using the following representation*

$$P(t,x) = \int_\Omega \kappa(x,y)u(t,y)dy,$$

*where $\kappa$ is a convolution kernel which can be represented by the sum of eigenfunctions of the operator $(I-\chi\Delta)^{-1}$ in $L^2(\Omega)$.*

### The invariance of domain $\Omega$ and the well-posedness of the model

Note that in System (2.1)-(2.2) we do not impose any boundary condition directly on $u$. Instead, the boundary condition here is induced by $\nabla P \cdot \nu = 0$. If we consider the associated characteristics flow of (2.1)-(2.2)

$$\begin{cases} \frac{\partial}{\partial t}\Pi(t,s;x) = -d\,\nabla P(t,\Pi(t,s;x)) \\ \Pi(s,s;x) = x \in \Omega. \end{cases} \tag{2.4}$$

We can prove (see Appendix C) the characteristics can not leave the domain $\Omega$ (see Figure 3.2 for an illustration). In fact, we can prove for any $t > 0$, the mapping $x \mapsto \Pi(t,0;x)$ is a bijection from $\Omega$ to itself (see Lemma 2.10). We consider the solution along the characteristics

$$w(t,x) := u(t,\Pi(t,0;x)) \quad x \in \Omega, t > 0.$$

Taking any $x \in \Omega$, there exists $y \in \Omega$ such that $x = \Pi(t,0;y)$, and since

$$w(t,y) = w(t,\Pi(0,t;x)) = u(t,x),$$

we can reconstruct the solution $u(t,\cdot)$ from $w(t,\cdot)$ and $\{\Pi(t,s,\cdot)\}_{t,s\in[0,T]}$ on $\Omega$.

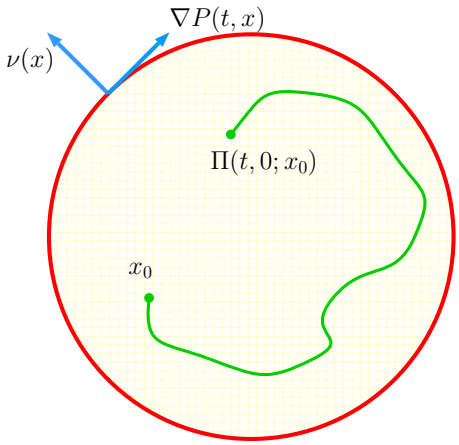


Figure 3.2: *An illustration for the invariance of domain $\Omega$. The green curve represents a trajectory of the characteristics.*

**Assumption 2.3.** *Assume the vector field $(t,x) \mapsto \nabla P(t,x)$ is continuous in $[0,T]\times\overline{\Omega}$ and lipschitzian with respect to $x$ in $[0,T]\times\overline{\Omega}$.*

**Remark 2.4.** *Assumption 2.3 is a sufficient condition for the existence and uniqueness of the characteristic flow $\{\Pi(t,s;\cdot)\}_{t,s\in[0,T]}$ in (2.4).*

**Definition 2.5.** *For any bounded open domain $\Omega$. If $u:\Omega\to\mathbb{R}$ is bounded and continuous, we write*

$$\|u\|_{C(\overline{\Omega})} := \sup_{x\in\Omega}|u(x)|.$$

*For any $\alpha\in(0,1]$, the $\alpha^{th}$–Hölder norm of $u:\Omega\to\mathbb{R}$ is*

$$\|u\|_{C^{0,\alpha}(\overline{\Omega})} := \|u\|_{C(\overline{\Omega})} + [u]_{C^{0,\alpha}(\overline{\Omega})},$$

*where*

$$[u]_{C^{0,\alpha}(\overline{\Omega})} := \sup_{\substack{x,y\in\Omega\\ x\neq y}} \left\{ \frac{|u(x)-u(y)|}{|x-y|^\alpha} \right\}.$$

*The Hölder space* $C^{k,\alpha}(\overline{\Omega})$ *consists of all functions* $u \in C^k(\overline{\Omega})$ *for which the norm*

$$\|u\|_{C^{k,\alpha}(\overline{\Omega})} := \sum_{|\alpha|\leq k} \|D^\alpha u\|_{C(\overline{\Omega})} + \sum_{|\alpha|=k} [D^\alpha u]_{C^{0,\alpha}(\overline{\Omega})}$$

*is finite.*

**Lemma 2.6.** *[50, Theorem 6.30 and 6.31] Let* $\Omega \subset \mathbb{R}^2$ *to be a unit open disk. Consider the following elliptic equation*

$$\begin{cases} (I-\chi\Delta)P(x) = u(x) & x\in\Omega \\ \nabla P(x)\cdot\nu(x) = 0 & x\in\partial\Omega, \end{cases} \tag{2.5}$$

*where* $\nu$ *is the outward unit normal vector on* $\partial\Omega$*. Then for all* $u \in C^{0,\alpha}(\overline{\Omega})$*, the elliptic problem (2.5) has a unique solution* $P \in C^{2,\alpha}(\overline{\Omega})$*. Moreover,*

$$\|P\|_{C^{2,\alpha}(\overline{\Omega})} \leq C\|u\|_{C^{0,\alpha}(\overline{\Omega})},$$

*where* $C = C(\alpha,\chi,\Omega)$*.*

The following theorem tells us if we choose our initial value $u_0$ to be smooth enough, then Assumption 2.3 can be satisfied and the existence and uniqueness of solutions follow.

**Theorem 2.7 (Existence and uniqueness of solutions).** *Let* $u_0 \in W^{1,\infty}(\Omega)\cap C^0_+(\overline{\Omega})$*. Then for some* $T>0$ *there exists a unique non-negative solution* $u \in C\left([0,T];C^0_+(\overline{\Omega})\right)$ *to (2.1)-(2.2) which satisfies* $u(t=0,x)=u_0(x)$*. Moreover for any* $t\in[0,T]$*, we have* $u(t,\cdot)\in W^{1,\infty}(\Omega)$ *and* $\sup_{t\in[0,T]}\|u(t,\cdot)\|_{W^{1,\infty}(\Omega)} < \infty$*.*

The proof the above theorem will be detailed in Appendix D.

**Remark 2.8.** *Since for any* $t\in[0,T]$ *and for any* $\alpha\in(0,1)$*, we have* $u(t,\cdot)\in W^{1,\infty}(\Omega)\hookrightarrow C^{0,\alpha}(\overline{\Omega})$*, we deduce from Lemma 2.6 that* $P(t,\cdot)\in C^{2,\alpha}(\overline{\Omega})$*. Therefore,* $(t,x)\to\nabla P(t,x)$ *is continuous (since* $P\in C([0,T];C^1(\overline{\Omega}))$*) and lipchitzian with respect to* $x$ *which implies Assumption 2.3.*

### Conservation law on a volume

If the reaction term $h\equiv 0$ in System (2.1)-(2.2), the boundary condition implies the conservation law for $u$. This can be seen through the solution along the characteristics. In fact, we have the following conservation law.

**Theorem 2.9.** *For each volume* $A\subset\Omega$ *and each* $0\leq s\leq t$ *we have*

$$\int_{\Pi(t,s;A)} u(t,x)\mathrm{d}x = \int_A \exp\left(\int_s^t h\left(u\left(l,\Pi(l,s;z)\right)\right)\mathrm{d}l\right) u(s,z)\mathrm{d}z.$$

*In particular, if we have* $h=0$*, then for any* $0\leq s\leq t$

$$\int_{\Pi(t,s;A)} u(t,x)\mathrm{d}x = \int_A u(s,z)\mathrm{d}z.$$

*This means the total number of cell in the volume $A$ is constant along the volumes $\Pi(t,s;A)$.*

Before proving Theorem 2.9, we need the following lemma.

**Lemma 2.10.** *Let $T>0$ and $\{\Pi(t,s;x)\}_{t,s\in[0,T]}$ to be the characteristic flow generated by (2.4). Then the map $x\mapsto\Pi(t,s;x)$ is continuously differentiable and one has the determinant of Jacobi matrix:*

$$\det J_\Pi(t,s;x)=\exp\left(\int_s^t\frac{d}{\chi}\left(u(l,\Pi(l,s;x))-P(l,\Pi(l,s;x))\right)\mathrm{d}l\right). \tag{2.6}$$

*where $J_\Pi(t,s;x)$ is the Jacobian matrix of $\Pi(t,s;x)$ with respect to $x$ at point $(t,s;x)$.*

*Proof.* From Theorem 2.7 and Remark 2.8, the mapping $(t,x)\to P(t,x)$ is $C([0,T];C^1(\overline{\Omega}))$ and $P(t,\cdot)\in C^{2,\alpha}(\overline{\Omega})$ for any $\alpha\in(0,1)$ if $u_0\in W^{1,\infty}(\Omega)$. This ensures the characteristics $x\to\Pi(t,s;x)$ is continuously differentiable. Taking the partial derivative of Equation (2.4) with respect to $x$ yields

$$\begin{cases}\partial_t J_\Pi(t,s;x)=-d\,J_{\nabla P}(t,\Pi(t,s;x))J_\Pi(t,s;x)\\ J_\Pi(s,s;x)=\mathrm{Id},\end{cases}$$

where $J_{\nabla P}(t,\Pi(t,s;x))$ is the Jacobian matrix of $\nabla P(t,x)$ with respect to $x$ at point $(t,\Pi(t,s;x))$. For any matrix-valued $C^1$ function $A:t\mapsto A(t)$, the Jacobian formula reads as follows

$$\frac{\mathrm{d}}{\mathrm{d}t}\det A(t)=\det A(t)\times\mathrm{Trace}\left(A^{-1}(t)\frac{d}{dt}A(t)\right).$$

Hence, we obtain

$$\begin{aligned}\frac{\mathrm{d}}{\mathrm{d}t}\det J_\Pi(t,s;x)&=\det J_\Pi(t,s;x)\times\mathrm{Trace}\left(J_\Pi(t,s;x)^{-1}J_{\nabla P}(t,\Pi(t,s;x))J_\Pi(t,s;x)\right)\\&=\det J_\Pi(t,s;x)\times\mathrm{Trace}\left(J_{\nabla P}(t,\Pi(t,s;x))\right)\end{aligned}$$

and since $\mathrm{Trace}\left(J_{\nabla P}(t,\Pi(t,s;x))\right)=(\Delta P)(t,\Pi(t,s;x))=-\frac{1}{\chi}\left(u(t,\Pi(t,s;x))-P(t,\Pi(t,s;x))\right)$. Therefore, we have

$$\begin{cases}\dfrac{\mathrm{d}}{\mathrm{d}t}\det J_\Pi(t,s;x)=\det J_\Pi(t,s;x)\times\dfrac{d}{\chi}\left[u(t,\Pi(t,s;x))-P(t,\Pi(t,s;x))\right]\\ \det J_\Pi(s,s;x)=1.\end{cases}$$

Therefore the result follows. □

*Proof of Theorem 2.9.* Let $\{\Pi(t,s;x)\}_{t,s\in[0,T]}$ to be the characteristic flow generated by (2.4). Given any measurable set $A\subset\Omega$ and any $0\le s\le t$, we integrate $u(t,x)$ over the volume $\Pi(t,s;A)$ with respect to $x$

$$\int_\Omega\mathbb{1}_{\Pi(t,s;A)}(x)u(t,x)\mathrm{d}x=\int_\Omega\mathbb{1}_A(z)u(t,\Pi(t,s;z))\det J_\Pi(t,s;z)\mathrm{d}z, \tag{2.7}$$

where we changed the variable $x$ to $\Pi(t,s;z)$ on the right-hand-side.

For the right-hand-side, we will prove in (D.1) Appendix D that

$$u(t,\Pi(t,s;z)) = u(s,z)\exp\left(\int_s^t h(u(l,\Pi(l,s;z))) + \frac{d}{\chi}\left(P(l,\Pi(l,s;z)) - u(l,\Pi(l,s;z))\right)\mathrm{d}l\right).$$

Combining with (2.6) we obtain that

$$u(t,\Pi(t,s;z))\det J_\Pi(t,s;z) = u(s,z)\exp\left(\int_s^t h(u(l,\Pi(l,s;z)))\mathrm{d}l\right).$$

Substituting the above equation into (2.7) gives us

$$\int_\Omega \mathbb{1}_{\Pi(t,s;A)}(x)u(t,x)\mathrm{d}x = \int_\Omega \mathbb{1}_A(z)u(s,z)\exp\left(\int_s^t h(u(l,\Pi(l,s;z)))\mathrm{d}l\right)\mathrm{d}z,$$

which is equivalent to

$$\int_{\Pi(t,s;A)} u(t,x)\mathrm{d}x = \int_A \exp\left(\int_s^t h\left(u\left(l,\Pi(l,s;z)\right)\right)\mathrm{d}l\right)u(s,z)\mathrm{d}z.$$

The result follows. □

## 2.2 Multi-species model

### Multi-species ODE model

Let us consider the corresponding two species model without the spatial variable $x$ that is $u_i = u_i(t)$ for $i = 1, 2$.

$$\begin{cases} \dfrac{\mathrm{d}u_i}{\mathrm{d}t} = u_i h_i(u_1,u_2) \quad i=1,2, \\ u_i(0) = u_{i,0} \in \mathbb{R}_+. \end{cases} \tag{2.8}$$

We adopt the Lotka-Volterra model by letting

$$h_i(u_1,u_2) = b_i - \delta_i - \sum_{j=1}^{2} a_{ij}u_j, \quad i=1,2. \tag{2.9}$$

where $b_i > 0$, $i = 1, 2$ are the growth rates, $a_{ij} \geq 0$, $i \neq j$ represent the mutual competition between the species, $a_{ii}$ is the competition among the same species and $\delta_i$ is the additional mortality rate caused by drug treatment. In Section 2.2.1 we will always assume $\delta_i = 0$ for $i = 1, 2$ (when $\delta_i > 0$, one can regard $b_i - \delta_i$ as a whole). If we consider (2.8) in the absence of the other species, we can rewrite (2.9) as

$$h_i(u_1,u_2) = b_i - a_{ii}u_i, \quad i=1,2.$$

We always assume that for each $i$, $a_{ii} > 0$ meaning that each species alone exhibits logistic growth. This model has been considered by many authors (for example, see [80, 106]).

Here we give a short summary of some qualitative properties of the solution to (2.8) in order to compare with the PDE model.

**Equilibrium and stability for (2.8)-(2.9)**

One can easily compute the system has the following equilibrium

$$E_0 = (0,0), \quad E_1 = (P_1, 0), \quad E_2 = (0, P_2), \quad E^* = (u_1^*, u_2^*)$$

where

$$P_1 := \frac{b_1}{a_{11}}, \quad P_2 := \frac{b_2}{a_{22}}, \quad E^* = \left( \frac{a_{22}b_1 - a_{12}b_2}{a_{11}a_{22} - a_{12}a_{21}}, \frac{a_{21}b_1 - a_{11}b_2}{a_{12}a_{21} - a_{11}a_{22}} \right) \tag{2.10}$$

The solution $E^*$ is only of relevance when $a_{12}a_{21} \neq a_{11}a_{22}$ and $(u_1^*, u_2^*)$ is strictly positive, which is equivalent to say

$$\begin{cases} \frac{a_{12}}{a_{11}} > \frac{P_1}{P_2} \\ \frac{a_{21}}{a_{22}} > \frac{P_2}{P_1} \end{cases} \quad \text{or} \quad \begin{cases} \frac{a_{12}}{a_{11}} < \frac{P_1}{P_2} \\ \frac{a_{21}}{a_{22}} < \frac{P_2}{P_1} \end{cases} .$$

We adapt the main stability results from Zeeman [106] where the author considered a general $n$–species extinction case, Murray [80, Chapter 3.5] and Hirsch [59, Chapter 11] to system (2.8)-(2.9) for the following fours cases (i)-(iv) and discuss their biological implications.

**Proposition 2.11.** *For system (2.8)-(2.9), suppose for each $i = 1, 2$, $b_i > 0, a_{ii} > 0$ and $a_{ij} \geq 0$ for any $i \neq j$. Let $P_1 = a_{11}/b_1, P_2 = a_{22}/b_2$ be the equilibrium for each species alone and assume the initial value $(u_{1,0}, u_{2,0})$ lies strictly in the first quadrant that is $u_{1,0} > 0$ and $u_{2,0} > 0$. Then for the following four cases we have*

(i). *$a_{12}/a_{11} < P_1/P_2$, $a_{21}/a_{22} < P_2/P_1$. This case corresponds to Figure 3.3 (a). The system (2.8) has four positive equilibrium, namely $E_0, E_1, E_2$ and $E^*$. In such case, only $E^*$ is global globally asymptotic stable in the region $\{(u_1, u_2) \in \mathbb{R}^2 \,|\, u_1 > 0, u_2 > 0\}$.*

(ii). *$a_{12}/a_{11} > P_1/P_2, a_{21}/a_{22} < P_2/P_1$. This case corresponds to Figure 3.3 (b). The system (2.8) has three positive equilibrium, namely $E_0, E_1$ and $E_2$. Only $E_2$ is globally stable in the positive quadrant excepted for the axis $u_1 = 0$.*

(iii). *$a_{12}/a_{11} < P_1/P_2, a_{21}/a_{22} > P_2/P_1$. This case corresponds to Figure 3.3 (c). The analysis of the stability is similar to the case (ii). Only $E_1$ is globally stable in the positive quadrant excepted for the axis $u_2 = 0$.*

(iv). *$a_{12}/a_{11} > P_1/P_2, a_{21}/a_{22} > P_2/P_1$. This case corresponds to Figure 3.3 (d). In this case, system (2.8) has four equilibrium, where $E_1$ and $E_2$ are stable while $E^*$ is a saddle point. The steady states $E_1$ and $E_2$ have two non-overlapping domains of attraction, separated by the stable manifold $\boldsymbol{S}$ of equilibria $E^*$.*

**Remark 2.12.** *Although among the four cases,* (ii) *and* (iii) *always lead to the principle of exclusion and so do (iv) due to the natural perturbation in population levels, we still have the case* (i) *where the two species can coexist in the long term. As we further develop our*

*PDE model for* (2.8)*, we can show numerically that the principle of exclusion dominates even when case* (i) *is satisfied and this is a evident difference compared to ODE model* (2.8)*.*

A scheme of the qualitative behavior of the phase trajectory is given in Figure 3.3 by numerical simulations.

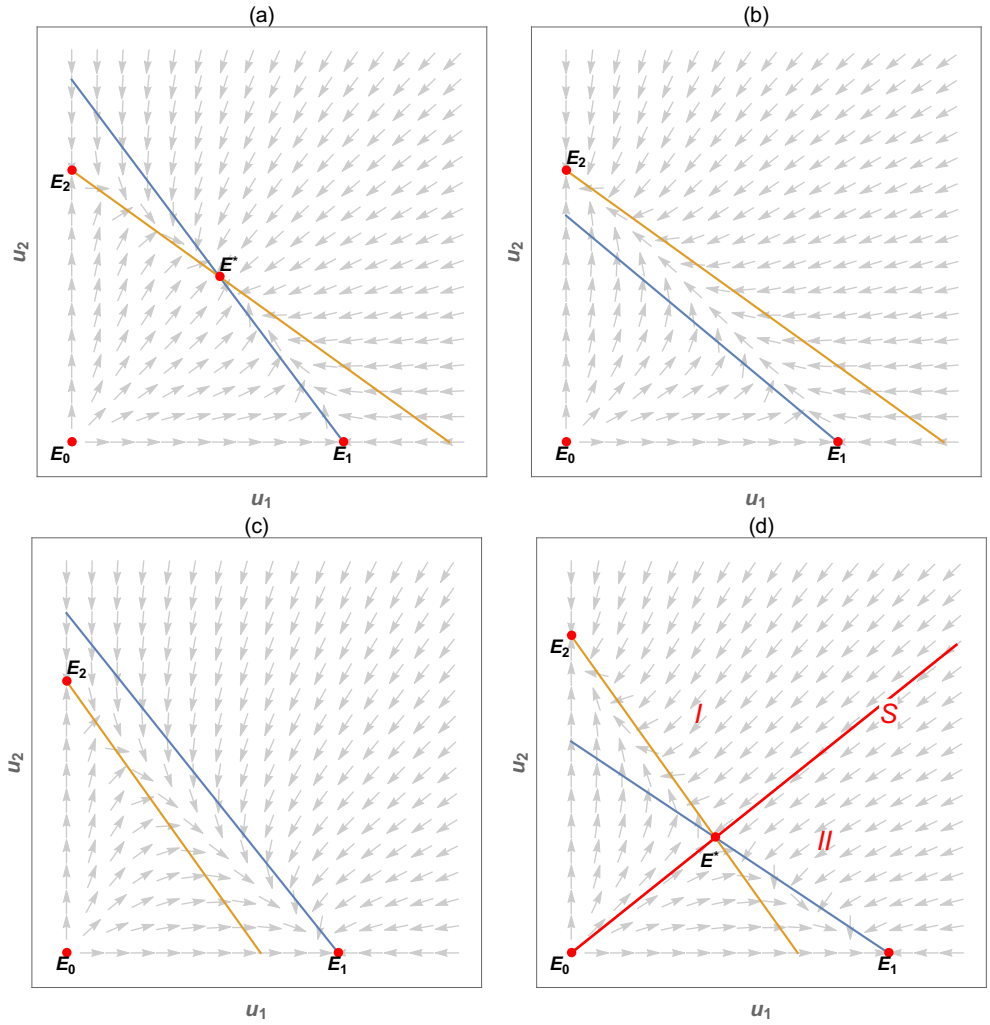


Figure 3.3: *A scheme of the qualitative behavior of the phase trajectory for various cases.* **(a)** $a_{12}/a_{11} < P_1/P_2, a_{21}/a_{22} < P_2/P_1$*. Only the positive steady state* $E^*$ *is stable and all trajectories tend to it.* **(b)** $a_{12}/a_{11} > P_1/P_2, a_{21}/a_{22} < P_2/P_1$*. Only one stable steady state* $E_2$ *exists with the whole positive quadrant its domain of attraction.* **(c)** $a_{12}/a_{11} < P_1/P_2, a_{21}/a_{22} > P_2/P_1$*. Only one stable steady state* $E_1$ *exists with the whole positive quadrant its domain of attraction.* **(d)** $a_{12}/a_{11} > P_1/P_2, a_{21}/a_{22} > P_2/P_1$*.* $E_1$ *and* $E_2$ *are stable steady states, each of which has a domain of attraction namely* ***I*** *and* ***II****, separated by a separatrix* ***S*** *which is the stable manifold of equilibria* $E^*$*.*

### Multi-species PDE model

We study a two species population dynamic model on a unit open disk $\Omega \subset \mathbb{R}^2$ given as follows

$$\begin{cases} \partial_t u_1(t,x) - d_1 \operatorname{div}\big(u_1(t,x)\nabla P(t,x)\big) = u_1(t,x)h_1((u_1,u_2)(t,x)) \\ \partial_t u_2(t,x) - d_2 \operatorname{div}\big(u_2(t,x)\nabla P(t,x)\big) = u_2(t,x)h_2((u_1,u_2)(t,x)) & \text{in } [0,T]\times\Omega \\ \big(I-\chi\Delta\big)P(t,x) = u_1(t,x)+u_2(t,x) \\ \nabla P(t,x)\cdot\nu(x) = 0 & \text{on } [0,T)\times\partial\Omega, \end{cases} \tag{2.11}$$

where $\nu$ is the outward normal vector, $d_i$ is the dispersion coefficient, $\chi$ is the sensing coefficient. Recall the function $h_i$ is of form

$$h_i(u_1,u_2) = b_i - \delta_i - \sum_{j=1}^{2} a_{ij}u_j, \quad i=1,2.$$

System (2.11) is supplemented with initial distribution

$$\mathbf{u}_0(\cdot) := (u_1(0,\cdot),u_2(0,\cdot)) \in C^1(\overline{\Omega})^2. \tag{2.12}$$

### Segregation property

From the mono-layer cell populations co-culture experiments, we can see that once the two cell populations confront each other, they will stop growing, thus, forming the separated islets. We can prove that our model (2.11) preserves such segregation property.

**Theorem 2.13.** *Suppose* $\mathbf{u} = (u_1,u_2)(t,x)$ *is the solution of* (2.11)-(2.12) *and assume* $d_1 = d_2 = d$ *in* (2.11). *Then for any initial distribution with* $u_1(0,x)u_2(0,x) = 0$ *for all* $x\in\Omega$, *we have* $u_1(t,x)u_2(t,x) = 0$ *for any* $t>0$ *and* $x\in\Omega$.

*Proof.* We argue by contradiction, assume there exist $t^*>0, x^*\in\Omega$ such that

$$u_1(t^*,x^*)u_2(t^*,x^*) > 0.$$

Suppose the characteristic flow satisfies the following equation

$$\begin{cases} \frac{\partial}{\partial t}\Pi(t,s;x) = -d\,\nabla P(t,\Pi(t,s;x)) \\ \Pi(s,s;x) = x\in\Omega. \end{cases}$$

Since $x\to\Pi(t,s;x)$ is invertible from $\Omega$ to itself, there exists some $x_0\in\Omega$ such that $\Pi(t^*,0;x_0) = x^*$. Then for any $i=1,2$, we have

$$u_i(t^*,\Pi(t^*,0;x_0)) = u_i(0,x_0)\, e^{\int_0^{t^*} h_i((u_1,u_2)(l,\Pi(l,0;x_0)))+\frac{d}{\chi}(P(l,\Pi(l,0;x_0))-(u_1+u_2)(l,\Pi(l,0;x_0)))\mathrm{d}l} > 0, \tag{2.13}$$

which implies

$$u_i(0,x_0) > 0, \quad i=1,2.$$

This is a contradiction. □

For the one dimensional case $N = 1$, suppose $u_1, u_2$ are solutions to (2.11)-(2.12), we give an illustration (see Figure 3.4) of the segregation for the solutions integrated along the characteristics $u_i(t, \Pi(t, 0; x))$ for $i = 1, 2$. In fact, if there exists for some $x_0$ such that $u_i(0, x_0) = 0$ for $i = 1, 2$. Then from Equation (2.13) we obtain

$$u_1(t, \Pi(t, 0; x_0)) = u_2(t, \Pi(t, 0; x_0)) = 0, \ \forall t > 0.$$

Therefore, the characteristics $t \mapsto \Pi(t, 0; x_0)$ forms a segregation barrier for the two cell populations.

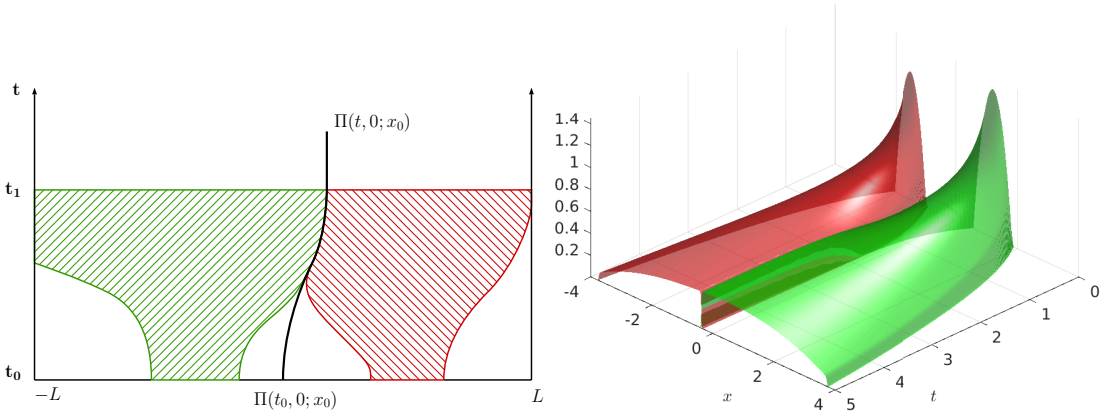


Figure 3.4: *In this figure we illustrate the notion of segregation with a one dimensional bounded domain. Figure (a) shows the characteristic $t \mapsto \Pi(t, 0; x_0)$ forms a segregation "wall". Figure (b) shows the temporal-spatial evolution of the two species.*

### Conservation law on a volume

If we assume that $d_1 = d_2 = d$ in system (2.11), we have the following similar conservation law for two species case. Suppose volume $A \subset \Omega$ and each $0 \leq s \leq t$:

$$\int_{\Pi(t,s;A)} u_i(t, x)\mathrm{d}x = \int_A \exp\left[\int_s^t h_i\left((u_1, u_2)\left(l, \Pi(l, s; z)\right)\right)\mathrm{d}l\right] u_i(s, z)\mathrm{d}z, i = 1, 2.$$

Therefore, if we have $h_i = 0$ for any $0 \leq s \leq t$

$$\int_{\Pi(t,s;A)} u_i(t, x)\mathrm{d}x = \int_A u_i(s, z)\mathrm{d}z, i = 1, 2.$$

This means the total cell number of the species $u_i$ is constant along the characteristics starting from the volume $A$.

# 3 Numerical simulations

## 3.1 Impact of the segregation on the competitive exclusion

We set $U_i$ to be the total number at time $t = 0$

$$U_i = \int_\Omega u_i(0, x)\mathrm{d}x, \quad i = 1, 2. \tag{3.1}$$

We give the parameter values used in the simulations and their interpretations in Table 3.1. The parameter fitting for the growth rate $b_i$ and the intraspecific coefficients $a_{ii}$ are detailed in Appendix E.

| Symbol | Interpretation | Value | Unit | Method | Dimensionless value |
|---|---|---|---|---|---|
| $t$ | time | 1 | $day$ | - | 1 |
| $r$ | inner radius of the dish | 2.62 | $cm$ | [89] | 1 |
| $U_i$ | cell total number at $t = 0$ | $10^5$ | – | [89] | 0.01 |
| $b_1$ | growth rate of cell $u_1$ | 0.6420 | $day^{-1}$ | fitted | 0.6420 |
| $b_2$ | growth rate of cell $u_2$ | 0.6359 | $day^{-1}$ | fitted | 0.6359 |
| $a_{11}$ | intraspecific competition of $u_1$ | $1.07 \times 10^{-6}$ | $cm^2/day$ | fitted | 1.5588 |
| $a_{22}$ | intraspecific competition of $u_2$ | $1.06 \times 10^{-6}$ | $cm^2/day$ | fitted | 1.5415 |
| $d_1$ | dispersion coefficient of $u_1$ | 13.73 | $cm^4/day$ | fitted | 2 |
| $d_2$ | dispersion coefficient of $u_2$ | 13.73 | $cm^4/day$ | fitted | 2 |
| $\chi$ | sensing coefficient | $6.86 \times 10^{-2}$ | $cm^2$ | fitted | 0.01 |

Table 3.1: *List of the model parameters, their interpretations, values and symbols. Here $u_1$ represents MCF-7 (sensitive cell) and $u_2$ represents MCF-7/Doxo (resistant cell). From [89], the surface of the dish is $21.5\,cm^2$. Thus the inner radius of the dish $r$ is calculated by $r^2\pi = 21.5\,cm^2$.*

The goal of our simulations is to compare the various cases discussed in Proposition 2.11 (ODE case) with our PDE model with segregation. As we will see in the numerical simulations, the model with spatial structure can present totally different results compared to the previous ODE model. To that aim, we firstly consider the case where the drug (doxorubicine) concentration is low in the cell co-culture for MCF-7 and MCF-7/Doxo. The drug treatment causes an additional mortality to the sensitive population MCF-7 represented by $u_1$ while no extra mortality to the resistant population MCF-7/Doxo represented by $u_2$ (MCF-7/Doxo is resistant to a small quantity of drug treatment see Table E.1 in Appendix E).

Now since we consider the presence of the drug, the equilibrium (2.10) in the ODE case should be rewritten as

$$\bar{P}_1 = \frac{b_1 - \delta_1}{a_{11}}, \quad \bar{P}_2 = \frac{b_2 - \delta_2}{a_{22}}. \tag{3.2}$$

Moreover we assume the drug concentration is low such that $b_1 - \delta_1 > 0$ and $\delta_2 = 0$, therefore we have

$$\bar{P}_1 < \bar{P}_2.$$

The case when $\bar{P}_1 > \bar{P}_2$ is similar and will be discussed in the end of this section.

Case (i): $a_{12}/a_{11} < \bar{P}_1/\bar{P}_2$, $a_{21}/a_{22} < \bar{P}_2/\bar{P}_1$. By using (3.2), the condition in Case (i) can be interpreted by

$$\frac{a_{12}}{a_{22}} < \frac{b_1 - \delta_1}{b_2 - \delta_2}, \quad \frac{a_{21}}{a_{11}} < \frac{b_2 - \delta_2}{b_1 - \delta_1}.$$

Since we have $b_1 - \delta_1 > 0$ and $\delta_2 = 0$, if the coefficients $a_{12}$ and $a_{21}$ are small, then Case (i) holds. We give a possible set of parameters satisfying Case (i) :

$$\delta_1 = 0.4,\ \delta_2 = 0,\ a_{12} = 0.2,\ a_{21} = 1. \tag{3.3}$$

We assume that for each species $u_i$, the initial distribution follows the uniform distribution on a disk with 20 initial cell clusters (represented by the red/green dots in Figure 3.5 (a)). The initial total cell number is $U_i = 0.01$ in (3.1) for each species and we assume each cluster contains the same quantity of cells. We present its numerical simulation in Figure 3.5 from day 0 to day 6. We also plot the relative cell numbers in Figure 3.5 (f) where we define the relative cell number for species $i$ as

$$\frac{U_i(t)}{U_1(t) + U_2(t)}, \qquad \text{where } U_i(t) := \int_\Omega u_i(t,x)\mathrm{d}x,\ i = 1, 2.$$

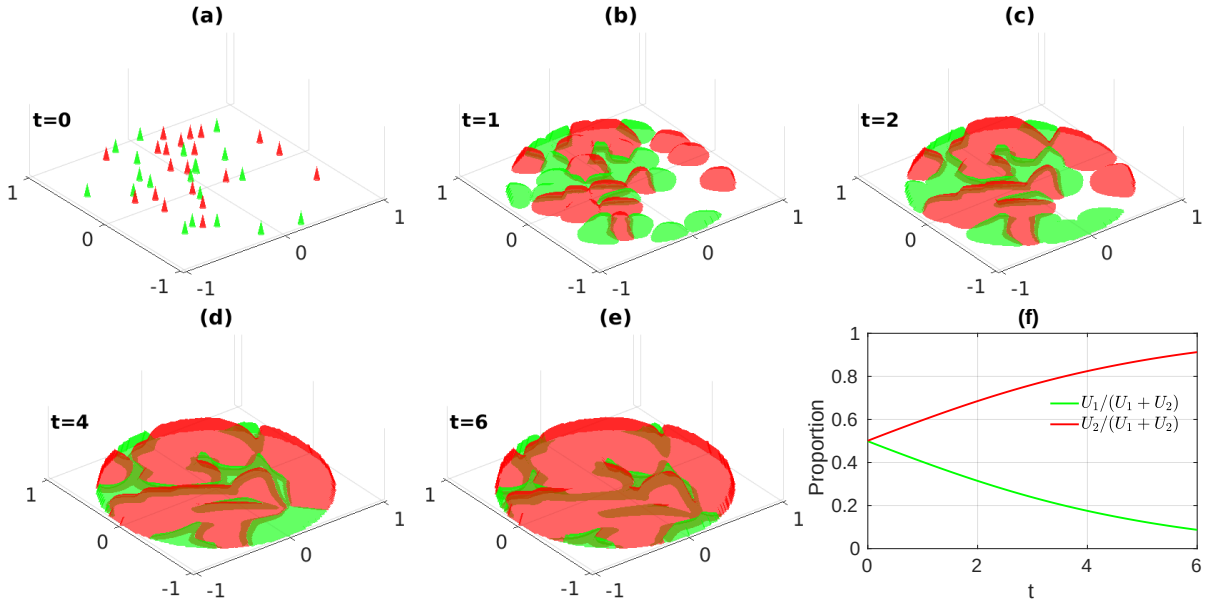


Figure 3.5: *Spatial-temporal evolution of the two species $u_1$ and $u_2$ and its relative proportion. Figures (a)-(e) correspond to the evolution of cell growth form day 0 to day 6 and Figure (f) is the relative proportion plot from day 0 to day 6. We fix the parameters $\delta_1 = 0.4$, $\delta_2 = 0$, $a_{12} = 0.2$, $a_{21} = 1$ in (3.3). The initial distribution follows the uniform distribution on a disk with 20 initial cell clusters. The initial total cell number is $U_1 = U_2 = 0.01$ for each species and cells are equally distributed in each cluster. The other parameters are given in Table 3.1.*

In Case (i) of the ODE system (2.8), Proposition 2.11 shows that the two species can coexist with the equilibrium

$$\bar{E}^* := \left( \frac{a_{22}(b_1 - \delta_1) - a_{12}(b_2 - \delta_2)}{a_{11}a_{22} - a_{12}a_{21}}, \frac{a_{21}(b_1 - \delta_1) - a_{11}(b_2 - \delta_2)}{a_{12}a_{21} - a_{11}a_{22}} \right) \approx (0.11, 0.34).$$

However, as shown in Figure 3.5, we can see the population density $u_1$ tends to 0 and $u_2$ tends to 1. Next, we consider the Cases (ii)-(iv) in Proposition 2.11 by choosing the parameters in each case as follows.

| **Parameters** | $\delta_1$ | $\delta_2$ | $a_{12}$ | $a_{21}$ | Relations |
|---|---|---|---|---|---|
| **Case (ii)** | 0.4 | 0 | 1 | 1 | $a_{12}/a_{11} > \bar{P}_1/\bar{P}_2$, $a_{21}/a_{22} < \bar{P}_2/\bar{P}_1$. |
| **Case (iii)** | 0.4 | 0 | 0.2 | 5 | $a_{12}/a_{11} < \bar{P}_1/\bar{P}_2$, $a_{21}/a_{22} > \bar{P}_2/\bar{P}_1$. |
| **Case (iv)** | 0.4 | 0 | 1 | 5 | $a_{12}/a_{11} > \bar{P}_1/\bar{P}_2$, $a_{21}/a_{22} > \bar{P}_2/\bar{P}_1$. |

Table 3.2: *List of the parameters used in the simulations for Cases (ii)-(iv). Other parameters are given in Table 3.1.*

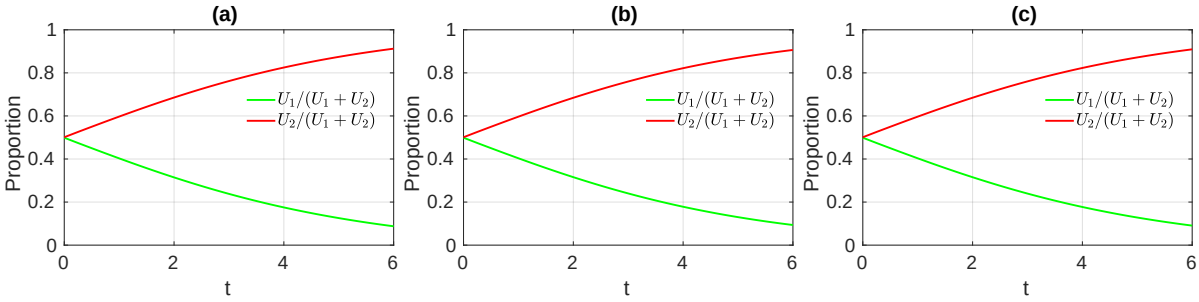


Figure 3.6: *Evolution of the relative cell numbers for two species $u_1$ and $u_2$. Figure (a)-(c) correspond to the parameter values chosen as in Table 3.2 for Cases (ii)-(iv) and other parameters are given in Table 3.1.*

With the simulations in Figure 3.5, Figure 3.6 and the results in Proposition 2.11, by setting

$$\bar{E}_1 = (\bar{P}_1, 0) \quad \bar{E}_2 = (0, \bar{P}_2) \quad \bar{E}^* = \left( \frac{a_{22}(b_1 - \delta_1) - a_{12}(b_2 - \delta_2)}{a_{11}a_{22} - a_{12}a_{21}}, \frac{a_{21}(b_1 - \delta_1) - a_{11}(b_2 - \delta_2)}{a_{12}a_{21} - a_{11}a_{22}} \right),$$

we can compare the stability between ODE model (2.8) and PDE model (2.11) under four different cases.

| $\bar{P}_1 < \bar{P}_2$ | Case (i) | Case (ii) | Case (iii) | Case (iv) |
|---|---|---|---|---|
| **Global attractor in ODE** | Coexistence $\bar{E}^*$ | $\bar{E}_2$ | $\bar{E}_1$ | Region dependent |
| **Stable steady state in PDE** | $\bar{E}_2$ | $\bar{E}_2$ | $\bar{E}_2$ | $\bar{E}_2$ |

Table 3.3: *A summary for the stability to four cases (i)-(iv) under ODE model and PDE model with segregation.*

The numerical simulation strongly indicates that the stable steady states only depend on the relation between $\bar{P}_1$ and $\bar{P}_2$. If $\bar{P}_1 < \bar{P}_2$ (resp. $\bar{P}_1 > \bar{P}_2$), the population $u_2$ (resp. $u_1$) will dominate and the other species will die out. We also did the four cases when $\bar{P}_1 > \bar{P}_2$, the results showed that $\bar{E}_1$ is the only stable steady state, which verifies our conjecture. Since the results are similar we omit the numerical simulations.

One can notice that unlike the ODE system (2.8), the segregation property for the PDE model implies that it is impossible for the two species to coexist at a same position $x \in \Omega$. Moreover, through the numerical simulations we observed that the PDE model (2.11) always undergoes a competitive exclusion principle, unless the equilibrium $\bar{P}_1 = \bar{P}_2$ in (3.2).

## 3.2 Impact of the initial distribution on the population ratio

In the previous section, we considered the competitive exclusion principle for the two species. By studying the relative proportions of $u_1$ and $u_2$, we presented the relation of the interspecific competition in our numerical simulation. Moreover, we can discover in Figure 3.5 (f) and in Figure 3.6 (a)-(c) that the increase of the proportion of the dominant population $u_2$ (red curve) is varying with time. It is evident to see from day 0 to day 2 the increase of the dominant population $u_2$ is faster than the increase from day 4 to day 6. If we further study the spatial-temporal evolution of the cell co-culture presented in Figure 3.5 (a)-(e), we can observe that from day 0 to day 2 the competition between the two groups is mainly expressed in the competition for space resources. However, from day 4 to day 6, when the surface of the dish is almost fully occupied by cells, the reaction term $u_i h_i(u_1, u_2)$ in the equation begins to play a major role in influencing the change of the number of cells. In order to explore the major factors in cell competition, we consider the impact on the initial distribution. We will mainly focus on two factors, namely the initial cell total number and the law of initial distribution, which might influence the proportions for $u_1$ and $u_2$. To that aim, we set the following parameters

$$\delta_1 = 0.15,\ \delta_2 = 0,\ a_{12} = 0,\ a_{21} = 0. \tag{3.4}$$

and the other parameters are given in Table 3.1.

### Dependency on the initial total cell number

In cell culture, the initial number of cell cluster is an important factor. Bailey et al. [6] study the sphere-forming efficiency of MCF-7 human breast cancer cell by comparing the cell culture with different initial numbers of cell cluster. Here we consider the impact of initial cluster number on the final proportion of species. To that aim, we assume the initial distribution follows the uniform distribution on a disk. We consider two sets of initial condition, that is

$$\begin{aligned} &U_1 = U_2 = 0.005, \quad N_{u_1} = N_{u_2} = 10, \\ &U_1 = U_2 = 0.1, \quad N_{u_1} = N_{u_2} = 200, \end{aligned} \tag{3.5}$$

where $U_1$ and $U_2$ are defined in (3.1) and $N_{u_1}$ (respectively $N_{u_2}$) is the initial number of cell clusters of species $u_1$ (respectively species $u_2$).

The above initial conditions correspond to different types of seeding in the experiment, namely cells are sparsely seeded or densely seeded. We assume the total cell number is proportional to the initial number of cell cluster, meaning the dilution procedure adopted in the experiment is the same, thus the number of cells in each cell cluster is a constant.

In Figure 3.7, we first give a numerical simulation for the cell growth with sparse seeding. In Figure 3.8, we present the simulation under the dense seeding condition, tracking from day 0 to day 6.

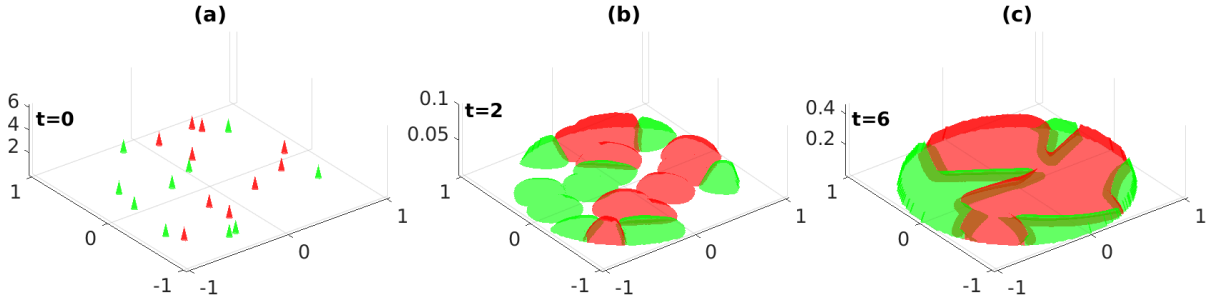


Figure 3.7: *Cell co-culture for species $u_1$ and $u_2$ over 6 days. We plot the case where cells are sparsely seeded, i.e., $U_1 = U_2 = 0.005$, $N_{u_1} = N_{u_2} = 10$ for day $0, 2$ and day $6$. We set parameters as $\delta_1 = 0.15$, $\delta_2 = 0$, $a_{12} = 0$, $a_{21} = 0$ in (3.4). Other parameters are given in Table 3.1.*

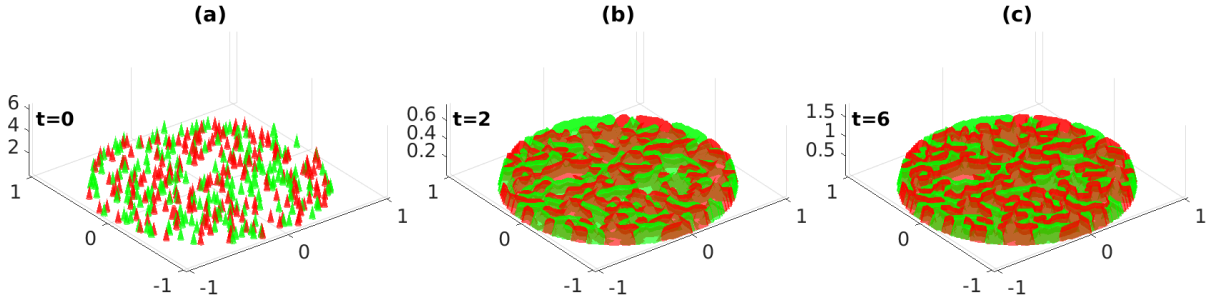


Figure 3.8: *Cell co-culture for species $u_1$ and $u_2$ over 6 days. We plot the case where where cells are densely seeded, i.e., $U_1 = U_2 = 0.1$, $N_{u_1} = N_{u_2} = 200$ for day $0, 2$ and day $6$. We set parameters as $\delta_1 = 0.15$, $\delta_2 = 0$, $a_{12} = 0$, $a_{21} = 0$ in (3.4). Other parameters are given in Table 3.1.*

In Figure 3.9 we plot the evolution of the total number and its proportion for species $u_1$ and $u_2$ over 6 days of the simulation.

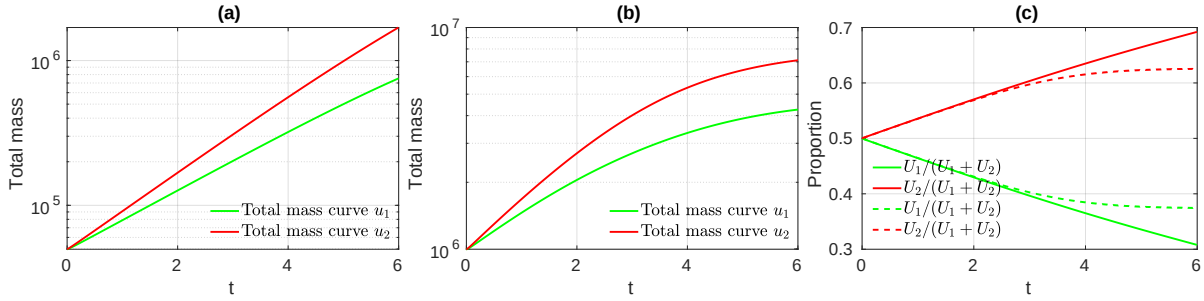


Figure 3.9: *Evolution of the total number (in log scale) and its proportion for species $u_1$ and $u_2$ over 6 days. Figure (a) is the total number plot corresponding to the simulations in Figure 3.7 while Figure (b) corresponds to the simulations in Figure 3.8. In Figure (c), the solid lines represents the proportion when the number of initial cell cluster equals $N_{u_1} = N_{u_2} = 10$ and the dash lines represents the proportion when $N_{u_1} = N_{u_2} = 200$. Parameters are given in Table 3.1 and $\delta_1 = 0.15$, $\delta_2 = 0$, $a_{12} = 0$, $a_{21} = 0$ in (3.4).*

From Figure 3.9 (a)-(b), since $u_2$ is resistant to the drug, the number of population $u_2$ is much greater than $u_1$. However, we can also observe a difference in their cell growth curves. In Figure (a) we can see that both cells are in the period of exponential growth from day 0 to day 6 (a base-10 log scale is used for the y-axis). Conversely, in Figure (b) the growth curves for both cells are converging to a constant from day 4 to day 6, implying that the cell co-culture is reaching a saturation stage. More importantly, in Figure (c), we observe a significant difference in the development of population ratios. In fact, since the spatial competition is still the dominant factor in the first two days, we can hardly see any difference between the dashed lines and solid lines. The proportion of the dominant population grows almost linearly. However, the proportion of the densely seeded group changed much slower after day 4, while the sparsely seeded group still grows linearly. This shows that although the growth rate of $u_1$ is at a competitive disadvantage, due to the sufficient number of cluster in the initial stage, and due to the segregation principle, $u_1$ does not die out in a short time in the competition. Although the competitive exclusion applies in this case, the time for the extinction of $u_1$ will be very long.

### Dependency on the law of the initial distribution

In the experiment, the size of the cell dish can be a factor to determine the law of the initial distribution for the cell. In general, under the same total cell number, a small size cell dish will lead to a biased initial distribution and cells are more likely to aggregate at the border. While a big size cell dish will make the cell distribution more homogeneous, thus the initial distribution follows a uniform distribution. Therefore, in this section, we study whether the population ratio can be affected by the law of initial distribution. We will choose the beta distribution for the choice of the radius $r$ and the angle $\theta$ follows the uniform distribution on $[0, 2\pi]$, that is

$$\{r_n\}_{n=1,\dots,N} \sim \text{Beta}(\alpha, \beta), \quad \{\theta_n\}_{n=1,\dots,N} \sim \text{U}(0, 2\pi).$$

The coordinate transformation of the initial distribution to a unit disk is as follows

$$\begin{cases} x_n = \sqrt{r_n}\cos(\theta_n) \\ y_n = \sqrt{r_n}\sin(\theta_n) \end{cases} \quad n = 1, 2, \ldots, N. \tag{3.6}$$

In Figure 3.10, we plot the density function of the beta distribution for different $\alpha, \beta$

$$f_{\alpha,\beta}(x) = 1/B(\alpha,\beta)\, x^{\alpha-1}(1-x)^{\beta-1},$$

where $B(\alpha,\beta)$ is a normalization constant to ensure that the total integral is 1.

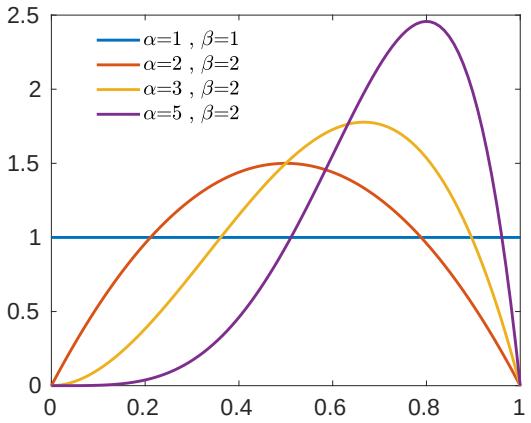


Figure 3.10: *Density function of the initial distribution* $f_{\alpha,\beta}(x) = 1/B(\alpha,\beta)\, x^{\alpha-1}(1-x)^{\beta-1}$ *for different* $\alpha$ *and* $\beta$*, where* $B(\alpha,\beta)$ *is a normalization constant to ensure that the total integral is* 1.

Our simulation will mainly compare the following two cases

$$(\alpha_1, \beta_1) = (1, 1), \quad (\alpha_2, \beta_2) = (3, 2).$$

We plot the initial distributions of the two different cases in Figure 3.11 where we choose 40 cell clusters (i.e., $N_{u_1} = 40$ and $N_{u_2} = 40$ in (3.6)) for species $u_1$ and species $u_2$.

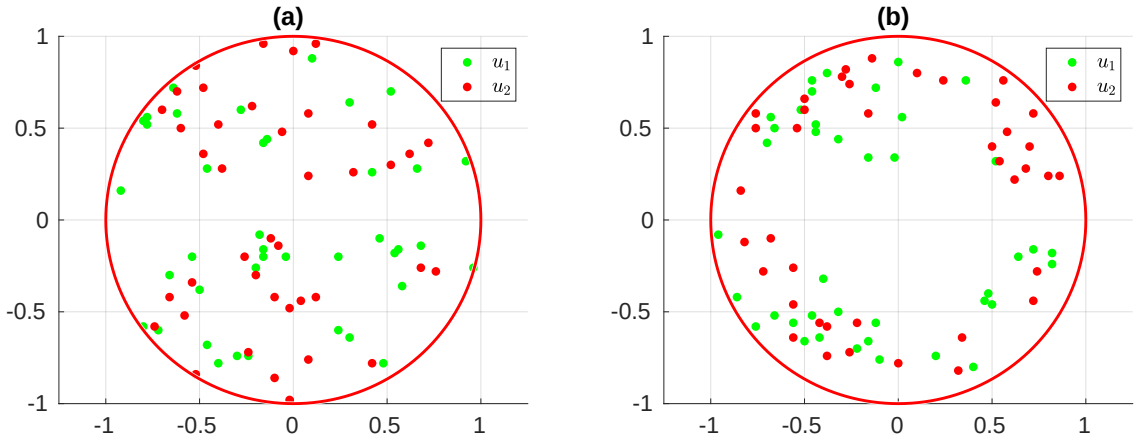


Figure 3.11: *Spatial distribution of the initial values when* $(\alpha,\beta) = (1,1)$ *(Figure (a)) and* $(\alpha,\beta) = (3,2)$ *(Figure (b)). Here red dots and green dots in Figure 3.11 represent cell clusters. We take the cell cluster number* $N_{u_1} = 40$ *and* $N_{u_2} = 40$ *for both cases.*

Suppose the initial cell clusters $N_{u_1} = N_{u_2} = 40$ and cell total number $U_1 = U_2 = 0.02$, which is equally distributed in each cell cluster. Typical numerical solutions are shown in Figure 3.12 when $(\alpha_1, \beta_1) = (1, 1)$ and in Figure 3.13 when $(\alpha_2, \beta_2) = (3, 2)$.

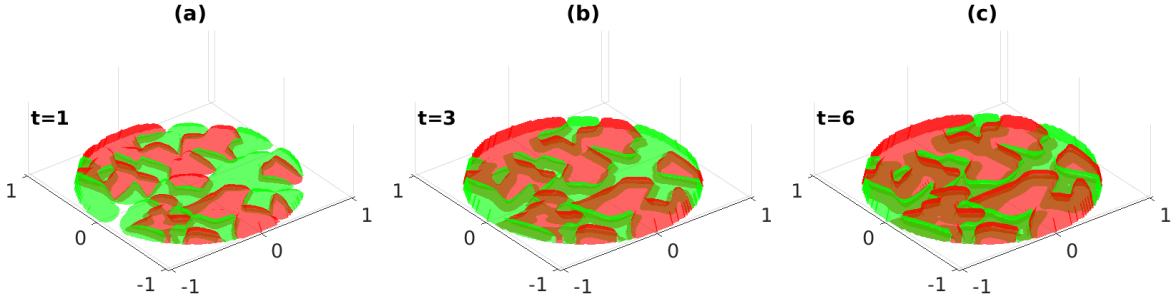


Figure 3.12: *Cell co-culture for species $u_1$ and $u_2$ over 6 days. We plot the case where the initial distribution follows beta function with parameters $(\alpha, \beta) = (1, 1)$, namely the uniform distribution, for day $1, 3$ and day $6$. Parameters are given in Table 3.1 and $\delta_1 = 0.15$, $\delta_2 = 0$, $a_{12} = 0$, $a_{21} = 0$ in (3.4).*

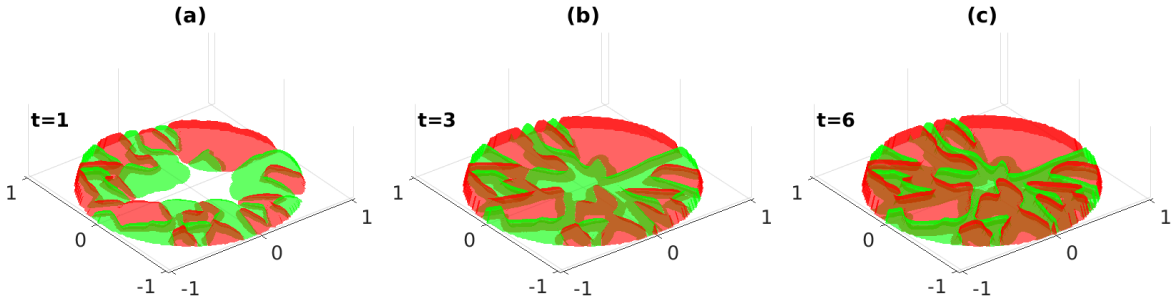


Figure 3.13: *Cell co-culture for species $u_1$ and $u_2$ over 6 days. We plot the case where the initial distribution follows beta function with parameters $(\alpha, \beta) = (3, 2)$, namely a biased distribution, for day $1, 3$ and day $6$. Parameters are given in Table 3.1 and $\delta_1 = 0.15$, $\delta_2 = 0$, $a_{12} = 0$, $a_{21} = 0$ in (3.4).*

Now we plot the evolution of the total number for species $u_1$ and $u_2$ over 6 days.

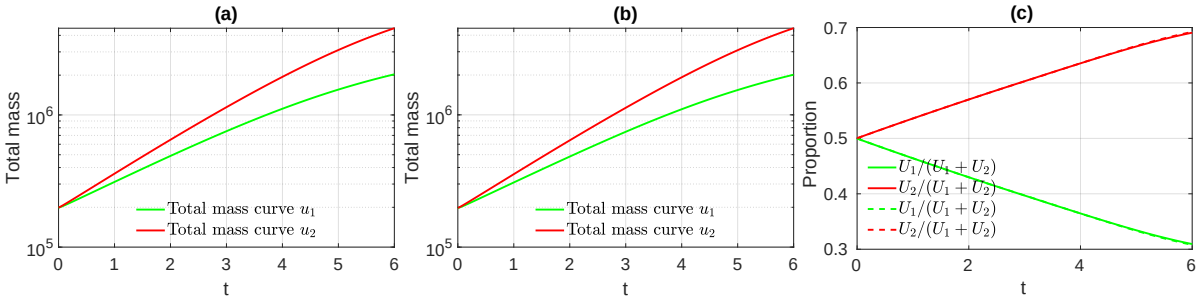


Figure 3.14: *Evolution of the total number (in log scale) and its proportion for species $u_1$ and $u_2$ over 6 days. Figure (a) is the total number plot corresponding to the simulation with an uniform initial distribution in Figure 3.12 while Figure (b) corresponds to the simulation with a biased initial distribution in Figure 3.13. In Figure (c), the solid lines represents the proportion when the initial distribution follows uniform distribution, i.e., $(\alpha, \beta) = (1, 1)$ and the dash lines represents the proportion to the case $(\alpha, \beta) = (3, 2)$. From Figure (c), we can see that they are overlapped. Parameters are given in Table 3.1 and $\delta_1 = 0.15$, $\delta_2 = 0$, $a_{12} = 0$, $a_{21} = 0$ in (3.4).*

From Figure 3.14 we can see that the law of initial distribution has almost no influence on the final proportion of species. We also tried different scenarios when the cell total numbers are 20, 50 and 100 or with different extra mortality rate $\delta_1 = 0, 0.2$ and 0.5, the results are similar. Thus we can deduce that the final relative proportion is stable under the variation of the law of the initial distribution.

Combining the above numerical experiments in Section 3.2.1 and Section 3.2.2, we can see that under the competitive principle, the difference in the spatial resources can change the competition induced by the cell dynamics. To be more precise, under the case of sufficient spatial resources, the competitive mechanism can be more sufficiently expressed than in the case of less spatial resources. In Section 3.2.2, although we changed the law of the initial distribution of the cell seeding, as for the overall spatial resources, it is the same for both species. Therefore, the result of the competitive principle is almost the same in terms of the total number and the population ratio of the two populations.

## 3.3 Impact of the dispersion coefficient on the population ratio

In Section 3.2, when the parameters of the model are the same, the competition induced by the cell dynamics can be reflected by the difference in the spatial resource. Now we assume the spatial resource is the same and we investigate the role of the dispersion coefficient in the evolution of the species.

To that aim, we let the initial distribution of the two species follow the same uniform distribution and they are sparsely seeded on the dish. Furthermore, we let the cell dynamics for the two population to be almost the same, the only variable we control here is the dispersion coefficient for the population. We take the same uniform initial distribution at day 0, with the same number of initial cluster and the same amount of cell total number, i.e.,

$$U_1 = U_2 = 0.005, \quad N_{u_1} = N_{u_2} = 10, \quad a_{12} = a_{21} = 0. \tag{3.7}$$

We compare the following two scenarios in Table 3.4 where the only difference is the dispersion parameters.

| Parameters | $d_1$ | $d_2$ | $\delta_1$ | $\delta_2$ |
|---|---|---|---|---|
| **scenario 1:** | 2 | 2 | 0 | 0 |
| **scenario 2:** | 2 | 0.2 | 0 | 0 |

Table 3.4: *Two sets of dispersion coefficients for $u_1$ and $u_2$.*

In scenario 1, the dispersion coefficients of the two species are the same, while in scenario 2 we suppose the species $u_1$ has an advantage in the spatial competition over its competitor $u_2$.

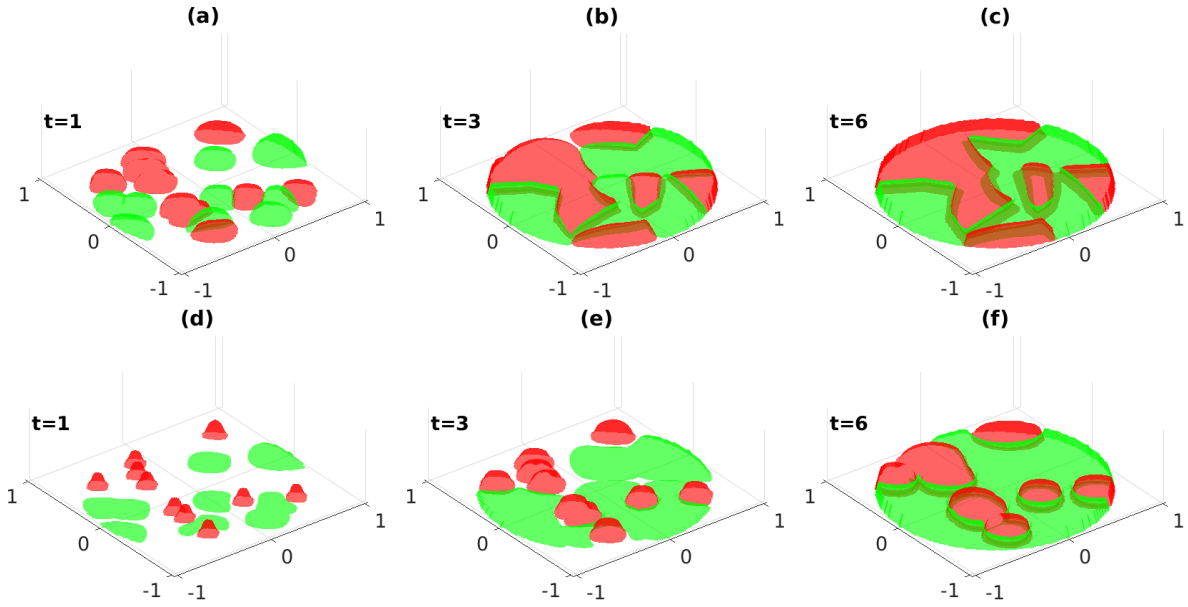


Figure 3.15: *Cell co-culture for species $u_1$ and $u_2$ over 6 days. Figure (a)-(c) corresponds to scenario 1 (i.e. with the parameters $d_1 = 2, d_2 = 2, \delta_1 = \delta_2 = 0$) while Figure (d)-(f) corresponds to scenario 2 (i.e. with $d_1 = 2, d_2 = 0.2, \delta_1 = \delta_2 = 0$). In both scenarios, the number of initial cluster and the cell total number are the same and follow (3.7) and the same uniform distribution. We plot the simulations for day $1, 3$ and day $6$. Other parameters are given in Table 3.1.*

Now we plot the evolution of the total number and the population ratios for species $u_1$ and $u_2$ over 6 days.

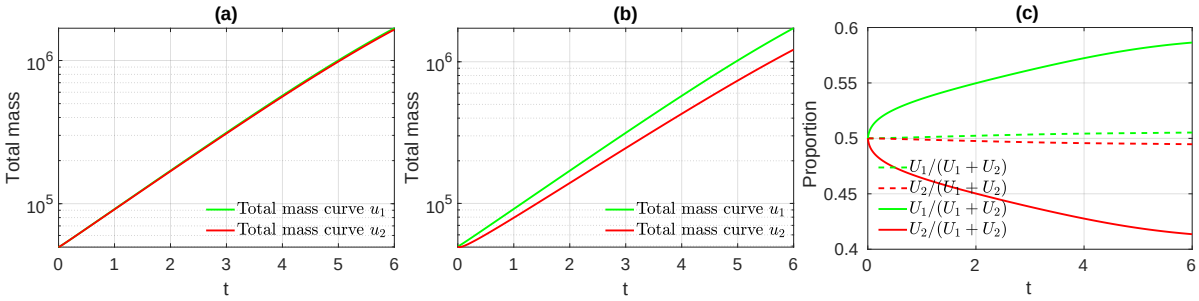


Figure 3.16: *Evolution of the total number (in log scale) and its proportion for species $u_1$ and $u_2$ over 6 days. In Figure (a) we plot the total number of cells corresponding to the scenario 1. In Figure (b) we plot the total number of cells corresponding to the scenario 2. In Figure (c) we plot the population ratios and the dashed lines corresponds to scenario 1 while the solid lines corresponds to scenario 2 in 3.4. Other parameters are given in Table 3.1 and (3.7).*

The main result from Figure 3.16 is that the dispersion coefficient can have a great impact on the population ratio after 6 days. Next, we consider the following scenario where $u_1$ has the advantage in dispersion coefficient but is at a disadvantage induced by drug treatment. Therefore

| Parameters | $d_1$ | $d_2$ | $\delta_1$ | $\delta_2$ |
|---|---|---|---|---|
| **scenario 3:** | 2 | 0.2 | **0.1** | 0 |

Table 3.5: *This scenario corresponds to the case where the species $u_1$ spreads faster than the species $u_2$. Moreover, due to a drug treatment, the mortality of the species $u_1$ is strictly positive while the mortality of the species $u_2$ is zero (i.e. the drug treatment does not affect the second species). In the context of cancer cell, the species $u_1$ would correspond to the sensitive cells to the drug while $u_2$ would correspond to the cell resistant to the drug treatment.*

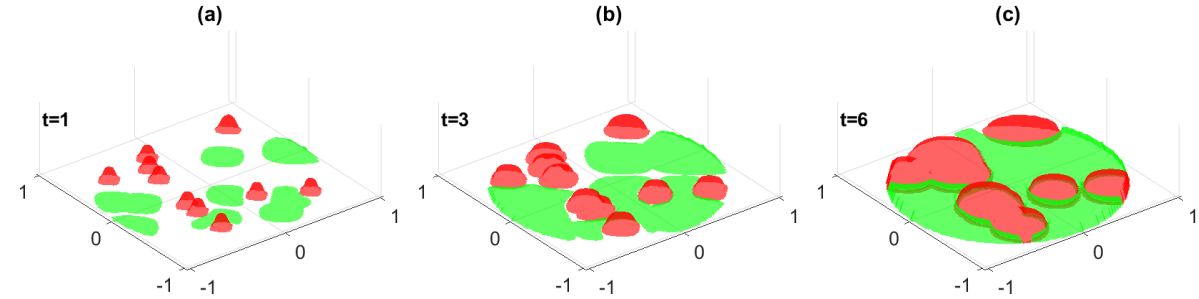


Figure 3.17: *Cell co-culture for species $u_1$ and $u_2$ over 6 days. Figure (a)-(c) corresponds to the scenario 3 with $d_1 = 2, d_2 = 0.2, \delta_1 = 0.1, \delta_2 = 0$ in Table 3.5. The number of initial cluster and cell total number follow (3.7). Other parameters are given in Table 3.1.*

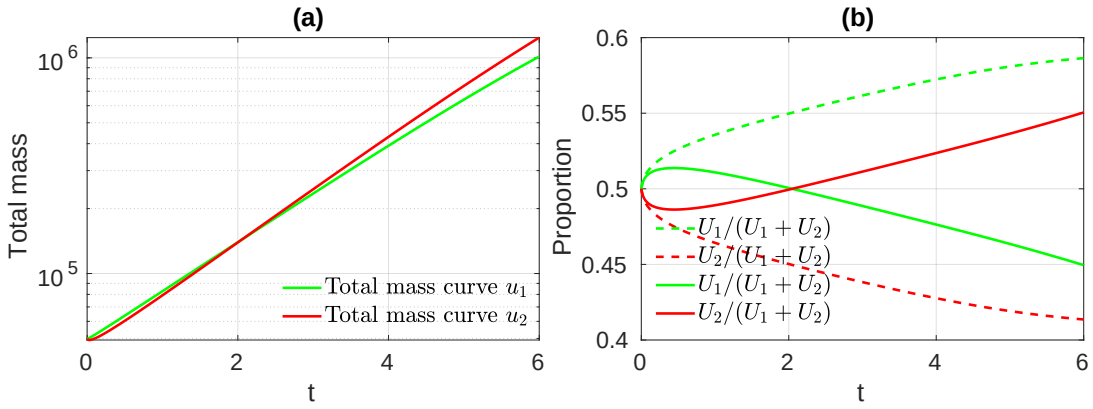


Figure 3.18: *Evolution of the total number (in log scale) and its proportion for species $u_1$ and $u_2$ over 6 days. Figure (a) is the total number plot corresponding to the scenario 3 in Figure 3.17. In Figure (b), the dashed lines corresponds to the population ratios of scenario 2 with $d_1 = 2, d_2 = 0.2, \delta_1 = 0, \delta_2 = 0$ in Table 3.4 and while the solid lines corresponds to scenario 3 with $d_1 = 2, d_2 = 0.2, \delta_1 = 0.1, \delta_2 = 0$ in Table 3.5. Other parameters are given in Table 3.1 and (3.7).*

By including now a drug treatment, we can see from Figure 3.17 and Figure 3.18 that between day 0 and day 2, the population $u_1$ dominates over $u_2$ thanks to a larger dispersion rate. After day 2, since the drug is killing the cell for species $u_1$ while the drug has no effect on the species $u_2$, the species $u_2$ finally takes over the species $u_1$. It leads to a gradual increase in its proportion of the population ratio.

In the numerical simulations for the scenarios 1 and 2 in Table 3.4, we let the cell dynamics of the two species be almost equal. Thus the competition due to the cell dynamics is almost negligible. We have shown the dispersion coefficient of populations can have a great impact on the population ratio after 6 days.

In the simulation for scenario 3 in Table 3.5, we can observe that despite the competitive exclusion, a larger dispersion coefficient can lead to a short-term advantage in the population. In the long term, the competitive exclusion principle still dominates.

# 4 Conclusion and discussion

From the experimental data in the work of Pasquier et al. [89], we modeled the monolayer cell co-culture by a hyperbolic Keller-Segel equation (2.11). We proved the local existence and uniqueness of solutions by using the notion of the solution integrated along the characteristics in Theorem 2.7 and proved the conservation law in Theorem 2.9. For the asymptotic behavior, we analyzed the problem numerically in Section 3.

In Section 3.1 we discussed the competitive exclusion principle, indicating that the asymptotic behavior of the population depends only on the relationship between the steady states $\bar{P}_1$ and $\bar{P}_2$ (see (3.2) for definition) which is different from the ODE case. We found that except for the case $P_1 = P_2$, the model with spatial segregation always exhibits an exclusion principle.

Even though the long term dynamics of cell density is decided by the relative values of the equilibrium, the short term behavior need a more delicate description. We studied two factors which may influence the population ratios. The first factor is the initial cell distribution, as measured by the initial total cell number and the law of initial distribution. We found that the impact of the initial distribution on the population ratio lies in the initial total cell number but not in the law of initial distribution.

The second factor influencing the population ratio is the cell movement in space, as measured by the dispersion coefficient $d_i$. In the transient stage (i.e. before the dish is saturated), the dispersion rate $d_i$ are the dominant factor. Once the surface of the dish is saturated by cells, cell dynamics $u_i\, h(u_1, u_2)$ becomes the key factor. Note that the coefficients $a_{12}, a_{21}$ do not play any role in the competition because of the segregation principle.

We can briefly summarize the following main factors that can influence the population ratio in cell culture for model (2.11):

(a). The difference of cell dynamics in the two species (internal factor): if the equilibrium $\bar{P}_1 > \bar{P}_2$ (see (3.2) for definition), then $u_1$ will dominate, $u_2$ will die out (and vice-versa when $\bar{P}_1 < \bar{P}_2$) (see Figures 3.5-3.6 and Table 3.3);

(b). If cells are densely seeded at the beginning, despite of competitive advantage, the dominant species can not take out its competitor in a short time (see Figures 3.7-3.8). We also concluded that the law of initial distribution has almost no influence on the population ratio (see Figures 3.12-3.13);

(c). If cells are sparsely seeded at the beginning, we need to distinguish the period of time needed for the cell to occupy the surface of the dish and the time needed for each species to reach a saturation stage (see Figure 3.16 and Figure 3.18).

# Conclusion

## 1 Contributions of the thesis

The motivation of this thesis is to study the cell movement with separation phenomenon found in cell co-culture experiments through a mathematical model. In the 1970s, Shigesada et al. [95] proposed a self-diffusion and cross-diffusion model to study the effects of separation between two competing species. They found the segregation can allow the populations to maintain their respective living areas, thus leading to the coexistence of two populations. This result provides a different perspective on the exclusion principle of the classic Lotka-Volterra ODE model. Although the separation of solutions can be rigorously proved in nonlinear diffusion equations, one of the mathematical drawbacks of such models is that it is difficult to obtain the uniqueness of solutions. Therefore, based on the work of other researchers, we proposed an alternative model – a reaction-diffusion equation with nonlocal advection term. We rigorously proved the existence and uniqueness of solutions. Particularly, when the viscosity equals 0, we can also prove the segregation property of solutions.

### 1.1 A reaction-diffusion equation with nonlocal advection

In Chapter 1 and 2, we mainly dealt with a class of reaction-diffusion equation with nonlocal advection term.

In Chapter 1 we mainly discussed the case when the viscosity coefficient $\varepsilon > 0$. Under rather general assumption on the nonlocal kernel, we studied the local well-posedness of the problem in suitable fractional spaces by using the semigroup theory. We obtained stability results for the homogeneous steady state. A bifurcation analysis was performed to understand the emerging complex patterns when the positive homogeneous steady state becomes unstable. With a symmetric step function kernel, Turing bifurcation of equilibrium may occur. As a result, we obtained the existence of a stable branch of spatially heterogeneous steady states. More surprisingly, when this symmetry is broken by shifting the step function, the homogeneous steady state may undergo what we called Turing-Hopf bifurcation yielding the existence of a branch of spatially heterogeneous and time periodic solutions.

Lastly, by letting the kernel function converge to a Dirac measure, we can see whether the solution will converge formally to the solution of porous medium equation (Barenblatt solution) depends highly on the sign of the Fourier coefficients of the kernel. To be more

precise, if the kernel has only positive Fourier coefficients, then we observed that the solution does converge to Baranblatt solution while if the kernel possesses a negative Fourier coefficient, it may lead to spatially heterogeneous solution.

In Chapter 2 we studied the case when the viscosity equals 0, our equation becomes a hyperbolic nonlocal advection equation. In such case, the classical semigroup theory is not enough to prove the well-posedness of the equation. To that aim, inspired by the work of Ducrot and Magal [39], we considered the notion of solutions integrated along the characteristics. In Chapter 2, we generalized the single-species equation in [39] and we investigated the competition between two species. Moreover, by using the solution integrated along the characteristics, we proved that the solutions admit segregation property. Besides, under the framework of Young measure theory, we extended the results on the asymptotic behavior of solutions in [39] to two-species case. From a numerical perspective, we found that under the effect of segregation, the PDE model admits a competitive exclusion principle and the finial proportion of populations is also affected by the initial distributions.

### 1.2 An application to cell co-culture

From the experimental data in the work of Pasquier et al. [89], we modeled the monolayer cell co-culture by a hyperbolic Keller-Segel equation. We proved the competitive exclusion principle, indicating that the asymptotic behavior of populations only depends on the relationship between the steady states for two species. We found that except for the case when the two steady states are equal, the model with spatial segregation always exhibits an exclusion principle. This result is different from the ODE case.

Even though the long term dynamics of cell density is decided by the relative values of the steady states, the short term behavior need a more delicate description. We studied two factors which may influence the population ratios. The first factor is the initial cell distribution, as measured by the initial total cell number and the law of initial distribution. We found that the impact of the initial distribution on the population ratio lies in the initial total cell number but not in the law of initial distribution.

The second factor having an impact on the population ratio is the cell movement in space, as measured by the dispersion coefficients. In the transient stage (i.e., before the dish is saturated), the dispersion rates are the dominant factor. Once the surface of the dish is saturated by cells, cell dynamics becomes the key factor. Our numerical results also confirm the work in [95], the segregation property can suppress the competition in the sense that each species can live on its separated domain (depending on the initial distribution), thus the dominant species needs an extremely long time to take out its competitor.

## 2 Research perspectives

One of the important problems that we are interested in is the traveling wave solution for such a nonlocal advection equation. Aronson [4] and Atikinson [5], using the phase-plane

analysis, studied the porous medium equation with logistic source

$$u_t = (u^m)_{xx} + u(1-u), \text{ with } m > 1,$$

and confirmed the existence of the sharp-type traveling wave with the critical wave speed $c^*$.

From the case when $m = 1$ which corresponds to the Fisher-KPP equation, to some recent work dealing with the large time behavior of solutions and stability of the wavefronts for $m > 1$ in higher dimension, the traveling wave solutions for classic porous medium equation still attracts many mathematicians. We refer to the references [4, 5, 35, 37, 63] in the topic of traveling wave solutions for porous medium equations.

As for the reaction-diffusion equation with nonlocal advection, we refer to the recent work by Hamel and Henderson [52]. They considered the following model

$$u_t + \partial_x(u\,(K * u)) = u_{xx} + u(1-u),$$

where the bounded odd kernel function $K \in L^p(\mathbb{R})$ for $p \in [1, \infty]$. They obtained the explicit upper and lower bounds on the propagation speed which are asymptotically sharp in the above cases.

In fact, our on-going work will focus on the existence of the traveling wave solution of the following problem defined on $\mathbb{R}$

$$u_t - (u(\rho * u)_x)_x = u(1-u),$$

where kernel $\rho(x) = \frac{1}{2}e^{-|x|}$ corresponds to the Keller-Segel model with negative chemotaxis.

Contrast to the porous medium case where the sharp-type traveling wave solutions are continuous, in the case of nonlocal advection with logistic source we can show the traveling wave solution (if exists) is necessarily discontinuous. This is also observed by our numerical simulations. Our numerical simulation is under the following regime :

- Given a bounded interval $[-L, L]$ and an initial distribution of $\phi \in C([-L, L])$ satisfying $\phi(-L) = 1$ and for some $z^* \in [-L, L]$,

$$\phi(z) = 0, \text{ for any } z \geq z^*.$$

- Extend the initial profile by letting $\phi(z) \equiv 1$ for any $z < -L$ and $\phi(z) \equiv 0$ for any $z > L$;
- Solve numerically the following PDE using upwind scheme

$$\begin{cases} \partial_t u(t,x) - \partial_x\big(u(t,x)\partial_x p(t,x)\big) = u(t,x)(1-u(t,x)), \\ u(t,x) = 1,\ x \leq -L, \quad u(t,x) = 0,\ x \geq L, \qquad\qquad t > 0,\ x \in [-L, L]. \\ u(0,x) = \phi(x), \end{cases} \tag{2.1}$$

with the convolution term defined as

$$\begin{aligned} p(t,x) &= \int_{\mathbb{R}} \rho(x-y)u(t,y)dy \\ &= \int_{-\infty}^{L} \rho(x-y)dy + \int_{-L}^{L} \rho(x-y)u(t,y)dy \end{aligned}$$

where $\rho(x) = \frac{1}{2}e^{-|x|}$.

Our initial value $\phi$ is chosen as

$$\phi(x) = \frac{(x-x_0)^2}{(L+x_0)^2}\mathbb{1}_{[-L,x_0]}(x) \in C^1([-L,L]). \tag{2.2}$$

In the following numerical simulations, we always set

$$L = 20,\ x_0 = -15.$$

Figure 3.1 is the propagation of the profile.

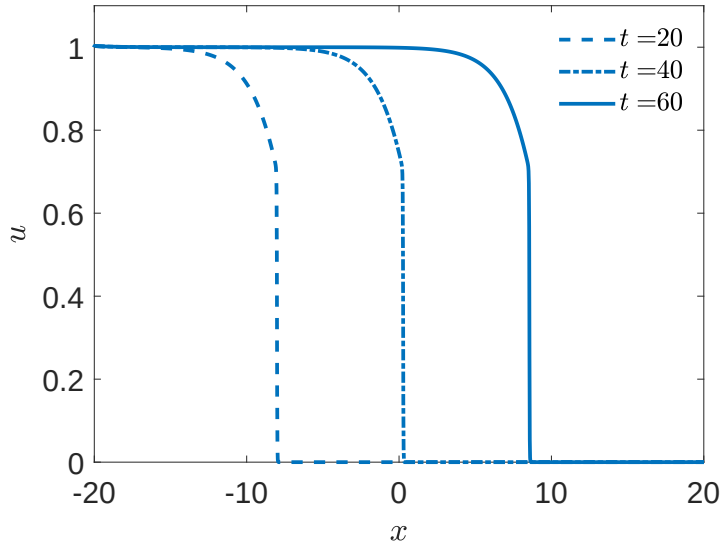


Figure 3.1: *We plot the propagation of the front under system (2.1). Our initial distribution is taken as (2.2). We plot the propagation profile at $t = 20, 40$ and 60 (reps. dashed lines, dotted-dashed lines and solid lines).*

The above simulation shows that even though the initial profile is $C^1$ smooth, there is the formation of discontinuity in large time behavior.

We also plot the propagation speeds at different $u$ values, namely, when $u = 0, 0.2, 0.5, 0.8$ and 0.9 (here $u = 0$ means the position of the largest point which is nonzero), this will help us to identify if the above profile is a traveling wave or not.

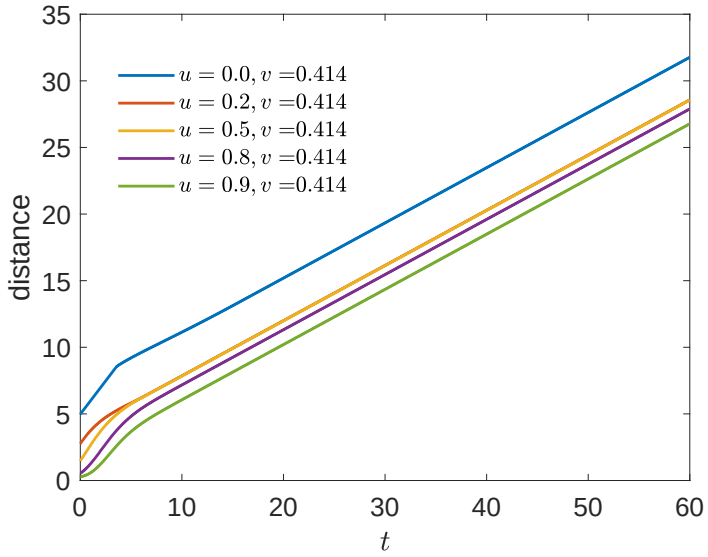


Figure 3.2: *We plot the propagating speed of the front under system* (5.1). *Our initial distribution is taken as* (5.2). *We trace the propagating speeds of the profile at* $u = 0, 0.2, 0.5, 0.8$ *and* $0.9$. *The x-axis represents the time and the y-axis is the relative moving distance at different* $u$ *values.*

Since the dynamics of cell growth can either be described through individual-based models as well as continuum models, for the extension of our work in the modeling aspect we can consider the comparison of these two different approaches. We refer to Byrne and Drasdo [20], Motsch and Peurichard [78] for the comparison of individual-based models with the limiting continuum models. In fact, in order to formally derive a continuous model from the microscopic model with non-overlapping constraint and cell division, Motsch and Peurichard [78] obtained a nonlocal advection equation with a threshold constraint for the density function. In the aforementioned papers, the microscopic and macroscopic models showed numerically a good agreement in their large time dynamics. Therefore, the continuum model solves the large computational time raised by the individual-based model but stays closely linked to the microscopic dynamics.

Comparing the individual-based models with the limiting continuum models can also be a guiding direction for the future work of this thesis. In the introduction part, we mentioned if the interactions between the particles follow the potential $V^n$ satisfying

$$V^n(x) = n^\beta V\left(n^{\frac{\beta}{N}} x\right),$$

and the following convergence

$$\lim_{n\to\infty} V^n(x) = \delta_0(x),$$

where $\delta_0$ is the Dirac measure at 0. Then as the number of the particles goes to infinity, we can obtain a nonlocal advection model when $\beta = 0$ (Mckean-Vlasov limit). Here it is interesting to consider the influence of the choice of the potential $V$. One may ask whether there are some restrictions on the Fourier coefficients of $V$ as mentioned in the work [48, 58]. Whether the continuous model requires some modifications after considering the volume of cells and the non-overlapping limitation? Under what conditions can we

say the individual-based model is a good approximation? Finally, when we have the simulations for the individual-based model, we can gain a better understanding of the co-culture, separation, boundary formation, and competing relationships of cell co-culturing.

# Appendix A

# Reduced system for Theorem 3.8

In this subsection, we give a brief calculation of the center manifold reduction as a supplement of Theorem 3.8. Recall our equation reads as follows

$$\frac{d}{dt}\begin{pmatrix} w(t) \\ \gamma(t) \end{pmatrix} = L\begin{pmatrix} w(t) \\ \gamma(t) \end{pmatrix} + R\begin{pmatrix} w(t) \\ \gamma(t) \end{pmatrix},$$

wherein we have set

$$L = \begin{pmatrix} \left(A + \partial_w \tilde{F}(0,\gamma_0)\right) & 0 \\ 0 & 0 \end{pmatrix} \in \mathcal{L}\left(H^2 \times \mathbb{R}, H^0 \times \mathbb{R}\right),$$

and

$$R\begin{pmatrix} w \\ \gamma \end{pmatrix} = \begin{pmatrix} \tilde{F}(w,\gamma) - \partial_w \tilde{F}(0,\gamma_0)w \\ 0 \end{pmatrix}.$$

Recall also that $\tilde{F}$ and $B$ are defined by

$$\tilde{F}(w,\gamma) = \frac{b-\mu}{\gamma\mu}(K \circ w)'' + B(w,w) + \left(\frac{\mu^2}{b+\gamma\mu w} - \mu\right)w + w,$$
$$B(w,w) = \frac{d}{dx}\left(w\frac{d}{dx}K \circ w\right),$$

and we define

$$G(w,\gamma) = \tilde{F}(w,\gamma) - \partial_w \tilde{F}(0,\gamma_0)w.$$

Moreover, we also define $\hat{A} = A + \partial_w \tilde{F}(0,\gamma_0)$ and let us observe that $\hat{A}e_n = \lambda_n(\gamma_0)e_n$ for all $n \in \mathbb{Z}$. Recall that the framework of 3.8 implies that we have, for some $n_0 \geq 1$,

$$\lambda_{\pm n_0}(\gamma_0) \in i\mathbb{R}, \quad \mathrm{Re}(\lambda_n(\gamma_0)) < 0,\ \forall n \neq \pm n_0.$$

To perform our center manifold reduction we will need the following computations:

- $K \circ e_n = c_n(K)e_n$ for all $n \in \mathbb{Z}$

- $B(e_n, e_m) = -\left(\frac{\pi}{L}\right)^2 c_m(K)m(m+n)e_{m+n}$ for all $(n,m) \in \mathbb{Z}^2$.

Define the center space $\mathcal{E}^c = \text{span}\,(e_{\pm n_0}) \times \mathbb{R}$ and the stable space $\mathcal{E}^s = \text{span}\,(e_{\pm n_0})^\perp \times \{0\}$ where $\text{span}\,(e_{\pm n_0})$ denotes the vector space spanned by eigenfunctions $e_{\pm n_0}$ while $\text{span}\,(e_{\pm n_0})^\perp$ denotes its orthogonal space for the $L^2(-L,L)-$inner product. We denote by $\tilde{\Psi} : \mathcal{E}^c \to \mathcal{E}^s$ the local center manifold and in the sequel we will make use of the following notation

$$\tilde{\Psi}(x^c, \gamma) = (\Psi(x^c, \gamma), 0) \in \mathcal{E}^s, \text{ for } (x^c, \gamma) \in \mathcal{E}^c \text{ close to } (0, \gamma_0),$$

and $x^c = x_- e_{-n_0} + x_+ e_{n_0}$. Since the center manifold is smooth (here $C^\infty$) we rewrite it as follows:

$$\Psi(x^c, \gamma) = \sum_{n \neq \pm n_0} \Psi_n(x^c, \gamma) e_n = \sum_{n \neq \pm n_0} P_n(x^c, \gamma) e_n + O\left(\left(\|x_c\| + |\gamma - \gamma_0|\right)^3\right) \text{ in } H^2,$$

where, for each $n \in \mathbb{Z} \setminus \{\pm n_0\}$, $P_n(x^c, \gamma)$ is homogeneous polynomial of degree 2 for the variables $x_-$, $x_+$ and $(\gamma - \gamma_0)$. For notational simplicity we also denote by $P_{\pm n_0}(x^c, \gamma)$ the first order polynomials

$$P_{-n_0}(x^c, \gamma) = x_- \text{ and } P_{n_0}(x^c, \gamma) = x_+.$$

Note that since the center manifold is real valued, one has

$$x_+ = \overline{x}_- \text{ and } \Psi_{-n}(x^c, \gamma) = \overline{\Psi_n(x^c, \gamma)}, \, \forall n \neq \pm n_0.$$

To compute the – center manifold – reduced system, let us introduce the center and stable projectors $\Pi^c$ and $\Pi^s$ as follows:

$$\Pi^c \varphi = \sum_{n = \pm n_0} c_n(\varphi) e_n \text{ and } \Pi^s \varphi = \sum_{n \neq \pm n_0} c_n(\varphi) e_n,$$

as well as the center and stable part of the linear operator $\hat{A}$, respectively denoted by $\hat{A}^c$ and $\hat{A}^s$ and defined by

$$\hat{A}^c \varphi = \sum_{n = \pm n_0} c_n(\varphi) \lambda_n(\gamma_0) e_n \text{ and } \hat{A}^s \varphi = \sum_{n \neq \pm n_0} \lambda_n(\gamma_0) c_n(\varphi) e_n.$$

Next the reduced system reads as

$$\begin{cases} \dfrac{dx^c(t)}{dt} = \hat{A}^c x^c(t) + \Pi^c G\left(x^c(t) + \Psi\left(x^c(t), \gamma(t)\right), \gamma(t)\right), \\ \dfrac{d\gamma(t)}{dt} = 0, \end{cases} \tag{A.1}$$

and the center manifold satisfies the following equation in the neighbourhood of $(x^c, \gamma) = (0, , \gamma_0)$:

$$\partial_{x^c} \Psi(x^c, \gamma) \left[A^c x^c + \Pi^c G(x^c + \Psi(x^c, \gamma), \gamma)\right] = A^s \Psi(x^c, \gamma) + \Pi^s G(x^c + \Psi(x^c, \gamma), \gamma). \tag{A.2}$$

Our goal is to obtain a Taylor expansion up to order 3 of the above reduced system. To that aim we shall first compute a Taylor expansion of $\Pi^c G(x^c + \Psi(x^c, \gamma), \gamma)$ and

$\Pi^s G(x^c + \Psi(x^c, \gamma), \gamma)$ respectively up to order 3 and 2. To do so, first note that for $\|w\|$ small enough and $\gamma$ close to $\gamma_0$ one has the series expansion

$$\tilde{F}(w, \gamma) = \frac{b-\mu}{\gamma\mu} (K \circ w)'' + B(w, w) + w(1-\mu) + \frac{\mu^2}{b} \sum_{p=0}^{\infty} \frac{\gamma^p \mu^p w^{p+1}}{b^p},$$

and

$$\partial_w \tilde{F}(0, \gamma_0) w = \frac{b-\mu}{\gamma_0\mu} (K \circ w)'' + w(1-\mu) + \frac{\mu^2}{b} w.$$

As a consequence one has, for all $w$ and $|\gamma - \gamma_0|$ small enough,

$$G(w, \gamma) = \frac{b-\mu}{\mu} \frac{\gamma_0 - \gamma}{\gamma_0 \gamma} (K \circ w)'' + B(w, w) + \frac{\mu^2}{b} \sum_{p=1}^{\infty} \frac{\gamma^p \mu^p w^{p+1}}{b^p}.$$

Hence this leads us to the following order 3 Taylor expansion

$$\begin{aligned} G(w, \gamma) =& \frac{b-\mu}{\gamma_0\mu} \frac{(2\gamma_0 - \gamma)(\gamma_0 - \gamma)}{\gamma_0^2} (K \circ w)'' + B(w, w) + \frac{\mu^3 \gamma_0}{b^2} w^2 \\ &+ \frac{\mu^3(\gamma - \gamma_0)}{b^2} w^2 + \frac{\mu^4 \gamma_0^2}{b^3} w^3 + O((|w| + |\gamma - \gamma_0|)^4). \end{aligned}$$

Now choosing the following form for $w$

$$w = x^c + \Psi(x^c, \gamma) = x_- e_{-n_0} + x_+ e_{n_0} + \sum_{n \neq \pm n_0} P_n(x^c, \gamma) + O\left((\|x^c\| + |\gamma - \gamma_0|)^3\right) \text{ in } H^2,$$

yields

$$\begin{aligned} (K \circ w)'' =& -\left( \left(\frac{n_0 \pi}{L}\right)^2 c_{-n_0}(K) x_- e_{-n_0} + \left(\frac{n_0 \pi}{L}\right)^2 c_{n_0}(K) x_+ e_{n_0} \right) \\ &- \sum_{n \neq \pm n_0} \left(\frac{n\pi}{L}\right)^2 c_n(K) P_n(x^c, \gamma) e_n + O\left((\|x^c\| + |\gamma - \gamma_0|)^3\right) \text{ in } H^0, \end{aligned}$$

and

$$\begin{aligned} B(w, w) =& \sum_{m,n \in \mathbb{Z}^2} P_n(x^c, \gamma) P_m(x^c, \gamma) B(e_n, e_m) \\ =& -\sum_{m,n} P_n(x^c, \gamma) P_m(x^c, \gamma) \left(\frac{\pi}{L}\right)^2 c_m(K) m(m+n) e_{m+n} \\ &+ O\left((\|x^c\| + |\gamma - \gamma_0|)^4\right) \text{ in } H^0, \end{aligned}$$

Now, we calculate those terms of $B(w, w)$ up to order 2, which are given by

$$\text{order 2} \begin{cases} -x_+^2 \left(\frac{\pi}{L}\right)^2 c_{n_0}(K) 2n_0^2 e_{2n_0}, & n = m = n_0; \\ -x_-^2 \left(\frac{\pi}{L}\right)^2 c_{-n_0}(K) 2n_0^2 e_{-2n_0}, & n = m = -n_0; \\ 0, & n = n_0, m = -n_0; \text{ or } n = -n_0, m = n_0. \end{cases}$$

For further normal form computation, we list all possible situations of order 3 of $\Pi^c B(w,w)$, that the components along the vectors $e_{n_0}$ and $e_{-n_0}$. They reads as follows

$$\text{order 3}\begin{cases} 0, & n=n_0,\ m=0;\\ -x_+P_{-2n_0}(x^c,\gamma)\left(\frac{\pi}{L}\right)^2 c_{-2n_0}(K)2n_0^2e_{-n_0}, & n=n_0,\ m=-2n_0;\\ 0, & n=-n_0,\ m=0;\\ -x_-P_{2n_0}(x^c,\gamma)\left(\frac{\pi}{L}\right)^2 c_{2n_0}(K)2n_0^2e_{n_0}, & n=-n_0,\ m=2n_0;\\ -x_+P_0(x^c,\gamma)\left(\frac{\pi}{L}\right)^2 c_{n_0}(K)n_0^2e_{n_0}, & n=0,\ m=n_0;\\ x_+P_{-2n_0}(x^c,\gamma)\left(\frac{\pi}{L}\right)^2 c_{n_0}(K)n_0^2e_{-n_0}, & n=-2n_0,\ m=n_0;\\ -x_-P_0(x^c,\gamma)\left(\frac{\pi}{L}\right)^2 c_{-n_0}(K)n_0^2e_{-n_0}, & n=0,\ m=-n_0;\\ x_-P_{2n_0}(x^c,\gamma)\left(\frac{\pi}{L}\right)^2 c_{-n_0}(K)n_0^2e_{n_0}, & n=2n_0,\ m=-n_0; \end{cases}$$

Finally, we compute the term $\Pi^c w^2$ and $\Pi^c w^3$. To that aim, note that one has

$$\begin{aligned} w^2 &= \left(x_-e_{-n_0}+x_+e_{n_0}+\sum_{n\neq\pm n_0}P_n(x^c,\gamma)e_n\right)^2\\ &= x_+^2e_{2n_0}+2x_+x_-e_0+x_-^2e_{-2n_0}+(x_-e_{-n_0}+x_+e_{n_0})\sum_{n\neq\pm n_0}P_n(x^c,\gamma)e_n\\ &\quad+O((\|x^c\|+|\gamma-\gamma_0|)^4). \end{aligned}$$

Therefore

$$\begin{aligned} \Pi^c w^2 &= \left(x_+P_0(x^c,\gamma)+x_-P_{2n_0}(x^c,\gamma)\right)e_{n_0}+\left(x_+P_{-2n_0}(x^c,\gamma)+x_-P_0(x^c,\gamma)\right)e_{-n_0}\\ &\quad+O((\|x^c\|+|\gamma-\gamma_0|)^4). \end{aligned}$$

Next, one has

$$w^3=(x_-e_{-n_0}+x_+e_{n_0})^3+O((\|x^c\|+|\gamma-\gamma_0|)^4),$$

so that we get

$$\Pi^c w^3=3x_+^2x_-e_{n_0}+3x_+x_-^2e_{-n_0}+O((\|x^c\|+|\gamma-\gamma_0|)^4).$$

Coupling the above computations allows us to compute a Taylor expansion up to order 3 for the quantity $\Pi^c G(x^c+\Psi(x^c,\gamma),\gamma)$ and more precisely we get

$$\begin{aligned} &\Pi^c G(x^c+\Psi(x^c,\gamma),\gamma)\\ &=\frac{b-\mu}{\gamma_0\mu}\frac{(2\gamma_0-\gamma)(\gamma-\gamma_0)}{\gamma_0^2}\left(\frac{n_0\pi}{L}\right)^2(c_{-n_0}(K)x_-e_{-n_0}+c_{n_0}(K)x_+e_{n_0})\\ &\quad+\left(\frac{n_0\pi}{L}\right)^2(x_-P_{2n_0}(x^c,\gamma)c_{-n_0}(K)-2x_-P_{2n_0}(x^c,\gamma)c_{2n_0}(K)-x_+P_0(x^c,\gamma)c_{n_0}(K))\,e_{n_0}\\ &\quad+\left(\frac{n_0\pi}{L}\right)^2(x_+P_{-2n_0}(x^c,\gamma)c_{n_0}(K)-2x_+P_{-2n_0}(x^c,\gamma)c_{-2n_0}(K)-x_-P_0(x^c,\gamma)c_{-n_0}(K))\,e_{-n_0} \end{aligned}$$

$$+\frac{\mu^3\gamma_0}{b^2}(x_+P_0(x^c,\gamma)+x_-P_{2n_0}(x^c,\gamma))e_{n_0}+\frac{\mu^3\gamma_0}{b^2}(x_+P_{-2n_0}(x^c,\gamma)+x_-P_0(x^c,\gamma))e_{-n_0}$$
$$+\frac{\mu^4\gamma_0^2}{b^3}\left(3x_+^2x_-e_{n_0}+3x_+x_-^2e_{-n_0}\right)+O((\|x^c\|+|\gamma-\gamma_0|)^4)\text{ in }H^0. \tag{A.3}$$

Similarly, we also obtain a Taylor expansion for the quantity $\Pi^sG(x^c+\Psi(x^c,\gamma),\gamma)$ up to order 2 as follows,

$$\begin{aligned}\Pi^sG(x^c+\Psi(x^c,\gamma),\gamma)=&2\left(\frac{n_0\pi}{L}\right)^2\left(c_{n_0}(K)x_+^2e_{2n_0}+c_{-n_0}(K)x_-^2e_{-2n_0}\right)\\&+\frac{\mu^3\gamma_0}{b^2}\left(x_+^2e_{2n_0}+2x_+x_-e_0+x_-^2e_{-2n_0}\right)+O((\|x^c\|+|\gamma-\gamma_0|)^3).\end{aligned}$$

We now plug the above Taylor expansion into (A.4) to identify the polynomials $P_n$ needed to obtain a Taylor expansion up to order 3 of the reduced system.

First note that the left-hand side of (A.2) can be rewritten as

$$\begin{aligned}&\partial_{x^c}\Psi(x^c,\gamma)\left[A^cx^c+\Pi^cG(x^c+\Psi(x^c,\gamma),\gamma)\right]\\=&\partial_{x^c}\Psi(x^c,\gamma)\left[\lambda_{n_0}(\gamma_0)x_+e_{n_0}+\lambda_{-n_0}(\gamma_0)x_-e_{-n_0}+h.o.t.\geq 2\right]\\=&\lambda_{n_0}(\gamma_0)x_+\partial_{x^c}\Psi(x^c,\gamma)e_{n_0}+\lambda_{-n_0}(\gamma_0)x_-\partial_{x^c}\Psi(x^c,\gamma)e_{-n_0}+h.o.t.\geq 3\end{aligned} \tag{A.4}$$

where $h.o.t.\geq 2$ (resp. 3) means those terms with order greater than 2 (resp. 3). And similarly, the right-hand side of (A.2) can be re-written as

$$\begin{aligned}&A^s\Psi(x^c,\gamma)+\Pi^sG(x^c+\Psi(x^c,\gamma),\gamma)\\=&\sum_{n\neq\pm n_0}\lambda_n(\gamma_0)P_n(x^c,\gamma)e_n-2\left(\frac{n_0\pi}{L}\right)^2\left(c_{n_0}(K)x_+^2e_{2n_0}+c_{-n_0}(K)x_-^2e_{-2n_0}\right)\\&+\frac{\mu^3\gamma_0}{b^2}\left(x_+^2e_{2n_0}+2x_+x_-e_0+x_-^2e_{-2n_0}\right)+h.o.t.\geq 3\\=&\sum_{n\neq\pm n_0}\lambda_n(\gamma_0)P_n(x^c,\gamma)e_n+C_0x_+x_-e_0+C_{2n_0}x_+^2e_{2n_0}+C_{-2n_0}x_-^2e_{-2n_0}+h.o.t.\geq 3,\end{aligned} \tag{A.5}$$

wherein we have set

$$\begin{aligned}C_0&=2\frac{\mu^3\gamma_0}{b^2},\\C_{2n_0}&=-2\left(\frac{n_0\pi}{L}\right)^2c_{n_0}(K)+\frac{\mu^3\gamma_0}{b^2},\\C_{-2n_0}&=-2\left(\frac{n_0\pi}{L}\right)^2c_{-n_0}(K)+\frac{\mu^3\gamma_0}{b^2}.\end{aligned} \tag{A.6}$$

According to (A.3) we only need to compute those terms when $n=0,\pm 2n_0$. Next since (A.4) and (A.5) are equal, identifying the terms of order 2 yields

$$\lambda_{n_0}(\gamma_0)x_+\frac{\partial}{\partial x_+}P_n(x^c,\gamma)+\lambda_{-n_0}(\gamma_0)x_-\frac{\partial}{\partial x_-}P_n(x^c,\gamma)=\lambda_n(\gamma_0)P_n(x^c,\gamma)+Q_n(x^c)$$

for $n=0,\pm 2n_0$, where we have defined

$$Q_0(x^c)=C_0x_+x_-,\ Q_{2n_0}(x^c)=C_{2n_0}x_+^2,\ Q_{-2n_0}(x^c)=C_{-2n_0}x_-^2.$$

Recalling that $P_n$ are homogeneous polynomials of degree 2 with respect to the three variables $x_-$, $x_+$ and $(\gamma - \gamma_0)$, obtains that

$$\begin{aligned} P_0(x^c, \gamma) &= -\frac{C_0}{\lambda_0(\gamma_0)} x_+ x_-, \\ P_{2n_0}(x^c, \gamma) &= -\frac{C_{2n_0}}{\lambda_{2n_0}(\gamma_0)} x_+^2, \\ P_{-2n_0}(x^c, \gamma) &= -\frac{C_{-2n_0}}{\lambda_{-2n_0}(\gamma_0)} x_-^2, \end{aligned}$$

where the constants $C_0$, $C_{\pm 2m_0}$ are defined in (A.6). Finally substituting the above expression into the Taylor expansion of $\Pi^c G(x^c + \Psi(x^c, \gamma), \gamma)$ yields the following reduced system up to order 3,

$$\begin{cases} \dfrac{dx_+(t)}{dt} & = [i\omega + a(\gamma)]\, x_+ + x_- x_+^2 \beta + h.o.t \geq 4, \\ x_-(t) & = \overline{x}_+(t), \\ \dfrac{d\gamma(t)}{dt} & = 0. \end{cases}$$

Here we have set $\lambda_{n_0}(\gamma_0) = i\omega$,

$$a(\gamma) = \left(\frac{n_0 \pi}{L}\right)^2 \frac{b - \mu}{\gamma_0 \mu} c_{n_0}(K) \frac{(2\gamma_0 - \gamma)(\gamma - \gamma_0)}{\gamma_0^2},$$

and

$$\begin{aligned} \beta = \frac{3\gamma_0^2 \mu^4}{b^3} &+ \frac{2\gamma_0 \mu^3 \left(\pi^2 b^2 n_0^2 c_{n_0}(K) - \gamma_0 \mu^3 L^2\right)}{b^4 L^2 \lambda_0(\gamma_0)} \\ &+ \frac{\left(2\pi^2 b^2 n_0^2 c_{n_0}(K) - \gamma_0 \mu^3 L^2\right) \left(\pi^2 b^2 n_0^2 \left(c_{-n_0}(K) - 2c_{2n_0}(K)\right) + \gamma_0 \mu^3 L^2\right)}{b^4 L^4 \lambda_{2n_0}(\gamma_0)}. \end{aligned}$$

The first equation in the above system turns out to be the Poincaré normal form. It allows us to study the stability of the bifurcated periodic solution. To that aim observe that

$$\mathrm{Re}(a(\gamma)) = \left(\frac{n_0 \pi}{L}\right)^2 \varepsilon_0 \frac{(2\gamma_0 - \gamma)(\gamma - \gamma_0)}{\gamma_0^2},$$

so that $\mathrm{Re}(a(\gamma)) > 0$ for $\gamma > \gamma_0$ and negative for $\gamma < \gamma_0$ but close to $\gamma_0$. The stability of the bifurcating period orbit is fully determined by the sign of the real part of the $\beta$. However we are not able to conclude about this sign. To summarize the Hopf bifurcation at $\gamma_0$ is:

1. **supercritical** if $\mathrm{Re}\,\beta < 0$, namely the origin is stable for $\gamma < \gamma_0$ and unstable for $\gamma > \gamma_0$. Moreover when $\gamma > \gamma_0$ the system has a stable limit cycle. Here the circular limit cycle has a radius proportional to $\sqrt{\gamma - \gamma_0}$.
2. **subcritical** if $\mathrm{Re}\,\beta > 0$, namely the origin is stable for $\gamma < \gamma_0$ and unstable when $\gamma > \gamma_0$. Moreover when $\gamma < \gamma_0$ the system has an unstable limit cycle, with a radius proportional to $\sqrt{\gamma_0 - \gamma}$.

# Appendix B

# Numerical scheme

## 1 Numerical scheme for the hyperbolic Keller-Segel equation

For simplicity, we give the numerical scheme for the following one species and one dimensional model

$$\begin{cases} \partial_t u + d\,\partial_x (uv) = f(u) & \\ v(t,x) = -\partial_x P(t,x) & \text{in } (0,T]\times[-L,L] \\ (I-\chi\Delta)P(t,x) = u(t,x) & \\ \partial_x P(t,\pm L) = 0 & \text{on } [0,T]. \end{cases} \tag{B.1}$$

The numerical method used is based on finite volume method. We refer to [67, 101] for more results about this subject. Our numerical scheme reads as follows

$$\begin{aligned} &u_i^{n+1} = u_i^n - d\,\frac{\Delta t}{\Delta x}\Big(\phi(u_{i+1}^n, u_i^n) - \phi(u_i^n, u_{i-1}^n)\Big) + \Delta t\, f(u_i^n), \\ &i = 1,2,\dots,M,\ n = 0,1,2,\dots,N, \end{aligned} \tag{B.2}$$

with $\phi(u_{i+1}^n, u_i^n)$ defined as

$$\phi(u_{i+1}^n, u_i^n) = (v_{i+\frac{1}{2}}^n)^+ u_i^n - (v_{i+\frac{1}{2}}^n)^- u_{i+1}^n = \begin{cases} v_{i+\frac{1}{2}}^n u_i^n, & v_{i+\frac{1}{2}}^n \geq 0, \\ v_{i+\frac{1}{2}}^n u_{i+1}^n, & v_{i+\frac{1}{2}}^n < 0. \end{cases}$$

and

$$v_{i+\frac{1}{2}}^n = -\frac{p_{i+1}^n - p_i^n}{\Delta x},\ i = 0,1,2,\cdots,M,$$

where we define

$$P^n := (I-\chi A)^{-1}U^n, \quad n = 0,1,2,\dots,N, \quad P^n = \left(p_i^n\right)_{M\times 1} \quad U^n = \left(u_i^n\right)_{M\times 1}.$$

where $\chi$ is a constant and $A = (a_{i,j})_{M\times M}$ is the usual linear diffusion matrix with Neumann boundary condition. Therefore, since by Neumann boundary condition $p_0 = p_1$ and $p_{M+1} = p_M$, for Equation (B.2) when $i = 1, M$ we have

$$\begin{aligned} \phi(u_1^n, u_0^n) &= 0, \\ \phi(u_{M+1}^n, u_M^n) &= 0. \end{aligned}$$

which gives

$$u_1^{n+1} = u_1^n - d\,\frac{\Delta t}{\Delta x}\phi(u_2^n, u_1^n) + \Delta t\, f(u_1^n),$$
$$u_M^{n+1} = u_M^n + d\,\frac{\Delta t}{\Delta x}\phi(u_M^n, u_{M-1}^n) + \Delta t\, f(u_M^n).$$

By this boundary condition, we have the conservation of mass for Equation (B.1) when the reaction term $f \equiv 0$.

## 2 Numerical Scheme for a nonlocal advection equation

For simplicity, we give the numerical scheme for the following one species and one dimensional model with periodic boundary condition

$$\begin{cases} \partial_t u + \partial_x (u\, v) &= \varepsilon \partial_x^2 u + uh(u),\ t > 0,\ x \in \mathbb{T}, \\ v(t,x) &= -\partial_x (K \circ u(t,\cdot))(x), \\ u(0,x) &= u_0(x) \in L^1_{per}(\mathbb{T}). \end{cases}$$

The numerical method is based on finite volume scheme. We briefly illustrate our numerical scheme in this section: the approximation of the convolution term is as follows

$$(K \circ u(t,\cdot))(x) = \int_{\mathbb{T}} u(t,y)K(x-y)dy \approx \sum_j K(x-x_j)u(t,x_j)\Delta x.$$

In addition, we define

$$p_i^n := \sum_{j=1}^{M} K(x_i - x_j)u(t_n, x_j)\Delta x,$$

for $i = 1, 2, \ldots, M,\ n = 0, 1, 2, \ldots, N$. We use the numerical scheme as illustrated in [101] to deal with the nonlocal convection term and the scheme reads as follows

$$\begin{aligned} u_i^{n+1} = u_i^n &+ \varepsilon \frac{\Delta t}{\Delta x^2}\left(u_{i+1}^{n+1} - 2u_i^{n+1} + u_{i-1}^{n+1}\right) \\ &- \frac{\Delta t}{\Delta x}\left(\phi(u_{i+1}^{n,-}, u_i^{n,+}) - \phi(u_i^{n,-}, u_{i-1}^{n,+})\right) + \Delta t\, u_i^n h(u_i^n), \\ i = 1, 2, \ldots, M,&\ \ n = 0, 1, 2, \ldots, N, \end{aligned}$$

with $\phi(u_{i+1}^n, u_i^n)$ defined as

$$\phi(u_{i+1}^{n,-}, u_i^{n,+}) = (v_{i+\frac{1}{2}}^n)^+ u_i^{n,+} - (v_{i+\frac{1}{2}}^n)^- u_{i+1}^{n,-} = \begin{cases} v_{i+\frac{1}{2}}^n u_i^{n,+}, & v_{i+\frac{1}{2}}^n \geq 0, \\ v_{i+\frac{1}{2}}^n u_{i+1}^{n,-}, & v_{i+\frac{1}{2}}^n < 0. \end{cases}$$

where

$$v_{i+\frac{1}{2}}^n = -\frac{p_{i+1}^n - p_i^n}{\Delta x},\ i = 1, 2, \cdots, M-1,$$

and

$$\begin{aligned} u_i^{n,-} &= u_i^n - \frac{1}{2}\text{minmod}(u_{i+1}^n - u_i^n, u_i^n - u_{i-1}^n), \\ u_i^{n,+} &= u_i^n + \frac{1}{2}\text{minmod}(u_{i+1}^n - u_i^n, u_i^n - u_{i-1}^n), \end{aligned} \qquad i = 1, 2, \cdots, M-1,$$

where the function $\text{minmod}(a, b)$ is defined as

$$\text{minmod}(a,b) = \begin{cases} \text{sign}(a)\min\{a,b\}, & \text{sign}(a) = \text{sign}(b), \\ 0, & \text{otherwise.} \end{cases}$$

By the periodic boundary condition, let $v_{\frac{1}{2}}^n = v_{M+\frac{1}{2}}^n$ and $u_0^n = u_M^n$, $u_1^n = u_{M+1}^n$. Thus,

$$u_0^{n,\pm} = u_M^{n,\pm},\ u_1^{n,\pm} = u_{M+1}^{n,\pm},$$

the conservation law holds when the reaction term equals zero.

# Appendix C

# Invariance of the domain $\Omega$

In this section, we prove the invariance of domain $\Omega$ for the characteristic equation.
**Assumption 0.1.** *Let $\Omega \subset \mathbb{R}^2$ be an open bounded subset with $\partial\Omega$ of class $C^2$.*

Since $\Omega$ is a bounded domain of class $C^2$, there exists $U$ a neighborhood of the boundary $\partial\Omega$ such that the distance function $x \to \text{dist}(x, \partial\Omega) := \inf_{y\in\partial\Omega} \|x - y\|$ restricted to $U$ has the regularity $C^2$ (see Foote [47, Theorem 1]). Furthermore, by Foote [47, Theorem 1] and Ambrosio [2, Theorem 1 p.11], we have the following properties for $\Omega$.
**Lemma 0.2.** *Let Assumption 0.1 be satisfied. Then*

(i). *There exists a small neighborhood $U$ of $\partial\Omega$ with $U \subset \overline{\Omega}$ such that, for every $x \in U$ there is a unique projection $P(x) \in \partial\Omega$ satisfying* $\text{dist}(x, P(x)) = \text{dist}(x, \partial\Omega)$.

(ii). *The distance function $x \mapsto \delta(x) := \text{dist}(x, \partial\Omega)$ is $C^2$ on $U\backslash\partial\Omega$.*

(iii). *For any $x \in U$, $\nabla\delta(x) = -\nu(P(x))$ where $\nu(x)$ is the outward normal vector.*

We consider the following non-autonomous differential equation on $\Omega$

$$\begin{cases} x'(t) = f(t, x(t)) \quad t > 0 \\ x(0) = x_0 \in \Omega. \end{cases} \tag{C.1}$$

**Assumption 0.3.** *The vector field $f : [0, \infty) \times \overline{\Omega} \to \mathbb{R}^2$ is continuous and satisfies*

$$\nu(x) \cdot f(t, x) \leq 0, \quad \forall t > 0, \forall x \in \partial\Omega. \tag{C.2}$$

*Moreover, for any $T > 0$, there exists a constant $K = K(T)$ such that vector field $f$ satisfies*

$$|f(t, x) - f(t, y)| \leq K|x - y|, \quad \forall x, y \in \overline{\Omega}, t \in [0, T]. \tag{C.3}$$

By (C.3), we have the existence and uniqueness of the solutions of (C.1) and the solutions may eventually reach the boundary $\partial\Omega$ in finite time. We will prove that (C.2) implies that the solutions of (C.1) actually stay in $\Omega$ and can not attain boundary $\partial\Omega$ in finite time under Assumption 0.1.
**Theorem 0.4.** *Let Assumption 0.1 and 0.3 be satisfied. For any $T > 0$, let $x(t)$ be the solution of (C.1) on $[0, T]$. Then $x(t) \in \Omega$ for any $t \in [0, T]$.*

*Proof.* We prove this theorem by contradiction. Let $t^* \in (0, T]$ be the first time when $x(t)$ reaches boundary $\partial\Omega$, i.e.,

$$t^* = \inf\{0 < t \leq T : \delta(x(t)) = 0\}.$$

We can find a $\theta > 0$ such that, $x(t) \in U \cap \overline{\Omega}$ for any $t \in [t^* - \theta, t^*]$. Since $t \to x(t)$ is $C^1$, the mapping $t \mapsto \delta(x(t))$ is $C^1$ on $[t^* - \theta, t^*]$. By Lemma 0.2 (iii), we have

$$\frac{d}{dt}\delta(x(t)) = x'(t) \cdot \nabla\delta(x(t)) = -f(t, x(t)) \cdot \nu(y(t)), \tag{C.4}$$

where $\nu$ is the outward normal vector and $y(t) := P_{\partial\Omega}(x(t))$ is the unique projection of $x(t)$ onto $\partial\Omega$. By assumption (C.2), we have

$$-f(t,x(t))\cdot\nu(y(t)) = \big(f(t,y(t))-f(t,x(t))\big)\cdot\nu(y(t))-f(t,y(t))\cdot\nu(y(t)) \geq \big(f(t,y(t))-f(t,x(t))\big)\cdot\nu(y(t)).$$

Hence (C.4) becomes

$$\begin{aligned}\frac{d}{dt}\delta(x(t)) =& - f(t,x(t)) \cdot \nu(y(t)) \\ \geq& \big(f(t,y(t)) - f(t,x(t))\big) \cdot \nu(y(t)) \\ \geq& - |f(t,y(t)) - f(t,x(t))|\,|\nu(y(t))| \\ \geq& - K|y(t) - x(t)| = -K\delta(x(t)), \quad t \in [t^* - \theta, t^*],\end{aligned}$$

which yields

$$\delta(x(t)) \geq \delta(x(t^* - \theta))e^{-K(t-t^*+\theta)}, \quad \forall t \in [t^* - \theta, t^*],$$

and $\delta(x(t^* - \theta)) > 0$ implies $\delta(x(t^*)) > 0$ which contradicts our assumption $\delta(x(t^*)) = 0$. □

# Appendix D

# Proof of Theorem 2.7

**Solution integrated along the characteristics.** Let us temporarily suppose $u \in C^1([0,T]\times\Omega)$ where $\Omega$ is the two dimensional open unit disk, we can rewrite the first equation in (2.1) as

$$\begin{aligned}\partial_t u(t,x) - d\,\nabla u(t,x)\cdot\nabla P(t,x) &= u(t,x)h(u(t,x)) + d\,u(t,x)\Delta P(t,x)\\ &= u(t,x)\left(h(u(t,x)) + \frac{d}{\chi}(P(t,x)-u(t,x))\right).\end{aligned}$$

Moreover, if we differentiate the solution along the characteristic with respect to $t$ then

$$\begin{aligned}&\frac{\mathrm{d}}{\mathrm{d}t}u(t,\Pi(t,0;x))\\ &= \partial_t u(t,\Pi(t,0;x)) + \nabla u(t,\Pi(t,0;x))\cdot\partial_t\Pi(t,0;x)\\ &= \partial_t u(t,\Pi(t,0;x)) - d\,\nabla u(t,\Pi(t,0;x))\cdot\nabla P(t,\Pi(t,0;x))\\ &= u(t,\Pi(t,0;x))\left(h(u(t,\Pi(t,0;x))) + \frac{d}{\chi}\left(P(t,\Pi(t,0;x)) - u(t,\Pi(t,0;x))\right)\right).\end{aligned}$$

The solution along the characteristics can be written as

$$\begin{aligned}&u(t,\Pi(t,0;x))\\ &= u_0(x)\exp\left(\int_0^t h(u(l,\Pi(l,0;x))) + \frac{d}{\chi}\big(P(l,\Pi(l,0;x)) - u(l,\Pi(l,0;x))\big)\mathrm{d}l\right).\end{aligned}$$

Similarly, we can deduce for any $0\le s\le t$

$$\begin{aligned}&u(t,\Pi(t,s;x))\\ &= u(s,x)\exp\left(\int_s^t h(u(l,\Pi(l,s;x))) + \frac{d}{\chi}\big(P(l,\Pi(l,s;x)) - u(l,\Pi(l,s;x))\big)\mathrm{d}l\right).\end{aligned}\tag{D.1}$$

For the simplicity of notation, we let $d=\chi=1$ in our following discussion and define $w(t,x) := u(t,\Pi(t,0;x))$. We construct the following Banach fixed point problem for the pair $(w,P)$. For each $(w,P)$, we let

$$w^1(t,x) = u_0(x)\exp\Big(\int_0^t F(w(l,x)) + P(l,\Pi(l,0;x))\mathrm{d}l\Big).\tag{D.2}$$

where we set $F(u) = h(u) - u$ for any $u \geq 0$ and we define

$$\mathcal{T}\begin{pmatrix} w(t,x) \\ P(t,x) \end{pmatrix} := \begin{pmatrix} w^1(t,x) \\ (I-\Delta)^{-1} w^1(t, \Pi(0,t;\cdot))(x) \end{pmatrix} = \begin{pmatrix} w^1(t,x) \\ P^1(t,x) \end{pmatrix}, \tag{D.3}$$

where $(I-\Delta)^{-1}$ is the resolvent of the Laplacian operator with Neumann boundary condition.

We define

$$\begin{aligned} X^\tau &:= C^0\big([0,\tau], C^0(\overline{\Omega})\big), \quad Y^\tau := C^0\big([0,\tau], C^1(\overline{\Omega})\big), \\ \tilde{X}^\tau &:= \left\{ w \in C^0\big([0,\tau], C^0(\overline{\Omega})\big) \,\middle|\, w \geq 0, \sup_{t\in[0,\tau]} \|w(t,\cdot)\|_{W^{1,\infty}(\Omega)} \leq C_1 \right\}, \\ \tilde{Y}^\tau &:= \left\{ P \in C^0\big([0,\tau], C^1(\overline{\Omega})\big) \,\middle|\, \sup_{t\in[0,\tau]} \big\|P(t,\cdot)\big\|_{W^{2,\infty}(\Omega)} \leq C_2 \right\}, \end{aligned} \tag{D.4}$$

where $C_i, i = 1, 2$ are two constants to be fixed later. Recall $W^{1,\infty}(\Omega)$ is equivalent to Lipschitz continuous function on $\Omega$ [45, Chapter 5. Theorem 4. p.279]. We also set

$$Z^\tau := X^\tau \times Y^\tau, \quad \tilde{Z}^\tau := \tilde{X}^\tau \times \tilde{Y}^\tau.$$

Notice $\tilde{Z}^\tau$ is a complete metric space for the distance induced by the norm $(\|\cdot\|_{X^\tau}, \|\cdot\|_{Y^\tau})$. For simplicity, we denote $\|\cdot\|_{C^{\alpha,k}} := \|\cdot\|_{C^{\alpha,k}(\Omega)}$ and $\|\cdot\|_{W^{k,\infty}} := \|\cdot\|_{W^{k,\infty}(\Omega)}$ for $\alpha \in (0,1], k \in \mathbb{N}_+$.

**Theorem 0.1** (Existence and uniqueness of solutions)**.** *For any initial value $u_0 \in W^{1,\infty}(\Omega)$ and $u_0 \geq 0$, for any $C_1$, $C_2$ large enough in (D.4), there exists $\tau = \tau(C_1, C_2) > 0$ such that the mapping $\mathcal{T}$ has a unique fixed point in $\tilde{Z}^\tau$.*

*Proof.* For any positive initial value $u_0 \in W^{1,\infty}(\Omega)$ and $r > 0$, we fix $C_1$ to be a constant such that $4\|u_0\|_{W^{1,\infty}} \leq C_1$ and $C_2$ is a constant defined in (D.15) later in the proof.

We also denote

$$\begin{pmatrix} w^0 \\ P^0 \end{pmatrix} = \begin{pmatrix} u_0 \\ (I-\Delta)^{-1}_{\mathcal{N}} u_0 \end{pmatrix}$$

and let $\overline{B_{\tilde{Z}^\tau}}\left(\begin{pmatrix} w^0 \\ P^0 \end{pmatrix}, r\right)$ be the closed ball centered at $\begin{pmatrix} w^0 \\ P^0 \end{pmatrix}$ with radius $r$ in $\tilde{Z}^\tau = \tilde{X}^\tau \times \tilde{Y}^\tau$ with usual product norm

$$\left\| \begin{pmatrix} w \\ P \end{pmatrix} \right\|_{\tilde{Z}^\tau} := \|w\|_{X^\tau} + \|P\|_{Y^\tau}$$

and we set

$$\kappa := \left\| \begin{pmatrix} w^0 \\ P^0 \end{pmatrix} \right\|_{\tilde{Z}^\tau} + r.$$

Suppose $\begin{pmatrix} w \\ P \end{pmatrix} \in \overline{B_{Z^\tau}}\left(\begin{pmatrix} w^0 \\ P^0 \end{pmatrix}, r\right)$, we need to prove that there exits a $\tau$ small enough such that the following properties hold

(a). For any $t \in [0,\tau]$, $(w^1(t,\cdot), P^1(t,\cdot))$ in (D.2) and (D.3) belong to $W^{1,\infty}(\Omega)\times W^{2,\infty}(\Omega)$ and their norms satisfy

$$\sup_{t\in[0,\tau]} \|w^1(t,\cdot)\|_{W^{1,\infty}} \le C_1, \tag{D.5}$$

$$\sup_{t\in[0,\tau]} \|P^1(t,\cdot)\|_{W^{2,\infty}} \le C_2. \tag{D.6}$$

(b). Moreover, we have

$$\|w^1 - w^0\|_{X^\tau} \le \frac{r}{2}, \tag{D.7}$$

$$\|P^1 - P^0\|_{Y^\tau} \le \frac{r}{2}. \tag{D.8}$$

Moreover, we plan to show that the mapping is a contraction: there exists a $\theta \in (0,1)$ such that for any $\begin{pmatrix} \tilde{w} \\ \tilde{P} \end{pmatrix}, \begin{pmatrix} w \\ P \end{pmatrix} \in \overline{B_{\tilde{Z}^\tau}}\left(\begin{pmatrix} w^0 \\ P^0 \end{pmatrix}, r\right)$ we have

$$\left\|\mathcal{T}\begin{pmatrix} \tilde{w} \\ \tilde{P} \end{pmatrix} - \mathcal{T}\begin{pmatrix} w \\ P \end{pmatrix}\right\|_{\tilde{Z}^\tau} \le \theta \left\|\begin{pmatrix} \tilde{w} \\ \tilde{P} \end{pmatrix} - \begin{pmatrix} w \\ P \end{pmatrix}\right\|_{\tilde{Z}^\tau}. \tag{D.9}$$

**Step 1.** We show that there exists a $\tau$ small enough such that for any $(w,P) \in \tilde{X}^\tau \times \tilde{Y}^\tau$ then

$$\sup_{t\in[0,\tau]} \|w^1(t,\cdot)\|_{W^{1,\infty}} \le C_1,$$

where $w^1$ is defined in (D.2).

Indeed, since $\nabla P(t,\cdot)$ is Lipschitz continuous, then $x \to \Pi(t,0,x)$ is also Lipschitz continuous. Since $\Pi(t,0;\cdot)$ maps $\Omega$ into $\Omega$, we have

$$\begin{aligned}\|P(t,\Pi(t,0;\cdot))\|_{W^{1,\infty}} &\le \|P(t,\Pi(t,0;\cdot))\|_{L^\infty} + \|\nabla P(t,\cdot)\|_{L^\infty}\|\Pi(t,0;\cdot)\|_{W^{1,\infty}} \\ &\le \|P(t,\cdot)\|_{W^{1,\infty}} \max\{\|\Pi(t,0;\cdot)\|_{W^{1,\infty}}, 1\}.\end{aligned}$$

For any $t \in [0,\tau]$, we let $\tilde{F} := \sup_{u\in[0,\kappa]}\{|F(u)| + |F'(u)|\}$. By the definition of $w^1$ in (D.2), we have

$$\begin{aligned}&\|w^1(t,\cdot)\|_{W^{1,\infty}} \\ &\quad\le \|u_0\|_{W^{1,\infty}} \left\|\exp\left\{\int_0^t F(w(l,\cdot)) + P(l,\Pi(l,0,\cdot))\mathrm{d}l\right\}\right\|_{W^{1,\infty}} \\ &\quad\le \|u_0\|_{W^{1,\infty}} \left\|\exp\left\{\int_0^t F(w(l,\cdot)) + P(l,\Pi(l,0,\cdot))\mathrm{d}l\right\}\right\|_{L^\infty}\end{aligned}$$

$$
\begin{aligned}
&\times \left(1+\int_0^t \|F(w(l,\cdot))\|_{W^{1,\infty}} + \|P(l,\Pi(l,0,\cdot))\|_{W^{1,\infty}}\mathrm{d}l\right)\\
&\leq \|u_0\|_{W^{1,\infty}} \exp\left\{\int_0^t \|F(w(l,\cdot))\|_{L^\infty} + \|P(l,\Pi(l,0,\cdot))\|_{L^\infty}\mathrm{d}l\right\}\\
&\quad\times \left(1+\tau\tilde{F}\max\{\sup_{l\in[0,\tau]}\|w(l,\cdot)\|_{W^{1,\infty}},1\} + \tau\|P(l,\cdot)\|_{W^{1,\infty}}\max\{\|\Pi(l,0,\cdot)\|_{W^{1,\infty}},1\}\right)\\
&\leq \|u_0\|_{W^{1,\infty}} e^{\tau\left(\tilde{F}+\kappa\right)}\left(1+\tau\tilde{F}\max\{C_1,1\}+\tau\kappa\max\{\|\Pi(l,0,\cdot)\|_{W^{1,\infty}},1\}\right). \qquad \text{(D.10)}
\end{aligned}
$$

Next we estimate $\max\left\{\sup_{l\in[0,\tau]}\|\Pi(l,0,\cdot)\|_{W^{1,\infty}},1\right\}$. We have for any $t,s\in[0,\tau]$

$$
\Pi(t,s;x) = x - \int_s^t \nabla P(l,\Pi(l,s;x))\mathrm{d}l.
$$

Since $\Omega$ is the unit open disk, $\|x\|_{W^{1,\infty}(\Omega)} = 2$. We can obtain the following estimate

$$
\begin{aligned}
\|\Pi(t,s;\cdot)\|_{W^{1,\infty}} &\leq 2 + \int_s^t \|\nabla P(l,\Pi(l,s;\cdot))\|_{W^{1,\infty}}\mathrm{d}l\\
&\leq 2 + \sup_{l\in[s,t]}\|\nabla P(l,\cdot)\|_{W^{1,\infty}}\int_s^t \max\left\{\|\Pi(l,s;\cdot)\|_{W^{1,\infty}},1\right\}\mathrm{d}l\\
&\leq 2 + C_2\int_s^t \max\{\|\Pi(l,s;\cdot)\|_{W^{1,\infty}},1\}\mathrm{d}l.
\end{aligned}
$$

Thanks to Grönwall's inequality, we have

$$
\sup_{t,s\in[0,\tau]}\|\Pi(t,s;\cdot)\|_{W^{1,\infty}} \leq 2e^{\tau C_2}. \qquad \text{(D.11)}
$$

Substituting the (D.11) into (D.10) yields

$$
\|w^1(t,\cdot)\|_{W^{1,\infty}} \leq \|u_0\|_{W^{1,\infty}} e^{\tau\left(\tilde{F}+\kappa\right)}\left(1+\tau\tilde{F}\max\{C_1,1\}+2\tau\kappa e^{\tau C_2}\right).
$$

Since $C_1 \geq 4\|u_0\|_{W^{1,\infty}}$, we can choose $\tau \leq \min\left\{\frac{\ln 2}{\tilde{F}+\kappa}, \frac{1}{\tilde{F}\max\{C_1,1\}+2\kappa e^{C_2}}, 1\right\}$ and we obtain

$$
\sup_{t\in[0,\tau]}\|w^1(t,\cdot)\|_{W^{1,\infty}} \leq C_1. \qquad \text{(D.12)}
$$

Thus, Equation (D.5) holds.

Let us now check that $w^1$ satisfies (D.7). Let $\chi[u] := ue^u$, we remark that $|e^u - 1| \leq ue^u = \chi[u]$ for all $u \geq 0$. We have

$$
\begin{aligned}
|w^1(t,x) - u_0(x)| &\leq |u_0(x)|\left|\exp\left\{\int_0^t F(w(l,x)) + P(l,\Pi(l,0,x))\mathrm{d}l\right\} - 1\right|\\
&\leq \|u_0\|_{C^0}\chi\left[\int_0^t \|F(w(l,\cdot))\|_{C^0} + \|P(l,\Pi(l,0,\cdot))\|_{C^0}\mathrm{d}l\right]\\
&\leq \|u_0\|_{C^0}\chi\left[\tau\tilde{F} + \tau\sup_{l\in[0,\tau]}\|P(l,\cdot)\|_{C^0}\right]
\end{aligned}
$$

$$\leq \|u_0\|_{C^0}\chi\left[\tau\tilde{F}+\tau\kappa\right], \tag{D.13}$$

where $\tilde{F}=\sup_{u\in[0,\kappa]}\{|F(u)|+|F'(u)|\}$. From (D.13) we have

$$\sup_{t\in[0,\tau]}\|w^1(t,\cdot)-u_0(\cdot)\|_{C^0}\leq\|u_0\|_{C^0}\chi\left[\tau\tilde{F}+\tau\kappa\right]. \tag{D.14}$$

Since $\lim_{u\to 0}\chi[u]=0$, it suffice to take $\tau$ small enough to ensure (D.7).

**Step 2.** Next we verify (D.6) and (D.8) for $P^1$ where $P^1$ is defined as the second component of (D.3). We show that there exists $\tau$ small enough such that for any $(w,P)\in\tilde{X}^\tau\times\tilde{Y}^\tau$

$$\sup_{t\in[0,\tau]}\|P^1(t,\cdot)\|_{W^{2,\infty}}\leq C_2.$$

Thanks to the Schauder estimate [50, Theorem 6.30], there exists a constant $C$ depending only on $\Omega$ such that

$$\|P^1(t,\cdot)\|_{C^{2,\frac{1}{2}}}\leq C\|w^1(t,\Pi(0,t;\cdot))\|_{C^{0,\frac{1}{2}}}.$$

Recalling $\sup_{t\in[0,\tau]}\|\Pi(0,t;\cdot)\|_{W^{1,\infty}}\leq 2e^{\tau C_2}$ as a consequence of (D.11), we have

$$\begin{aligned}\|P^1(t,\cdot)\|_{W^{2,\infty}}&\leq\|P^1(t,\cdot)\|_{C^{2,\frac{1}{2}}}\\&\leq C\|w^1(t,\Pi(0,t;\cdot))\|_{C^{0,\frac{1}{2}}}\\&\leq C\|w^1(t,\Pi(0,t;\cdot))\|_{W^{1,\infty}}\\&\leq C\|w^1(t,\cdot)\|_{W^{1,\infty}}\max\{\|\Pi(0,t;\cdot)\|_{W^{1,\infty}},1\}\\&\leq 2\,C\,C_1e^{\tau C_2}.\end{aligned}$$

We can now define

$$C_2=4\,C\,C_1, \tag{D.15}$$

which only depends on $\Omega$ and $\|u_0\|_{W^{1,\infty}}$. Finally, we let $\tau\leq(\ln 2)/C_2$ and we have

$$\|P^1(t,\cdot)\|_{W^{2,\infty}}\leq 4\,C\,C_1=C_2.$$

In particular, we have shown (D.6).

Next we prove (D.8). Since $\Omega$ is a two-dimensional unit disk, using Morrey's inequality [45, Chapter 5. Theorem 6], we have

$$\|P^1(t,\cdot)-P_0(\cdot)\|_{C^{1,\frac{1}{2}}}\leq C\|P^1(t,\cdot)-P_0(\cdot)\|_{W^{2,4}}, \tag{D.16}$$

where $C$ is a constant depending only on $\Omega$. For the sake of simplicity, we use the same notation $C$ for a universal constant depending only on $\Omega$ in the following estimates. Moreover, by the classical elliptic estimates (Agmon–Douglis–Nirenberg [1]) we have

$$\|P^1(t,\cdot)-P_0(\cdot)\|_{W^{2,4}}\leq C\|w^1(t,\Pi(0,t;\cdot))-u_0(\cdot)\|_{L^4}. \tag{D.17}$$

Equations (D.16) and (D.17) imply that

$$\|P^1(t,\cdot)-P_0(\cdot)\|_{C^1}\leq\|P^1(t,\cdot)-P_0(\cdot)\|_{C^{1,\frac{1}{2}}}$$

$$
\begin{aligned}
&\leq C\|w^1(t,\Pi(0,t;\cdot))-u_0(\cdot)\|_{L^4}\\
&\leq C\|w^1(t,\Pi(0,t;\cdot))-u_0(\cdot)\|_{C^0}\\
&\leq C\|w^1(t,\Pi(0,t;\cdot))-w^1(t,\cdot)\|_{C^0}+C\|w^1(t,\cdot)-u_0(\cdot)\|_{C^0}\\
&\leq C\|w^1\|_{W^{1,\infty}}\|\Pi(0,t;\cdot)-\cdot\|_{C^0}+C\|w^1(t,\cdot)-u_0(\cdot)\|_{C^0}\\
&\leq C\,C_1\|\Pi(0,t;\cdot)-\cdot\|_{C^0}+C\|w^1(t,\cdot)-u_0(\cdot)\|_{C^0}\\
&\leq C\,C_1\,\tau\sup_{t\in[0,\tau]}\|\nabla P(t,\cdot)\|_{C^0}+C\|w^1(t,\cdot)-u_0(\cdot)\|_{C^0}\\
&\leq C\,C_1\,\tau\,\kappa+C\|w^1(t,\cdot)-u_0(\cdot)\|_{C^0}\\
&\leq C\,C_1\,\tau\,\kappa+C\|u_0\|_{C^0}\chi\left[\tau\tilde{F}+\tau\kappa\right],
\end{aligned}
$$

where we have used (D.14) for the last inequality . We can conclude

$$
\sup_{t\in[0,\tau]}\|P^1(t,\cdot)-P_0(\cdot)\|_{C^1}\to 0,\quad \tau\to 0.
$$

Thus, it suffice to take $\tau$ small enough to ensure the neighborhood condition (D.8).

**Step 3. Contraction mapping** In order to verify (D.9), we let $\begin{pmatrix}\tilde{w}\\ \tilde{P}\end{pmatrix},\begin{pmatrix}w\\ P\end{pmatrix}\in \overline{B_{\tilde{Z}^\tau}}\left(\begin{pmatrix}w^0\\ P^0\end{pmatrix},r\right)$. We observe that

$$
\begin{aligned}
\left|\tilde{w}^1(t,x)-w^1(t,x)\right| = \Big|&u_0(x)\exp\Big(\int_0^t F(w(l,x))+P(l,\Pi(l,0;x))\mathrm{d}l\Big)\\
&-u_0(x)\exp\Big(\int_0^t F(\tilde{w}(l,x))+\tilde{P}(l,\tilde{\Pi}(l,0;x))\mathrm{d}l\Big)\Big|.
\end{aligned}
$$

Due to the classical inequality $|e^x-e^y|\leq e^{x+y}|x-y|$ which holds for any $x,y\in\mathbb{R}$, we deduce

$$
\begin{aligned}
&\left|\tilde{w}^1(t,x)-w^1(t,x)\right|\\
&\quad\leq \|u_0\|_{C^0}e^{2\tau(\tilde{F}+\kappa)}\Big[\int_0^t\|F(\tilde{w}(l,\cdot))-F(w(l,\cdot))\|_{C^0}\mathrm{d}l\\
&\qquad+\int_0^t\|\tilde{P}(l,\tilde{\Pi}(l,0;\cdot))-P(l,\Pi(l,0;\cdot))\|_{C^0}\mathrm{d}l\Big]\\
&\quad\leq \|u_0\|_{C^0}e^{2\tau(\tilde{F}+\kappa)}\Big[\tau\tilde{F}\sup_{l\in[0,\tau]}\|\tilde{w}(l,\cdot)-w(l,\cdot)\|_{C^0}\\
&\qquad+\tau\sup_{l\in[0,\tau]}\|\tilde{P}(l,\tilde{\Pi}(l,0;\cdot))-P(l,\tilde{\Pi}(l,0;\cdot))\|_{C^0}\\
&\qquad+\tau\sup_{l\in[0,\tau]}\|P(l,\tilde{\Pi}(l,0;\cdot))-P(l,\Pi(l,0;\cdot))\|_{C^0}\Big]\\
&\quad\leq \|u_0\|_{C^0}e^{2\tau(\tilde{F}+\kappa)}\Big[\tau\tilde{F}\sup_{l\in[0,\tau]}\|\tilde{w}(l,\cdot)-w(l,\cdot)\|_{C^0}+\tau\sup_{l\in[0,\tau]}\|\tilde{P}(l,\cdot)-P(l,\cdot)\|_{C^0}
\end{aligned}
$$

$$
\begin{aligned}
&+\tau \sup_{l\in[0,\tau]} \|P(l,\cdot)\|_{W^{1,\infty}} \sup_{l\in[0,\tau]} \|\tilde{\Pi}(l,0;\cdot)-\Pi(l,0;\cdot)\|_{C^0}\Big] \\
&\le \tau\|u_0\|_{C^0} e^{2\tau(\tilde{F}+\kappa)}\Big[\tilde{F}\|\tilde{w}-w\|_{X^\tau}+\|\tilde{P}-P\|_{Y^\tau} \\
&\quad + C_2 \sup_{l\in[0,\tau]} \|\tilde{\Pi}(l,0;\cdot)-\Pi(l,0;\cdot)\|_{C^0}\Big]. \qquad \text{(D.18)}
\end{aligned}
$$

To estimate $\sup_{l\in[0,\tau]} \|\tilde{\Pi}(l,0;\cdot)-\Pi(l,0;\cdot)\|_{C^0}$ in (D.18), we claim that

$$
\sup_{t,s\in[0,\tau]} \|\tilde{\Pi}(t,s;\cdot)-\Pi(t,s;\cdot)\|_{C^0} \le \tau e^{\tau C_2} \sup_{t\in[0,\tau]} \|\tilde{P}(l,\cdot)-P(l,\cdot)\|_{C^1}. \qquad \text{(D.19)}
$$

Indeed, we can obtain that

$$
\begin{aligned}
\Big|\tilde{\Pi}(t,s;x)-\Pi(t,s;x)\Big| &= \left|\int_s^t \nabla\tilde{P}(l,\tilde{\Pi}(l,s;x))-\nabla P(l,\Pi(l,s;x))\mathrm{d}l\right| \\
&\le \int_s^t \|\nabla\tilde{P}(l,\tilde{\Pi}(l,s;\cdot))-\nabla P(l,\tilde{\Pi}(l,s;\cdot))\|_{C^0}\mathrm{d}l \\
&\quad + \int_s^t \|\nabla P(l,\tilde{\Pi}(l,s;\cdot))-\nabla P(l,\Pi(l,s;\cdot))\|_{C^0}\mathrm{d}l \\
&\le \tau \sup_{l\in[0,\tau]} \|\nabla\tilde{P}(l,\tilde{\Pi}(l,s;\cdot))-\nabla P(l,\tilde{\Pi}(l,s;\cdot))\|_{C^0} \\
&\quad + \sup_{l\in[0,\tau]} \|\nabla P(l,\cdot)\|_{W^{1,\infty}} \int_s^t \|\tilde{\Pi}(l,s;\cdot)-\Pi(l,s;\cdot)\|_{C^0}\mathrm{d}l.
\end{aligned}
$$

This leads to

$$
\begin{aligned}
\sup_{t,s\in[0,\tau]} \|\tilde{\Pi}(t,s;\cdot)-\Pi(t,s;\cdot)\|_{C^0} &\le \tau \sup_{l\in[0,\tau]} \|\tilde{P}(l,\cdot)-P(l,\cdot)\|_{C^1} \\
&\quad + C_2 \int_s^t \|\tilde{\Pi}(l,s;\cdot)-\Pi(l,s;\cdot)\|_{C^0}\mathrm{d}l.
\end{aligned}
$$

Again due to Grönwall's inequality, we conclude that (D.19) holds.

Inserting (D.19) into (D.18) we have

$$
\begin{aligned}
&\sup_{t\in[0,\tau]} \left\|\tilde{w}^1(t,\cdot)-w^1(t,\cdot)\right\|_{C^0} \\
&\quad \le \|u_0\|_{C^0} e^{2\tau(\tilde{F}+\kappa)}\Big[\tau\tilde{F}\|\tilde{w}-w\|_{X^\tau}+\tau\|\tilde{P}-P\|_{Y^\tau}+\tau^2 C_2\, e^{\tau C_2}\|\tilde{P}-P\|_{Y^\tau}\Big] \\
&\quad \le \tau\|u_0\|_{C^0} e^{2\tau(\tilde{F}+\kappa)}\Big[\tilde{F}\|\tilde{w}-w\|_{X^\tau}+\big(1+\tau C_2\, e^{\tau C_2}\big)\|\tilde{P}-P\|_{Y^\tau}\Big] \\
&\quad \le L_1(\tau)\Big[\|\tilde{w}-w\|_{X^\tau}+\|\tilde{P}-P\|_{Y^\tau}\Big], \qquad \text{(D.20)}
\end{aligned}
$$

where we set

$$
L_1(\tau) := \tau\|u_0\|_{C^0} e^{2\tau(\tilde{F}+\kappa)}\Big(\tilde{F}+\big(1+\tau C_2\, e^{\tau C_2}\big)\Big)
$$

and $L_1(\tau)\to 0$ as $\tau\to 0$.

Next we prove the contraction property for $\|\tilde{P}^1 - P^1\|_{Y^\tau}$. As before, applying the same argument of Morrey's inequality (D.16) and classical elliptic estimates (D.17), we can deduce

$$\begin{aligned}
\|\tilde{P}^1(t,\cdot) - P^1(t,\cdot)\|_{C^1} &\le C\|\tilde{w}^1(t,\tilde{\Pi}(0,t;\cdot)) - w^1(t,\Pi(0,t;\cdot))\|_{L^4} \\
&\le C\|\tilde{w}^1(t,\tilde{\Pi}(0,t;\cdot)) - w^1(t,\Pi(0,t;\cdot))\|_{C^0} \\
&\le C\|\tilde{w}^1(t,\tilde{\Pi}(0,t;\cdot)) - w^1(t,\tilde{\Pi}(0,t;\cdot))\|_{C^0} \\
&\quad + C\|w^1(t,\tilde{\Pi}(0,t;\cdot)) - w^1(t,\Pi(0,t;\cdot))\|_{C^0} \\
&\le C\|\tilde{w}^1(t,\cdot) - w^1(t,\cdot)\|_{C^0} + C\|w^1\|_{W^{1,\infty}}\|\tilde{\Pi}(0,t;\cdot) - \Pi(0,t;\cdot)\|_{C^0} \\
&\le C\|\tilde{w}^1(t,\cdot) - w^1(t,\cdot)\|_{C^0} + C\,C_1\|\tilde{\Pi}(0,t;\cdot) - \Pi(0,t;\cdot)\|_{C^0} \\
&\le C\|\tilde{w}^1(t,\cdot) - w^1(t,\cdot)\|_{C^0} + C\,C_1\,\tau\,e^{\tau C_2}\sup_{t\in[0,\tau]}\|\tilde{P}(t,\cdot) - P(t,\cdot)\|_{C^1},
\end{aligned}$$

where we used (D.19) in the last inequality and $C$ is a constant depending only on $\Omega$. Defining $L_2(\tau) := C\,C_1\,\tau\,e^{\tau C_2}$ and together with (D.20) we obtain

$$\sup_{t\in[0,\tau]}\|\tilde{P}^1(t,\cdot) - P^1(t,\cdot)\|_{C^1} \le C\,L_1(\tau)\Big[\|\tilde{w} - w\|_{X^\tau} + \|\tilde{P} - P\|_{Y^\tau}\Big] + L_2(\tau)\|\tilde{P} - P\|_{Y^\tau}. \tag{D.21}$$

Combing with (D.20) and (D.21) we deduce

$$\|\tilde{w}^1 - w^1\|_{X^\tau} + \|\tilde{P}^1 - P^1\|_{Y^\tau} \le \big(C\,L_1(\tau) + L_2(\tau)\big)\Big[\|\tilde{w} - w\|_{X^\tau} + \|\tilde{P} - P\|_{Y^\tau}\Big], \tag{D.22}$$

where $L_i(\tau) \to 0$, $i = 1, 2$ as $\tau \to 0$. If $\tau$ is small enough, this implies (D.9) for some $\theta \in (0,1)$. Since $\tilde{Z}^\tau$ is complete metric space for the distance induced by the norm $(\|\cdot\|_{X^\tau}, \|\cdot\|_{Y^\tau})$ in $Z_\tau$, the result follows by the classical Banach fixed point theorem. □

# Appendix E

# Parameter fitting

From the work in [89], MCF-7 and MCF-7/Doxo cells are cultured at $10^5$ initial cell number separately in $60 \times 15$ mm cell dish with or without doxorubicine. We use the cell proliferation data followed every 12 hours during six days to fit the parameters of the following ordinary differential equation

$$\begin{cases} \dfrac{du_i}{dt} = u_i(b_i - a_{ii}u_i) - \delta_i u_i \quad i = 1, 2. \\ u_i(0) = u_{i,0}. \end{cases} \tag{E.1}$$

Here we use $u_1$ to represent the MCF-7 (sensitive to drug) and $u_2$ to represent the MCF-7/Doxo (resistant to drug) and $b_i > 0$ is the growth rate $\delta_i$ is the extra mortality rate caused by drug (doxorubicine) treatment and $a_{ii} > 0$ is a coefficient which controls the number of saturation.

In the work [98] cell proliferation kinetics for MCF-7 is studied over 11 days in 150 $cm^2$ flask. Following an inoculation of $3 \times 10^5$ cells at day 0, a maximum cell density of 8 to $9 \times 10^7$ cells/flask was reached at day 11. Therefore, we assume the saturation number for each species in $60 \times 15$ mm (surface of $21.5\, cm^2$) dish satisfies

$$\frac{b_i}{a_{ii}} \approx 9 \times 10^7 \times \frac{21.5\, cm^2}{150\, cm^2} = 1.29 \times 10^7, \quad i = 1, 2.$$

By fixing the saturation number, we first estimate the growth rate $b_i$ of each species under zero drug concentration, namely $\delta_i = 0$. We divide the cell number by $u_{i,0} = 10^5$ (the initial cell number) and rescale the parameters as follows

$$\tilde{u}_i = \frac{u_i}{10^5}, \quad \tilde{a}_i = a_{ii} \times 10^5, \quad \tilde{b}_i = b_i. \tag{E.2}$$

As seen in Figure E.1, without treatment, MCF-7 and MCF-7/Doxo displayed very similar growth rates, 0.6420 and 0.6359 per day, respectively.

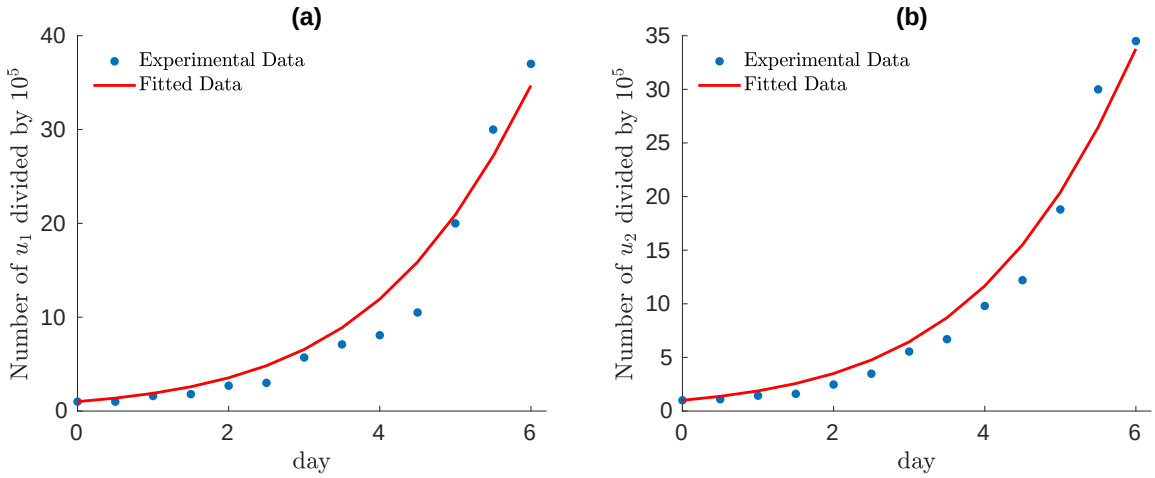


Figure E.1: *Fitting for the parameters (under rescaling (E.2)) in model (E.1). We plot the experimental data (dots in (a)) of MCF-7 (sensitive to drug) and (dots in (b)) MCF-7/Doxo (resistant to drug) with no drug concentration over 6 days. We obtain an estimation of the growth rates* $b_1 = 0.6420, b_2 = 0.6359$ *and* $a_{11} = 0.0050, a_{22} = 0.0049$.

By fixing the parameters

$$b_1 = 0.6420,\ a_{11} = 0.0050, \quad b_2 = 0.6359,\ a_{22} = 0.0049, \tag{E.3}$$

we consider different scenarios with the drug concentration varies from $0.1\,\mu M$ to $10\,\mu M$ (see Figure E.2) and we estimate the extra mortality rate $\delta_i$ for each population due to doxorubicine (see Table E.1).

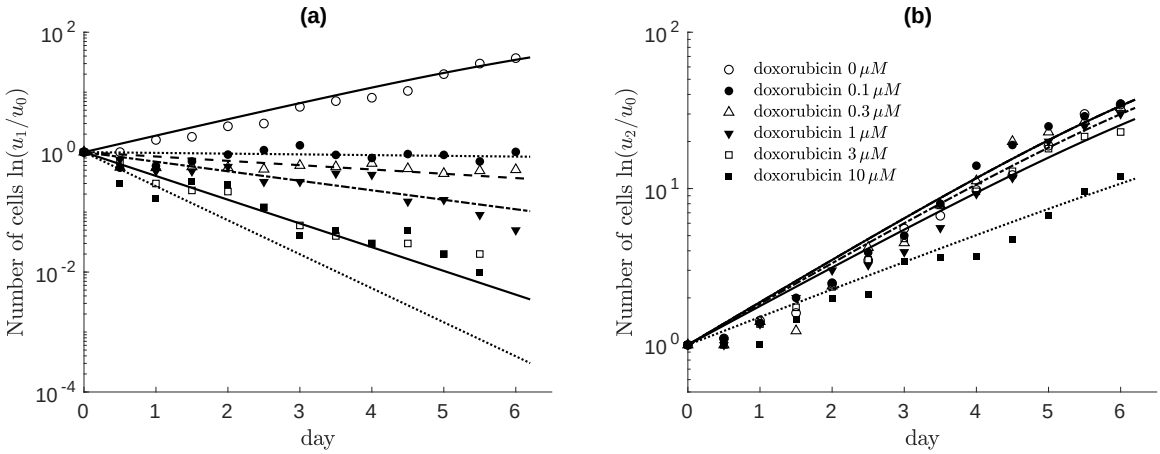


Figure E.2: *Fitting for the growth curves of MCF-7 (a) and MCF-7/Doxo (b) under different drug concentrations in model (E.1) over 6 days. Cells were grown in the absence or presence of doxorubicine (0.1 to 10 $\mu M$, corresponding symbols given in the legend in (b)) and counted every 12 hours in a Malassez chamber. Cell counts are expressed as the logarithm of the cell numbers ($u_i$) divided by the cell number at day 0 ($u_{i,0}$). We fix the growth rate $b_i$ and $a_{ii}$, $i = 1, 2$ as in (E.3).*

| **Drug concentration** ($\mu M$) | 0 | 0.1 | 0.3 | 1 | 3 | 10 |
|---|---|---|---|---|---|---|
| **Extra mortality** $\delta_1$ ($\text{day}^{-1}$) | 0 | 0.6619 | 0.8109 | 1.0118 | 1.5585 | 1.9545 |
| **Extra mortality** $\delta_2$ ($\text{day}^{-1}$) | 0 | 0 | 0 | 0.0246 | 0.0569 | 0.2192 |

Table E.1: *List of the estimation of extra mortality rate $\delta_1$ for the sensitive cell and $\delta_2$ for the resistant cell under different concentrations of doxorubicine.*

# Bibliography


[1] S. Agmon, A. Douglis and L. Nirenberg, Estimates near the boundary for solutions of elliptic partial differential equations satisfying general boundary value conditions I, *Comm. Pure Appl. Math.* **12** (1959), pp. 623–727.

[2] L. Ambrosio, Geometric evolution problems, distance function and viscosity solutions, *Calc. Var. Partial Differential Equations* Springer, Berlin, Heidelberg, (2000), 5-93.

[3] N. J. Armstrong, K. J., Painter and J. A. Sherratt, A continuum approach to modelling cell-cell adhesion, *J. Theoret. Biol.,* **243** (2006), 98-113.

[4] D. G. Aronson, *Density-dependent interaction-diffusion systems.* In Dynamics and Modelling of Reactive Systems (Proc. Adv. Sem., Math. Res. Center, Univ. Wisconsin, Madison, Wis., 1979), pp. 161-176, Publ. Math. Res. Center Univ. Wisconsin, 44, Academic Press, New York-London, 1980.

[5] C. Atkinson, G. E. H. Reuter and C. J. Ridler-Rowe, Traveling wave solution for some nonlinear diffu- sion equations. *SIAM J. Math. Anal.* **12** (1981), no. 6, 880-892.

[6] P. C. Bailey, R. M. Lee, M. I. Vitolo, S. J. Pratt, E. Ory, K. Chakrabarti, C. J. Lee, K. N. Thompson and S. S. Martin, Single-Cell Tracking of Breast Cancer Cells Enables Prediction of Sphere Formation from Early Cell Divisions, *iScience*, **8**, (2018) 29-39.

[7] J. Bedrossian, N. Rodriguez and A. L. Bertozzi, Local and global well-posedness for aggregation equations and Patlak-Keller-Segel models with degenerate diffusion, *Nonlinearity,* **24** (2011), 1683-1714.

[8] N. Bellomo, A. Bellouquid, J. Nieto and J. Soler, On the asymptotic theory from microscopic to macroscopic growing tissue models: An overview with perspectives, *Math. Models Methods Appl. Sci.*, **22(01)** (2012), 1130001.

[9] A. J. Bernoff and C. M. Topaz, A Primer of Swarm Equilibria, *SIAM J. Appl. Dyn. Syst.,* **10** (2011), 212-250.

[10] A. J. Bernoff, and C. M. Topaz, Nonlocal aggregation models: A primer of swarm equilibria. *SIAM Rev.*, **55(4)** (2013), 709-747.

[11] A. L. Bertozzi and D. Slepcev, Existence and uniqueness of solutions to an aggregation equation with degenerate diffusion, *Comm. Pur. Appl. Anal.,* **9** (2010), 1617-1637.

[12] A. L. Bertozzi, T. Laurent and J. Rosado, $L^p$ theory for the multidimensional aggregation equation, *Comm. Pur. Appl. Math.,* **64** (2011), 45-83.

[13] A. L. Bertozzi, J. B. Garnett and T. Laurent, Characterization of radially symmetric finite time blowup in multidimensional aggregation equations, *SIAM J. Math. Anal.,* **44** (2012), 651-681.

[14] M. Berstch, D. Hilhorst, H. Izuhara and M. Mimura, A nonlinear parabolic–hyperbolic system for contact inhibition of cell-growth, *Differ. Equations Appl.,* **4(1)** (2012), 137-157.

[15] M. Bertsch, D. Hilhorst, H. Izuhara, M. Mimura and T. Wakasa, Travelling wave solutions of a parabolic-hyperbolic system for contact inhibition of cell-growth, *Eur. J. Appl. Math.*, **26(03)** (2015), 297-323.

[16] P. Billingsley, *Convergence of Probability Measures*, Wiley, 2nd ed., 1999.

[17] M. Bodnar and J. J. L. Velazquez, An integro-differential equation arising as a limit of individual cell-based models, *J. Differential Equations*, **222** (2006), 341-380.

[18] M. Burger and M. Di Francesco, Large time behaviour of nonlocal aggregation models with nonlinear diffusion,*Netw. Heterog. Media,* **3** (2008), 749-785.

[19] M. Burger, R. Fetecau and Y. Huang, Stationary states and asymptotic behavior of aggregation models with nonlinear local repulsion, *SIAM J. Appl. Dyn. Syst.*, **13(1)** (2014), 397-424.

[20] H. Byrne and D. Drasdo, Individual-based and continuum models of growing cell populations: a comparison. *J. Math. Biol.* **58(4-5)** (2009), 657-687

[21] V. Calvez and Y. Dolak-Struß, Asymptotic behavior of a two-dimensional Keller-Segel model with and without density control, *In Mathematical Modeling of Biological Systems,* **Volume II** (2008) (pp. 323-337). Birkhäuser Boston.

[22] V. Calvez, L. Corrias and M.A. Ebde, Blow-up, concentration phenomenon and global existence for the Keller-Segel model in high dimension, *Comm. Partial Differential Equations*, **37(4)** (2012), 561-584.

[23] R. S. Cantrell, C. Cosner, and Y. Lou, Approximating the ideal free distribution via reaction-diffusion-advection equations. *J. Differential Equations*, **245(12)** (2008), 3687-3703.

[24] V. Capasso, and D. Morale, Asymptotic behavior of a system of stochastic particles subject to nonlocal interactions. *Stochastic Anal. Appl.*, **27(3)** (2009), 574-603.

[25] J. A. Carrillo, Y. P. Choi and S. P. Perez, A review on attractive-repulsive hydrodynamics for consensus in collective behavior. In Active Particles, **Volume 1** (2017) pp. 259-298. Birkhäuser, Cham.

[26] J. A. Carrillo, H. Murakawa, M. Sato, H. Togashi and O. Trush, A population dynamics model of cell-cell adhesion incorporating population pressure and density saturation, *J. Theor. Biol.*, **474** (2019) 14-24.

[27] C. Castaing, P. Raynaud de Fitte and M. Valadier, *Young Measures on Topological Spaces: with Applications in Control Theory and Probability Theory*, Springer, 2004.

[28] T. Cazenave and A. Haraux, *An Introduction to Semilinear Evolution Equations*, Oxford Lect. Ser. Math. Appl. 13, Oxford, 1998

[29] M. G. Crandall and P. H. Rabinowitz, Bifurcation from simple eigenvalues. *Journal of Functional Analysis*, **8(2)** (1971), 321-340.

[30] M. G. Crandall and P. H. Rabinowitz, The Hopf bifurcation theorem in infinite dimensions. *Arch. Rational Mech. Anal.*, **67(1)** (1977), 53-72.

[31] K. C. Chang, *Methods in nonlinear analysis*, Springer Science & Business Media, 2006.

[32] S. N. Chow and K. Lu, Invariant manifolds and foliations for quasiperiodic systems, *J. Differential Equations* **117** (1995), 1-27.

[33] J. H. Cushman, B. X. Hu and F. W. Deng, Nonlocal reactive transport with physical and chemical heterogeneity: Localization errors. *Water Resources Research,* **31(9)** (1995), 2219-2237.

[34] C. Dahmann, A. C. Oates and M. Brand, Boundary formation and maintenance in tissue development. *Nat. Rev. Genet.*, **12(1)** (2011), 43.

[35] A. de Pablo, J. L. Vázquez, Travelling waves and finite propagation in a reaction-diffusion equation. *J. Differential Equations* **93** (1991), no. 1, 19-61.

[36] A. H. Delgoshaie, D. W. Meyer, P. Jenny and H. A. Tchelepi, Non-local formulation for multiscale flow in porous media. *Journal of Hydrology*, **531** (2015), 649-654.

[37] Y. Du, F. Quiros and M. Zhou, Logarithmic corrections in Fisher-KPP type Porous Medium Equations. (2018) arXiv preprint arXiv:1806.02022.

[38] A. Ducrot, F. Le Foll, P. Magal, H. Murakawa, J. Pasquier and G. F. Webb, An in Vitro Cell Population Dynamics Model Incorporating Cell Size, Quiescence, and Contact Inhibition, *Math. Model. Methods Appl. Sci.*, **21(supp01):871**, 2011.

[39] A. Ducrot and P. Magal, Asymptotic behaviour of a non-local diffusive logistic equation, *SIAM J. Math. Anal.*, **46** (2014), 1731-1753.

[40] A. Ducrot, X. Fu and P. Magal, Turing and Turing-Hopf bifurcations for a reaction diffusion qquation with nonlocal advection, *J. Nonlinear Sci.*, **28(5)** (2018), 1959-1997.

[41] R. M. Dudley, *Convergence of Baire measures*, Studia Mathematica, T. XXVII. (1966), 251–268.

[42] J. Dyson, S. A. Gourley, R. Villella-Bressan and G. F. Webb, Existence and asymptotic properties of solutions of a nonlocal evolution equation modeling cell-cell adhesion. *SIAM J. Math. Anal.,* **42(4)** (2010) 1784-1804.

[43] R. Eftimie, G. de Vries, M. A. Lewis and F. Lutscher, Modeling group formation and activity patterns in self-organizing collectives of individuals, *Bull. Math. Biol.*, **69** (2007), 1537-1565.

[44] B. Engquist and S. Osher, One-sided difference approximations for nonlinear conservation laws. *Math. Comp.*, **36 (154)** (1981), 321-351.

[45] L. C. Evans, *Partial differential equations*, American Mathematical Society, 1998.

[46] B. Fiedler and P. Polácik, Complicated dynamics of scalar reaction diffusion equations with a nonlocal term, *Proc. Royal Soc. Edinburgh*, **115** (1990), 263-276.

[47] R. L. Foote, Regularity of the distance function, *Proc. Amer. Math. Soc.*, **92(1)** (1984), 153-155.

[48] X. Fu and P. Magal, Asymptotic behavior of a nonlocal advection system with two populations. (2018) arXiv preprint arXiv:1812.06733.

[49] X. Fu, Q. Griette and P. Magal, A cell-cell repulsion model on a hyperbolic Keller-Segel equation. **(2019)** arXiv preprint arXiv:1907.11091.

[50] D. Gilbarg and N. S. Trudinger, *Elliptic partial differential equations of second order*, Classics in Mathematics. U.S. Government Printing Office, 2001.

[51] W. S. C. Gurney and R. M. Nisbet, The regulation of inhomogeneous populations. *J. Theoret. Biol.* **52** (1975), 441-457.

[52] F. Hamel and C. Henderson, Propagation in a Fisher-KPP equation with non-local advection. (2017) arXiv preprint arXiv:1709.00923.

[53] M. Haragus and G. Iooss, *Local Bifurcations, Center Manifolds, and Normal Forms in Infinite-Dimensional Dynamical Systems*, Universitext. Springer-Verlag London, Ltd., London; EDP Sciences, Les Ulis, 2011. xii+329 pp.

[54] B. D. Hassard, N. D. Kazarinoff and Y.-H. Wan, *Theory and Applications of Hopf Bifurcaton*, Cambridge Univ. Press, Cambridge, 1981.

[55] D. Henry, *Geometric Theory of Semilinear Parabolic Equation*, volume 840. Lecture Notes in Mathematics, Springer-Verlag, (1981).

[56] T. Hillen, K. J. Painter and C. Schmeiser, Global existence for chemotaxis with finite sampling radius, *Discrete Contin. Dyn. Syst. Ser. B* **7(1)** (2007), 125-144.

[57] T. Hillen and K. J. Painter, A user's guide to PDE models for chemotaxis, *J. Math. Biol.*, **58(1-2)** (2009), 183–217.

[58] T. Hillen, K. J. Painter and M. Winkler, Convergence of a cancer invasion model to a logistic chemotaxis model, *Math. Models Methods Appl. Sci.*, **23** (2013), pp. 165-198.

[59] M. W. Hirsch, S. Smale and R. L. Devaney, *Differential equations, dynamical systems, and an introduction to chaos*, (2012) Academic press.

[60] E. E. Holmes, M. A. Lewis, J. E. Banks and R. R. Veit, Partial differential equations in ecology: spatial interactions and population dynamics. *Ecology*, **75(1)** (1994), 17-29.

[61] D. Horstmann, From 1970 until present: the Keller-Segel model in chemotaxis and its consequences, *J. Jahresberichte DMV*, **105(3)** (2003), 103-165.

[62] X. Hu and J. H. Cushman, Nonequilibrium statistical mechanical derivation of a nonlocal Darcy's law for unsaturated/saturated flow. *Stochastic Hydrology and Hydraulics*, **8(2)** (1994), 109-116.

[63] R. Huang, C. Jin, M. Mei and J. Yin, Existence and stability of traveling waves for degenerate reaction-diffusion equation with time delay. *J. Nonlinear Sci.*, **28(3)** (2018), 1011-1042.

[64] S. Katsunuma, H. Honda, T. Shinoda, Y. Ishimoto, T. Miyata, H. Kiyonari, T. Abe, K. Nibu, Y. Takai and H. Togashi, Synergistic action of nectins and cadherins generates the mosaic cellular pattern of the olfactory epithelium, *J. Cell Biol.*, **212(5)** (2016), 561-575.

[65] K. Kawasaki, Diffusion and the formation of spatial distribution, *Mathematical Sciences* **16** (1978) 47-52

[66] E. F. Keller and L. A. Segel, Model for chemotaxis, *J. Theor. Biol.* **30** (1971), 225-234.

[67] R. J. Leveque, *Finite volume methods for hyperbolic problems*, Cambridge university press, 2002.

[68] A. J. Leverentz, C. M. Topaz and A. J. Bernoff, Asymptotic dynamics of attractive-repulsive swarms, *SIAM J. Appl. Dyn. Syst.*, **8** (2009), 880-908.

[69] Y. Lou and W. M. Ni, Diffusion, self-diffusion and cross-diffusion, *J. Differential Equations* , **131(1)** (1996), 79-131.

[70] Y. Lou and W. M. Ni, Diffusion vs cross-diffusion: an elliptic approach. *J. Differential Equations* , **154(1)** (1999), 157-190.

[71] A. Lunardi, *Analytic semigroups and optimal regularity in parabolic problems*, Springer Science & Business Media, 2012.

[72] P. Magal and S. Ruan, On semilinear Cauchy problems with non-dense domain, *Adv. Differential Equations* **14(11/12)** (2009), 1041-1084.

[73] P. Magal and S. Ruan, *Theory and Applications of Abstract Semilinear Cauchy Problems,* **Vol. 201**, Springer-Verlag (2018).

[74] M. Mimura and K. Kawasaki, Spatial segregation in competitive interaction-diffusion equations, *J. Math. Biol.*, **9(1)** (1980), 49-64.

[75] A. Mogilner and L. Edelstein-Keshet, A nonlocal model for a swarm, *J. Math. Biol.,* **38** (1999), 534-570.

[76] A. Mogilner, L. Edelstein-Keshet, L. Bent and A. Spiros, Mutual interactions, potentials, and individual distance in a social aggregation, *J. Math. Biol.*, **47** (2003), 353-389.

[77] D. Morale, V. Capasso and K. Oelschläger, An interacting particle system modelling aggregation behaviour: from individuals to populations, *J. Math. Biol.,* **50** (2005), 49-66.

[78] S. Motsch and D. Peurichard, From short-range repulsion to Hele-Shaw problem in a model of tumor growth. *J. Math. Biol.,* **76(1-2)** (2018), 205-234.

[79] H. Murakawa and H. Togashi, Continuous models for cell-cell adhesion, *J. Theor. Biol.*, **372** (2015), 1-12.

[80] J. D. Murray, *Mathematical Biology I: An Introduction*, volume I. Springer Science 2003.

[81] J. D. Murray, *Mathematical Biology II: Spatial Models and Biomedical Applications*, volume II. Springer Science 2003.

[82] G. Nadin, B. Perthame and L. Ryzhik, Traveling waves for the Keller-Segel system with Fisher birth terms. *Interfaces Free Bound.* **10(4)** (2008), 517-538.

[83] T. Nagai and M. Mimura, Asymptotic behaviour for a nonlinear degenerate diffusion equation in population dynamics. *SIAM J. Appl. Math.* **43** (1983), 449-464.

[84] K. Oelschläger, A law of large numbers for moderately interacting diffusion processes, *Z. Wahrsch. Verw. Gebiete*, **69** (1985), pp. 279–322.

[85] K. Oelschläger, Large systems of interacting particles and the porous medium equation, *J. Differential Equations*, **88** (1990), 294-346.

[86] K. J. Painter, J. M. Bloomfield, J. A. Sherratt and A. Gerisch, A nonlocal model for contact attraction and repulsion in heterogeneous cell populations. *Bull. Math. Biol.,* **77(6)** (2015), 1132-1165.

[87] C. S. Patlak, Random walk with persistence and external bias, *Bull. Math. Biophys.* **15** (1953), 311-338.

[88] J. Pasquier, L. Galas, C. Boulangé-Lecomte, D. Rioult, F. Bultelle, P. Magal, G.F. Webb, and F. Le Foll, Different modalities of intercellular membrane exchanges mediate cell-to-cell glycoprotein transfers in MCF-7 breast cancer cells, *J. Biol. Chem.*, **287(10)** (2012), 7374-7387.

[89] J. Pasquier, P. Magal, C. Boulangé-Lecomte, G. F. Webb and F. Le Foll, Consequences of cell-to-cell P-glycoprotein transfer on acquired multidrug resistance in breast cancer: a cell population dynamics model, *Biol. Direct*, **6(1):5**, (2011).

[90] B. Perthame and A. L. Dalibard, Existence of solutions of the hyperbolic Keller-Segel model, *Trans. Amer. Math. Soc.,* **361** (2009), 2319-2335.

[91] G. Raoul, Non-local interaction equations: stationary states and stability analysis, *Differential Integral Equations*, **25** (2012), 417-440.

[92] K. P. Rybakowski, An abstract approach to smoothness of invariant manifolds. *Appl. Anal.*, **49(1-2)** (1993), 119-150.

[93] M. Sen and E. Ramos, A spatially non-local model for flow in porous media. *Transport in porous media*, **92(1)** (2012), 29-39.

[94] D. Serre, *Systèmes de lois de conservation II*, Diderot Editeur Arts et Sciences, 1996.

[95] N. Shigesada, K. Kawasaki and E. Teramoto, Spatial segregation of interacting species. *J. Theoret. Biol.*, **79(1)** (1979), 83-99.

[96] J. Smoller, *Shock waves and reaction-diffusion equations* (Vol. 258). Springer Science & Business Media (1983).

[97] Y. Song, S. Wu and H. Wang, Spatiotemporal dynamics in the single population model with memory-based diffusion and nonlocal effect. *J. Differential Equations*, (2019) In Press.

[98] R. L. Sutherland, R. E. Hall and I. W. Taylor, Cell proliferation kinetics of MCF-7 human mammary carcinoma cells in culture and effects of tamoxifen on exponentially growing and plateau-phase cells, *Cancer research*, **43(9)** (1983), 3998-4006.

[99] H. B. Taylor, A. Khuong, Z. Wu, Q. Xu, R. Morley, L. Gregory, A. Poliakov, W.R. Taylor and D.G. Wilkinson. Cell segregation and border sharpening by Eph receptor-ephrin-mediated heterotypic repulsion. *J. Royal Soc. Interface*, **14(132)** (2017), p.20170338.

[100] R. Temam, *Infinite-dimensional dynamical systems in mechanics and physics* (Vol. 68). Springer Science & Business Media (2012).

[101] E. F. Toro, *Riemann solvers and numerical methods for fluid dynamics: a practical introduction,* Springer Science & Business Media. 2013

[102] M. Valadier, *Young measures. Methods of nonconvex analysis* (Varenna, 1989), 152-188, Lecture Notes in Math., 1446, Springer, Berlin, 1990.

[103] A. Vanderbauwhede and G. Iooss, Center manifold theory in infinite dimensions, *Dynamics Reported*, Vol. **1**, Springer-Verlag, Berlin, (1992), 125-163.

[104] J. L. Vázquez, *The Porous Medium Equation: Mathematical Theory*, Oxford University Press, 2007.

[105] A. Yagi, *Abstract Parabolic Evolution Equations and their Applications*, Springer-Verlag Berlin Heidelberg, 2010.

[106] M. L. Zeeman, Extinction in competitive Lotka-Volterra systems, *Proc. Amer. Math. Soc.*, **123(1)** (1995), 87-96.